

# MECHANICAL REGULATION OF CELL DEATH

---

A Dissertation Submitted to the Faculty of  
WORCESTER POLYTECHNIC INSTITUTE  
in Partial Fulfillment of the Requirements for the Degree of  
DOCTOR OF PHILOSOPHY  
in Biomedical Engineering

October 29<sup>th</sup> 2020

By:

---

Zachary Ethan Goldblatt

Approved by:

---

Kristen L. Billiar, PhD  
Dissertation Advisor  
Professor & Department Head  
Biomedical Engineering  
Worcester Polytechnic Institute

---

Glenn Gaudette, PhD  
Professor  
Biomedical Engineering  
Worcester Polytechnic Institute

---

Qi Wen, PhD  
Associate Professor  
Physics  
Worcester Polytechnic Institute

---

Nima Rahbar, PhD  
Associate Professor  
Civil & Environmental Engineering  
Worcester Polytechnic Institute

---

Venkat Maruthamuthu, PhD  
Associate Professor  
Mechanical & Aerospace Engineering  
Old Dominion University

## Acknowledgements

The completion of this dissertation work would not have been possible without the immeasurable help from the many people who have supported me over the last five years. First and foremost, I would like to thank my outstanding advisor, Dr. Kristen Billiar, for his endless guidance and friendship. Thank you for the opportunity to work on this exciting project, the continual encouragement through successes and failures, and the invaluable experience in grant/manuscript writing and student mentoring. I have enjoyed the discussions we have had about science and competing against each other on the basketball court. An additional thank you to the rest of my dissertation committee: Dr. Glenn Gaudette, Dr. Qi Wen, Dr. Nima Rahbar, and Dr. Venkat Maruthamuthu for their insight and the valuable expertise they have provided me throughout this project and my time in graduate school.

Thank you to the members of the Billiar Lab who have helped me design new experiments and techniques, troubleshoot issues, complete data analysis, and provided general advisement. Special thanks to Heather Cirka, who initially trained me in lab techniques and established the foundation of my project. Thank you to Habibeh Ashouri Choshali, who performed all the FE modeling of cell-stresses. And my biggest thanks to Leigh Whitehorn, my undergraduate student mentee who performed like a Ph.D. student and acted independently on her own research project. Without her, I would not have been able to complete all the aspects of my project in the time that I did.

I want to also thank all my amazing friends and colleagues I have made at WPI over the years. You are what makes graduate school worth it, and you have given me a lifetime of stories both inside and outside of the lab.

Last, but certainly not least, I would like to thank my family for their endless love, support, and most importantly, patience, as I finish up my 23<sup>rd</sup> year of schooling. I will finally no longer be labeled as a “student.” Thank you for encouraging me to be the best that I can, celebrating with me in my successes, and always being there. And thank you to my fiancé, Megan, who supports me unconditionally, sets the bar high, and always challenges me to be better.

# Table of Contents

Acknowledgements.....	i
Table of Contents.....	ii
Table of Figures.....	vi
Table of Tables.....	vii
List of Abbreviations and Symbols.....	viii
Abstract.....	1
Chapter 1: Introduction.....	3
1.1 References.....	6
Chapter 2: Background.....	8
2.1 Overview.....	8
2.2 Valvular interstitial cells.....	12
2.3 The role of apoptosis in cardiovascular diseases.....	12
2.3.1 Heart failure.....	13
2.3.2 Atherosclerosis.....	14
2.3.3 Aneurysm formation.....	15
2.3.4 Calcific aortic valvular disease.....	15
2.3.5 Pulmonary arterial hypertension.....	16
2.4 Canonical and non-canonical apoptotic pathways.....	16
2.5 Stages of apoptosis and stage-specific markers.....	20
2.5.1 Early stage apoptosis.....	20
2.5.2 Mid stage apoptosis.....	21
2.5.3 Late stage apoptosis.....	21
2.6 Mechanical induction of apoptosis.....	23
2.6.1 Mechanical stretch.....	27
2.6.2 Fluid shear stress.....	28
2.6.3 Microgravity.....	28
2.6.4 Regulation of cell spread area.....	29
2.6.5 Control of substrate modulus.....	30
2.6.6 Area-restricted multicellular systems.....	31
2.6.7 Modeling cell-stresses in multicellular systems.....	32
2.6.8 Separating the individual effects of correlated mechanical stimuli.....	35
2.7 Potential mechanical mechanisms regulating apoptosis.....	35
2.7.1 Canonical mechanotransduction pathways.....	35

2.7.2 Tension in the cytoskeleton.....	37
2.7.3 Cellular realignment due to strain avoidance.....	40
2.7.4 Yes-associated protein (YAP).....	40
2.7.5 Myocardin-related transcription factor-A (MRTF-A).....	42
2.8 Mechanomedicines as a potential therapeutic solution.....	43
2.9 Summary.....	45
2.10 References.....	46
Chapter 3: Cells on Soft Substrates Exhibit Partial Strain Avoidance.....	59
3.0 Abstract.....	60
3.1 Introduction.....	61
3.2 Materials and Methods.....	63
3.2.1 Cell Culture.....	63
3.2.2 Polyacrylamide Hydrogel Preparation.....	63
3.2.3 Cyclical Stretching Time-lapse Microscopy.....	64
3.2.4 Traction Force Microscopy.....	64
3.2.5 Immunofluorescence.....	65
3.3 Results.....	65
3.3.1 Cells stretched on stiff substrates exhibit strain avoidance behavior.....	65
3.3.2 Cells stretched on soft substrates display partial avoidance behavior.....	66
3.3.3 Cells reach steady state behavior after continuous cyclical stretch.....	69
3.3.4 Cells revert to initial state when continuous mechanical stimulus is removed.....	72
3.3.5 Cyclic stretch decreases apoptosis in cells on soft substrates.....	73
3.4 Discussion.....	74
3.4.1 Mechanism behind cell reorientation in response to cyclic stretch.....	75
3.4.2 Cells on stiff substrates reorient away from stretch.....	78
3.4.3 Mechanical stretch enables cells on soft substrates to elongate.....	79
3.4.4 Cells revert to initial state after cessation of cyclic stretch.....	79
3.4.5 Relevant mechanosensitive signaling pathways.....	80
3.5 Conclusions.....	80
3.6 Acknowledgements.....	81
3.7 References.....	81
Chapter 4: Heterogeneity profoundly alters emergent stress fields.....	85
4.0 Abstract.....	86
4.1 Significance.....	87
4.2 Introduction.....	88

4.3 Materials and Methods.....	89
4.3.1 Cell Culture.....	89
4.3.2 Microcontact Substrate Preparation.....	90
4.3.3 Live Cell Imaging.....	90
4.3.4 Traction Force Microscopy.....	90
4.3.5 Atomic Force Microscopy.....	91
4.3.6 Immunocytochemistry.....	91
4.3.7 Modeling.....	92
4.3.8 Developing Stable YAP-VIC Cell Line.....	98
4.3.9 Magnetic Induction of Stress.....	99
4.4 Results and Discussion.....	99
4.4.1 Homogeneous models predict high stresses and low traction forces.....	99
4.4.2 Distributions of high-stress biomarkers localize to aggregate periphery.....	102
4.4.3 Central cells vary in morphology, behavior, and properties compared to peripheral cells.....	105
4.4.4 Heterogeneous models predict stress distributions inverse to homogeneous models.....	108
4.4.5 MSM trends agree with thermal contraction models.....	110
4.4.6 Activation of YAP decreases apoptosis in multicellular aggregates.....	113
4.4.7 Interpretation of stress measurements relative to biological markers.....	114
4.5 Conclusions.....	117
4.6 Author Contributions.....	118
4.7 Acknowledgements.....	118
4.8 References.....	118
Chapter 5: Conclusions, Limitations, and Future Work.....	123
5.1 Conclusions.....	123
5.1.1 Conclusions: Aim 1.....	123
5.1.2 Conclusions: Aim 2.....	124
5.2 Experimental Limitations and Next Steps.....	126
5.2.1 Study Limitations: Aim 1.....	126
5.2.2 Study Limitations: Aim 2.....	128
5.3 Long-term Future Work for the Field.....	131
5.3.1 Future Work: Aim 1.....	131
5.3.2 Future Work: Aim 2.....	136
5.4 References.....	141
Appendix: Protocols.....	145
A.1 Valvular interstitial cell isolation.....	145

A.2 Preparation of Leibovitz's L-15 culture media .....	146
A.3 Activation of polyacrylamide gel .....	146
A.4 Micro-contact printing protocol .....	147
A.5 Attachment of polyacrylamide gels onto CellScale wells .....	148
A.6 Collagen attachment to control polyacrylamide gels .....	149
A.7 Preparing fluorescent micro-bead coat on glass coverslips .....	149
A.8 Caspase-3/7 live cell detection .....	150
A.9 Image acquisition for Traction Force Microscopy .....	151
A.10 Immunofluorescence staining protocol .....	151
A.11 Immunocytochemistry staining protocol for $\alpha$ -SMA .....	152
A.12 Immunocytochemistry staining protocol for YAP and MRTF-A .....	153
A.13 MATLAB code for radial distribution of caspase in aggregates .....	154

## Table of Figures

<b>Figure 2.1:</b> Apoptosis occurs naturally in organisms during various phases of their life .....	9
<b>Figure 2.2:</b> Unregulated apoptosis (insufficient or excessive) can lead to various diseases.....	10
<b>Figure 2.3:</b> Apoptosis is present in various types of heart failure.....	13
<b>Figure 2.4:</b> In <i>in vitro</i> models of CAVD, TGF- $\beta$ 1 causes cell aggregation .....	16
<b>Figure 2.5:</b> Overview of apoptotic pathways .....	17
<b>Figure 2.6:</b> Apoptosis occurs in three different stages: early, mid, and late .....	22
<b>Figure 2.7:</b> Mechanical stimuli that regulate apoptosis include mechanical stress from the ECM .....	26
<b>Figure 2.8:</b> Cells cultured on soft (1.2 kPa) substrates (top) are small with rounded morphology .....	31
<b>Figure 2.9:</b> High cell-stress markers localize to aggregate periphery .....	32
<b>Figure 2.10:</b> Schematic of stress components for thermal contraction model. ....	34
<b>Figure 2.11:</b> Schematic of stress components for monolayer stress microscopy model.....	35
<b>Figure 2.12:</b> Both excessive and insufficient mechanical stress can activate apoptotic signaling.....	37
<b>Figure 2.13:</b> Schematic of the relationship between intracellular stress levels.....	38
<b>Figure 2.14:</b> Schematic of the common Hippo signaling pathway. ....	41
<b>Figure 2.15:</b> Schematic of the MRTF signaling pathway. ....	43
<b>Figure 2.16:</b> Schematic of mechanomedicines .....	44
<b>Figure 3.1:</b> Cells on stiff gels are spread out and then reorient away .....	66
<b>Figure 3.2:</b> Cells on soft gels are rounded and then elongate .....	68
<b>Figure 3.3:</b> Cells on soft gels are rounded and then elongate .....	69
<b>Figure 3.4:</b> Cyclic stretch directly influences changes in cell behavior when on soft gels.....	70
<b>Figure 3.5:</b> Changes in cell behavior over 12 hr of continuous cyclical stretching .....	71
<b>Figure 3.6:</b> Changes in cell behavior over 6 hr after stretch cessation .....	73
<b>Figure 3.7:</b> Changes in apoptosis due to cyclic stretch depend on substrate stiffness .....	74
<b>Figure 3.8:</b> Relationship between cellular survival and internal cell tension .....	76
<b>Figure 3.9:</b> Schematic of possible mechanism behind strain avoidance behavior .....	77
<b>Figure 4.1:</b> Schematics of stress components for each computational model.....	92
<b>Figure 4.2:</b> Parametric study shows sensitivity of the stress distributions.....	94
<b>Figure 4.3:</b> Parametric study changing $\alpha$ (A-C) or the substrate modulus (D-F).....	95
<b>Figure 4.4:</b> Cell-layer and substrate stresses simulated by thermal contraction .....	96
<b>Figure 4.5:</b> Homogeneous thermal contraction and MSM modeling.....	101
<b>Figure 4.6:</b> Protein measurements for cell-layer stress .....	103
<b>Figure 4.7:</b> YAP and MRTF-A localize in the nucleus of peripheral cells.....	104
<b>Figure 4.8:</b> Cells within the central region of aggregates have on average .....	107
<b>Figure 4.9:</b> Cell-layer and substrate stresses simulated by thermal contraction .....	109
<b>Figure 4.10:</b> Continuous distribution for contractile stresses as a function of radius .....	110
<b>Figure 4.11:</b> Cell aggregates generate both positive ( <i>inward</i> ) and negative ( <i>outward</i> ) stresses.....	110
<b>Figure 4.12:</b> Heat maps from left to right show measured traction stresses .....	111
<b>Figure 4.13:</b> Cell-layer stresses calculated by MSM for step change heterogeneous condition.....	111
<b>Figure 4.14:</b> Cell-layer stresses calculated by MSM .....	113
<b>Figure 4.15:</b> Constitutively active YAP decreases occurrences of apoptosis .....	114
<b>Figure 4.16:</b> Additional mechanical load in aggregate center increases intracellular stress.....	117

## Table of Tables

<b>Table 2.1:</b> Mechanical stimuli cause cellular apoptosis or survival.....	24
<b>Table 3.1:</b> Time required to reach specified time constants.....	71
<b>Table 3.2:</b> Time required to reach specified time constants.....	72

## List of Abbreviations and Symbols

<b>AFM</b>	Atomic force microscopy
<b>CAVD</b>	Calcific aortic valvular disease
<b>ECM</b>	Extracellular matrix
<b>FFT</b>	Fast Fourier transform
<b>MSM</b>	Monolayer stress microscopy
<b>MRTF-A</b>	Myocardin-related transcriptional factor-A
<b>PA</b>	Polyacrylamide
<b>PDMS</b>	Polydimethylsiloxane
<b>TFM</b>	Traction force microscopy
<b>VIC</b>	Valvular interstitial cell
<b>YAP</b>	Yes-associated protein
<b><math>\alpha</math>-SMA</b>	Alpha smooth muscle actin

## Abstract

Valvular disease is the cause of over 300,000 heart valve replacement surgeries each year worldwide. Calcific aortic valvular disease (CAVD), the most common valvular pathology, results in the stiffening and mineralization of the aortic valve leaflets, which hinders proper opening and closing of the leaflets. Previously thought to be a passive disease, CAVD is now known to be an active process mediated by valvular cells. Currently, there are no therapies available for the reversal or prevention of CAVD; treatments mostly comprise invasive surgeries and complete replacement of the valve. The mechanisms that initiate and regulate this disease remain largely unknown. However, studies have shown that the regulation of cell tension and programmed cell death (apoptosis) by the extracellular mechanical environment may be an underlying cause. It is generally hypothesized that cells maintain homeostatic levels of internal tension, and when mechanical forces such as external loading or cell-cell contact adversely affect that tension state, cells react in attempt to reestablish homeostasis. If internal tension remains too high or low, apoptosis can occur, triggering disease progression. Therefore, understanding the fundamental mechanisms that regulate cell tension and apoptosis is a critical step toward developing therapeutic treatments for CAVD.

This dissertation examines cell behavior in response to different mechanical stress stimuli. We first investigated how mechanical stress affects cell survival and cytoskeletal remodeling in single cells that are dynamically stretched. We found that cyclically stretching cells in low-stress environments facilitates cellular spreading and decreases in apoptosis. While studies of single cells allow for the isolation of specific cellular behaviors independent of cell-cell contacts, multicellular systems are more characteristic of *in vivo* environments. Therefore, we next identified specific mechanical stress parameters and mechanotransduction pathways that mediate cell tension and apoptosis in two-dimensional multicellular aggregates. We determined that cells in aggregates display regional differences in stress-associated biomarkers, with low stress in central regions and high stress in peripheral regions. Additionally, the mechanosensitive transcriptional cofactors, YAP and MRTF-A, localize to the nucleus in regions of high stress and help promote cell survival. Overall, we found that low-stress conditions, such as those found on soft substrates or in the central region of aggregates, initiate apoptosis, and cells can be rescued if

intracellular tensional levels are restored to homeostatic levels by external cyclic stretch or cell-to-cell stress transfer. This work offers new insight into how mechanical stress regulates cell fate through mechanotransduction pathways.

## Chapter 1: Introduction

Cardiovascular disease has been the leading cause of death in the United States since the early 1920s. It is currently responsible for nearly one in every three deaths in the United States and has an estimated annual cost of \$350 billion as of 2014 (Virani *et al.*, 2020). Valvular disease contributes to over 300,000 heart valve replacement surgeries each year worldwide (Manji *et al.*, 2012). Calcific aortic valvular disease (CAVD) is the most common valvular pathology and the third most common type of cardiovascular disease (Freeman and Otto, 2005; Dweck *et al.*, 2012). It arises from calcification of heart valve leaflets, which decreases the ability of valves to open and close properly. Previously thought to be passive, CAVD is a dynamic and cell-mediated disease; activated valvular cells have been shown to aggregate together and colocalize with diseased areas such as fibrosis and calcification (Aikawa *et al.*, 2006). Recent studies have found from histology and immunohistochemistry samples from explants and *in vivo* that cellular programmed death (apoptosis) is an underlying cause of CAVD and other cardiovascular diseases (Kim, 1995; Proudfoot *et al.*, 2001; Clarke *et al.*, 2006; Van Vré *et al.*, 2012). Understanding the fundamental mechanisms that regulate apoptosis, and how they contribute to these disease pathologies, is critical for developing better therapeutic treatments.

Apoptosis is the result of a complex signaling cascade whereby extrinsic or intrinsic signals are interpreted by the cell and result in self-termination. It is a highly conserved physiological process, critical to the continuing health of the organism and its development, tissue maintenance, and overall homeostasis. Proper regulation of this process is crucial as a variety of diseases can result from either excessive apoptosis (atrophy, degenerative disease) or reduced apoptotic rates (cancer, fibrosis). The current belief is that apoptosis is a product of downstream signaling cascades from extrinsic cellular signals initiated by inflammatory cytokines or other environmental factors (Thompson, 1995; Elmore, 2007). Recent evidence suggests that the extracellular mechanical environment plays a role in apoptosis (Kulms *et al.*, 2002; Gourlay and Ayscough, 2005; Ndozangue-Touriguine *et al.*, 2008; Desouza *et al.*, 2012), but the mechanical mechanisms that regulate this process are still unknown. Therefore, there is an increasing need to identify the signaling mechanisms by which cells transduce mechanical signals into an apoptotic response.

Cells sense and respond to mechanical signals through mechanotransduction, a process by which mechanical stimuli are sensed, transferred, and converted into biochemical signals or cellular behaviors. In response to their environment, cells will rapidly change their intracellular tension by remodeling their cytoskeleton, which is adaptive and dynamic. The cytoskeleton is made up of F-actin and G-actin; their levels have been linked to various mechanosensitive signaling pathways, which are associated with cellular behaviors such as proliferation and possibly apoptosis. Cytoskeletal remodeling allows cells to maintain a tension homeostasis with their surrounding environment (Chien, 2007; Cox and Erler, 2011; Humphrey *et al.*, 2014). For instance, cells adhered to high-modulus (stiff) substrates are able to assemble a stable cytoskeleton and attain homeostatic tension. When an external mechanical stimulus is introduced, such as uniaxial cyclic stretch, cell tension increases. To reduce their intracellular tension levels, cells remodel their cytoskeleton and reorient away from the direction of stretch to an angle of optimal stress. For cells on stiff substrates, this angle is perpendicular to the direction of stretch. If the stretch is equibiaxial, cells pull in their filopodia and/or reduce spread area to reduce stress. Alternatively, cells adhered to very low-modulus (soft) substrates are not able to generate optimal tension levels. Cyclic stretch allows cells to generate a more stable cytoskeleton and increase tension inside cells towards their optimal levels. Like cells on stiff substrates, we have shown that cells on soft substrates will reorient to an angle of optimal stress if the stretch level is large enough; however, this angle is less than perpendicular from the direction of stretch.

Actin destabilization has been linked to apoptosis; however, studies investigating this phenomenon have not elucidated the underlying mechanisms connecting these events (Gourlay *et al.*, 2004; Croft *et al.*, 2005; Leadsham *et al.*, 2010). There remains a significant gap in our understanding regarding how particular physical stimuli trigger apoptosis through mechanotransduction signaling pathways, such as the Hippo and MRTF pathways and their transcriptional coactivators, Yes-associated protein (YAP) and myocardin-related transcription factor A (MRTF-A), respectively.

The motivation of this project arises from the need to develop a method to determine the mechanisms by which mechanical properties of the extracellular matrix and intracellular stress affect the integrity of the actin cytoskeleton, and to investigate signaling pathways that regulate

apoptosis. The proposed research offers an addition to the current paradigm that inflammatory and chemical environmental factors, exclusively, induce apoptosis in cardiovascular disease. These factors play a large role in apoptosis; however, we propose that mechanical stress can also regulate apoptosis. We have created powerful methods to finely adjust mechanical stimulation of cells and observe subsequent cellular behavior both in single cells and in multicellular aggregates. Two aims have been established to explore these research areas. In the first aim, we investigate how mechanical stress and substrate modulus affect the cytoskeletal network organization and apoptosis in single cells that are dynamically stretched. In the second aim, we determine specific mechanical stress parameters and mechanotransduction pathways that mediate apoptosis in multicellular systems.

The first aim is addressed in Chapter 3, where we investigate the effects of cyclical mechanical stretch on cytoskeletal remodeling and subsequent cell survival in individual valvular interstitial cells (VIC) on soft substrates. We hypothesize that cells respond to their mechanical environment by remodeling their cytoskeleton to optimize their intracellular stress, and that insufficient mechanical feedback causes cytoskeletal depolymerization, triggering apoptosis. We characterize single cell behavior on soft and stiff substrates, which helps modulate basal cell-stress levels, as well as use cyclic stretch to dynamically modulate stress. We examine the relationship between cell-stress state and stress-associated biomarkers. Additionally, we explore the reversibility of cell survival and behavior when mechanical inputs are removed. This aim is important as it increases our understanding of how mechanical stimuli initiate cytoskeletal reorganization, which then regulates mechanosensitive pathways that control apoptosis.

The second aim is outlined in Chapter 4, where we investigate collective cell behavior in multicellular aggregates and correlate the emergent stress fields in the cell layer to regional differences in behavior and cell fate. We postulate that intercellular interactions leading to low intracellular stresses initiate apoptosis in multicellular systems. We culture VICs in restrictive multicellular aggregates in order to systematically examine the relationship between cell geometry, mechanical stress parameter distribution, and apoptosis. We also correlate and validate modeled stress fields with distributions of biomarkers indicative of stress. Additionally, we investigate the mechanism by which YAP and MRTF-A signaling pathways regulate apoptosis.

This aim is significant as it describes the spatial relationship between intracellular cell stress, mechanosensitive pathways, and apoptosis within multicellular aggregates.

The conclusions, limitations, and future directions of this project are discussed in Chapter 5. A quantitative understanding of how external mechanical signals regulate cell fate is critical for understanding the mechanisms underlying various diseases, such as cardiovascular disease, cancer, and tissue degeneration. Because this mechanical-biochemical relationship is bidirectional, the proposed research may offer two opportunities for novel treatments of cardiovascular disease. Pharmaceuticals targeting key modulators of cytoskeletal destabilization, as well as mechanical perturbations (“mechanomedicines”) capable of inhibiting apoptotic pathways, may be designed using results of these innovative experiments.

The contribution of this project is significant as it will be the first to bridge mechanotransduction signaling pathways with mechanical stresses that may regulate apoptosis. The results from this project will pave the way to identify new biophysical predictors of apoptosis to better monitor cardiovascular pathologies.

## 1.1 References

- Aikawa, E., Whittaker, P., Farber, M., Mendelson, K., Padera, R. F., Aikawa, M., and Schoen, F. J. (2006). Human semilunar cardiac valve remodeling by activated cells from fetus to adult: Implications for postnatal adaptation, pathology, and tissue engineering. *Circulation* *113*, 1344–1352.
- Chien, S. (2007). Mechanotransduction and endothelial cell homeostasis: the wisdom of the cell. *Am. J. Physiol. Heart Circ. Physiol.* *292*, H1209–H1224.
- Clarke, M. C. H., Figg, N., Maguire, J. J., Davenport, A. P., Goddard, M., Littlewood, T. D., and Bennett, M. R. (2006). Apoptosis of vascular smooth muscle cells induces features of plaque vulnerability in atherosclerosis. *Nat. Med.* *12*, 1075–1080.
- Cox, T. R., and Erler, J. T. (2011). Remodeling and homeostasis of the extracellular matrix: implications for fibrotic diseases and cancer. *Dis. Model. Mech.* *4*, 165–178.
- Croft, D. R., Coleman, M. L., Li, S., Robertson, D., Sullivan, T., Stewart, C. L., and Olson, M. F. (2005). Actin-myosin-based contraction is responsible for apoptotic nuclear disintegration. *J. Cell Biol.* *168*, 245–255.
- Desouza, M., Gunning, P. W., and Stehn, J. R. (2012). The actin cytoskeleton as a sensor and

- mediator of apoptosis. *Bioarchitecture* 2, 75–87.
- Dweck, M. R., Boon, N. A., and Newby, D. E. (2012). Calcific aortic stenosis: a disease of the valve and the myocardium. *J. Am. Coll. Cardiol.* 60, 1854–1863.
- Elmore, S. (2007). Apoptosis: a review of programmed cell death. *Toxicol. Pathol.* 35, 495–516.
- Freeman, R. V., and Otto, C. M. (2005). Spectrum of calcific aortic valve disease: Pathogenesis, disease progression, and treatment strategies. *Circulation* 111, 3316–3326.
- Gourlay, C. W., and Ayscough, K. R. (2005). The actin cytoskeleton: a key regulator of apoptosis and ageing? *Nat. Rev. Mol. Cell Biol.* 6, 583–589.
- Gourlay, C. W., Carpp, L. N., Timpson, P., Winder, S. J., and Ayscough, K. R. (2004). A role for the actin cytoskeleton in cell death and aging in yeast. *J. Cell Biol.* 164, 803–809.
- Humphrey, J. D., Dufresne, E. R., and Schwartz, M. A. (2014). Mechanotransduction and extracellular matrix homeostasis. *Nat. Rev. Mol. Cell Biol.* 15, 802–812.
- Kim, K. M. (1995). Apoptosis and Calcification. *Scanning Microsc.* 9, 1137–1178.
- Kulms, D., Düssmann, H., Pöppelmann, B., Ständer, S., Schwarz, A., and Schwarz, T. (2002). Apoptosis induced by disruption of the actin cytoskeleton is mediated via activation of CD95 (Fas/APO-1). *Cell Death Differ.* 9, 598–608.
- Leadsham, J. E., Kotiadis, V. N., Tarrant, D. J., and Gourlay, C. W. (2010). Apoptosis and the yeast actin cytoskeleton. *Cell Death Differ.* 17, 754–762.
- Manji, R. A., Menkis, A. H., Ekser, B., and Cooper, D. K. C. (2012). The future of bioprosthetic heart valves. *Indian J. Med. Res.* 135, 150–151.
- Ndozangue-Touriguine, O., Hamelin, J., and Bréard, J. (2008). Cytoskeleton and apoptosis. *Biochem. Pharmacol.* 76, 11–18.
- Proudfoot, D., Skepper, J. N., Hegyi, L., Farzaneh-Far, A., Shanahan, C. M., and Weissberg, P. L. (2001). The role of apoptosis in the initiation of vascular calcification. *Z. Kardiol.* 90, 43–46.
- Thompson, C. B. (1995). Apoptosis in the Pathogenesis and Treatment of Disease. *Sci. New Ser.* 267, 1456–1462.
- Virani, S. S. *et al.* (2020). Heart Disease and Stroke Statistics—2020 Update.
- Van Vré, E. A., Ait-Oufella, H., Tedgui, A., and Mallat, Z. (2012). Apoptotic cell death and efferocytosis in atherosclerosis. *Arterioscler. Thromb. Vasc. Biol.* 32, 887–893.

## Chapter 2: Background

The following subsections appear in Goldblatt et al. "Mechanical Regulation of Apoptosis in the Cardiovascular System." *In-press, Annals of Biomedical Engineering*. (2020) and are reproduced here with permission. Specific figures were reproduced with permissions from The Society of Thoracic Surgeons, American College of Cardiology Foundation, Massachusetts Medical Society, The Royal Society of Chemistry, and Biophysical Journal. Sections with an asterisk (\*) indicate additional sections not included in the original article.

### 2.1 Overview

Apoptosis, also known as programmed cell death, involves a complex signaling cascade whereby extracellular or intracellular signals result in the orderly termination of cells. Although apoptosis results in the demise of cells, it is critical to the continuing health of the organism as a whole, especially during embryogenesis, growth, and tissue maintenance. Common examples of homeostatic apoptosis include digit individualization on the hands/feet, loss of tails in tadpoles, and cellular reorganization in dorsal closure in *Drosophila* (Figure 2.1) (Suzanne and Steller, 2013). On the other hand, when apoptosis is incorrectly regulated, unchecked cell growth can lead to fibrosis and tumor formation, while excessive apoptosis can lead to degenerative diseases, such as degenerative disc disease and muscle atrophy (Figure 2.2). In fact, one of the hallmarks of cancer is the ability of malignant cells to evade apoptosis (Hanahan and Weinberg, 2011).

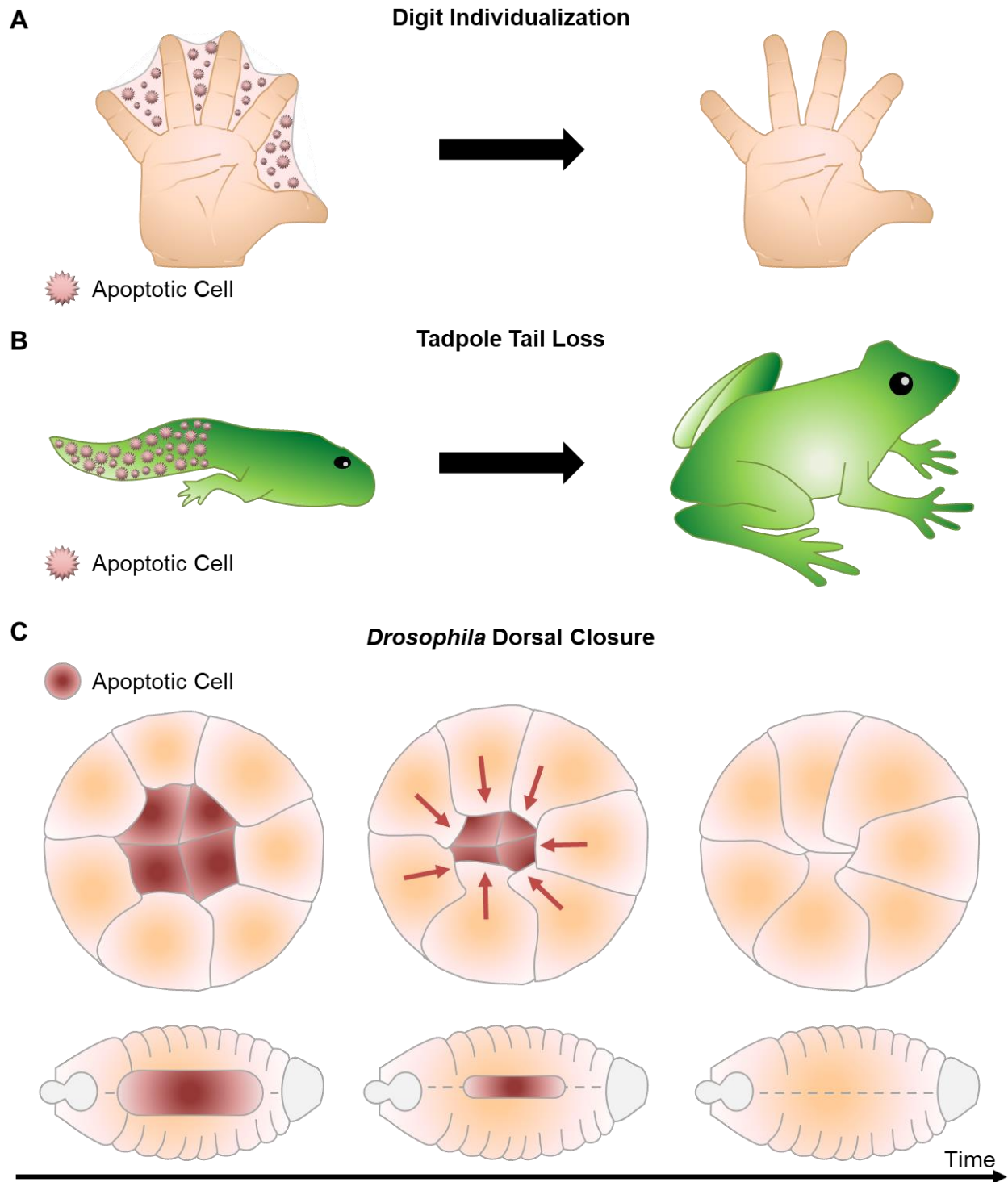


**Figure 2.1: Apoptosis occurs naturally in organisms during various phases of their life, such as morphogenesis and embryogenesis.** A) Morphogenetic apoptosis helps separate digits in the hand and feet. B) Apoptosis in tadpole tails helps transition their growth into frogs, causing tadpoles to lose their tails. C) During the embryonic stage, *Drosophila* undergo a process called dorsal closure, where an elliptical gap in the dorsal region converges and undergoes compression and apoptosis.

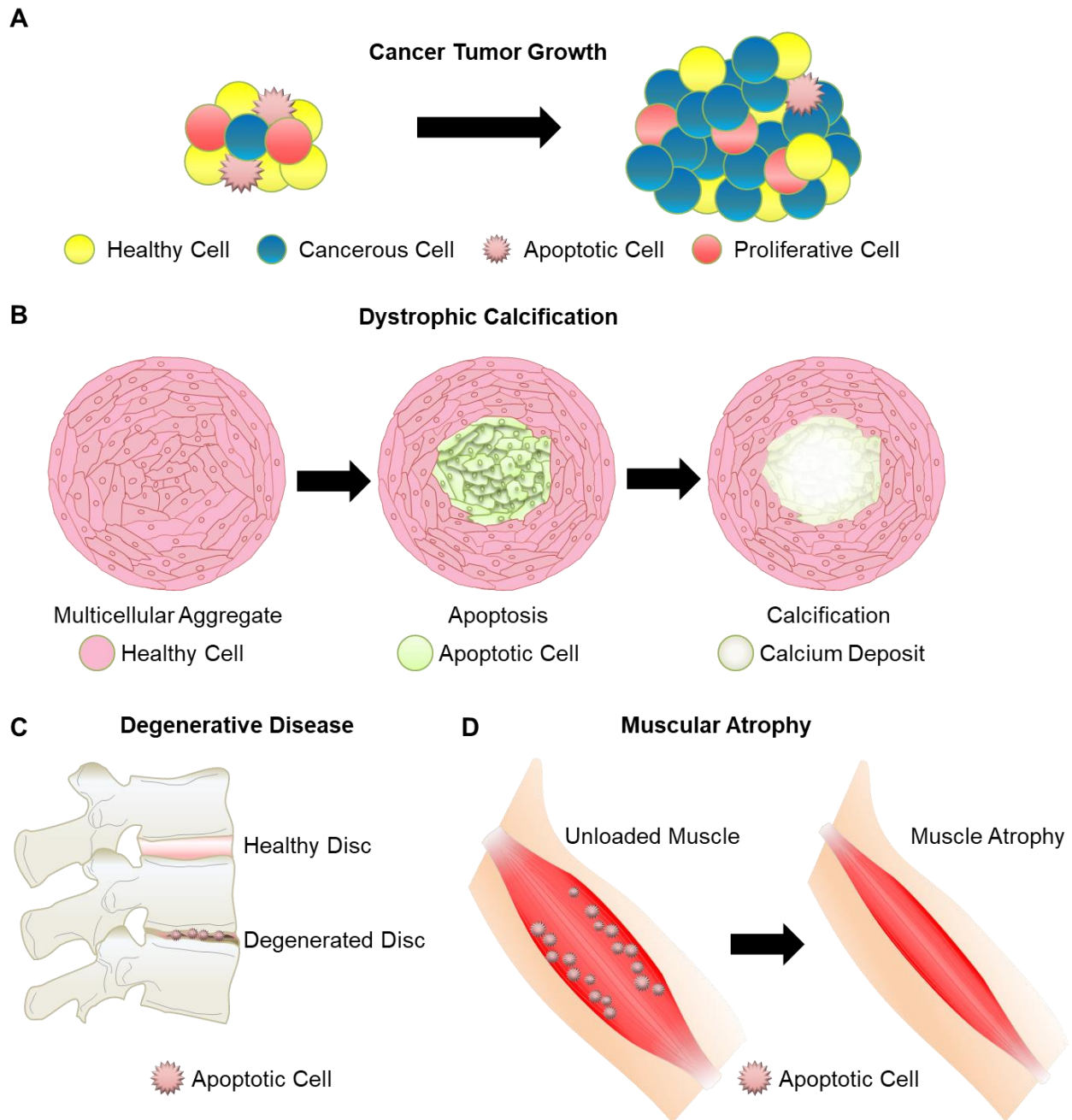


**Figure 2.2: Unregulated apoptosis (insufficient or excessive) can lead to various diseases. A)** Healthy tissues have a balance between apoptotic and proliferative cells; in contrast, the unregulated growth of cancerous cells which evade apoptosis lead to tumor formation. **B)** In dystrophic calcification, a symptom of heart valve disease, cells aggregate triggering apoptosis of the central compressed cells which promotes calcium deposition and disease progression. Uncontrolled apoptosis can also lead to degenerative diseases such as degenerated discs in the spine (**C**) and atrophy of the muscles (**D**).

There are many environmental factors that can initiate apoptosis, such as pH, oxygen concentration, radiation, infection, cytokines and inflammatory signaling molecules (Kannan and

Jain, 2000; Lagadic-Gossmann *et al.*, 2004; Roos and Kaina, 2006). Increasingly, the mechanical environment is being recognized as a key regulator of apoptosis as well (Gourlay and Ayscough, 2005b; Desouza *et al.*, 2012). Externally applied mechanical stimuli (stretch and forces) and external physical factors (ECM stiffness, geometric constraints, topography) which regulate internally generated cell forces are all referred to as mechanical stimuli within this review. How mechanical stimulation is interpreted by the cell and transduced into an apoptotic response is an active area of research in cell mechanobiology. Currently, there are no well-defined mechanisms of action for how mechanical stimuli regulate cell health and initiate apoptosis. Teasing apart specific conditions which initiate apoptosis has been challenging, as factors inducing cell death are dependent upon the specific loading conditions and the extracellular mechanical environment is constantly evolving. Most studies correlate mechanical stimuli with observed cell responses. For example, elevated mechanical loading has been shown to initiate apoptosis by causing excessive DNA damage, while trauma from mechanical forces induces apoptosis by altering mitochondria permeability (Clark *et al.*, 1999; Mayr *et al.*, 2002). Apoptosis also occurs following wound healing and results in the removal of excess myofibroblasts; these cells are shielded from stresses by the mature collagen matrix that they produce and remodel around themselves (Tomasek *et al.*, 2002). No real mechanisms have been offered linking mechanics to apoptosis; this is the direction that the field needs to improve next.

In this chapter, we analyze mechanically regulated apoptosis with a focus on the cardiovascular system. We provide a brief introduction to aberrant apoptosis present in different types of cardiovascular diseases and describe the canonical signaling pathways of apoptosis. We then review the literature demonstrating mechanical-induced apoptosis and discuss potential mechanosensing pathways. Where and how mechanics acts on cells is not yet known. These are the questions research needs to explore in the future. We attempt to specify a potential unifying mechanism for how mechanical stimuli initiate apoptosis. We hypothesize that regulation of cytoskeletal stability may link mechanics to apoptosis. Finally, we conclude by examining the potential of mechanomedicines for treatment by regulation of apoptosis. The goal of this chapter is to summarize the current state of understanding of the mechanobiology of apoptosis and encourage promising directions to explore for future research.

## 2.2 Valvular interstitial cells\*

While the work in this dissertation is transferrable to many cell lines (e.g., cancer cell growth or stem cell differentiation), our focus is on the heart valve and how heart valve cells are linked to valvular disease via mechanoregulation. The heart valve is composed of two cell types: valvular endothelial cells (VEC) and valvular interstitial cells (VIC). While VECs form a monolayer on the external sides of the valve leaflets, VICs occupy the interstitial space of the valve. VICs are fibroblast-like cells that adapt their phenotypes in response to their microenvironment (Komuro, 1990). They are crucial for the repair and general maintenance of valvular tissue. They lay down the structural proteins for the valve including collagen, elastin, and fibronectin that make up the extracellular matrix (ECM), and provides the mechanical characteristics that are unique to the heart valve. Biochemical and mechanical cues can activate VICs to differentiate into myofibroblasts, which enhances their matrix deposition. Myofibroblast-like VICs can overexpress ECM proteins which can lead to fibrosis. Additionally, it has been shown that VICs can adopt osteogenic characteristics that lead to calcification (Liu *et al.*, 2007; Pillai *et al.*, 2017). Human VICs would be the most relevant cell type to use for heart research, but healthy human VICs are difficult to obtain. Human VICs generally come from days-old, unused heart transplants or “healthier” portions of diseased valves procured from valve replacement surgeries. Since human VICs are rare to have in heart studies, porcine VICs are the next most relevant cell line and are therefore the most common source of cells for studying VIC biology and mechanobiology. They are a more biologically relevant cell model than immortalized mesenchymal cells; not only have they been derived from the tissue of interest, VICs also display propensities, like the aforementioned calcification, that appear to be lacking in reports of more conventional, available cell types such as dermal fibroblasts or mesenchymal stem cells. Additionally, porcine VICs have been used in many disease models, such as calcific aortic valvular disease models, which show high occurrences of apoptosis correlated with high instances of calcification (Proudfoot *et al.*, 2001; Clarke *et al.*, 2008; Cirka *et al.*, 2017).

## 2.3 The role of apoptosis in cardiovascular diseases

Apoptosis is required for the orderly removal of cells within an organism. In contrast, necrosis is premature cell death caused by external disease, injury, or lack of blood supply. As necrotic cells

die, an inflammatory response can be triggered causing collateral damage to surrounding cells. Apoptosis allows the removal of cells without initiating undesirable immune responses. When apoptosis is unregulated, cell death can contribute to disease initiation and progression. Apoptosis is believed to contribute to various cardiovascular diseases such as heart failure, atherosclerosis, aneurysm formation, calcific aortic valve disease, and pulmonary arterial hypertension (Rowe *et al.*, 2000; Mohler *et al.*, 2001; Jurasz *et al.*, 2010; Chiong *et al.*, 2011; Ohsawa *et al.*, 2018). Combined, these diseases represent a significant source of morbidity and mortality in the United States, highlighting the immense burden aberrant apoptosis places on society.

### 2.3.1 Heart failure

Chronic heart failure is marked by progressive loss of cardiomyocytes over time (Kim and Kang, 2010; Chiong *et al.*, 2011). Numerous studies suggest that apoptosis of cardiomyocytes plays a role in cardiomyopathy and heart failure (Kim and Kang, 2010; Chiong *et al.*, 2011), and apoptotic cardiomyocyte death has been shown to accompany irreversible congestive heart failure (Olivetti *et al.*, 1997). Further, examination of diseased explanted hearts from cardiac transplantation patients with idiopathic dilated cardiomyopathy and ischemic cardiomyopathy revealed high levels of apoptosis indicating a link between cardiomyocyte apoptosis and end-stage heart disease (Figure 2.3) (Narula *et al.*, 1996). Conversely, inhibiting apoptosis of cardiomyocytes has been shown to reduce the development of cardiac dilation and contractile dysfunction, both of which are hallmarks of heart failure (Wencker *et al.*, 2003).

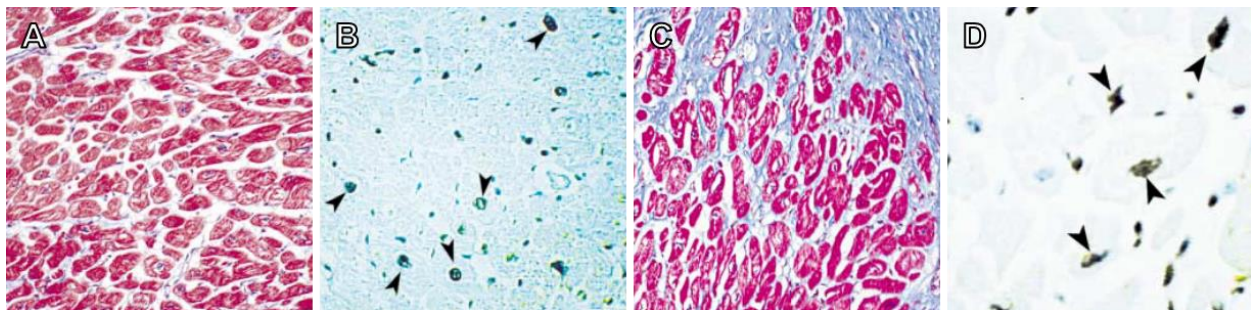


**Figure 2.3: Apoptosis is present in various types of heart failure.** **A)** In end-stage idiopathic dilated cardiomyopathy, myocardial sectioning shows normal myocytes and no fibrosis. **B)** Apoptotic myocytes (arrowheads) are generally observed in aggregated cells (not isolated) and varies regionally (TUNEL+ cells stained black) (x250 magnification). **C)** In ischemic cardiomyopathy, myocardial section shows mild

myocardial hypertrophy and extensive interstitial fibrosis. **D**) Apoptosis is found in myocytes (arrowheads) and can vary regionally in sections (TUNEL+ cells stained black) (x350 magnification). These sections are evidence of the link between high levels of cardiomyocyte apoptosis and end-stage heart disease. **A-D**) Images are adapted from Narula et al. (Narula *et al.*, 1996).

### 2.3.2 Atherosclerosis

Coronary heart disease is the most common form of cardiovascular disease, affecting one in fifteen Americans each year (Virani et al., 2020). A hallmark of coronary heart disease is the progressive narrowing and stiffening of the coronary arteries, also known as atherosclerosis. Atherosclerosis is characterized by the loss of integrity of the intimal (inner) surface of arteries and deposition of plaques of fatty material and cells. Although the early disease mechanisms are still an active area of research, it is known that the contiguous vascular endothelial cell (VEC) layer which lines the arterial wall is disrupted. The endothelial layer continuously proliferates to renew the intimal layer of blood vessels. As a result of overcrowding or injury, VECs undergo apoptosis and are then extruded from the endothelium to make room for new cells (Ohsawa et al., 2018). External stresses, such as mechanical stresses from overcrowding, can stimulate the sphingosine-1-phosphate pathway in endothelial cells (Mleynek. Tara M. et al., 2018). This pathway activates contraction of actin and myosin II fibers of neighboring VECs and physically forces apoptotic cells from the endothelial layer while preventing any gap formation. This permits the elimination of aberrant or unfit cells from the endothelial layer while maintaining membrane integrity. On the other hand, when endothelial cells undergo apoptosis and are not properly extruded, their remnants may contribute to atherosclerosis. Apoptotic cells become more pro-coagulant and pro-adhesive for platelets, possibly through activated  $\beta 1$  integrin signaling, which can promote plaque formation (Zhang et al., 2015). Additionally, apoptotic cells can cause plaque instability leading to rupture (Zhang et al., 2015).

Another known mechanism for atherosclerosis progression occurs when smooth muscle cells, which normally reside in the medial layer of the arterial wall, migrate and proliferate into the intimal plaques. High rates of apoptosis in smooth muscle cells remaining in the tunica media accelerate the disease state, promoting medial layer degeneration (Clarke et al., 2008).

Additionally, high rates of smooth muscle cell apoptosis within plaques decrease plaque stability

and increase the risk of rupture (Clarke et al., 2006). Plaque rupture can be life threatening, causing complications including heart attack and stroke.

### 2.3.3 Aneurysm formation

Aortic aneurysms contribute to over 10,000 deaths each year in the United States (Virani *et al.*, 2020). Aneurysms are localized bulges in an artery initiated from a weakened arterial wall. Examination of human pathological tissue specimens show higher rates of apoptosis and decreased vascular smooth muscle cell density in the medial layer of aneurysmal tissues compared to healthy control tissues (Rowe *et al.*, 2000). Additionally, the rho kinase inhibitor, Fasudil, was shown to prevent apoptosis and formation of aneurysms when administered to ApoE-deficient mice (Wang *et al.*, 2005b). These findings implicate excessive apoptosis as an aneurysm initiating mechanism.

### 2.3.4 Calcific aortic valvular disease

Calcific aortic valvular disease (CAVD) is the most common valvular pathology, and the third most common type of cardiovascular disease (Freeman and Otto, 2005; Dweck *et al.*, 2012). CAVD arises from mineral deposits which form on the leaflets. A study of 350 explanted valves from surgeries found over 83% of the valves demonstrated evidence of dystrophic calcification (Mohler *et al.*, 2001). Examination of diseased explanted valves show the fibrous protein structure highly disarrayed with loss of the tri-layer tissue architecture (Leopold, 2012; Rodriguez *et al.*, 2014). Valvular interstitial cell aggregation coinciding with large increases in cell density is linked to increased instances of apoptosis and subsequent dystrophic calcification (Figure 2.4) (Jian *et al.*, 2003; Tanaka *et al.*, 2005; Cirka *et al.*, 2017). Studies utilizing *in vitro* models of valve calcification demonstrate that preventing apoptosis with pan-caspase inhibitor Z-VAD-FMK prevents calcifications from forming, suggesting that apoptosis is a critical step in the disease process (Jian *et al.*, 2003; Cirka *et al.*, 2017).

### 2.3.5 Pulmonary arterial hypertension

Pulmonary arterial hypertension (PAH) is a rare disease with very poor prognosis (Peacock *et al.*, 2007). PAH results from adaptive pulmonary remodeling, vasoconstriction, and thrombosis (Gurbanov and Shiliang, 2006). Interestingly, unlike heart failure, CAVD, aneurysm formation, and atherosclerosis where abnormal apoptosis increases the severity of the disease, increasing apoptosis in pulmonary arterial smooth muscle (PASM) cells has been proposed as a possible treatment to reverse the hyper-proliferative state of PASMs (Huang *et al.*, 2010).

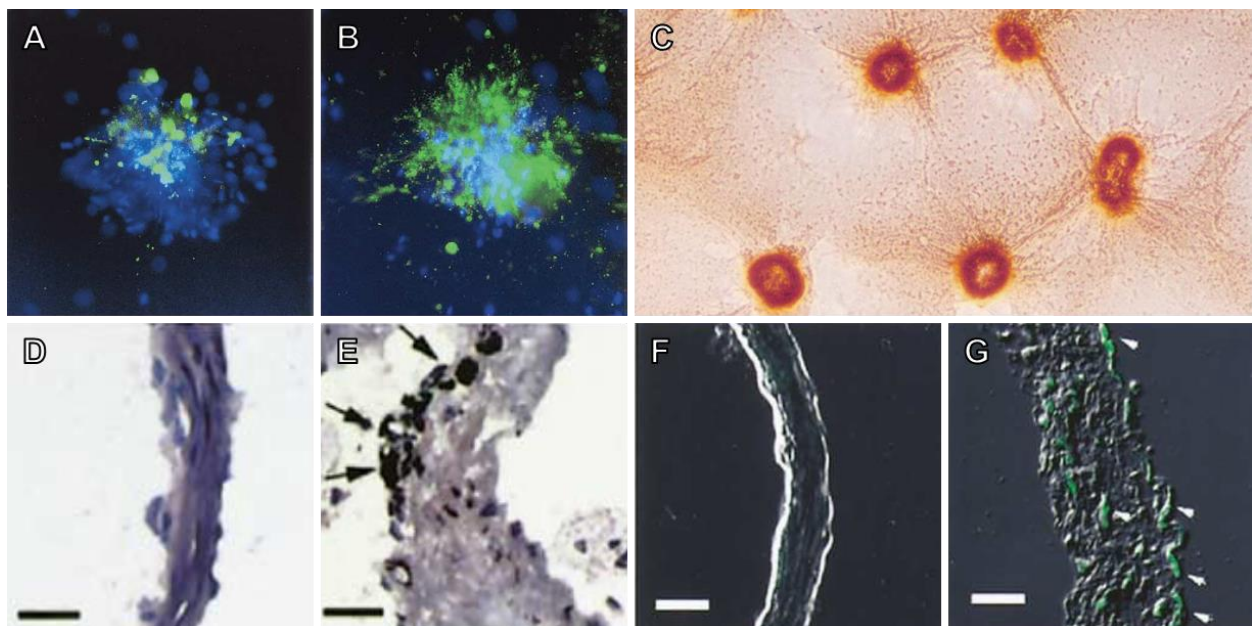


**Figure 2.4:** In *in vitro* models of CAVD, TGF- $\beta$ 1 causes cell aggregation to occur in monolayers of valvular interstitial cells. Cells in the center of the aggregates begin to apoptose after 3 days (A) and show high rates of apoptosis after 7 days (B). Cells are stained for nuclei (blue, DAPI) and apoptosis (green, Annexin V) (x200 magnification). C) Cell aggregates stain positive for calcification after 14 days (red, Alizarin Red S) (x100 magnification). In *in vivo* models, hearts from wild-type mice (D) are negative for calcification, while ApoE deficient mice (E) stain positive for ectopic calcification (von Kossa). Arrows indicate positive area. Apoptotic death is absent in wild-type mice (F) but present in ApoE deficient mice (G). Arrows indicate apoptotic cells, which are TUNEL stained (green). Scale bars = 20  $\mu$ m. A-C) Images are adapted from Jian *et al.* (Jian *et al.*, 2003). D-G) Images are adapted from Tanaka, *et al.* (Tanaka *et al.*, 2005).

## 2.4 Canonical and non-canonical apoptotic pathways

Currently, there are two defined canonical pathways recognized in the apoptotic process: the intrinsic pathway and the extrinsic pathway (Figure 2.5). There is growing evidence of other

non-canonical pathways that initiate apoptosis in cells, such as ones that are mechanosensitive. In these pathways, mechanical forces can induce and modulate the extrinsic and intrinsic pathways.

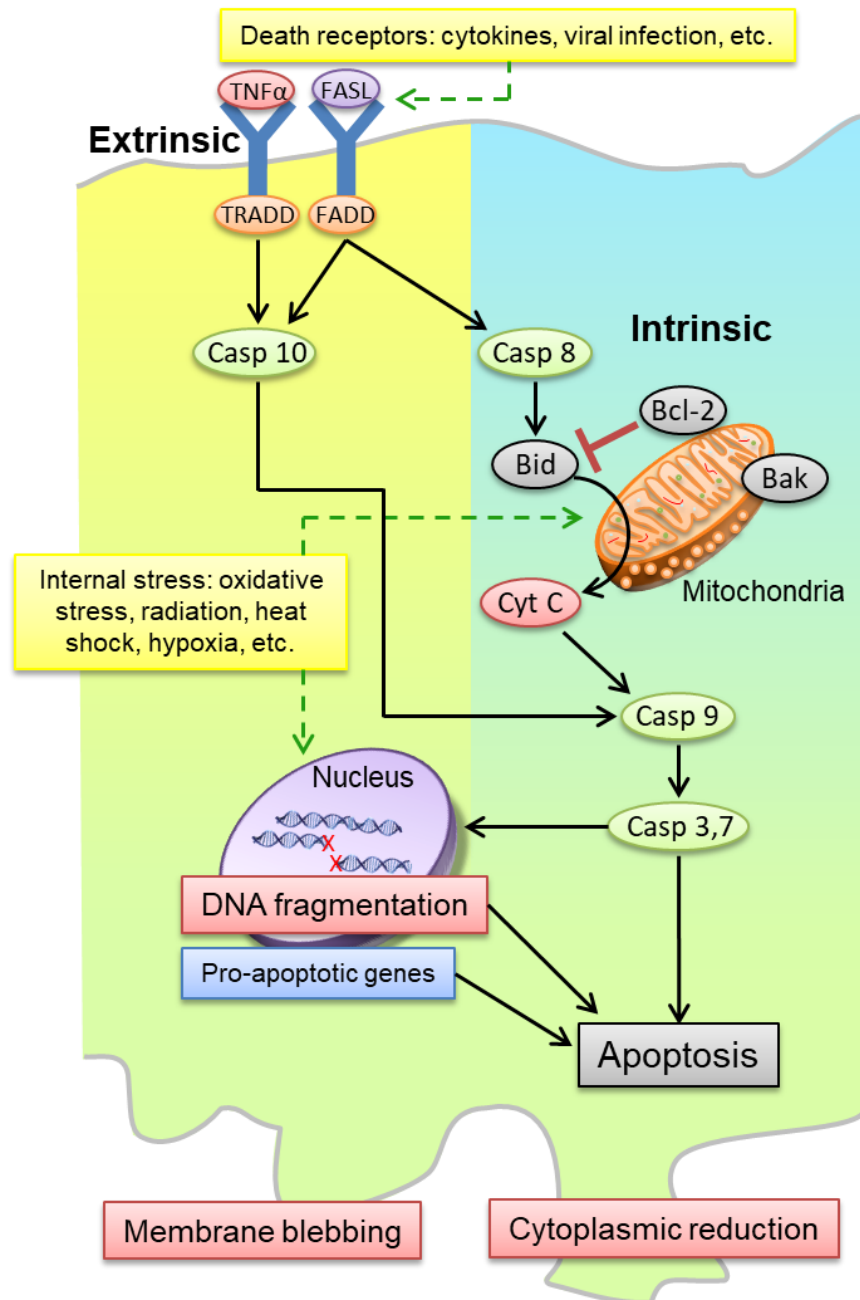


**Figure 2.5:** Overview of apoptotic pathways. Apoptosis can be triggered by the intrinsic pathway (mitochondria mediated) or extrinsic pathway (receptor mediated). External factors, such as cytokines and infection, can initiate the extrinsic pathway, while internal factors, such as oxidative stress and radiation, can initiate the intrinsic pathway. The two pathways can interact with one another through mechanical and chemical signaling, and progress with activated caspases.

The extrinsic pathway is activated by external stimuli that bind to various cell transmembrane “death” receptors. Two common death receptors are TNF- $\alpha$  and FAS, which are part of the tumor necrosis factor (TNF) family (Locksley *et al.*, 2001). Upon activation of the receptors, multiple intracellular proteins interact with one another in order to form a death-inducing signaling complex (DISC). These complexes then recruit and activate downstream initiator caspases, such as caspases 8 and 10. These initiator caspases can then activate parts of the intrinsic pathway by inducing mitochondrial stress, or can activate downstream effector caspases, such as caspase-3 and 7, which directly initiate degradation of cellular components and facilitate cell death. When proceeding through the stages of apoptosis, caspases interact with numerous downstream proteins as a form of intracellular chemical signaling. Although distinct from one another, there is evidence that the intrinsic and extrinsic pathways are connected and that signaling molecules in one pathway can stimulate the other (Igney and Krammer, 2002).

The intrinsic pathway, also known as the mitochondrial pathway, is activated through signals generated inside the cell. This pathway can be triggered by various positive or negative stimuli. Positive stimuli include DNA damage (Norbury and Zivnotovsky, 2004), oxidative stress (Kannan and Jain, 2000), heat shock (Song, 2014), radiation (Watters, 1999), viral infection, (Hardwick, 2001), hypoxia (Sendoel and Hengartner, 2014), as well as a positive induction from cytokines (Arstall *et al.*, 1999). Negative stimuli can include the absence of specific hormones, such as growth factors (Araki *et al.*, 1990) and cytokines (Lotem and Sachs, 1999), which results in a failure to repress apoptosis. The Bcl-2 protein family plays a major role in regulating the intrinsic pathway, as it serves dual functions in apoptosis with some protein members serving as anti-apoptotic stimuli and others being pro-apoptotic (Tsujimoto, 2003; Czabotar *et al.*, 2014). Mechanical stimuli have been found to cause changes in Bcl-2 anti-apoptotic and pro-apoptotic protein levels and thus interact with the intrinsic pathway (Su *et al.*, 2006; Kong *et al.*, 2013). Bcl-2 and Bcl-xL proteins act as anti-apoptotic cues, prompting cell survival and inhibiting apoptosis, while Bax, Bad/Bid, and Bik proteins serve as pro-apoptotic cues, which advance apoptosis by promoting permeabilization of the mitochondrial membrane (Tsujimoto, 2003; Czabotar *et al.*, 2014). Cytochrome c, the main chemical mediator of downstream apoptosis signaling, is released from the permeabilized mitochondrial intermembrane compartment into the cytosol (Tsujimoto, 2003). Cytochrome c then binds with apoptotic protease activating factor 1

(APAF1) to create apoptosomes. Apoptosomes activate downstream caspases leading to the final stages of apoptosis, such as membrane blebbing and the formation of apoptotic bodies (Wernig and Xu, 2002).

In addition to the traditional extrinsic and intrinsic pathways, there exist many secondary signaling apoptotic pathways, some of which are mechanically linked. Mechanical stretch has been found to activate both the extrinsic and intrinsic pathways but the mechanisms remain unknown (Liao *et al.*, 2005). Mechanically induced apoptosis may be a result of cytoskeletal destabilization, which can cause deformities in mitochondrial and nuclear structure (Anesti and Scorrano, 2006; Houben *et al.*, 2007). These organelles are directly connected to the cytoskeleton, where external mechanical forces can transfer directly from the cell boundary to internal organelles (Kim *et al.*, 2012; Li *et al.*, 2014). Cytoskeletal disruption can cause changes in gene expression, subsequently altering cell behavior and possibly inducing apoptosis (Tamada *et al.*, 2004; Jaalouk and Lammerding, 2009). Additionally, mechanical stresses have been found to activate various caspases and death receptors in the apoptotic pathway (Roy and Nicholson, 2000; Wu *et al.*, 2016). The mechanisms behind transducing external mechanical signals into an apoptotic response remain unknown but are possibly accomplished via cytoskeletal reorganization.

The state of the cytoskeleton can also regulate mitochondrial permeabilization. Reduced actin dynamics increase instances of apoptosis in yeast with actin point mutations (Gourlay and Ayscough, 2005a). F-actin with decreased turnover forms clumps and results in increased accumulation of reactive oxygen species (ROS) as well as prolonged opening of voltage dependent anion channels (VDAC). Open VDACs result in a loss of mitochondrial membrane potential and increased apoptosis. To this effect, the enzyme gelsolin helps promote F-actin turnover. Gelsolin overexpression results in the closure of VDACs resulting in a reduction of cytochrome c release, maintenance of membrane potential, and reduction in apoptosis (Kusano *et al.*, 2000).

Actin-associated molecules can initiate apoptosis when they dissociate from cytoskeletal fibers. Bmf, a pro-apoptotic protein, is normally sequestered within actin-associated myosin motors and inactive (Puthalakath *et al.*, 2001). CD95/FAS, another pro-apoptotic protein, associates with

actin at the cellular membrane via the protein ezrin (Parlato *et al.*, 2000). Additionally, Akt (protein kinase B, PKB) is activated through integrin signaling and the phosphatidylinositol 3-kinase (PI3K) pathway (Flusberg *et al.*, 2001). Upon actin depolymerization by cell detachment or cytochalasin D treatment, Bmf is released from myosin, initiating mitochondrial-dependent apoptosis, ezrin-FAS association is reduced, initiating FAS-dependent apoptosis, and Akt activity is reduced, which increases instances of apoptosis (Figure 2.7).

## 2.5 Stages of apoptosis and stage-specific markers

Studying the timing of apoptosis is important to understand how mechanics plays a role in the different stages of apoptosis. Apoptosis is a process that progresses over time, with specific characteristics within each stage. Determining the stages in which mechanics plays a role may lead to new targets in the apoptotic pathway aimed at increasing or reversing apoptosis. There are five common apoptosis detection assays: morphological changes, membrane alteration, caspase detection, DNA fragmentation, and mitochondrial membrane potential (Porter and Jänicke, 1999; Gottlieb *et al.*, 2003; Huang *et al.*, 2005; Galluzzi *et al.*, 2007; Bailey *et al.*, 2009). There are pros and cons to each assay as each one is used to measure a different characteristic of apoptosis. Some proteins, such as caspases, are temporary and need to be measured at the correct times, while others are permanent, such as DNA fragmentation.

### 2.5.1 Early stage apoptosis

In early-stage apoptosis, signaling cascades begin to activate after death-receptors or internal triggers are activated. The cascades include the activation of caspases, which are transient proteins (Kumar, 2007; McIlwain *et al.*, 2015). Caspases can be detected by numerous means including western blots, immunoprecipitation, and immunostaining. Caspase-3 and 7 are two of the most commonly activated caspases during apoptosis and are therefore a common target for researchers (Porter and Jänicke, 1999). Staining for caspase can be done on live cells, fixed cells, or cell pellets. Additionally, mitochondria begin to permeabilize in early apoptosis leading to changes in the mitochondrial membrane potential due to ion leakage. This depolarization can be detected through the use of fluorescent dyes, which bind to ions that are translocated across the mitochondrial membrane, coupled with fluorescent microscopy (Perry *et al.*, 2011).

## 2.5.2 Mid stage apoptosis

During mid-stage apoptosis, caspase signaling cascades continue to be active, and the mitochondria continue to permeabilize, causing more ion leakage. Also, during mid-stage apoptosis, membrane alteration in apoptotic cells occurs which is characterized by the externalization of phosphatidylserine, a membrane residue. At first, phosphatidylserine translocation may be reversible, but as apoptosis progresses, this process becomes permanent. These residues can easily be visualized by staining cells with Annexin V (Fadeel, 2004). This allows simple detection of single apoptotic cells; however, this marker is also shared with cells that are undergoing necrosis. Therefore, a control is necessary to distinguish between these two types of cell death, such as co-staining with propidium iodide. Morphological changes such as cytoplasmic reduction may also occur during the mid-stage of apoptosis. Most of these changes are visually distinguishable via light microscopy.

## 2.5.3 Late stage apoptosis

In late-stage apoptosis, permanent transformations occur in apoptotic cells. Additional morphological changes occur including nuclear fragmentation/condensation, disorganization of cytoplasmic organelles, formation of apoptotic bodies, and blebbing of the cell membrane (Kerr *et al.*, 1972; Galluzzi *et al.*, 2007). Further, DNA fragmentation occurs within the nucleus (Darzynkiewicz *et al.*, 2008; Darzynkiewicz and Zhao, 2011). A terminal deoxynucleotidyl transferase dUTP nick end labeling (TUNEL) assay, which labels the ends of DNA breaks, can be used to observe fragmented DNA in apoptotic cells (Darzynkiewicz and Zhao, 2011; Musumeci *et al.*, 2011).

Apoptosis has previously been considered a unidirectional process; once initiated, the process ends in cell death. However, it is possible to reverse apoptosis if cells have not progressed too far down the apoptotic cascade (Figure 2.6). It has been shown in numerous studies that removing an apoptotic inducer can allow cells to revert back to a healthy state, sometimes as late as mid-stage apoptosis (Geske *et al.*, 2001; Wang *et al.*, 2005a; Tang *et al.*, 2009). For example, murine hepatocytes show increased levels of caspase-3 and caspase-8 when cells are induced with glycochenodeoxycholate (GCDC), yet they return to control levels after the removal of GCDC

(Wang *et al.*, 2005a). After returning to higher culture temperatures, low-temperature-stressed p53 MOD cells have decreased levels of Annexin V, which is indicative of phosphatidylserine internalization, and undergo DNA repair (low temperature is apoptotic inducer in these cells) (Geske *et al.*, 2001). HeLa cells revert to their typical morphology and have decreased rates of apoptosis when inducers like jasplakinolide, ethanol, or staurosporine are removed if early in the apoptotic process (Tang *et al.*, 2009). However, if nuclear fragmentation occurs, cells cannot be rescued even after the removal of the apoptotic inducer. Finally, in various cancer lines, such as human A375 (skin), HepG2 (liver), MCF7 (breast), and PC3 (prostate) cancer cells, cells treated with jasplakinolide (a reagent that disrupts actin filaments and induces polymerization of monomeric actin into amorphous masses) exhibit early apoptotic markers, yet the cells revert back to their apoptosis-resistant homeostatic state if the chemical inducer is washed before the later stages of apoptosis are reached. These findings indicate that certain stages of the apoptotic pathway can be reversible while others are permanent (Figure 2.6).

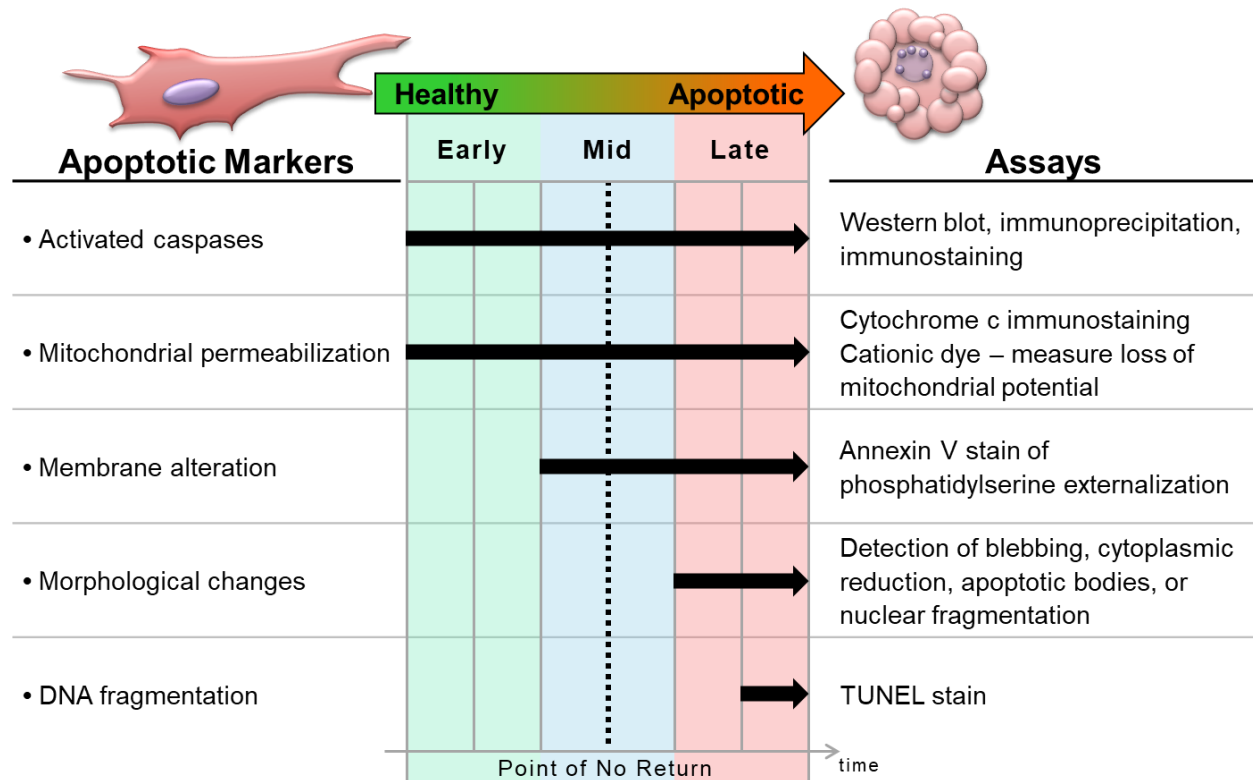


**Figure 2.6:** Apoptosis occurs in three different stages: early, mid, and late. Different stage-specific markers (left list) are activated/initiated at specific times within the apoptotic process and can be measured with associated assays (right list). Apoptosis is a reversible process up until the dotted line, which indicates the point of no return, where a cell reaching this point will always complete apoptosis.

## 2.6 Mechanical induction of apoptosis

Recently, there is increasing evidence that the mechanical environment plays a critical role in cardiovascular apoptosis (Gourlay and Ayscough, 2005b; Desouza *et al.*, 2012). It includes external forces applied to the cells and the material properties of the extracellular matrix (ECM) which resist cell-generated forces. The mechanical environment affects cells through mechanotransduction, the processes by which mechanical stimuli are sensed, transferred, and then converted into biochemical signals and subsequent gene expression that regulate cell fate (Figure 2.7). There are various mechanical forces that are physiologically and pathologically present within the cardiovascular system. The chambers of the heart, heart valves, and blood vessels reside in diverse conditions which give rise to heterogeneous structures and properties of each component. These cell environments have varying levels of stiffness, are exposed to cyclical mechanical loading and can experience fluid shear stress from flowing blood. To study the effects of these stimuli in controlled environments, researchers recapitulate substrate stiffness, stretch, and shear *in vitro*. Culture on compliant hydrogels allow for the tuning of the substrate stiffness, enabling the study of cells on a variety of elastic moduli, which can replicate a range of environments found within the body. A number of devices have been developed commercially or custom-designed within research labs that can apply stretch to cells, either uniaxially or biaxially. Cells cultured within compliant stretchable wells fit within device actuators, and when the device is run, the substrate and adhered cells undergo mechanical stretch. Various stretch waveforms are programmable, allowing for the study of different mechanical stretch cues and potential thresholds. Shear stress is applied by replicating fluid flow patterns in microfluidic devices, parallel flow plates, and cone-in-plate devices. Combinations and interactions between mechanical stimuli are also studied by integrating multiple of the aforementioned platforms together, e.g., stretching cells cultured on tunable modulus substrates (Cui *et al.*, 2015; Cirka *et al.*, 2016). These mechanical stimuli have different effects on cell survival individually and in combination (Table 2.1).

**Table 2.1:** Mechanical stimuli cause cellular apoptosis or survival. “↑” indicates increase, “↓” indicates decrease, and “–” indicates no change. All cell lines listed under *substrate stiffness* are stiffness-dependent unless otherwise indicated.

Stimulus	Parameter	Cell Line	Source	Result	Reference
<b>Substrate stiffness</b>	Low modulus (<1 kPa) vs high modulus (~5 kPa) (moduli estimated from acrylamide/bis-acrylamide concentrations)	<b>Stiffness-dependent</b> NIH 3T3 fibroblasts  <b>Stiffness-independent</b> H- <i>ras</i> -transformed NIH 3T3 cells	murine (mouse)	↓ proliferation (BrdU) ↑ apoptosis (TUNEL)  – proliferation – apoptosis	Wang (Wang <i>et al.</i> , 2000)
	Low modulus (1 kPa) vs intermediate modulus (32 kPa) vs high modulus (63 kPa)	annulus fibrosus cells	murine (rat)	↓ proliferation (hemocytometer)  ↑ apoptosis (Annexin V, caspase-3)	Zhang (Zhang <i>et al.</i> , 2011b)
	Low modulus (0.4 kPa) vs intermediate modulus (5 kPa) vs high modulus (60 kPa)	normal murine mammary gland epithelial cells (NMuMG)	murine (mouse)	↑ apoptosis (caspase-3)	Leight (Leight <i>et al.</i> , 2012)
		Madin–Darby canine kidney epithelial cells (MDCK)	canine	↑ apoptosis (caspase-3)	
	Low modulus (0.15 kPa) vs high modulus (4.8 kPa)	<b>Stiffness-dependent</b> A549 (lung) MDA-MB-231 (breast) <b>Stiffness-independent</b> PC-3 (prostate) mPanc96 (pancreas)	human	↓ proliferation (CyQuant kit) ↑ apoptosis (TUNEL)  – proliferation – apoptosis	Tilghman (Tilghman <i>et al.</i> , 2010)
	No stiffness – suspended in solution (anoikis)	capillary endothelial cells	human, bovine	↓ proliferation (BrdU) ↑ apoptosis (TUNEL)	Chen (Chen <i>et al.</i> , 1997)
	No stiffness – suspended in solution (anoikis)	capillary endothelial cells	bovine	↑ apoptosis (TUNEL, caspase-3)	Flusberg (Flusberg <i>et al.</i> , 2001)
	No stiffness – suspended in solution (anoikis)	FSK-7 mammary epithelial cells	murine (mouse)	↑ apoptosis (caspase-3, cytochrome c release, Hoechst 33258)	Wang (Wang <i>et al.</i> , 2003)
<b>Substrate strain</b>	7%, 25% strain	vascular smooth muscle cells (VSMC)	porcine	↑ apoptosis (LM-PCR) in 25% strain	Sotoudeh (Sotoudeh <i>et al.</i> , 2002)
	5%, 10%, 15% strain Sine, triangle, square wave	Tca8113 - human tongue squamous carcinoma cells	human	↑ apoptosis (Annexin V) with increasing strain  ↑ apoptosis (Annexin V) in square>triangle>sine wave	Wang (Wang <i>et al.</i> , 2009)
	5%, 15%, 25%	vascular smooth muscle cells	murine (rat, mice), human	↑ apoptosis (Annexin V, TUNEL) with higher strains in all cell lines  human>rat>mouse	Mayr (Mayr <i>et al.</i> , 2000)
	15% cyclic strain	vascular smooth muscle cells	murine (rat)	↑ apoptosis (Annexin V, TUNEL) only on collagen I	Wernig (Wernig <i>et al.</i> , 2003)
	100 mmHg in organ culture system	aortic heart valve	porcine	↓ proliferation (BrdU) in static condition ↑ apoptosis (caspase-3) in static condition	Konduri (Konduri <i>et al.</i> , 2005)

<b>Fluid flow shear stress</b>	Fluid flow present $12 \pm 4$ dyn/cm <sup>2</sup>	HUVEC	human	↓ apoptosis (Annexin V) flowed parallel to long axis of patterned cells  – apoptosis (Annexin V) flowed perp. to long axis of patterned cells	Wu (Wu <i>et al.</i> , 2007)
	Fluid flow present 0.05-0.1 dyn/cm <sup>2</sup>	HUVEC	human	↓ apoptosis (DAPI)	Kaiser (Kaiser <i>et al.</i> , 1997)
<b>Surface patterning</b>	Small cell area (78μm <sup>2</sup> vs ~314μm <sup>2</sup> vs unrestricted)	capillary endothelial cells	human, bovine	↓ proliferation (BrdU) ↑ apoptosis (TUNEL)	Chen (Chen <i>et al.</i> , 1997)
	Small cell area (78μm <sup>2</sup> vs unrestricted)	capillary endothelial cells	bovine	↑ apoptosis (TUNEL, caspase-3)	Flusberg (Flusberg <i>et al.</i> , 2001)
	Small cell area (314μm <sup>2</sup> , 615μm <sup>2</sup> , 1256μm <sup>2</sup> ) Increased circularity (0.1, 0.2, 0.4, 1)	MC3T3-E1	murine (mouse)	↑ apoptosis (TUNEL) ↑ apoptosis (TUNEL)	Fu (Fu <i>et al.</i> , 2013)
	Small cell area (300 μm <sup>2</sup> , 1024 μm <sup>2</sup> , 2025 μm <sup>2</sup> , 10,000 μm <sup>2</sup> )	human mesenchymal stem cells (MSC) human lung microvascular endothelial cells (HMVEC)	human human	↓ proliferation (BrdU) ↑ apoptosis (TUNEL)	Dupont (Dupont <i>et al.</i> , 2011)
	Multicellular aggregate (heterogeneous stress)	valvular interstitial cells (VIC)	porcine	↑ apoptosis in central region (caspase-3)	Cirka (Cirka <i>et al.</i> , 2017)
	Multicellular aggregate (heterogeneous stress)	valvular interstitial cells (VIC)	porcine	↑ apoptosis in central low stress region (caspase-3)	Goldblatt (Goldblatt <i>et al.</i> , 2020)
	<b>Surface composition</b>	Fibronectin (FN) Matrigel Collagen I	normal murine mammary gland epithelial cells (NmuMG)	murine (mouse)	↑ apoptosis (caspase-3) collagen I higher than Matrigel and FN
Collagen I Elastin Laminin Pronectin		vascular smooth muscle cells	murine (rat)	↑ apoptosis (Annexin V, TUNEL) only on collagen I with stretch	Wernig (Wernig <i>et al.</i> , 2003)

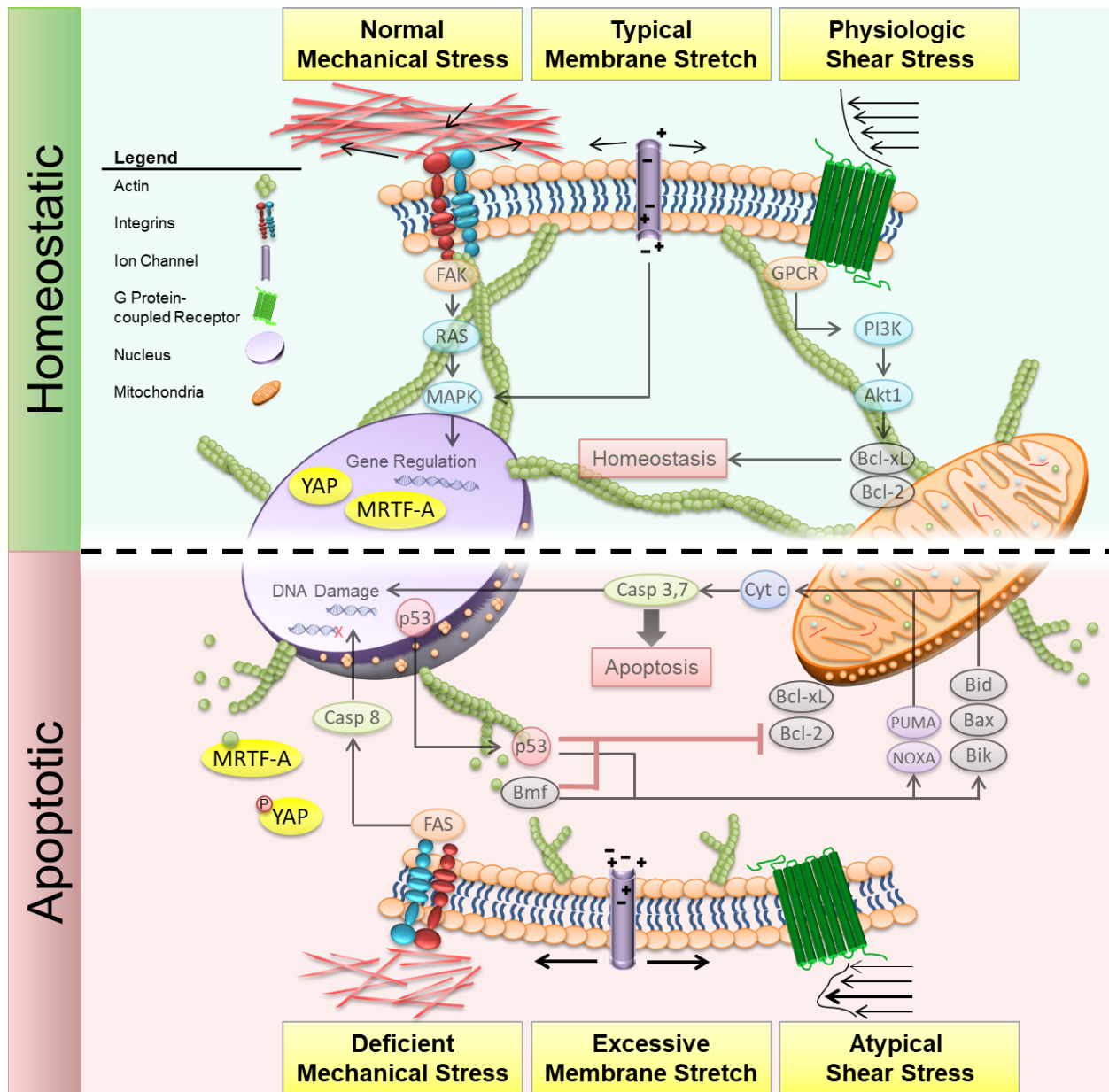


**Figure 2.7:** Mechanical stimuli that regulate apoptosis include mechanical stress from the ECM, stretching of the cellular membrane, and shear stress, which activate signaling pathways via integrins, ion channels, and G-protein coupled receptors (GPCR). *Top:* mechanical stimuli at physiological levels activate pro-survival pathways, such as the PI3K and MAPK pathways, which maintain cells at a homeostatic state. The cytoskeletal network is highly stable and remains as a fiber network. Mechanosensitive proteins, regulated by the cytoskeleton, such as YAP and MRTF-A, are activated and localized to the nucleus. *Bottom:* mechanical stimuli at sub- or supra-physiological levels activate pro-apoptotic pathways, such as the p53 tumor-suppressor and Bmf pathways, which inhibit anti-apoptotic molecules and activate pro-apoptotic molecules, subsequently advancing the apoptotic process. These mechanical stimuli can be excessive or deficient mechanical stress from a fragmented ECM, excessive stretch of transmembrane channels, or abnormal shear stress. The cytoskeletal network is destabilized and fragments. Mechanosensitive proteins, such as YAP and MRTF-A, are deactivated and localized to the cytosol.

### 2.6.1 Mechanical stretch

Increased rates of apoptosis have been observed in tissues exposed to supraphysiologic stretch, such as in individuals with hypertension and subsequent pathological vascular remodeling (Bing, 1994; Wernig and Xu, 2002; Jurasz *et al.*, 2010). Different locations within the cardiovascular system undergo different magnitudes of mechanical stretch and therefore stress. It is well known that the pressures and loads experienced by arteries are much greater than those of veins. Cells within each environment are accustomed to those specific loading conditions and aberrant apoptosis is seen when this loading is changed. For example, in *in vivo* murine models, higher rates of apoptosis were seen in vein vascular smooth muscle cells (VSMC) grafted to arteries when compared to veins grafted to other veins, indicating that the increase in arterial pressure resulted in more apoptotic events. A potential molecular mechanism was later discovered that VSMCs subjected to this cyclic stretch activated the p53 tumor-suppression pathway (Mayr *et al.*, 2002). The activation of p53 subsequently changed the ratios of pro- and anti-apoptotic markers (Bax; Bcl-2 and Bcl-xL), therefore stimulating the apoptosis process (Figure 2.7). These marker levels changed in parallel with the observed apoptosis rates from the previous experiment. In contrast, it has been shown that cells naturally found in dynamically stretching environments can have increased rates of apoptosis with the cessation of mechanical stretch. Yoganathan and colleagues excised porcine aortic valves and found no differences in leaflet cell (endothelial cells, smooth muscle cells, and fibroblasts) death between fresh controls and dynamically cultured valves. However, when valves were inserted into static culture, apoptosis increased suggesting that reduction of cyclic stretch can induce apoptosis (Konduri *et al.*, 2005).

In *in vitro* studies, the magnitude, rate, and type of stretch have been shown to have varying effects on apoptosis in isolated cells. High, pathological-level strains of 20-25% in cyclically stretched VSMCs and endothelial cells have been shown to increase apoptotic rates (Mayr *et al.*, 2000; Sotoudeh *et al.*, 2002; Liu *et al.*, 2003). Increasing stretch amplitude (5%-25%) has also been shown to increase apoptosis (Liu *et al.*, 2003; Wang *et al.*, 2009). On the other hand, when apoptosis was induced in endothelial cells via TNF $\alpha$ , stretching cells at physiological levels of 6-10% had positive effects on cell survival (Liu *et al.*, 2003). VSMCs exhibit higher rates of apoptosis over longer time durations (6hrs) at high strain (15%) (Mayr *et al.*, 2000).

Additionally, the stretch waveform has been shown to affect apoptosis. Human carcinoma tongue cells, Tca8113, have increases in apoptotic occurrences when the waveform of stretch changes from a sine wave to a triangular wave to a square wave (Wang *et al.*, 2009).

Cell adhesion proteins and their respective signaling pathways play a large role in transducing mechanical signals inside a cell. Wernig *et al.* found that murine VSMCs cultured on collagen undergo higher rates of apoptosis when cyclically stretched compared to VSMCs cells cultured on elastin, laminin, or Pronectin (Wernig *et al.*, 2003). This result suggests that  $\beta$ 1-integrin signaling pathways are associated with apoptosis through mechanical mechanisms.

### 2.6.2 Fluid shear stress

Hemodynamic shear stress is an important mechanical stimulus that helps regulate function, structure, and gene expression in endothelial cells in blood vessels. Both increasing and decreasing shear stress *in vitro* via fluid flow has been shown to alter the prevalence of apoptosis in endothelial cells. Directional shear flow parallel to the long axis of human umbilical vein endothelial cell (HUVEC) was found to enhance stress fiber polymerization and reduce instances of apoptosis, while perpendicular flow did not counteract apoptotic events (Wu *et al.*, 2007). In an environment lacking mechanical stimuli, the absence of shear flow triggered apoptosis in vascular endothelial cells (Kaiser *et al.*, 1997). Reduced levels of shear stress appears to induce apoptosis of endothelial cells in human samples, which may lead to the onset of cardiovascular diseases such as atherosclerosis (Asakura and Karino, 1990; Malek *et al.*, 1999).

### 2.6.3 Microgravity

Decreased gravitational forces, as experienced in a microgravity environment simulated with the use of a random positioning machine (RPM) on Earth or in space flight, can inhibit survival signaling pathways and have been shown to initiate apoptosis. Microgravity conditions cause mechanical unloading on cells and are known to cause cellular changes in shape, size, and migration related to modifications to the cytoskeleton (Hughes-Fulford *et al.*, 1998; Infanger *et al.*, 2006). In an RPM, ONCO-DG 1 cells (papillary thyroid cancer cells) underwent significant cytoskeletal depolymerization followed by apoptosis when under hypogravitational conditions

(Infanger *et al.*, 2006). Additionally, in porcine aortic vascular endothelial cells and BL6-10 cells, cells downregulate anti-apoptotic genes, such as Bcl-2 and Bnip3, express higher levels of pro-apoptotic genes, such as p53, Bax, FasL, Bok, caspases-3, 7, and 8, and various death-domain genes, and undergo higher rates of apoptosis than those in earth-level gravity conditions (Morbidelli *et al.*, 2005; Zhao *et al.*, 2016). Further, Vidyasekar *et al.* found microgravity causes increases in apoptotic rates in DLD-1 cells (colorectal cancer cells) and MOLT-4 cells (lymphoblast leukemic cells) (Vidyasekar *et al.*, 2015). Apoptosis was coupled with inhibition of anti-apoptotic protein Bcl-2 and had up regulation of pro-apoptotic proteins, such as PARP, p-53, and BAX.

#### 2.6.4 Regulation of cell spread area

In high density monolayers, there are higher instances of apoptosis compared to sparse cultures (Qiao and Farrell, 1999). High density monolayers naturally cause size restrictions of cell spread area. Geometric constraints also have significant repercussions on other cell behavior such as changes in cytoskeleton dynamics (Lunova *et al.*, 2016), cell migration (Chen *et al.*, 2013), proliferation (Streichan *et al.*, 2014), and differentiation (Kilian *et al.*, 2010). Microcontact printing of small protein “island” enables the creation of patterned substrates with varying size and shapes. Cells are non-adhesive to the areas outside of the protein geometries, allowing high control of both individual cell shape and multicellular assembly shape. In these single-cell cultures, restricting cell spread area in human capillary endothelial cells and MC3T3-E1 osteoblast-like cells induces apoptosis in a dose-dependent manner with rates of apoptosis increasing from 30% to 50% as the protein island size is decreased from as high as  $1256 \mu\text{m}^2$  (40  $\mu\text{m}$  diameter circle) to as low as  $78 \mu\text{m}^2$  (10  $\mu\text{m}$  diameter circle) (Chen *et al.*, 1997; Fu *et al.*, 2013). Chen *et al.* further demonstrated that the amount of integrin binding was not responsible for the altered rates of apoptosis. By constricting cells to small sizes, they are unable to generate high traction forces on their ECM. It is possible that it is the decrease in cell-generated stress, rather than the restriction in cell area, that initiates apoptosis (Dupont *et al.*, 2011; Cirka *et al.*, 2017), as decreased cell forces and increased apoptosis are also observed on low modulus substrates compared to stiff substrates as described below (Kilian *et al.*, 2010).

### 2.6.5 Control of substrate modulus

Similar to cell spread area, substrate modulus affects many cellular functions including cell migration, proliferation, and differentiation (Klein *et al.*, 2009; Tilghman *et al.*, 2010; Chaudhuri *et al.*, 2015). Cells need to generate mechanical tension through cell-ECM adhesions to maintain homeostatic stress conditions (Egerbacher *et al.*, 2008; Humphrey *et al.*, 2014). When cultured on low modulus substrates (often referred to as “soft” substrates), cells are unable to generate substantial traction forces and often appear rounded, unlike the spread morphology of cells cultured on high modulus (“stiff”) substrates (Solon *et al.*, 2007; Califano and Reinhart-King, 2010) (Figure 2.8); this has been correlated to higher incidences of apoptotic events (Wang *et al.*, 2000; Tilghman *et al.*, 2010; Zhang *et al.*, 2011b; Leight *et al.*, 2012). Wang and colleagues demonstrated that primary fibroblasts generate lower traction forces and have smaller spread area on soft substrates compared to stiff substrates; in contrast, transformed cells have no observable differences in generated traction forces or spread area between soft and stiff substrates (Wang *et al.*, 2000). Interestingly, when cells are confluent, mechanical interactions between multiple cells abrogate the effects of substrate modulus (Yeung *et al.*, 2005). These cell monolayers show indistinguishable morphologies between soft and stiff substrates. Complete lack of cell-ECM (“zero modulus”) attachment results in a specific type of apoptosis called anoikis. The detachment of cells or inhibition of focal adhesions signals anoikis and leads to subsequent programmed cell death (Paoli *et al.*, 2013). It is unclear if it is the lack of physical feedback that cells receive from their environment, the lack of integrin binding, or other related signals that activate the apoptotic pathways in anoikis. There may be a common mechanism between cells in different low modulus conditions (e.g. cytoskeletal disassembly); however, studies that tease out the varying mechanical inputs need to be performed.

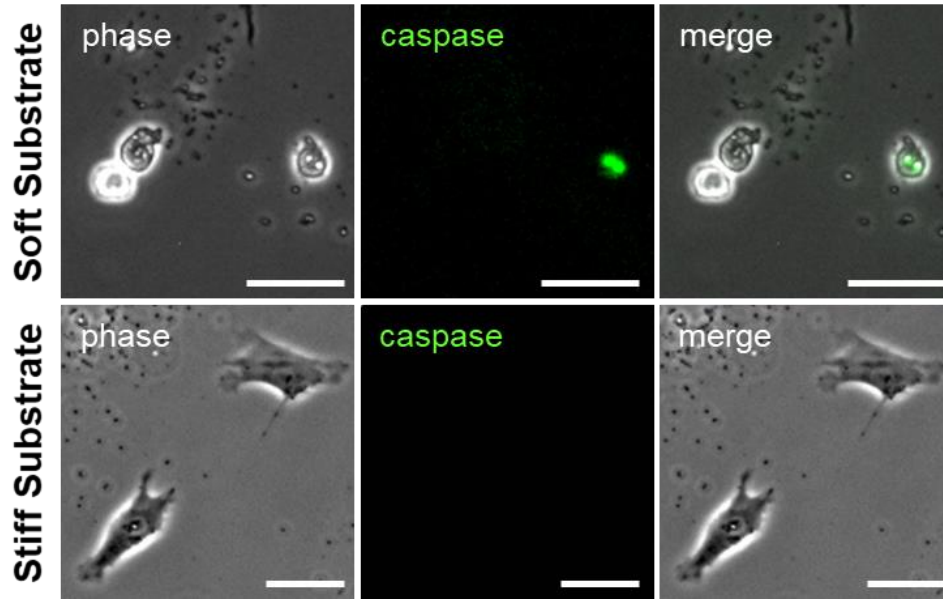


**Figure 2.8:** Cells cultured on soft (1.2 kPa) substrates (top) are small with rounded morphology and stain positive for apoptosis (green, caspase-3/7). Cells cultured on stiff (40 kPa) substrates (bottom) have larger spread area, are more elongated, and stain negative for apoptosis (green, caspase-3/7). Scale bars = 50  $\mu\text{m}$ . [Unpublished data]

### 2.6.6 Area-restricted multicellular systems

Mechanical stress fields arise from force transfer between cells and the ECM as well as cells with other cells. As previously stated in the *restricted cell spread area* section, apoptotic rates are higher for single cells cultured on small protein islands compared to large islands. In multicellular systems, constricting monolayers is a powerful means of creating heterogeneous monolayers with reproducible regions of differing cell stress, density, and spread areas which emerge from collective cell interactions. In multicellular aggregates, high cell densities and low spread areas localize in the central region contrary to the peripheral region, which has lower cell densities and high spread areas. We have previously shown that enhanced rates of apoptosis occur in these central regions with restricted valvular interstitial cell spreading and low traction forces (Figure 2.9, A and B) (Cirka *et al.*, 2017; Goldblatt *et al.*, 2020). Additionally, other studies have shown increased proliferation in the peripheral regions of aggregates (aggregates consisting of NIH 3T3 fibroblasts or bovine pulmonary artery endothelial cells) where cells are elongated and have high spread area (Nelson *et al.*, 2005; Li *et al.*, 2009). We are currently examining possible mechanisms for apoptotic signaling that correlate with cell-stresses. Previous models that predict and calculate stresses in the cell aggregates assume homogeneous cell

properties which produces high stresses in aggregate centers (opposite of where proliferation, apoptosis, and traction forces localize). Using more realistic heterogeneous parameters, our models predict low cell-layer stress in central regions, which correlates well with apoptosis. Additionally, we observe higher G/F-actin ratios in central regions which indicates cytoskeletal remodeling may play a role (Figure 2.9C). Accurate estimation of cell-stresses in these aggregates will lead to a better understanding how specific mechanical factors drive cell fate (Figure 2.9D). Further, being able to accurately determine where stresses are localized within cell monolayers will allow for more precise design of methods for mechanical control of cell fate.

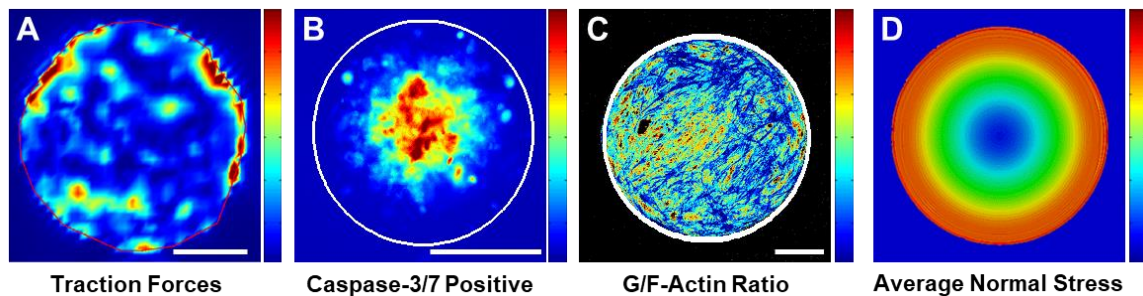


**Figure 2.9: High cell-stress markers localize to aggregate periphery while low cell-stress markers localize to aggregate center.** Heat map of traction forces (A) shows localization at aggregate periphery, while heat maps of active caspase-3/7 (B) and G/F-actin ratio (C) indicate low-stress localization in central region. D) Heat map of average normal stress from thermal contraction model using heterogeneous mechanical properties predicts low cell-layer stress in aggregate center colocalizing with the apoptotic cells. Scale bars = 100  $\mu\text{m}$ . Images are adapted from Cirka *et al.* and Goldblatt *et al.* (Cirka *et al.*, 2017; Goldblatt *et al.*, 2020).

### 2.6.7 Modeling cell-stresses in multicellular systems\*

In multicellular systems, such as in monolayers and restricted aggregates, collective cell contact has major effects on observed cellular behavior. Groupings of cells behave very differently than single, isolated cells. In a large aggregate, diffusion of growth factors and cytokines alone are not sufficient to explain the diversity seen in behaviors of cells just microns apart, especially in 2D culture where all cells are exposed to bulk media on their apical surfaces. Besides the direct exchange of molecules between neighboring cells, cells also physically pull on one another. There is growing evidence that mechanical stress fields are pivotal in controlling differences in

cellular behaviors. Mechanical stress fields that emerge from force transmission between cells are likely major contributors to cellular regulation.

Accurately determining the cellular stresses within monolayers is critical for quantifying the effect of mechanical factors on cell behaviors in multicellular systems. However, these cell-layer stresses cannot be directly measured and require computational modeling for estimated values. In this dissertation, we used two different computational models to simulate cell-stresses: a forward predictive model and a direct back-calculation model from measured traction forces. For forward predictions of stresses, we and other researchers use continuum models with pre-strain and FE models with thermal cooling to simulate active cell contraction (Nelson *et al.*, 2005; Li *et al.*, 2009; Banerjee and Cristina Marchetti, 2013; He *et al.*, 2015). For calculation of cell-stresses from measured substrate traction forces, monolayer stress microscopy (MSM) (Treat *et al.*, 2009) and other force-balancing methods (Maruthamuthu *et al.*, 2011; Moussus *et al.*, 2014; Liu *et al.*, 2016; Nier *et al.*, 2016) have been developed. Calculation of stresses within cell clusters require assumptions about isotropy, elastic constants, and uniformity of the cell layer (Ng *et al.*, 2014). Past studies assume these parameters to be homogeneous throughout the entire cell aggregate (Nelson *et al.*, 2005; Li *et al.*, 2009; He *et al.*, 2015; Liu *et al.*, 2016). In our models, we use heterogeneous parameters to better represent the heterogeneity of the cell aggregate.

### Thermal contraction model

One forward predictive FE modeling technique to estimate cell stresses is the thermal cooling or contraction model. The thermal contraction model is a three-dimensional, forward predictive model that “cools” a continuum to simulate cell contraction. As the model imposes a simulated temperature drop (input) in the cell layer (active layer), the cell layer cannot contract as it is fixed to the substrate layer (passive layer) (Figure 2.10). This constraint causes stresses to be generated (output) in both the cell layer (cell stress) and substrate layer (traction stress). These stresses are dependent on the distribution of mechanical parameters such as the cell layer modulus, substrate modulus, and coefficient of thermal expansion value ( $\alpha$ , representing the extent of “cell contraction”).

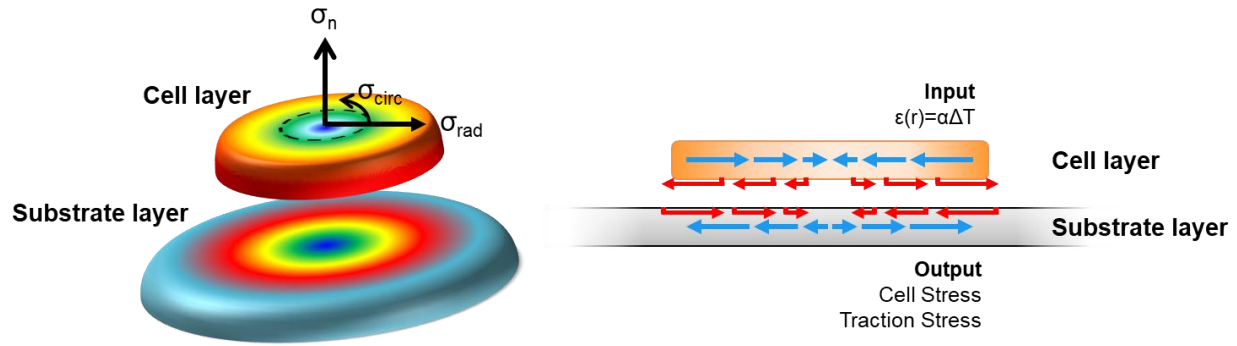


**Figure 2.10:** Schematic of stress components for thermal contraction model. An active layer (cell layer) is fixed to a passive layer (substrate layer) that is fixed at the bottom. Cooling of the active layer causes contraction, which is dependent on the coefficient of thermal expansion. Stresses build up in each layer due to the constraints on each layer.

### Monolayer stress microscopy

A different FE modeling technique is a direct back-calculation of cell-stresses from measured forces. Monolayer stress microscopy (MSM) is a computational method that directly calculates cell stresses using experimentally measured traction forces. MSM is a three-dimensional model that consists of a cell layer alone. In MSM, experimentally measured traction forces are input onto a fixed cell layer; these forces are balanced by internal cell-layer stresses (Figure 2.11). Cell stress and traction stresses are calculated from FE models which are dependent on the distribution of modulus for the cell layer. The MSM model is a force-balance model using real experimental measured forces, which are representative of real stress values. On other hand, the thermal contraction model is a powerful tool for predicting distributions of stresses based on contractility of the material, rather than real forces. The magnitude of forces that are predicted are dependent on the coefficient of thermal expansion and temperature drop which are not physical quantities relevant to actual cell aggregates. Thus, the MSM model predicts stress values representative of actual cell aggregates, whereas the thermal contraction model provides relative distributions of stresses.

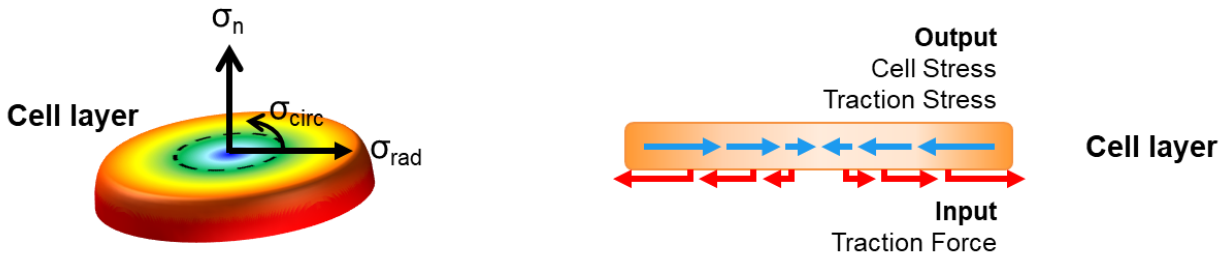


**Figure 2.11:** Schematic of stress components for monolayer stress microscopy model. There is one layer (cell layer) that is fixed at the bottom. Traction forces are input into the MSM model, which causes cell and traction stresses to form in the layer due to constraints on the layer. The calculated stresses in the layer are dependent on the distribution of modulus for the cell layer.

### 2.6.8 Separating the individual effects of correlated mechanical stimuli

The mechanical parameters initiating apoptosis are interdependent in that multiple mechanical stimuli occur simultaneously. For instance, both culturing cells on soft substrates and restricting cell spread area by microcontact printing inhibit the ability of cells to spread and generate traction forces and internal cell stress. Do low spread area, low traction forces, and/or low cell stress initiate apoptosis? Isolation experiments are needed to determine which mechanical signals and subsequent mechanotransduction pathways most directly regulate apoptosis. The pathways that tie these different mechanical signals together and induce similar cellular responses also need to be elucidated. It is likely that similar mechanisms connect all of these mechanical stimuli together in order to regulate apoptosis, such as their combinatorial roles on actin dynamics. For instance, if apoptosis is strongly regulated by actin dynamics, then inhibition of spread area and low traction force generation could induce apoptosis, as both independently inhibit actin dynamics. Further, a decrease in the ability of the actin cytoskeleton to remodel would have reciprocal effects on spread area and traction forces contributing to a positive feedback loop.

## 2.7 Potential mechanical mechanisms regulating apoptosis

### 2.7.1 Canonical mechanotransduction pathways

Very little is known regarding the mechanisms by which mechanical stimuli regulate apoptosis. Many of the signaling pathways already known to be critical for mechanotransduction interact with and modulate the canonical intrinsic and/or extrinsic apoptotic pathways. There is evidence

that signaling molecules associated with mitogen-activated protein kinases (MAPK), protein kinase C (PKC), and phosphatidylinositol 3-kinase (PI3K) pathways play a role in cell survival (Figure 2.12).

There are three main MAPK cascades that modulate cell fate: extracellular signal-related kinases (ERK), c-Jun N-terminal kinases (JNK), and p38-MAPKs (Wernig and Xu, 2002; Wada and Penninger, 2004). The ERK pathway tends to activate survival signals, while JNK and p38-MAPK pathways have been shown to contribute to both cell survival and apoptotic signaling (Mayr *et al.*, 2000; Wada and Penninger, 2004).

PKC and PI3K pathways are also signaling cascades that play a role in cell survival. PKCs can activate survival proteins such as NF- $\kappa$ B and inhibit apoptotic proteins such as BAD. PI3K activates Akt1, which activates survival proteins like Bcl-xL, while inactivating pro-apoptotic proteins like BAD (Figure 2.12). Mechanical stretch can also induce ion transport within transmembrane ion channels in cardiomyocytes (Yamazaki *et al.*, 1998; Peyronnet *et al.*, 2016). Calcium as well as chloride ion influxes have been shown to activate caspases and subsequent apoptosis (Bortner and Cidlowski, 2014).

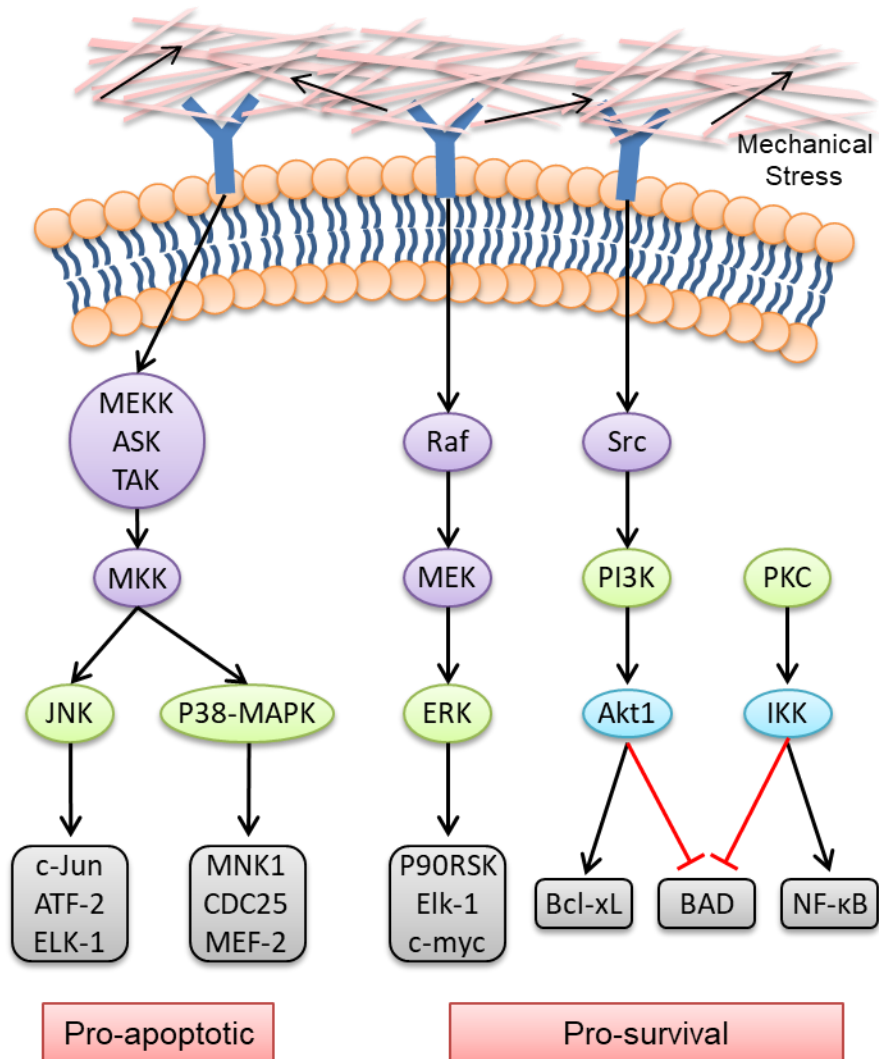


**Figure 2.12:** Both excessive and insufficient mechanical stress can activate apoptotic signaling pathways leading to cell death since both pro-apoptotic and pro-survival pathways are mechanically regulated. Mechanosensitive signaling pathways of apoptosis include the MAPK (JNK, p38-MAPK, ERK), PI3K, and PKC pathways. Certain branches of the JNK and p38-MAPK pathways can also promote cell survival (not shown).

### 2.7.2 Tension in the cytoskeleton

Cells require an intracellular tension homeostasis for continued proper cell health (Chan *et al.*, 2011). The actomyosin cytoskeleton directly controls the tensional state of cells, which plays a critical role in apoptotic pathways. Cytoskeletal reorganization can initiate apoptosis and also plays a role throughout the entire process (Gourlay *et al.*, 2004; Gourlay and Ayscough, 2005a; Leadsham *et al.*, 2010). Healthy cells under homeostatic conditions have low instances of apoptosis and high cytoskeletal stability (Figure 2.13, region B). In supraphysiological

conditions, such as when cells are excessively stretched *in vitro* or in fibrosis *in vivo*, cells experience atypically high inputs of external stresses which increases their intracellular stress levels (Figure 2.13, region C). Here, cytoskeletal stability decreases and occurrences of apoptosis increase. Cells will attempt to revert to homeostatic levels (region B) through reorganization of the cytoskeleton (e.g., strain avoidance in cyclically stretched cells); however, they will apoptose if they cannot reduce the stress on them. In subphysiological conditions, such as when cells are seeded on soft substrates or restricted to small areas through microcontact printing, cells experience unusually low inputs of external stress which decreases their intracellular stress levels (Figure 2.13, region A). Low internal cell tension will cause cytoskeletal stability to decrease and apoptosis to increase. In the central region of multicellular aggregates, we have found that low cell-stresses co-localize with high levels of G/F-actin ratio (low cytoskeletal stability) and high instances of apoptosis (Figure 2.9C) (Goldblatt *et al.*, 2020). By introducing external stresses (such as mechanical stretch), cells can increase their intracellular tension to reach homeostatic levels (region B). A mechanomedicine could help cells in low stress (region A) or high stress (region C) re-achieve homeostasis.

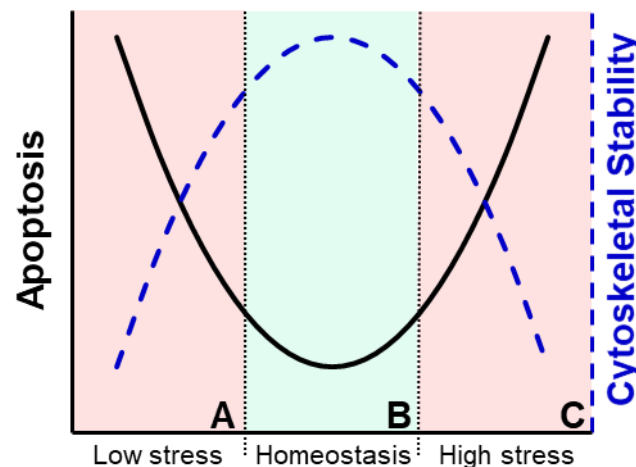


**Figure 2.13:** Schematic of the relationship between intracellular stress levels, apoptosis (black solid line), and cytoskeletal stability (blue dotted line). Healthy cells in physiological conditions are under standard stress levels and exist in region B. Cells experiencing atypically low (region A) or high (region C) inputs of external stress undergo higher instances of apoptosis with lower cytoskeletal stability. Figure is adapted from Chan *et al.* (Chan *et al.*, 2011).

Actin stress fibers can directly regulate apoptosis by pulling on organelles, such as the nucleus or mitochondria, or indirectly via actin-associated molecules or activation of mechanosensitive

pathways regulated by cytoskeletal dynamics (Anesti and Scorrano, 2006; Houben *et al.*, 2007; Mana-Capelli *et al.*, 2014). Studies have shown that stabilizing cytoskeletal dynamics can allow cells to overcome apoptosis (observed in Jurkat T, HeLa, and NIH3T3 cells) (Ohtsu *et al.*, 1997; Kusano *et al.*, 2000; Gourlay and Ayscough, 2005b). Overexpression of gelsolin helps promote F-actin turnover and has been shown to reduce apoptotic rates. By depolymerizing F-actin, gelsolin stimulates VDAC closure in mitochondria thereby preventing cytochrome c release. Additionally, gelsolin causes the accumulation of short F-actin segments; once it dissociates from the F-actin caps, these segments are readily available for repolymerization into longer F-actin stress fibers again.

On the other hand, destabilizing the cytoskeleton through excessive polymerization or depolymerization has been shown to initiate the apoptotic process (Odaka *et al.*, 2000; Gourlay *et al.*, 2004; Leadsham *et al.*, 2010; Desouza *et al.*, 2012). Jasplakinolide causes robust actin stabilization and promotes further polymerization of F-actin. This polymerization can cause F-actin fibers to clump together into aggregates as well as distinct changes in cellular activity indicative of apoptosis. An increase in caspase-3 activation has been shown in jasplakinolide treated yeast and Jurkat T cells, in addition to DNA fragmentation in rat thymocytes, lymph node cells, and COS cells, potentially from DNase-1 that is dissociated from G-actin monomers that are newly polymerized into F-actin (Peitsch *et al.*, 1993; Odaka *et al.*, 2000; Gourlay *et al.*, 2004). Conversely, depolymerization of the cytoskeletal network via cytochalasin D also initiates apoptosis. It has been shown to induce caspase activation as well as cytochrome c release in fibrosarcoma L929 and 3C6 T cells (Suria *et al.*, 1999; Paul *et al.*, 2002). Furthermore, organelles require mechanical feedback for proper function, and a decrease in cytoskeletal integrity may activate apoptotic pathways. The cytoskeleton directly connects to nuclear actin via linker proteins, such as nesprins and lamins. Both of these proteins are critical for nuclear mechanosensing and can cause alterations in gene expression due to transduced forces into the nucleus. When nesprins or lamins are inhibited, the nucleus cannot respond to mechanical signals, and as seen in neonatal mouse cardiomyocytes and HeLa cells, cells have been shown to undergo apoptosis (Steen and Collas, 2001; Banerjee *et al.*, 2014).

### 2.7.3 Cellular realignment due to strain avoidance\*

As reviewed above, cells forced above or below their homeostatic tension are more likely to undergo apoptosis (Mayr *et al.*, 2000; Wang *et al.*, 2000; Sotoudeh *et al.*, 2002; Hsieh and Nguyen, 2005). For example, apoptosis is observed in cells in low tension states (low modulus), as well as in high tension states (cyclic stretch at high magnitudes). In *in vitro* studies, it has been shown that cells on high-modulus (stiff) substrates, which are thought to equilibrate to their homeostatic tension, undergo reorientation away from the direction of externally applied cyclic strain. Reorganization of the cytoskeleton leads to reorientation of the cell body towards a direction of minimal stress, why is hypothesized to promote reestablishment of homeostatic tension (Kaunas *et al.*, 2005; De *et al.*, 2007; Zhong *et al.*, 2011). On the other hand, culturing cells on very low-modulus (soft) substrates allows us to study cells with naturally occurring low levels of initial internal tension. Here, stress fibers depolymerize due to insufficient mechanical feedback from the ECM which feeds back into cells having low tension. Introducing cyclic stretch to cells on soft substrates allows cells to reinforce stress fiber formation in the direction of stretch. As cells continue to increase in internal tension, cells reorient away from stretch towards a direction of optimal tension; this angle is much less than cells on stiff substrates. With respect to substrate modulus and cyclic stretch, each cell maintains homeostatic tension by reorienting towards an angle of optimal stress.

### 2.7.4 Yes-associated protein (YAP)\*

Cytoskeletal stability indirectly regulates various mechanosensitive pathways that are potentially linked to apoptosis, such as the Hippo pathway and its transcriptional factor yes-associated protein (YAP). YAP is mediated by the tensional state of the cell, and it has been shown that in low stress environments, YAP is phosphorylated, inactivated, and excluded from the nucleus, while the opposite processes occur in high stress environments (Wada *et al.*, 2011; Calvo *et al.*, 2013; Mascharak *et al.*, 2017). Previous literature has shown that stretching cells in low stress environments makes cells behave as if they are in high stress environments, promoting YAP localization to the nucleus (Aragona *et al.*, 2013; Codelia *et al.*, 2017).

YAP is primarily studied regarding its role in cell proliferation; however, it has also been shown to play a role in apoptosis. In the canonical Hippo pathway, YAP is negatively regulated by LATS kinases, which phosphorylate YAP and promote cytoplasmic retention and degradation (Zhao *et al.*, 2007; Reuven *et al.*, 2013; Codelia *et al.*, 2017) (Figure 2.14). Active YAP can lead to stimulating the expression of prominent apoptosis inhibitors, such as BIRC3, BIRC5, and CYR61 (Zhang *et al.*, 2011a; Lin *et al.*, 2015; Codelia *et al.*, 2017). Further, YAP inhibits proapoptotic genes such as dendrin and Bcl-2 family proteins (Campbell *et al.*, 2013; Song *et al.*, 2016). The mechanical environment has been shown to directly regulate YAP via the tension state of the cytoskeleton (Aragona *et al.*, 2013) (Figure 2.14). This regulation occurs through Rho-GTPases which control the tension of the cytoskeleton (Dupont *et al.*, 2011; Das *et al.*, 2016). Angiomotins are proteins that bind to F-actin and are released upon F-actin depolymerization (Mana-Capelli *et al.*, 2014). Free angiomotins can bind and sequester cytoplasmic YAP thus keeping them inactive. YAP activation may also occur independent of the cytoskeleton; a recent study showed that direct application of force onto the nucleus of a cell caused YAP activation and translocation into the nucleus (Elosegui-Artola *et al.*, 2017).

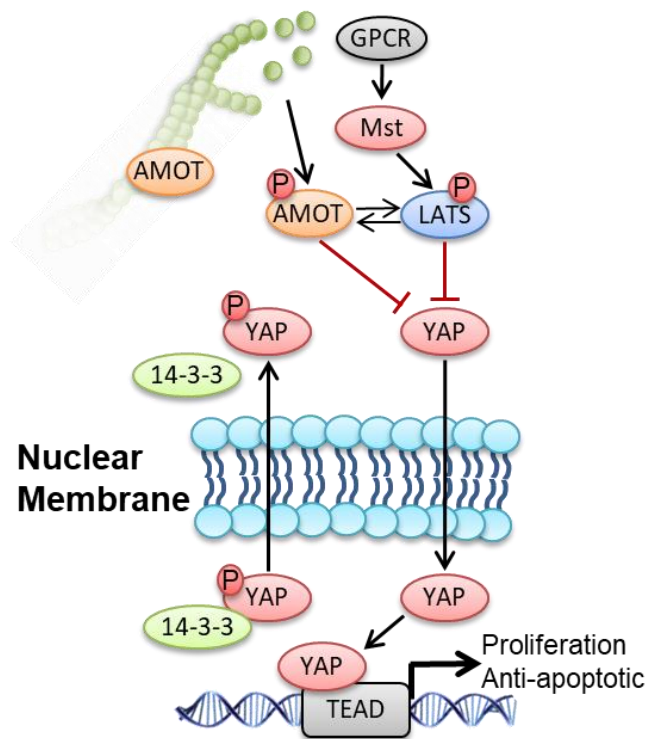


**Figure 2.14:** Schematic of the common Hippo signaling pathway. Activate YAP enters the nucleus to activate cell survival genes. Depolymerization of actin stress fibers (green) mechanically modulates the pathway to deactivate YAP with AMOTs. This is a potential role of actin in regulating apoptosis.

### 2.7.5 Myocardin-related transcription factor-A (MRTF-A)\*

The cytoskeleton also directly regulates the mechanosensitive MRTF pathway and its transcriptional factor myocardin-related transcription factor-A (MRTF-A) (Figure 2.15). MRTF-A, like YAP, is a cytoskeleton mediator that is mainly studied for its role in proliferation (Shaposhnikov *et al.*, 2012; Sisson *et al.*, 2015); however, it may also play a role in apoptosis. MRTF-A, a potent coactivator of serum response factor (SRF), induces transcription of many proliferative and cytoskeletal genes. MRTF-A is localized in the cytoplasm and is inactivated when making a complex with G-actin. When G-actin concentration decreases due to polymerization into F-actin, MRTF-A is released and allowed to translocate to the nucleus, which causes SRF-MRTF-A-directed gene activation (Olson and Nordheim, 2010). Nuclear G-actin can bind to nuclear MRTF-A in order to shuttle it back to the cytoplasm. Upstream from both YAP and MRTF-A are Rho and ROCK signaling. It was previously found that inhibition of ROCK can reduce the response to pressure induced apoptosis (Phrommintikul *et al.*, 2008), while constitutively active ROCK can enhance cardiomyocyte apoptosis (Chang *et al.*, 2006).

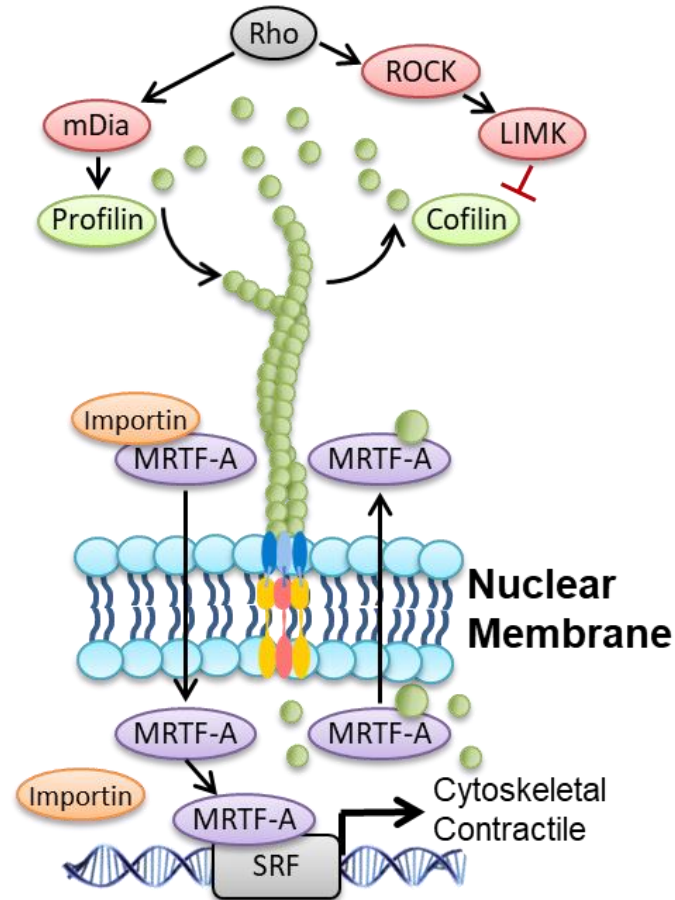


**Figure 2.15:** Schematic of the MRTF signaling pathway. Active MRTF-A is shuttled into the nucleus and activates cytoskeletal genes. Depolymerization of actin stress fibers (green) mechanically regulates MRTF-A by deactivation via free G-actin.

## 2.8 Mechanomedicines as a potential therapeutic solution

Understanding the mechanical mechanisms that regulate cell health in response to mechanical stress may inspire new therapeutic strategies which target these mechanically sensitive pathways. Chan and colleagues first introduced the concept of mechanomedicines in 2011 as a class of therapies which exploit mechanotransduction pathways and restore cells to their homeostatic stress state (Chan *et al.*, 2011). As both excessive apoptosis (e.g., atrophy and CAVD) and the absence of apoptosis (e.g., fibrosis and cancer) contribute to pathologies, mechanomedicines could treat disease by modulating rates of apoptosis as appropriate (Figure 2.16). Not only do mechanomedicines include pharmacological agents and inhibitory antibodies which may trigger or prevent apoptosis by interacting with the intrinsic/extrinsic apoptotic signaling cascade, but also potential biomimetic injectables that can modify the extracellular matrix environment

(Ingber, 2008). The mechanical environment created by the native ECM has been shown to regulate growth (Pickup *et al.*, 2014), differentiation (Guilak *et al.*, 2009), proliferation (Ulrich *et al.*, 2009), and sensitivity to cytokine-induced apoptosis (Farrelly *et al.*, 1999). Pathologies are often accompanied by noticeable changes in tissue properties (e.g., by physical palpitation in tumor discovery) (Huang and Ingber, 2005), and it has been proposed that many diseases arise due to degrading tissue architecture. Restoring the correct mechanical properties through ECM modification could help restore homeostasis by either preventing apoptosis or sensitizing target cells to apoptotic mechanical cues.

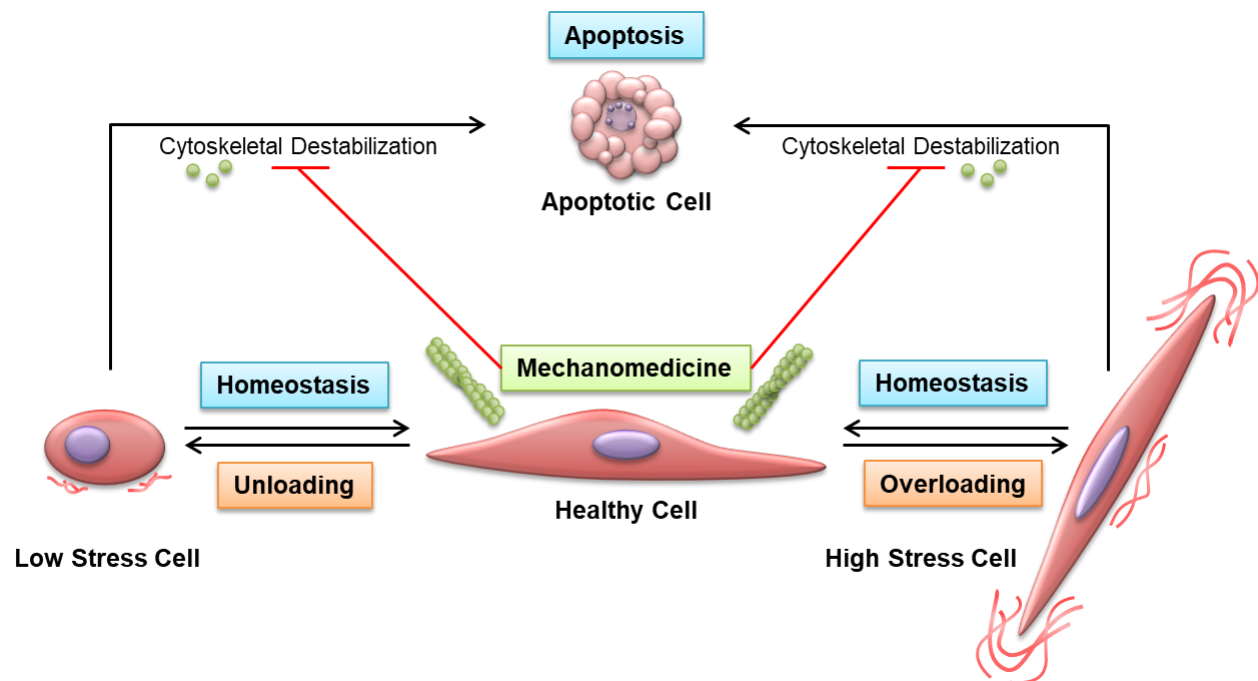


**Figure 2.16:** Schematic of mechanomedicines bringing the cell-stress state back to homeostatic levels. Overloading and underloading of cells can cause cytoskeletal destabilization which mechanomedicines can potentially target, allowing cells to reduce excessive apoptosis in degenerative diseases or uncontrolled growth (deficient apoptosis) in cancers.

To date, no pharmacologic treatment has been designed with the sole purpose of altering the mechanosensitive signaling pathways of cells, although there are medications that cause altered cytoskeletal tension as a side-effect. One such example is statins which are prescribed for treatment of high cholesterol or blood pressure. Statins inhibit HMG-CoA reductase which ultimately leads to the inhibition of isoprenylation of small GTPases such as Ras, Rho, Rab, and Rap (Rikitake and Liao, 2005). As Rho signaling is involved in cytoskeletal dynamics, decreased

Rho activity from statin use results in reduced cell contractility, as shown *in vitro* with decreased contractile protein expression in valvular interstitial cells (Gu and Masters, 2011).

Pharmacological agents that affect the cytoskeleton are of interest for cancer therapies to promote apoptosis in diseased cells, as well as impede cell metastasis. A number of groups have reported altered cytoskeletal dynamics within transformed cells, including altered G- to F-actin ratios and an inability to sense substrate stiffness in normal and malignant human lymphocytes and endometrial cells (Stournaras *et al.*, 1996). Additionally, a number of drugs which interact with microtubules or tubulin in order to prevent mitosis/proliferation, such as taxol and taxol-like compounds, molidine and epothilone, alter microtubule dynamics and have been shown to promote apoptosis in transformed cells (Jordan and Wilson, 1998; Kavallaris, 2010). As the cytoskeleton is critical to numerous cell processes such as migration and proliferation, which can be exploited in cancer during metastasis and tumorigenesis, the cytoskeleton has become a promising target for pharmacological intervention. A number of compounds have been identified which interfere with actin polymerization and dynamics through a variety of mechanisms. These compounds include cytochalasins, jasplakinolide, misakinolide and latrunculin (Olson and Nordheim, 2010). Although these compounds are heavily used *in vitro* to gain an understanding of the relationship between actin dynamics and apoptosis, similar acting pharmaceuticals have yet to be approved for clinical use. There is promise in cytoskeletal tension modulation as a therapy for cancer; however, this approach has yet to be taken for development of mechanomedicines for cardiovascular diseases.

## 2.9 Summary

Apoptosis is a highly regulated cellular process which plays a critical role in organism development and tissue maintenance. Dysregulation of apoptosis is implicated in a number of disease processes. Despite numerous correlations between physical stimuli and apoptosis, there remains a significant gap in our understanding in how particular mechanical inputs trigger apoptosis through mechanotransduction signaling pathways. Continued work is needed in identifying the mechanotransductive events which result in apoptosis via both extracellular and intracellular cues. Uncovering these mechanical mechanisms that regulate cell health is the first

step in creating ways to manipulate mechanically sensitive pathways. We believe one such mechanism is the regulation of cytoskeletal stability and how it directly modulates cell health in response to mechanical stimuli. The reversibility of apoptosis highlights the potential of developing promising mechanomedicines that alter cellular mechanics to reverse disease progression. By controlling rates of apoptosis, mechanomedicines could treat diseases ranging from cancer (increasing apoptosis) to degenerative diseases (decreasing apoptosis). Discovering how specific mechanotransduction pathways regulate apoptosis is critical for identifying therapeutic targets that may be treated with mechanomedicines and mechanotherapies.

## 2.10 References

- Anesti, V., and Scorrano, L. (2006). The relationship between mitochondrial shape and function and the cytoskeleton. *Biochim. Biophys. Acta - Bioenerg.* *1757*, 692–699.
- Aragona, M., Panciera, T., Manfrin, A., Giulitti, S., Michielin, F., Elvassore, N., Dupont, S., and Piccolo, S. (2013). A mechanical checkpoint controls multicellular growth through YAP/TAZ regulation by actin-processing factors. *Cell* *154*, 1047–1059.
- Araki, S., Shimada, Y., Kaji, K., and Hayashi, H. (1990). Apoptosis of vascular endothelial cells by fibroblast growth factor deprivation. *Biochem. Biophys. Res. Commun.* *168*, 1194–1200.
- Arstall, M. A., Sawyer, D. B., Fukazawa, R., and Kelly, R. A. (1999). Cytokine-mediated apoptosis in cardiac myocytes. *Circ. Res.* *85*, 829–840.
- Asakura, T., and Karino, T. (1990). Flow patterns and spatial distribution of atherosclerotic lesions in human coronary arteries. *Circ. Res.* *66*, 1045–1066.
- Bailey, R. W., Nguyen, T., Robertson, L., Gibbons, E., Nelson, J., Christensen, R. E., Bell, J. P., Judd, A. M., and Bell, J. D. (2009). Sequence of physical changes to the cell membrane during glucocorticoid-induced apoptosis in S49 lymphoma cells. *Biophys. J.* *96*, 2709–2718.
- Banerjee, I. *et al.* (2014). Targeted ablation of nesprin 1 and nesprin 2 from murine myocardium results in cardiomyopathy, altered nuclear morphology and inhibition of the biomechanical gene response. *PLoS Genet.* *10*, e1004114.
- Banerjee, S., and Cristina Marchetti, M. (2013). Controlling cell-matrix traction forces by extracellular geometry. *New J. Phys.* *15*.
- Bing, O. H. L. (1994). Hypothesis: apoptosis may be a mechanism for the transition to heart failure with chronic Pressure overload. *J. Mol. Cell. Cardiol.* *26*, 943–948.
- Bortner, C. D., and Cidlowski, J. A. (2014). Ion channels and apoptosis in cancer. *Philos. Trans. R. Soc. B Biol. Sci.* *369*, 1–9.
- Califano, J. P., and Reinhart-King, C. A. (2010). Substrate stiffness and cell area predict cellular

traction stresses in single cells and cells in contact. *Cell. Mol. Bioeng.* 3, 68–75.

Calvo, F. *et al.* (2013). Mechanotransduction and YAP-dependent matrix remodelling is required for the generation and maintenance of cancer-associated fibroblasts. *Nat Cell Biol* 15, 637–646.

Campbell, K. N., Wong, J. S., Gupta, R., Asanuma, K., Sudol, M., He, J. C., and Mundel, P. (2013). Yes-associated protein (YAP) promotes cell survival by inhibiting proapoptotic dendrin signaling. *J. Biol. Chem.* 288, 17057–17062.

Chan, D. D., Van Dyke, W. S., Bahls, M., Connell, S. D., Critser, P., Kelleher, J. E., Kramer, M. A., Pearce, S. M., Sharma, S., and Neu, C. P. (2011). Mechanostasis in apoptosis and medicine. *Prog. Biophys. Mol. Biol.* 106, 517–524.

Chang, J., Xie, M., Shah, V. R., Schneider, M. D., Entman, M. L., Wei, L., and Schwartz, R. J. (2006). Activation of Rho-associated coiled-coil protein kinase 1 (ROCK-1) by caspase-3 cleavage plays an essential role in cardiac myocyte apoptosis. *Proc. Natl. Acad. Sci.* 103, 14495–14500.

Chaudhuri, O. *et al.* (2015). Hydrogels with tunable stress relaxation regulate stem cell fate and activity. *Nat. Mater.* 15, 326–334.

Chen, B., Kumar, G., Co, C. C., and Ho, C.-C. (2013). Geometric control of cell migration. *Sci. Rep.* 3, 2827.

Chen, C. S., Mrksich, M., Huang, S., Whitesides, G. M., and Ingber, D. E. (1997). Geometric control of cell life and death. *Science* 276, 1425–1428.

Chiong, M., Wang, Z. V, Pedrozo, Z., Cao, D. J., Troncoso, R., Ibacache, M., Criollo, A., Nemchenko, A., Hill, J., and Lavandero, S. (2011). Cardiomyocyte death: mechanisms and translational implications. *Cell Death Dis.* 2, e244.

Cirka, H. A., Uribe, J., Liang, V., Schoen, F. J., and Billiar, K. L. (2017). Reproducible in vitro model for dystrophic calcification of cardiac valvular interstitial cells: insights into the mechanisms of calcific aortic valvular disease. *Lab Chip* 17, 814–829.

Cirka, H., Monterosso, M., Diamantides, N., Favreau, J., Wen, Q., and Billiar, K. (2016). Active traction force response to long-term cyclic stretch is dependent on cell pre-stress. *Biophys. J.* 110, 1845–1857.

Clark, R. S. B., Kochanek, P. M., Chen, M., Watkins, S. C., Marion, D. W., Chen, J., Hamilton, R. L., Loeffert, J. E., and Graham, S. H. (1999). Increases in Bcl-2 and cleavage of caspase-1 and caspase-3 in human brain after head injury. *FASEB J* 13, 813–821.

Clarke, M. C. H., Figg, N., Maguire, J. J., Davenport, A. P., Goddard, M., Littlewood, T. D., and Bennett, M. R. (2006). Apoptosis of vascular smooth muscle cells induces features of plaque vulnerability in atherosclerosis. *Nat. Med.* 12, 1075–1080.

Clarke, M. C. H., Littlewood, T. D., Figg, N., Maguire, J. J., Davenport, A. P., Goddard, M., and Bennett, M. R. (2008). Chronic apoptosis of vascular smooth muscle cells accelerates atherosclerosis and promotes calcification and medial degeneration. *Circ. Res.* 102, 1529–1538.

Codelia, V. A., Sun, G., and Irvine, K. D. (2017). Regulation of YAP by mechanical strain

- through Jnk and Hippo signaling. *Curr. Biol.* *24*, 2012–2017.
- Cui, Y., Hameed, F. M., Yang, B., Lee, K., Pan, C. Q., Park, S., and Sheetz, M. (2015). Cyclic stretching of soft substrates induces spreading and growth. *Nat. Commun.* *6*, 6333–6340.
- Czabotar, P. E., Lessene, G., Strasser, A., and Adams, J. M. (2014). Control of apoptosis by the BCL-2 protein family: implications for physiology and therapy. *Nat. Rev. Mol. Cell Biol.* *15*, 49–63.
- Darzynkiewicz, Z., Galkowski, D., and Zhao, H. (2008). Analysis of apoptosis by cytometry using TUNEL assay. *Methods* *44*, 250–254.
- Darzynkiewicz, Z., and Zhao, H. (2011). Detection of DNA strand breaks in apoptotic cells by flow- and image-cytometry. *Methods Mol. Biol.* *682*, 91–101.
- Das, A., Fischer, R. S., Pan, D., and Waterman, C. M. (2016). YAP nuclear localization in the absence of cell-cell contact is mediated by a filamentous actin-dependent, Myosin II and Phospho-YAP-independent pathway during extracellular matrix mechanosensing. *J. Biol. Chem.* *291*, 6096–6110.
- De, R., Zemel, A., and Safran, S. A. (2007). Dynamics of cell orientation. *Nat. Phys.* *3*, 655–659.
- Desouza, M., Gunning, P. W., and Stehn, J. R. (2012). The actin cytoskeleton as a sensor and mediator of apoptosis. *Bioarchitecture* *2*, 75–87.
- Dupont, S. *et al.* (2011). Role of YAP/TAZ in mechanotransduction. *Nature* *474*, 179–183.
- Dweck, M. R., Boon, N. A., and Newby, D. E. (2012). Calcific aortic stenosis: a disease of the valve and the myocardium. *J. Am. Coll. Cardiol.* *60*, 1854–1863.
- Egerbacher, M., Arnoczky, S. P., Caballero, O., Lavagnino, M., and Gardner, K. L. (2008). Loss of homeostatic tension induces apoptosis in tendon cells: an in vitro study. *Clin. Orthop. Relat. Res.* *466*, 1562–1568.
- Elosegui-Artola, A. *et al.* (2017). Force triggers YAP nuclear entry by regulating transport across nuclear pores. *Cell* *171*, 1397–1410.e14.
- Fadeel, B. (2004). Plasma membrane alterations during apoptosis: role in corpse clearance. *Antioxid. Redox Signal.* *6*, 269–275.
- Farrelly, N., Lee, Y.-J., Oliver, J., Dive, C., and Streuli, C. H. (1999). Extracellular matrix regulates apoptosis in mammary epithelium through a control on insulin signaling. *Cell* *144*, 1337–1347.
- Flusberg, D. A., Numaguchi, Y., and Ingber, D. E. (2001). Cooperative control of Akt phosphorylation, bcl-2 expression, and apoptosis by cytoskeletal microfilaments and microtubules in capillary endothelial cells. *Mol. Biol. Cell* *12*, 3087–3094.
- Freeman, R. V., and Otto, C. M. (2005). Spectrum of calcific aortic valve disease: Pathogenesis, disease progression, and treatment strategies. *Circulation* *111*, 3316–3326.
- Fu, R., Liu, Q., Song, G., Baik, A., Hu, M., Sun, S., Guo, X. E., Long, M., and Huo, B. (2013). Spreading area and shape regulate apoptosis and differentiation of osteoblasts. *Biomed. Mater.* *8*,

055005.

Galluzzi, L., Maiuri, M. C., Vitale, I., Zischka, H., Castedo, M., Zitvogel, L., and Kroemer, G. (2007). Cell death modalities: classification and pathophysiological implications. *Cell Death Differ.* *14*, 1237–1243.

Geske, F. J., Lieberman, R., Strange, R., and Gerschenson, L. E. (2001). Early stages of p53-induced apoptosis are reversible. *Cell Death Differ.* *8*, 182–191.

Goldblatt, Z. E., Ashouri Choshali, H., Cirka, H. A., Liang, V., Wen, Q., McCollum, D., Rahbar, N., and Billiar, K. L. (2020). Heterogeneity profoundly alters emergent stress fields in constrained multicellular systems. *Biophys. J.* *118*, 15–25.

Gottlieb, E., Armour, S., Harris, M., and Thompson, C. (2003). Mitochondrial membrane potential regulates matrix configuration and cytochrome c release during apoptosis. *Cell Death Differ.* *10*, 709–717.

Gourlay, C. W., and Ayscough, K. R. (2005a). A role for actin in aging and apoptosis. *Biochem. Soc. Trans.* *33*, 1260–1264.

Gourlay, C. W., and Ayscough, K. R. (2005b). The actin cytoskeleton: a key regulator of apoptosis and ageing? *Nat. Rev. Mol. Cell Biol.* *6*, 583–589.

Gourlay, C. W., Carpp, L. N., Timpson, P., Winder, S. J., and Ayscough, K. R. (2004). A role for the actin cytoskeleton in cell death and aging in yeast. *J. Cell Biol.* *164*, 803–809.

Gu, X., and Masters, K. S. (2011). Role of the Rho pathway in regulating valvular interstitial cell phenotype and nodule formation. *Am. J. Physiol. Circ. Physiol.* *300*, H448–H458.

Guilak, F., Cohen, D. M., Estes, B. T., Gimble, J. M., Liedtke, W., and Chen, C. S. (2009). Control of stem cell fate by physical interactions with the extracellular matrix. *Cell Stem Cell* *5*, 17–26.

Gurbanov, E., and Shiliang, X. (2006). The key role of apoptosis in the pathogenesis and treatment of pulmonary hypertension. *Eur. J. Cardio-Thoracic Surg.* *30*, 499–507.

Hanahan, D., and Weinberg, R. A. (2011). Hallmarks of cancer: The next generation. *Cell* *144*, 646–674.

Hardwick, J. M. (2001). Apoptosis in viral pathogenesis. *Cell Death Differ.* *8*, 109–110.

He, S., Liu, C., Li, X., Ma, S., Huo, B., and Ji, B. (2015). Dissecting Collective Cell Behavior in Polarization and Alignment on Micropatterned Substrates. *Biophys. J.* *109*, 489–500.

Houben, F., Ramaekers, F. C. S., Snoeckx, L. H. E. H., and Broers, J. L. V. (2007). Role of nuclear lamina-cytoskeleton interactions in the maintenance of cellular strength. *Biochim. Biophys. Acta - Mol. Cell Res.* *1773*, 675–686.

Hsieh, M. H., and Nguyen, H. T. (2005). Molecular mechanism of apoptosis induced by mechanical forces. *Int. Rev. Cytol.* *245*, 45–90.

Huang, J., Liu, Y., Sun, P., Lv, X., Bo, K., and Fan, X. (2010). Novel strategy for treatment of pulmonary arterial hypertension: enhancement of apoptosis. *Lung* *188*, 179–189.

- Huang, S., and Ingber, D. E. (2005). Cell tension, matrix mechanics, and cancer development. *Cancer Cell* 8, 175–176.
- Huang, X., Halicka, H. D., Traganos, F., Tanaka, T., Kurose, A., and Darzynkiewicz, Z. (2005). Cytometric assessment of DNA damage in relation to cell cycle phase and apoptosis. *Cell Prolif.* 38, 223–243.
- Hughes-Fulford, M., Tjandrawinata, R., Fitzgerald, J., Gasuad, K., and Gilbertson, V. (1998). Effects of microgravity on osteoblast growth. *Gravit. Space Biol. Bull.* 11, 51–60.
- Humphrey, J. D., Dufresne, E. R., and Schwartz, M. A. (2014). Mechanotransduction and extracellular matrix homeostasis. *Nat. Rev. Mol. Cell Biol.* 15, 802–812.
- Igney, F. H., and Krammer, P. H. (2002). Death and anti-death: tumour resistance to apoptosis. *Nat. Rev. Cancer* 2, 277–288.
- Infanger, M. *et al.* (2006). Simulated weightlessness changes the cytoskeleton and extracellular matrix proteins in papillary thyroid carcinoma cells. *Cell Tissue Res.* 324, 267–277.
- Ingber, D. E. (2008). Can cancer be reversed by engineering the tumor microenvironment? *Semin. Cancer Biol.* 18, 356–364.
- Jaalouk, D. E., and Lammerding, J. (2009). Mechanotransduction gone awry. *Nat. Rev. Mol. Cell Biol.* 10, 63–73.
- Jian, B., Narula, N., Li, Q. Y., Mohler, E. R., and Levy, R. J. (2003). Progression of aortic valve stenosis: TGF- $\beta$ 1 is present in calcified aortic valve cusps and promotes aortic valve interstitial cell calcification via apoptosis. *Ann. Thorac. Surg.* 75, 457–465.
- Jordan, M. A., and Wilson, L. (1998). Microtubules and actin filaments: dynamic targets for cancer chemotherapy. *Curr. Opin. Cell Biol.* 10, 123–130.
- Jurasz, P., Courtman, D., Babaie, S., and Stewart, D. J. (2010). Role of apoptosis in pulmonary hypertension: from experimental models to clinical trials. *Pharmacol. Ther.* 126, 1–8.
- Kaiser, D., Freyberg, M.-A., and Friedl, P. (1997). Lack of hemodynamic forces triggers apoptosis in vascular endothelial cells. *Biochem. Biophys. Res. Commun.* 231, 586–590.
- Kannan, K., and Jain, S. K. (2000). Oxidative stress and apoptosis. *Pathophysiology* 7, 153–163.
- Kaunas, R., Nguyen, P., Usami, S., and Chien, S. (2005). Cooperative effects of Rho and mechanical stretch on stress fiber organization. *Proc Natl Acad Sci* 102.
- Kavallaris, M. (2010). Microtubules and resistance to tubulin-binding agents. *Nat. Rev. Cancer* 10, 194–204.
- Kerr, J. F. R., Wyllie, A. H., and Currie, A. R. (1972). Apoptosis: a basic biological phenomenon with wide-ranging implications in tissue kinetics. *J. Intern. Med.* 258, 479–517.
- Kilian, K. A., Bugarija, B., Lahn, B. T., and Mrksich, M. (2010). Geometric cues for directing the differentiation of mesenchymal stem cells. *Proc. Natl. Acad. Sci.* 107, 4872–4877.
- Kim, D. H., Khatau, S. B., Feng, Y., Walcott, S., Sun, S. X., Longmore, G. D., and Wirtz, D. (2012). Actin cap associated focal adhesions and their distinct role in cellular mechanosensing.

Sci. Rep. 2, 1–13.

Kim, N. H., and Kang, P. M. (2010). Apoptosis in cardiovascular diseases: mechanism and clinical implications. *Korean Circ. J.* 40, 299–305.

Klein, E. A., Yin, L., Kothapalli, D., Castagnino, P., Byfield, F. J., Xu, T., Levental, I., Hawthorne, E., Janmey, P. A., and Assoian, R. K. (2009). Cell-cycle control by physiological matrix elasticity and in vivo tissue stiffening. *Curr. Biol.* 19, 1511–1518.

Komuro, T. (1990). Re-evaluation of fibroblasts and fibroblast-like cells. *Anat. Embryol. (Berl)* 182, 103–112.

Konduri, S., Xing, Y., Warnock, J. N., He, Z., and Yoganathan, A. P. (2005). Normal physiological conditions maintain the biological characteristics of porcine aortic heart valves: An ex vivo organ culture study. *Ann. Biomed. Eng.* 33, 1158–1166.

Kong, D., Zheng, T., Zhang, M., Wang, D., Du, S., Li, X., Fang, J., and Cao, X. (2013). Static Mechanical Stress Induces Apoptosis in Rat Endplate Chondrocytes through MAPK and Mitochondria-Dependent Caspase Activation Signaling Pathways. *PLoS One* 8, 1–10.

Kumar, S. (2007). Caspase function in programmed cell death. *Cell Death Differ.* 14, 32–43.

Kusano, H., Shimizu, S., Koya, R. C., Fujita, H., Kamada, S., Kuzumaki, N., and Tsujimoto, Y. (2000). Human gelsolin prevents apoptosis by inhibiting apoptotic mitochondrial changes via closing VDAC. *Oncogene* 19, 4807–4814.

Lagadic-Gossmann, D., Huc, L., and Lecureur, V. (2004). Alterations of intracellular pH homeostasis in apoptosis: origins and roles. *Cell Death Differ.* 11, 953–961.

Leadsham, J. E., Kotiadis, V. N., Tarrant, D. J., and Gourlay, C. W. (2010). Apoptosis and the yeast actin cytoskeleton. *Cell Death Differ.* 17, 754–762.

Leight, J. L., Wozniak, M. A., Chen, S., Lynch, M. L., and Chen, C. S. (2012). Matrix rigidity regulates a switch between TGF- $\beta$ 1-induced apoptosis and epithelial-mesenchymal transition. *Mol. Biol. Cell* 23, 781–791.

Leopold, J. A. (2012). Cellular mechanisms of aortic valve calcification. *Circ. Cardiovasc. Interv.* 5, 605–614.

Li, B., Li, F., Puskar, K. M., and Wang, J. H. C. (2009). Spatial patterning of cell proliferation and differentiation depends on mechanical stress magnitude. *J. Biomech.* 42, 1622–1627.

Li, Q., Kumar, A., Makhija, E., and Shivashankar, G. V. (2014). The regulation of dynamic mechanical coupling between actin cytoskeleton and nucleus by matrix geometry. *Biomaterials* 35, 961–969.

Liao, X., Wang, X., Gu, Y., Chen, Q., and Chen, L. Y. (2005). Involvement of death receptor signaling in mechanical stretch-induced cardiomyocyte apoptosis. *Life Sci.* 77, 160–174.

Lin, Z., Zhou, P., Von Gise, A., Gu, F., Ma, Q., Chen, J., Guo, H., Van Gorp, P. R. R., Wang, D. Z., and Pu, W. T. (2015). Pi3kcb links Hippo-YAP and PI3K-AKT signaling pathways to promote cardiomyocyte proliferation and survival. *Circ. Res.* 116, 35–45.

- Liu, A. C., Joag, V. R., and Gotlieb, A. I. (2007). The emerging role of valve interstitial cell phenotypes in regulating heart valve pathobiology. *Am. J. Pathol.* *171*, 1407–1418.
- Liu, C., He, S., Li, X., Huo, B., and Ji, B. (2016). Mechanics of cell mechanosensing on patterned substrate. *J. Appl. Mech.* *83*, 1–8.
- Liu, X. M., Ensenat, D., Wang, H., Schafer, A. I., and Durante, W. (2003). Physiologic cyclic stretch inhibits apoptosis in vascular endothelium. *FEBS Lett.* *541*, 52–56.
- Locksley, R. M., Killeen, N., and Lenardo, M. J. (2001). The TNF and TNF receptor superfamilies: integrating mammalian biology. *Cell* *104*, 487–501.
- Lotem, J., and Sachs, L. (1999). Cytokines as suppressors of apoptosis. *Apoptosis* *4*, 187–196.
- Lunova, M., Zablotskii, V., Dempsey, N. M., Devillers, T., Jirsa, M., Sykova, E., Kubinova, S., Lunov, O., and Dejneka, A. (2016). Modulation of collective cell behaviour by geometrical constraints. *Integr. Biol.* *8*.
- Malek, A. M., Alper, S. L., and Izumo, S. (1999). Hemodynamic shear stress and its role in atherosclerosis. *Jama* *282*, 2035–2042.
- Mana-Capelli, S., Paramasivam, M., Dutta, S., and McCollum, D. (2014). Angiotensins link F-actin architecture to Hippo pathway signaling. *Mol. Biol. Cell* *25*, 1676–1685.
- Maruthamuthu, V., Sabass, B., Schwarz, U. S., and Gardel, M. L. (2011). Cell-ECM traction force modulates endogenous tension at cell-cell contacts. *Proc. Natl. Acad. Sci.* *108*, 4708–4713.
- Mascharak, S., Benitez, P. L., Proctor, A. C., Madl, C. M., Hu, K. H., Dewi, R. E., Butte, M. J., and Heilshorn, S. C. (2017). YAP-dependent mechanotransduction is required for proliferation and migration on native-like substrate topography. *Biomaterials* *115*, 155–166.
- Mayr, M., Hu, Y., Hainaut, P., and Xu, Q. (2002). Mechanical stress-induced DNA damage and rac- p38MAPK signal pathways mediate p53-dependent apoptosis in vascular smooth muscle cells. *FASEB J* *16*, 1423–1425.
- Mayr, M., Li, C., Zou, Y., Huemer, U., Hu, Y., and Xu, Q. (2000). Biomechanical stress-induced apoptosis in vein grafts involves p38 mitogen-activated protein kinases. *FASEB J* *14*, 261–270.
- McIlwain, D. R., Berger, T., and Mak, T. W. (2015). Caspase functions in cell death and disease. *Cold Spring Harb. Perspect. Biol.* *7*, 1–28.
- Mleynek, Tara M., Redd, M., Chan, A., Gu, Y., Li, D. Y., and Rosenblatt, J. (2018). Endothelia extrude apoptotic cells to maintain a constant barrier. *BioRxiv2* [Preprint].
- Mohler, E., Francis, G., Carol, R., Robert, Z., G., K. M., and S., K. F. (2001). Bone formation and inflammation in cardiac valves. *Circulation* *103*, 1522–1528.
- Morbidelli, L., Monici, M., Marziliano, N., Cogoli, A., Fusi, F., Waltenberger, J., and Ziche, M. (2005). Simulated hypogravity impairs the angiogenic response of endothelium by up-regulating apoptotic signals. *Biochem. Biophys. Res. Commun.* *334*, 491–499.
- Moussus, M., Loughian, C. Der, Fuard, D., Courçon, M., Gulino-Debrac, D., Delanoë-Ayari, H., and Nicolas, A. (2014). Intracellular stresses in patterned cell assemblies. *Soft Matter* *10*, 2414–

2423.

Musumeci, G., Loreto, C., Carnazza, M. L., Strehin, I., and Elisseeff, J. (2011). OA cartilage derived chondrocytes encapsulated in poly(ethylene glycol) diacrylate (PEGDA) for the evaluation of cartilage restoration and apoptosis in an in vitro model. *Histol. Histopathol.* *26*, 1265–1278.

Narula, J., Haider, N., Virmani, R., Disalvo, T. G., Kolodgie, F. D., Hajjar, R. J., Schmidt, U., Semigran, M. J., Dec, G. W., and Khaw, B. (1996). Apoptosis in myocytes in end-stage heart failure. *N. Engl. J. Med.* *335*, 1182–1189.

Nelson, C. M., Jean, R. P., Tan, J. L., Liu, W. F., Sniadecki, N. J., Spector, A. A., and Chen, C. S. (2005). Emergent patterns of growth controlled by multicellular form and mechanics. *Proc. Natl. Acad. Sci.* *102*, 11594–11599.

Ng, M. R., Besser, A., Brugge, J. S., and Danuser, G. (2014). Mapping the dynamics of force transduction at cell-cell junctions of epithelial clusters. *Elife* *3*, e03282.

Nier, V., Jain, S., Lim, C. T., Ishihara, S., Ladoux, B., and Marcq, P. (2016). Inference of Internal Stress in a Cell Monolayer. *Biophys. J.* *110*, 1625–1635.

Norbury, C. J., and Zhivotovsky, B. (2004). DNA damage-induced apoptosis. *Oncogene* *23*, 2797–2808.

Odaka, C., Sanders, M. L., and Crews, P. (2000). Jasplakinolide induces apoptosis in various transformed cell lines by a caspase-3-like protease-dependent pathway. *Clin. Diagn. Lab. Immunol.* *7*, 947–952.

Ohsawa, S., Vaughen, J., and Igaki, T. (2018). Cell extrusion: a stress-responsive force for good or evil in epithelial homeostasis. *Dev. Cell* *44*, 284–296.

Ohtsu, M. *et al.* (1997). Inhibition of apoptosis by the actin-regulatory protein gelsolin. *EMBO J.* *16*, 4650–4656.

Olivetti, G., Abbi, R., and Quaini, F. (1997). Apoptosis in the failing human heart. *N. Engl. J. Med.* *336*, 1131–1141.

Olson, E. N., and Nordheim, A. (2010). Linking actin dynamics and gene transcription to drive cellular motile functions. *Nat. Rev. Mol. Cell Biol.* *11*, 353–365.

Paoli, P., Giannoni, E., and Chiarugi, P. (2013). Anoikis molecular pathways and its role in cancer progression. *Biochim. Biophys. Acta - Mol. Cell Res.* *1833*, 3481–3498.

Parlato, S., Giammarioli, A. M., Logozzi, M., Lozupone, F., Matarrese, P., Luciani, F., Falchi, M., Malorni, W., and Fais, S. (2000). CD95 (APO-1/Fas) linkage to the actin cytoskeleton through ezrin in human T lymphocytes: a novel regulatory mechanism of the CD95 apoptotic pathway. *EMBO J.* *19*, 5123–5134.

Paul, C., Manero, F., Gonin, S., Kretz-Remy, C., Viro, S., and Arrigo, A.-P. (2002). Hsp27 as a negative regulator of cytochrome c release. *Mol. Cell. Biol.* *22*, 816–834.

Peacock, A. J., Murphy, N. F., McMurray, J. J., Caballero, L., and Stewart, S. (2007). An epidemiological study of pulmonary arterial hypertension. *Eur. Respir. J.* *30*, 104–109.

- Peitsch, M. C., Polzar, B., Stephan, H., Crompton, T., MacDonald, H. R., Mannherz, H. G., and Tschopp, J. (1993). Characterization of the endogenous deoxyribonuclease involved in nuclear DNA degradation during apoptosis (programmed cell death). *EMBO J.* *12*, 371–377.
- Perry, S. W., Norman, J. P., Barbieri, J., Brown, E. B., and Gelbard, H. A. (2011). Mitochondrial membrane potential probes and the proton gradient: a practical usage guide. *Biotechniques* *50*, 98–115.
- Peyronnet, R., Nerbonne, J. M., and Kohl, P. (2016). Cardiac mechano-gated ion channels and arrhythmias. *Circ Res.* *118*, 311–239.
- Phrommintikul, A., Tran, L., Kompa, A., Wang, B., Adrahtas, A., Cantwell, D., Kelly, D. J., and Krum, H. (2008). Effects of a Rho kinase inhibitor on pressure overload induced cardiac hypertrophy and associated diastolic dysfunction. *Am. J. Physiol. - Hear. Circ. Physiol.* *294*, 1804–1814.
- Pickup, M. W., Mouw, J. K., and Weaver, V. M. (2014). The extracellular matrix modulates the hallmarks of cancer. *EMBO Rep* *15*, 1243–1253.
- Pillai, I. C. L. *et al.* (2017). Cardiac Fibroblasts Adopt Osteogenic Fates and Can Be Targeted to Attenuate Pathological Heart Calcification. *Cell Stem Cell* *20*, 218-232.e5.
- Porter, A. G., and Jänicke, R. U. (1999). Emerging roles of caspase-3 in apoptosis. *Cell Death Differ.* *6*, 99–104.
- Proudfoot, D., Skepper, J. N., Hegyi, L., Farzaneh-Far, A., Shanahan, C. M., and Weissberg, P. L. (2001). The role of apoptosis in the initiation of vascular calcification. *Z. Kardiol.* *90*, 43–46.
- Puthalakath, H., Villunger, A., O'Reilly, L. A., Beaumont, J. G., Coultas, L., Cheney, R. E., Huang, D. C. S., and Strasser, A. (2001). Bmf: a proapoptotic BH3-only protein regulated by interaction with the myosin V actin motor complex, activated by anoikis. *Science* *293*, 1829–1832.
- Qiao, L., and Farrell, G. C. (1999). The effects of cell density, attachment substratum and dexamethasone on spontaneous apoptosis of rat hepatocytes in primary culture. *Vitr. Cell. Dev. Biol. - Anim.* *35*, 417–424.
- Reuven, N., Adler, J., Meltser, V., and Shaul, Y. (2013). The Hippo pathway kinase Lats2 prevents DNA damage-induced apoptosis through inhibition of the tyrosine kinase c-Abl. *Cell Death Differ* *20*, 1330–1340.
- Rikitake, Y., and Liao, J. K. (2005). Rho GTPases, statins, and nitric oxide. *Circ Res* *97*, 1232–1235.
- Rodriguez, K. J., Piechura, L. M., Porras, A. M., and Masters, K. S. (2014). Manipulation of valve composition to elucidate the role of collagen in aortic valve calcification. *BMC Cardiovasc. Disord.* *14*, 1–10.
- Roos, W. P., and Kaina, B. (2006). DNA damage-induced cell death by apoptosis. *Trends Mol. Med.* *12*, 440–450.
- Rowe, V. L., Stevens, S. L., Reddick, T. T., Freeman, M. B., Donnell, R., Carroll, R. C., and

- Goldman, M. H. (2000). Vascular smooth muscle cell apoptosis in aneurysmal, occlusive, and normal human aortas. *J. Vasc. Surg.* *31*, 567–576.
- Roy, S., and Nicholson, D. W. (2000). Cross-talk in cell death signaling. *J. Exp. Med.* *192*, F21–F25.
- Sendoel, A., and Hengartner, M. O. (2014). Apoptotic cell death under hypoxia. *Physiology* *29*, 168–176.
- Shaposhnikov, D., Descot, A., Schilling, J., and Posern, G. (2012). Myocardin-related transcription factor A regulates expression of Bok and Noxa and is involved in apoptotic signaling. *Cell Cycle* *11*, 141–150.
- Sisson, T. H. *et al.* (2015). Inhibition of myocardin-related transcription factor/serum response factor signaling decreases lung fibrosis and promotes mesenchymal cell apoptosis. *Am. J. Pathol.* *185*, 969–986.
- Solon, J., Levental, I., Sengupta, K., Georges, P. C., and Janmey, P. A. (2007). Fibroblast adaptation and stiffness matching to soft elastic substrates. *Biophys. J.* *93*, 4453–4461.
- Song, A. S. (2014). Thermally induced apoptosis, necrosis, and heat shock protein expression in 3D culture. *J. Biomech. Eng.* *136*, 1–10.
- Song, Y., Fu, J., Zhou, M., Xiao, L., Feng, X., Chen, H., and Huang, W. (2016). Activated Hippo/Yes-associated protein pathway promotes cell proliferation and anti-apoptosis in endometrial stromal cells of endometriosis. *J. Clin. Endocrinol. Metab.* *101*, 1552–1561.
- Sotoudeh, M., Li, Y.-S., Yajima, N., Chang, C.-C., Tsou, T.-C., Wang, Y., Usami, S., Ratcliffe, A., Chien, S., and Shyy, J. Y.-J. (2002). Induction of apoptosis in vascular smooth muscle cells by mechanical stretch. *Am. J. Physiol. Circ. Physiol.* *282*, H1709–H1716.
- Steen, R. L., and Collas, P. (2001). Mistargeting of B-type lamins at the end of mitosis: implications on cell survival and regulation of lamins A/C expression. *J. Cell Biol.* *152*, 621–626.
- Stournaras, C., Stiakaki, E., Koukouritaki, S. B., Theodoropoulos, P. A., Kalmanti, M., Fostinis, Y., and Gravanis, A. (1996). Altered actin polymerization dynamics in various malignant cell types: Evidence for differential sensitivity to cytochalasin B. *Biochem. Pharmacol.* *52*, 1339–1346.
- Streichan, S. J., Hoerner, C. R., Schneidt, T., Holzer, D., and Hufnagel, L. (2014). Spatial constraints control cell proliferation in tissues. *Proc. Natl. Acad. Sci.* *111*, 5586–5591.
- Su, B. Y., Shontz, K. M., Flavahan, N. A., and Nowicki, P. T. (2006). The effect of phenotype on mechanical stretch-induced vascular smooth muscle cell apoptosis. *J. Vasc. Res.* *43*, 229–237.
- Suria, H., Chau, L., Negrou, E., Kelvin, D., and Madrenas, J. (1999). Cytoskeletal disruption induces T cell apoptosis by a caspase-3 mediated mechanism. *Life Sci.* *65*, 2697–2707.
- Suzanne, M., and Steller, H. (2013). Shaping organisms with apoptosis. *Cell Death Differ.* *20*, 669–675.
- Tamada, M., Sheetz, M. P., and Sawada, Y. (2004). Activation of a signaling cascade by

cytoskeleton stretch. *Dev. Cell* 7, 709–718.

Tanaka, K., Sata, M., Fukuda, D., Suematsu, Y., Motomura, N., Takamoto, S., Hirata, Y., and Nagai, R. (2005). Age-associated aortic stenosis in apolipoprotein E-deficient mice. *J. Am. Coll. Cardiol.* 46, 134–141.

Tang, H. L., Yuen, K. L., Tang, H. M., and Fung, M. C. (2009). Reversibility of apoptosis in cancer cells. *Br. J. Cancer* 100, 118–122.

Tilghman, R. W., Cowan, C. R., Mih, J. D., Koryakina, Y., Gioeli, D., Slack-Davis, J. K., Blackman, B. R., Tschumperlin, D. J., and Parsons, J. T. (2010). Matrix rigidity regulates cancer cell growth and cellular phenotype. *PLoS One* 5, 1–13.

Tomasek, J. J., Gabbiani, G., Hinz, B., Chaponnier, C., and Brown, R. A. (2002). Myofibroblasts and mechanoregulation of connective tissue remodelling. *Nat. Rev. Mol. Cell Biol.* 3, 349–363.

Trepat, X., Wasserman, M. R., Angelini, T. E., Millet, E., Weitz, D. A., Butler, J. P., and Fredberg, J. J. (2009). Physical forces during collective cell migration. *Nat. Phys.* 5, 426–430.

Tsujimoto, Y. (2003). Cell death regulation by the Bcl-2 protein family in the mitochondria. *J. Cell. Physiol.* 195, 158–167.

Ulrich, T. A., de Juan Pardo, E. M., and Kumar, S. (2009). The mechanical rigidity of the extracellular matrix regulates the structure, motility, and proliferation of glioma cells. *Cancer Res.* 69, 4167–4174.

Vidyasekar, P., Shyamsunder, P., Arun, R., Santhakumar, R., Kapadia, N. K., Kumar, R., and Verma, R. S. (2015). Genome wide expression profiling of cancer cell lines cultured in microgravity reveals significant dysregulation of cell cycle and MicroRNA gene networks. *PLoS One* 10, 1–20.

Virani, S. S. *et al.* (2020). Heart Disease and Stroke Statistics—2020 Update.

Wada, K.-I., Itoga, K., Okano, T., Yonemura, S., and Sasaki, H. (2011). Hippo pathway regulation by cell morphology and stress fibers. *Development* 138, 3907–3914.

Wada, T., and Penninger, J. M. (2004). Mitogen-activated protein kinases in apoptosis regulation. *Oncogene* 23, 2838–2849.

Wang, G., Chen, W., Qu, H., and Li, X. (2009). The effect of cyclic stretch on apoptosis of human squamous carcinoma of tongue cell line Tca8113. In: *IEEE, IEEE*, 1–4.

Wang, H.-B. B., Dembo, M., and Wang, Y. L. (2000). Substrate flexibility regulates growth and apoptosis of normal but not transformed cells. *Am J Physiol Hear. Cell Physiol* 279, C1345–C1350.

Wang, K., Brems, J. J., Gamelli, R. L., and Ding, J. (2005a). Reversibility of caspase activation and its role during glycochenodeoxycholate-induced hepatocyte apoptosis. *J. Biol. Chem.* 280, 23490–23495.

Wang, P., Valentijn, A. J., Gilmore, A. P., and Streuli, C. H. (2003). Early events in the anoikis program occur in the absence of caspase activation. *J. Biol. Chem.* 278, 19917–19925.

- Wang, Y. X. *et al.* (2005b). Fasudil, a Rho-kinase inhibitor, attenuates angiotensin II-induced abdominal aortic aneurysm in apolipoprotein E-deficient mice by inhibiting apoptosis and proteolysis. *Circulation* *111*, 2219–2226.
- Watters, D. (1999). Molecular mechanisms of ionizing radiation-induced apoptosis. *Immunol. Cell Biol.* *77*, 263–271.
- Wencker, D., Chandra, M., Nguyen, K., Miao, W., Garantziotis, S., Factor, S. M., Shirani, J., Armstrong, R. C., and Kitsis, R. N. (2003). A mechanistic role for cardiac myocyte apoptosis in heart failure. *J. Clin. Invest.* *111*, 1497–1504.
- Wernig, F., Mayr, M., and Xu, Q. (2003). Mechanical stretch-induced apoptosis in smooth muscle cells is mediated by  $\beta$ 1-integrin signaling pathways. *Hypertension* *41*, 903–911.
- Wernig, F., and Xu, Q. (2002). Mechanical stress-induced apoptosis in the cardiovascular system. *Prog. Biophys. Mol. Biol.* *78*, 105–137.
- Wu, C.-C., Li, Y.-S., Haga, J. H., Kaunas, R., Chiu, J.-J., Su, F.-C., Usami, S., and Chien, S. (2007). Directional shear flow and Rho activation prevent the endothelial cell apoptosis induced by micropatterned anisotropic geometry. *Proc. Natl. Acad. Sci.* *104*, 1254–1259.
- Wu, Y., Zhao, D., Zhuang, J., Zhang, F., and Xu, C. (2016). Caspase-8 and caspase-9 functioned differently at different stages of the cyclic stretch-induced apoptosis in human periodontal ligament cells. *PLoS One* *11*, 1–15.
- Yamazaki, T., Komuro, I., Kudoh, S., Zou, Y., Nagai, R., Aikawa, R., Uozumi, H., and Yazaki, Y. (1998). Role of ion channels and exchangers in mechanical stretch-induced cardiomyocyte hypertrophy. *Circ. Res.* *82*, 430–437.
- Yeung, T., Georges, P. C., Flanagan, L. A., Marg, B., Ortiz, M., Funaki, M., Zahir, N., Ming, W., Weaver, V., and Janmey, P. A. (2005). Effects of substrate stiffness on cell morphology, cytoskeletal structure, and adhesion. *Cell Motil. Cytoskeleton* *60*, 24–34.
- Zhang, H., Pasolli, H. A., and Fuchs, E. (2011a). Yes-associated protein (YAP) transcriptional coactivator functions in balancing growth and differentiation in skin. *Proc Natl Acad Sci* *108*, 2270–2275.
- Zhang, T., Tian, F., Wang, J., Jing, J., Zhou, S. S., and Chen, Y. D. (2015). Atherosclerosis-associated endothelial cell apoptosis by MiR-429-mediated down regulation of Bcl-2. *Cell. Physiol. Biochem.* *37*, 1421–1430.
- Zhang, Y. H., Zhao, C. Q., Jiang, L. S., and Dai, L. Y. (2011b). Substrate stiffness regulates apoptosis and the mRNA expression of extracellular matrix regulatory genes in the rat annular cells. *Matrix Biol.* *30*, 135–144.
- Zhao, B. *et al.* (2007). Inactivation of YAP oncoprotein by the Hippo pathway is involved in cell contact inhibition and tissue growth control. *Genes Dev.* *21*, 2747–2761.
- Zhao, T., Tang, X., Umeshappa, C. S., Ma, H., Gao, H., Deng, Y., Freywald, A., and Xiang, J. (2016). Simulated microgravity promotes cell apoptosis through suppressing Uev1A/TICAM/TRAF/NF- $\kappa$ B-regulated anti-apoptosis and p53/PCNA- and ATM/ATR-Chk1/2-controlled DNA-damage response pathways. *J. Cell. Biochem.* *2148*, 2138–2148.

Zhong, Y., Kong, D., Dai, L., and Ji, B. (2011). Frequency-dependent focal adhesion instability and cell reorientation under cyclic substrate stretching. *Cell. Mol. Bioeng.* 4, 442–456.

## Chapter 3: Cells on Soft Substrates Exhibit Partial Strain Avoidance and Reduction in Apoptosis after Stretch-induced Spreading

Zachary E. Goldblatt<sup>1</sup>, Monica Leigh Whitehorn<sup>1</sup>, Kristen L. Billiar<sup>1</sup>

Department of Biomedical Engineering, Worcester Polytechnic Institute, Worcester, MA

### 3.0 Abstract

Cells actively sense and adapt to their mechanical environment by changing their cytoskeletal structure, adhesions, and gene expression. It is well documented that cells cultured on high modulus (stiff) substrates reorient away from the direction of stretch, presumably to regain their homeostatic cytoskeletal tension state. In contrast, cells on very low modulus (soft) substrates appear unable to spread and generate tension and have been shown to have weaker focal adhesions, fewer stress fibers, and a higher propensity for apoptosis. Although we previously demonstrated that cells on soft substrates spread out in response to cyclic stretch, little has been reported as to the effects of soft substrates on strain avoidance and rates of apoptosis in cells. The goal of this work is to determine the effect of cyclic stretch on the ability of cells to reorient and survive when cultured on soft substrates, and what happens when the external stretch is removed. We find that in response to stretch, cells on soft (1.2 kPa) substrates are able to spread out (doubling area to  $\sim 800 \mu\text{m}^2$ ) parallel to stretch and then reorient away from the direction of stretch to  $75^\circ \pm 28^\circ$ , which is much less than those on stiff substrates ( $87^\circ \pm 18^\circ$ ). After cessation of stretch, cells revert to their initial rounded state ( $\sim 400 \mu\text{m}^2$ ) within 2 hours. Additionally, we find that mechanically stretching cells on soft substrates greatly decreases occurrences of apoptosis to  $\sim 7\%$  compared to  $\sim 20\%$  for static controls. Combined, these data indicate that mechanical stretch provides sufficient external resistance to cell-generated forces allowing cells to remodel their cytoskeleton which increases cell survival.

### 3.1 Introduction

Cells reorganize their cytoskeleton in response to external mechanical signals in order to achieve and maintain a desired “homeostatic” level of internal tension. A tension state deviating from this desired set point can lead to programmed cell death, or apoptosis (Wang *et al.*, 2000; Ingber, 2003). Apoptosis is a highly conserved process required for the continued health of an organism, but dysregulation of this process can lead to a variety of diseases. Therefore, identifying the key regulators of apoptosis could have important implications for disease prevention and treatment. Cell death can be initiated by the external mechanical environment directly or indirectly. Physical stimuli, including external loading of adhesion ligands, environmental stiffness, matrix fiber alignment, shear flow, and forces at cell-cell contacts can directly influence apoptosis-mediate pathways (Orr *et al.*, 2006; Jaalouk and Lammerding, 2009; Humphrey *et al.*, 2014). Alternatively, there is also strong evidence that internal cell tension, arising from the external environment, influences mechanotransduction pathways responsible for cell health. However, in both cases, the underlying mechanisms of cell tension and specific mechanical triggers that drive apoptosis remain unknown.

The elastic modulus of the extracellular matrix is a relatively simple, static stimulus that has been shown to influence internal cell tension through cytoskeletal organization in controlled, experimental systems. Cells cultured on high-modulus (stiff) substrates have low instances of apoptosis (Wang *et al.*, 2000). Additionally, cells on stiff substrates spread out and elongate, and generate strong focal adhesions, defined stress fibers, and high traction forces, all of which are associated with favorable cell health (Rape *et al.*, 2011; Mih *et al.*, 2012). Cells also generally show nuclear localization of specific mechanosensitive proteins (indicative of pro-survival), such as yes-associated-protein (YAP) and myocardin-related transcription factor A (MRTF-A) (Seo *et al.*, 2020). In contrast, very low-modulus (soft) substrates do not offer sufficient resistance to cells pulling on the substrate, resulting in internal cell tension below homeostatic values and higher instances of apoptosis (Tilghman *et al.*, 2010; Zhang *et al.*, 2011b; Leight *et al.*, 2012). Cells cultured on soft substrates are not able to spread out and remain small and rounded, which is associated with low cell tension and poor cell health. These cells have weak focal adhesions, lack stress fibers, and generate low traction forces. Additionally, they have predominantly

cytoplasmic localization of YAP and MRTF-A (Wang *et al.*, 2000). These outcomes are similar to what is found in geometrically restricted cells in small microcontact printed patterns, which reveals that soft substrates and small micropatterns act as similar environmental conditions that induce the same cellular behavior (Chen *et al.*, 1997; Oakes *et al.*, 2014).

While challenging to implement experimentally, it is important to understand how the addition of dynamic stimuli such as cyclic stretch interact with stiffness in the regulation of apoptosis. When exposed to cyclic stretch, cells on stiff substrates generally reorient away from the direction of stretch. This strain avoidance is hypothesized to be an adaptive mechanism by which cells bring their tension back toward homeostatic levels, which limits occurrences of apoptosis (Brown *et al.*, 1998; Kaunas *et al.*, 2005; De *et al.*, 2007; Zhong *et al.*, 2011). When cells do not reorient away from stretch, such as when they are biaxially stretched or micropatterned, instances of apoptosis increases, supporting that cells save themselves by reorienting (Rannou *et al.*, 2004; Zhang *et al.*, 2011a; Abbott *et al.*, 2012). While this reorientation response is well characterized for cells on stiff substrates, the effect of stretching cells on soft substrates is not well documented or understood. It is possible that cells on soft substrates, which experience unfavorably low cell tension in static culture, may respond favorably to the introduction of mechanical stretch. We have previously shown that cells on soft substrates elongate away from the direction of stretch and increase traction force generation when cyclically stretched over 24 hr (Cirka *et al.*, 2016). However, we did not yet characterize this behavior over time in individual cells nor measure cell death. Sheetz and colleagues have shown stretching cells can induce activation of YAP and MRTF-A (translocation to nucleus), while stopping stretch deactivates YAP and MRTF-A (re-localization to cytoplasm) (Cui *et al.*, 2015). The behavior of YAP and MRTF-A in these conditions are indicative of an increase in cell tension and health when cyclically stretched, while static conditions decreased cell tension and health.

The purpose of this study was to examine the influence of cyclic stretch and substrate modulus on cell reorientation and survival. We hypothesize that cells respond to their mechanical environment to optimize intracellular tension, and that insufficient or excessive mechanical feedback causes cytoskeletal depolymerization, triggering apoptosis. Cells undergoing six hours of uniaxial stretch followed by six hours of static culture were compared to statically cultured

cells on stiff and soft substrates. The temporal influence of stretch and cessation of stretch on cellular reorientation was measured using time-lapse microscopy. Apoptosis was measured to determine the effect of these cellular behaviors on cell health. This work studies cellular responses to mechanical forces and characterizes the relationship between tension homeostasis and apoptosis.

## 3.2 Materials and Methods

### 3.2.1 Cell Culture

Valvular interstitial cells (VICs) isolated from porcine aortic heart valve leaflets were obtained from a local abattoir (Blood Farm, Groton, MA) using previous protocols (Gould and Butcher, 2011). Porcine VICs are relevant for aortic valve disease research, as they act similarly to their human complement, such as where apoptosis is implicated. VICs were maintained in Dulbecco's Modified Eagle Medium (DMEM; 4.5g/L glucose; Life Technologies, Grand Island NY), supplemented with 10% fetal bovine serum (FBS; GE Healthcare HyClone, Logan, UT), and 1% antibiotic-antimycotic (10,000 units/mL penicillin, 10,000  $\mu\text{g}/\text{mL}$  streptomycin, 25  $\mu\text{g}/\text{mL}$  Amphotericin B; Life Technologies). Cells were seeded at a density of 7800 cells/cm<sup>2</sup> and cultured at 37°C and 5% CO<sub>2</sub> for 18 hr before running experiments. Cells from passages 2–10 were used for all experiments

### 3.2.2 Polyacrylamide Hydrogel Preparation

Polyacrylamide (PA) hydrogels were prepared with a low modulus (“soft,” 1.2 kPa, 12%:0.12% acrylamide:bisacrylamide) and high modulus (“stiff,” 38.4 kPa, 3%:0.1% acrylamide:bisacrylamide) using previous polymerization methods (Throm Quinlan *et al.*, 2011). PA gels were attached to stretchable Elastasil silicone wells (CellScale) for time-lapse cyclical stretching experiments. Briefly, wells were plasma treated in a plasma cleaner for 2 min. Wells were then bathed in a silane (1% aminopropyl trimethoxysilane) solution followed by a 0.5% glutaraldehyde solution for 5 min each. After drying the wells with N<sub>2</sub> gas, 4  $\mu\text{L}$  of prepared PA gel were pipetted onto the middle of each well, and a 5 mm round coverslip was placed on top. Gels were allowed to polymerize under N<sub>2</sub> gas for 90 min and were then soaked in DI water for

60 min before removing the glass coverslip. To allow cell adhesion, PA gels were activated with 0.5 mg/mL sulfo-SANPAH (Thermo Fisher, Waltham, MA), and then coated with 200  $\mu$ g/mL of rat tail collagen Type I (Corning, Bedford, MA) overnight at 4 °C. Gels were then sterilized by treatment with PBS with antibiotics for 24 hr, and cells were seeded the following day.

### 3.2.3 Cyclical Stretching Time-lapse Microscopy

A high-throughput uniaxial stretching device (CellScale; MCFX) with 16-well elastomeric culture plates (CellScale; Elastosil) were used to cyclically stretch cells with uniform pure uniaxial strain fields. Cells were cultured overnight and stretched the next day following a triangular waveform at 5% or 10% uniaxial strain at 1 Hz. Time-lapse phase-contrast imaging was performed on a Zeiss Axiovert 200M inverted microscope equipped with an AxioCam MRm camera (1.4 MP, 1388 X 1040 pixels). Images were obtained at 15 min intervals for 12 hr at x10 magnification. Unless noted, after 6 hr of dynamic stretch, the motor was halted at zero strain and the cells were cultured statically an additional 6 hr to determine if cellular behaviors revert to that of the static control. Cells were maintained in a temperature-regulated and humidified incubator on the microscope in CO<sub>2</sub>-free Leibovitz's L-15 media (Life Technologies, Grand Island NY), supplemented with 10% FBS, 0.45% glucose, and 1% antibiotic-antimycotic. Static control cells were cultured on PA gels polymerized on glass coverslips using previous methods (Cirka *et al.*, 2017). These cells were not stretched and were analyzed at the same time points under the same conditions. All image analysis was performed using ImageJ (version 1.49, National Institutes of Health, Bethesda, MD).

### 3.2.4 Traction Force Microscopy

Plasma-treated glass coverslips were coated uniformly with a 0.2  $\mu$ m fluorescent bead solution (Life Technologies). Fluorescent beads were transferred from coated coverslips onto prepared PA gels as previously described (Cirka *et al.*, 2016). Phase-contrast and fluorescent images of single cells were taken over the course of the entire time-lapse. After the completion of the time-lapse, cells were imaged after trypsinization for undeformed gel bead pattern. Substrate traction data were obtained by stress calculation in ANSYS (Ansys Inc., Canonsburg, PA) (modulus: 1.2 kPa, 38.4 kPa; Poisson ratio: 0.4; material property: linear elastic) from displacement fields

computed from mass particle image velocimetry from a custom MATLAB code (Cirka *et al.*, 2016).

### 3.2.5 Immunofluorescence

For apoptosis experiments, CellEvent Caspase-3/7 reagent (Thermo Fisher) was added to cell culture wells and allowed to incubate for 1 hr prior to stretching and imaging. Phase-contrast and fluorescent imaging was performed over the course of the time-lapse.

## 3.3 Results

### 3.3.1 Cells stretched on stiff substrates exhibit strain avoidance behavior

VICs on stiff substrates (38.4 kPa) are thought to obtain homeostatic tension in static conditions, indicated by traction force generation reaching a steady state with increasing substrate stiffness (Ghibaudo *et al.*, 2008). Cells are initially spread out and oriented in random directions.

Introducing 10% mechanical strain via cyclic stretch causes cells to remodel their cytoskeleton to reorient and elongate along the perpendicular direction of stretch to reduce the input of stress (Figure 3.1A). Studying cell morphology over time revealed that cell area decreases when stretched, compared to static controls (Figure 3.1B). Additionally, stretched cells have slightly higher aspect ratios and very similar circularity values compared to control cells (Figure 3.1, C and D). Based on their initial orientation, individual cells respond differently to the input of stretch; however, over time, cells collectively begin to reorient orthogonally to the direction of stretch shortly after stretch is introduced (Figure 3.1E).

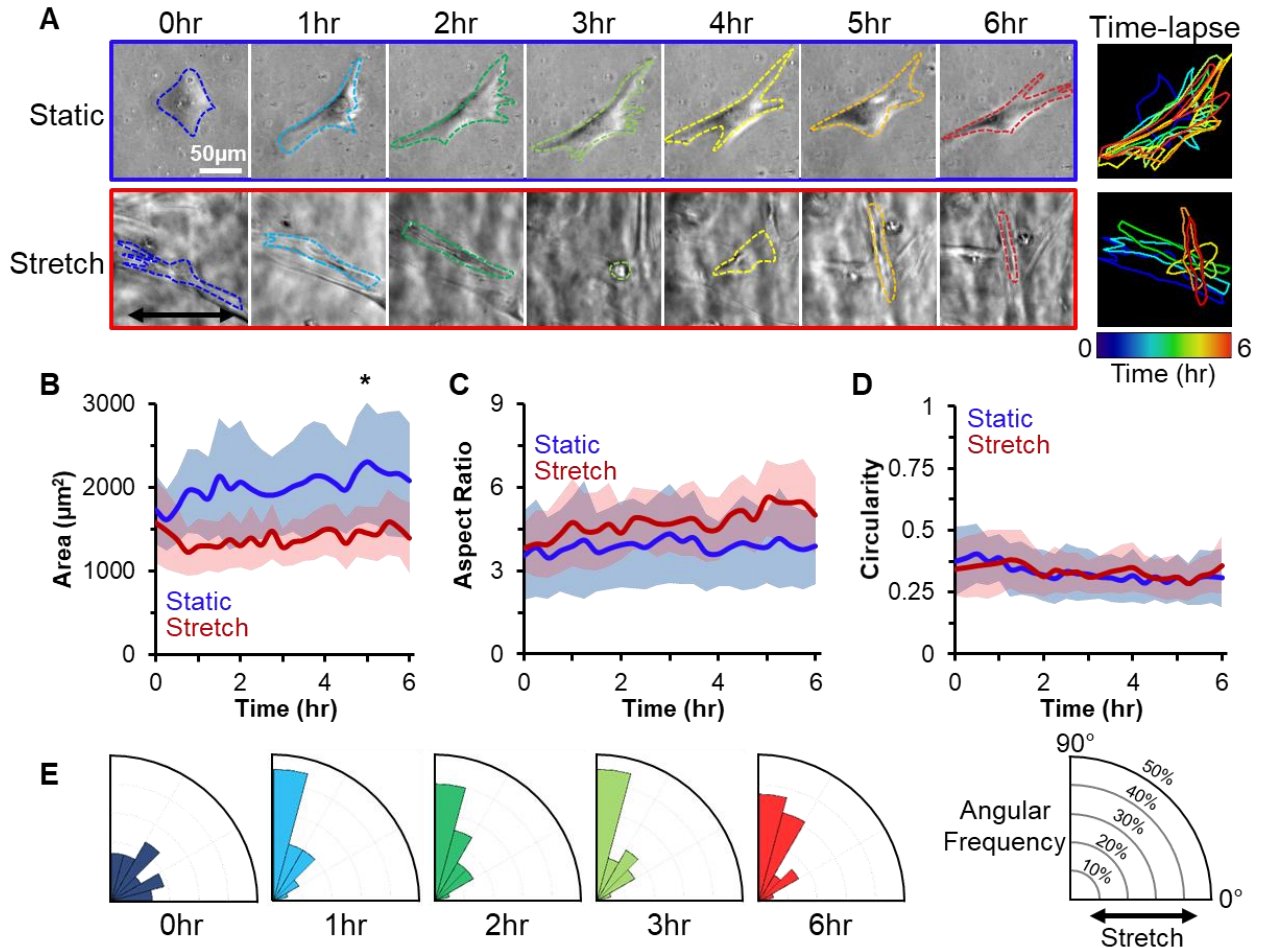


**Figure 3.1: Cells on stiff gels are spread out and then reorient away from direction of stretch when introduced to 10% mechanical stretch.** **A)** Representative time-lapse image series of static and stretched cells. Cell contours from 0-6 hr were color coded and overlaid. Arrow indicates direction of mechanical stretch. Scale bar = 50  $\mu\text{m}$ . Change in **(B)** average cell area ( $\pm\text{SE}$ ), **(C)** average aspect ratio ( $\pm\text{SE}$ ), and **(D)** average cell circularity ( $\pm\text{SE}$ ) with respect to time for static (blue) and stretched (red) cells.  $N = 20$  cells (3 replicates). **E)** Circular histograms showing distribution of cellular alignment over time. Cells begin normally distributed and quickly reorient perpendicular to the direction of stretch. Direction of stretch is parallel to  $0^\circ$ . \* $p < 0.05$  (5 hr Area) for two-way ANOVA with Tukey post-hoc test between static and stretch conditions.

### 3.3.2 Cells stretched on soft substrates display partial avoidance behavior

Contrary to cells on stiff gels, cells on very soft gels (1.2 kPa) start off small and rounded, which is indicative of cells having low internal tension levels. Roughly 35% ( $\pm 10\%$ ) of cells respond to mechanical stretch while the remaining proportion of cells remain balled up. The heterogeneity in cell behaviors in response to stretch may be due to differences in innate cell properties, which

can lead to the reduction in the ability of the other 65% of cells to respond to mechanical stretch when on very soft substrates. Here, we focus on cells that respond to the mechanical stimulus. These cells are able to elongate and spread out in response to 10% cyclical stretch over time (Figure 3.2A). Time-lapse images of cell morphology over time show that, for the cells which responded, the cell area on average significantly increases when stretched, compared to static controls, which maintain a constant cell area on average (Figure 3.2B). Additionally, over six hours, cells elongate and significantly increase in aspect ratio and significantly decrease in circularity when stretched; static cells retain a constant aspect ratio and circularity at nearly one (Figure 3.2, C and D). Once cyclic stretching begins, the average cell population begins to spread out parallel to the direction of stretch before reorienting to an angle substantially less than perpendicular, or roughly  $50\text{-}60^\circ$  from the direction of stretch (Figure 3.2E). Cells that initially spread out towards that intermediate angle remain elongated in that direction.

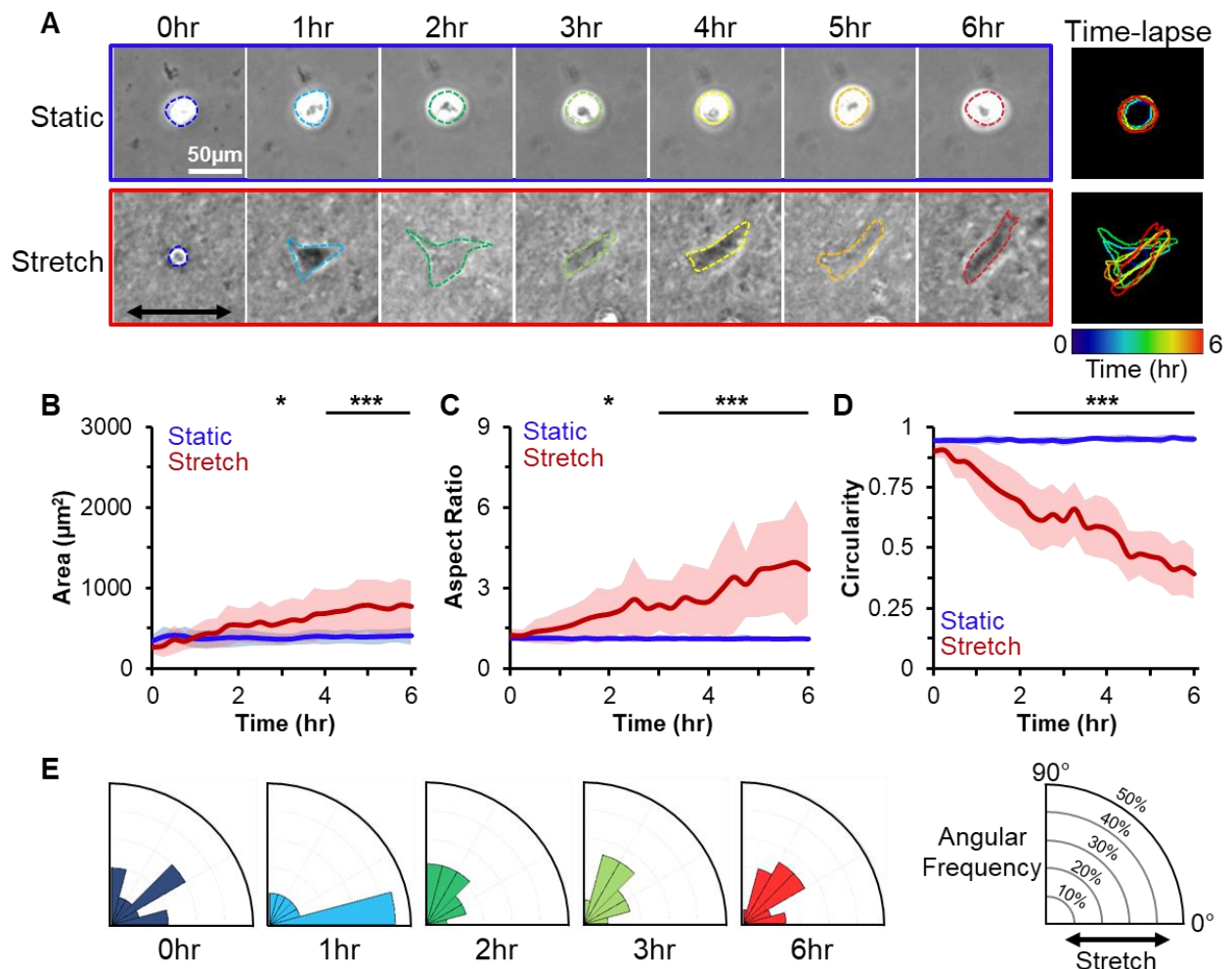


**Figure 3.2: Cells on soft gels are rounded and then elongate after introduced to 10% mechanical stretch.** **A)** Representative time-lapse image series of static and stretched cells. Cell contours from 0-6 hr were color coded and overlaid. Arrow indicates direction of mechanical stretch. Scale bar = 50  $\mu\text{m}$ . Change in **(B)** average cell area ( $\pm\text{SE}$ ), **(C)** average aspect ratio ( $\pm\text{SE}$ ), and **(D)** average cell circularity ( $\pm\text{SE}$ ) with respect to time for static (blue) and stretched (red) cells.  $N = 20$  cells (3 replicates). **E)** Circular histograms showing distribution of cellular alignment over time. Cells begin normally distributed and reorient towards the direction of stretch before reorienting away from stretch. Direction of stretch is parallel to  $0^\circ$ . \* $p < 0.05$  (3 hr Area, 2 hr AR) and \*\*\* $p < 0.001$  (4-6 hr Area, 3-6 hr AR, 2-6 hr Circ) for two-way ANOVA with Tukey post-hoc test between static and stretch conditions.

To further test the effects of cyclic stretch on cells on soft substrates, we lowered the mechanical strain applied to cells from 10% to 5% strain to see if cells would generate lower internal tension and spread out more parallel to the direction of stretch. We did not find any discernable differences between 10% and 5% strain. Both strains had similar significant increases in area and aspect ratio, a significant decrease in circularity, and realignment away from the direction of stretch (Figure 3.3).

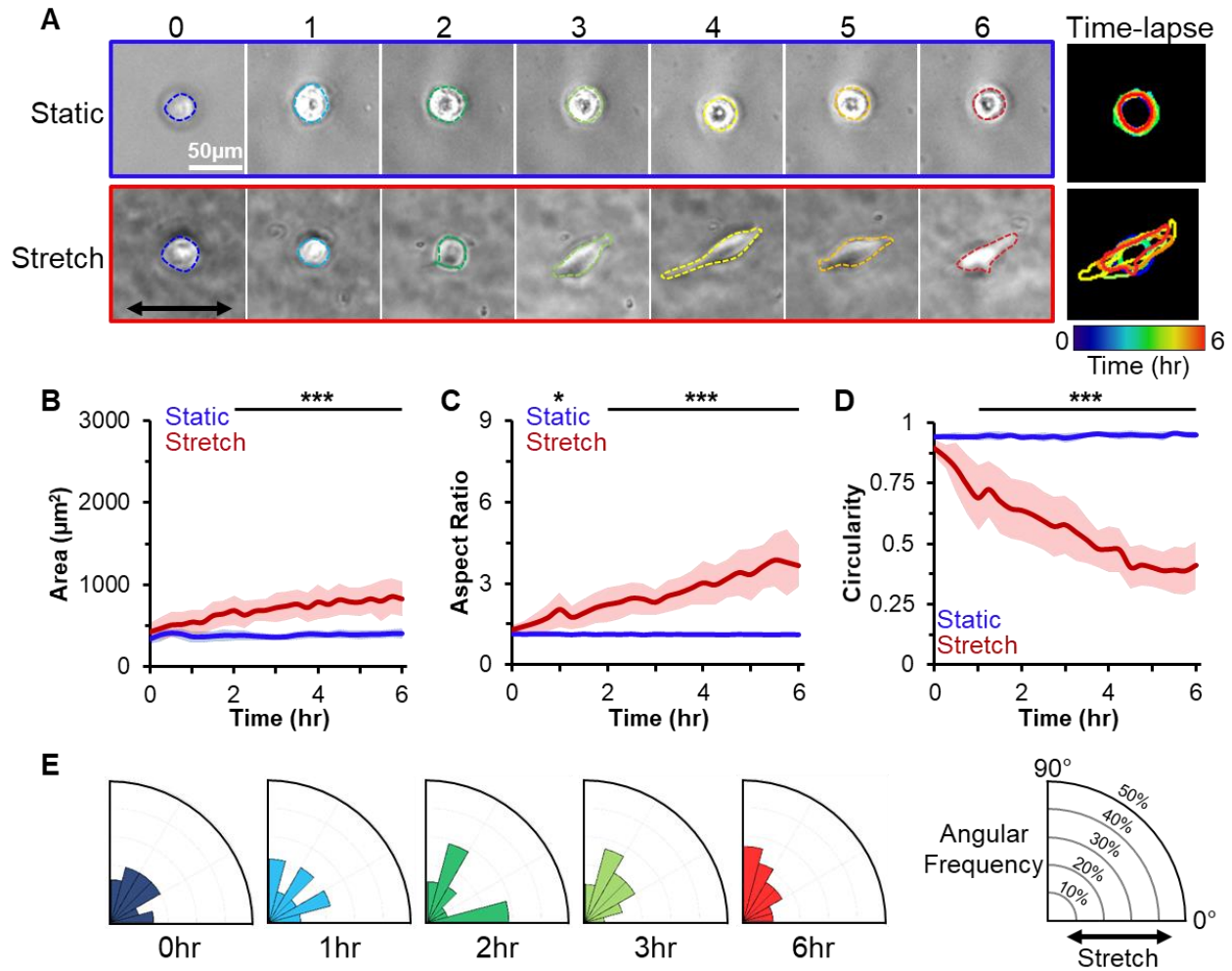


**Figure 3.3: Cells on soft gels are rounded and then elongate after introduced to 5% mechanical stretch.** A) Representative time-lapse image series of static and stretched cells. Cell contours from 0-6 hr were color coded and overlaid. Arrow indicates direction of mechanical stretch. Change in (B) average cell area ( $\pm$ SE), (C) average aspect ratio ( $\pm$ SE), and (D) average cell circularity ( $\pm$ SE) with respect to time for static (blue) and stretched (red) cells. N=20 cells (3 replicates). E) Circular histograms showing distribution of cellular alignment over time. Cells begin normally distributed and reorient towards the direction of stretch before reorienting perpendicular. Direction of stretch is parallel to 0°. \* $p < 0.05$  (2 hr AR) and \*\*\* $p < 0.001$  (2-6 hr Area, 2-6 hr AR, 1-6 hr Circ) for two-way ANOVA with Tukey post-hoc test between static and stretched conditions.

### 3.3.3 Cells reach steady state behavior after continuous cyclical stretch

Cells were stretched for 12 hr to determine if cell morphology parameters reach a steady state. Over time, cells continuously change their morphology which contributes to the fluctuations seen in average spread area, aspect ratio, and circularity. However, after 6 hr of continuous stretch, these measurements begin to level off and no longer change drastically with time (Figure 3.4A, B, and C). To calculate when steady state occurs, these data were fit with the exponential function,

$Ae^{Bx} + C$ , where  $A$ ,  $B$ , and  $C$  are constants that were mathematically determined to best fit the data (Figure 3.5). From this exponential relation, we calculated the theoretical steady state for each cell measurement. By 12 hr, cells have reached >89% of the predicted steady state value for each cell measurement (Table 3.1).

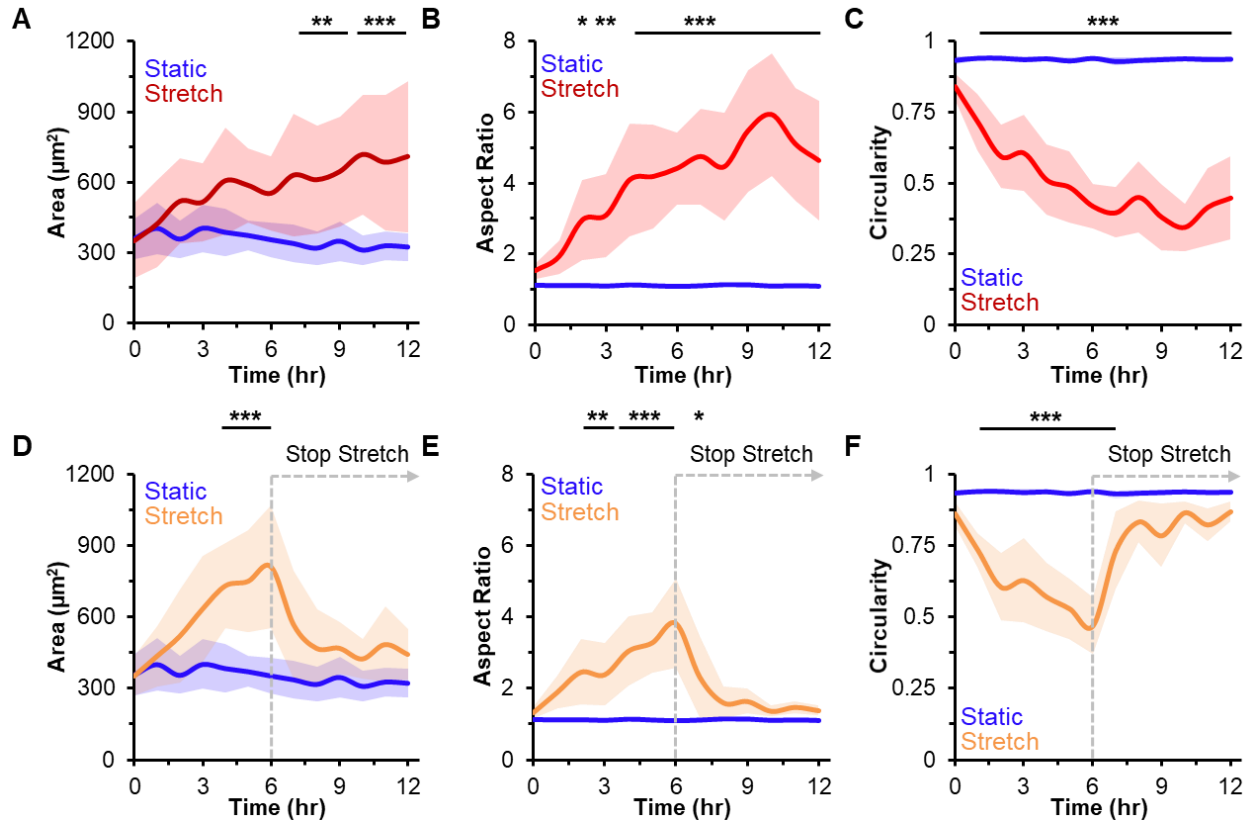


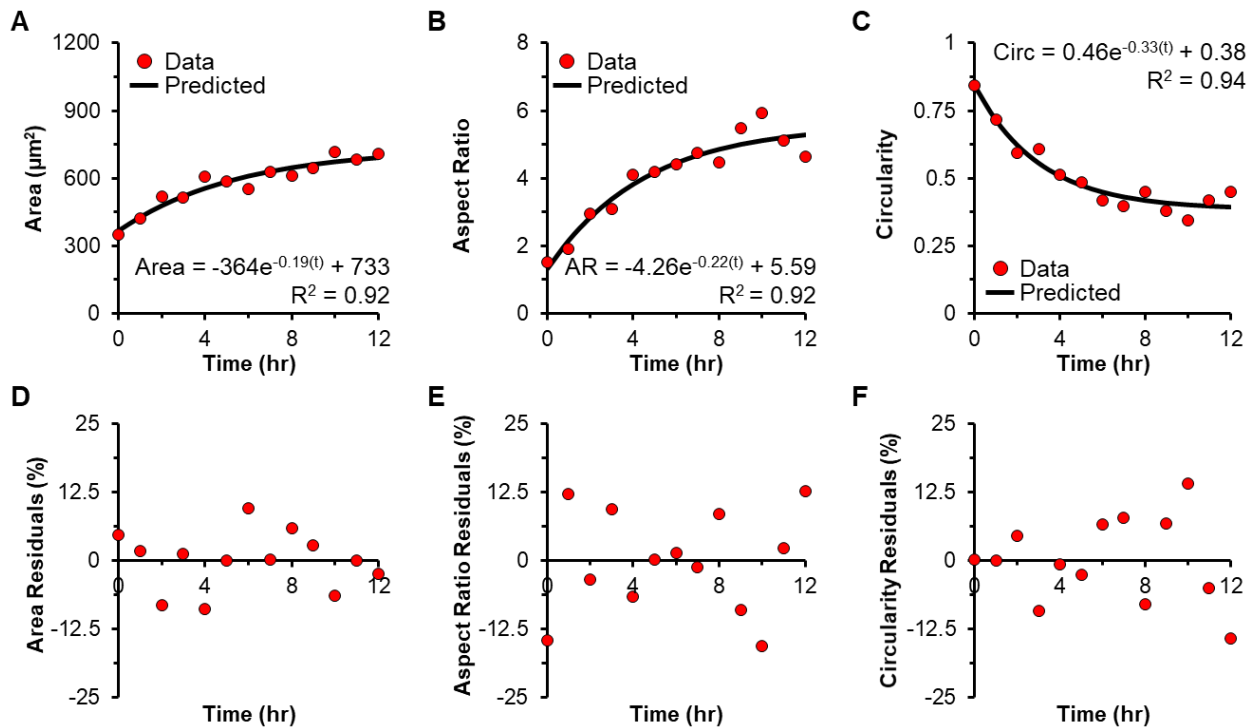
**Figure 3.4: Cyclic stretch directly influences changes in cell behavior when on soft gels. When that stimulus is removed, cells revert to previous behavior.** Change in average cell area (A), aspect ratio (B), and circularity (C) over time for static (blue) and cyclically stretched (red) cells over 12 hr of continuous stretching. Steady state behavior is achieved by 12 hr.  $N = 20$  cells (3 replicates). Change in average cell area (D), aspect ratio (E), and circularity (F) over time for static (blue) and cyclically stretched (orange) cells for 6 hr of stretch and 6 hr of no stretch. Dotted gray line indicates where stretch was stopped. After 2 hr of newly static conditions (after cessation of stretch), cells revert to almost initial state.  $N = 15$  cells (2 replicates). Top: \* $p < 0.05$  (1 hr AR), \*\* $p < 0.01$  (7-8 hr Area, 2 hr AR), and \*\*\* $p < 0.001$  (9-12 hr Area, 3-12 hr AR, 1-12 hr Circ) for two-way ANOVA with Tukey post-hoc test between static and stretch conditions. Bottom: \* $p < 0.05$  (7 hr AR), \*\* $p < 0.01$  (2-3 hr AR), and \*\*\* $p < 0.001$  (4-6 hr Area, 4-6 hr AR, 1-7 hr Circ) for two-way ANOVA with Tukey post-hoc test between static and stretch conditions.

**Table 3.1:** Time required to reach specified time constants for area, aspect ratio, and circularity after 12 hr of stretch (top). Percent of theoretical steady state reached after 6 hr and 12 hr of stretch for area, aspect ratio, and circularity (bottom).

		Time (hr) for Outcome to Reach Time Constant Value		
Time Constant (% of Limit)		Area	Aspect Ratio	Circularity
$0.7 \cdot \tau$	(50.3%)	3.84	3.15	2.14
$1 \cdot \tau$	(63.2%)	5.50	4.51	3.06
$2 \cdot \tau$	(86.5%)	11.01	9.02	6.12
$3 \cdot \tau$	(95%)	16.47	13.50	9.16

		Percent (%) of Steady State Reached		
Time		Area	Aspect Ratio	Circularity
6 hr Stretch		66%	74%	86%
12 hr Stretch		89%	93%	98%



**Figure 3.5: Changes in cell behavior over 12 hr of continuous cyclical stretching.** Predicted best fit (black line) vs data (red dot) for average cell area (A), aspect ratio (B), and circularity (C) with respect to time follow the exponential relationship  $Ae^{Bx} + C$ . Over time, a steady state limit is reached for a maximum area and aspect ratio and minimum circularity. Residuals (percent difference between experimental and predicted value) for cell area (D), aspect ratio (E), and circularity (F) reveal that the exponential function forms a strong correlation with the data. N = 20 cells (3 replicates).

### 3.3.4 Cells revert to initial state when continuous mechanical stimulus is removed

Stopping cyclic stretch of cells on stiff substrates results in a reversion of cell behavior back to its initial state, such as when traction forces recover to baseline pre-stretch values (Krishnan *et al.*, 2009, 2012). We next set out to answer the question of what would happen to cells on soft substrates when the external stretch stimulus is removed. Once stretch is removed, cells return to their original state within 2 hr having low spread area and aspect ratio and high circularity once again (Figure 3.4, D, E, and F). To calculate when steady state of reversion occurs, these data were also fit with the exponential function,  $Ae^{Bx} + C$ , with constants  $A$ ,  $B$ ,  $C$  determined for the best fit (Figure 3.6). After calculating the theoretical steady state for each cell measurement, we found that cells reached >92% of the predicted steady state by 2 hr, while after 6 hr, cells reached the steady state value (Table 3.2).

**Table 3.2:** Time required to reach specified time constants for area, aspect ratio, and circularity after 6 hr of static conditions (after 6 hr of stretch) (top). Percent of theoretical steady state reached after 2 hr and 6 hr of static conditions for area, aspect ratio, and circularity (bottom).

	<b>Time (hr) for Outcome to Reach Time Constant Value</b>		
<b>Time Constant (% of Limit)</b>	<b>Area</b>	<b>Aspect Ratio</b>	<b>Circularity</b>
<b>0.7 · τ</b> (50.3%)	0.58	0.68	0.56
<b>1 · τ</b> (63.2%)	0.83	0.97	0.81
<b>2 · τ</b> (86.5%)	1.67	1.95	1.62
<b>3 · τ</b> (95%)	2.49	2.91	2.42
<b>Percent (%) of Steady State Reached</b>			
<b>Time</b>	<b>Area</b>	<b>Aspect Ratio</b>	<b>Circularity</b>
<b>2 hr Static</b>	95%	92%	97%
<b>6 hr Static</b>	100%	100%	100%

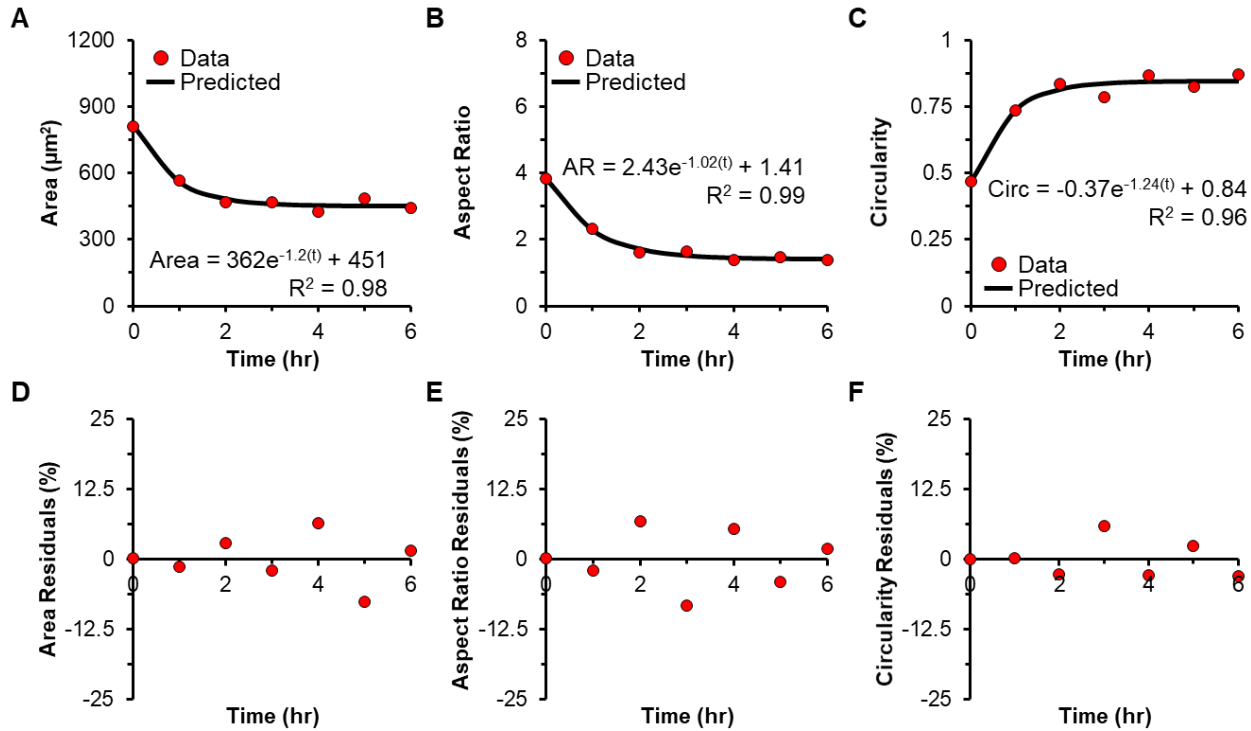


**Figure 3.6: Changes in cell behavior over 6 hr after stretch cessation.** Cells were stretched for 6 hr and then left in static conditions for another 6 hr (time 0). Predicted best fit (black line) vs data (red dot) for average cell area (A), aspect ratio (B), and circularity (C) with respect to time follow the exponential relationship  $Ae^{Bx} + C$ . Over time, a steady state limit is reached for a minimum area and aspect ratio and maximum circularity. Residuals (percent difference between experimental and predicted value) for cell area (D), aspect ratio (E), and circularity (F) reveal that the exponential function forms a strong correlation with the data. N = 15 cells (2 replicates).

### 3.3.5 Cyclic stretch decreases apoptosis in cells on soft substrates

Cells cultured statically on stiff substrates have very low instances of apoptosis over 12 hr. Additionally, cells on stiff substrates exposed to 6 hr of 10% stretching followed by 6 hr of static culture also have low instances of apoptosis (Figure 3.7A). On the other hand, cells cultured statically on soft substrates exhibit much higher proportions of apoptosis compared to cells on stiff substrates. Cyclic stretching of cells for 6 hr significantly reduces the proportion of caspase-positive cells observed (Figure 3.7B). When mechanical strain was removed, apoptosis rates increase back towards initial values.

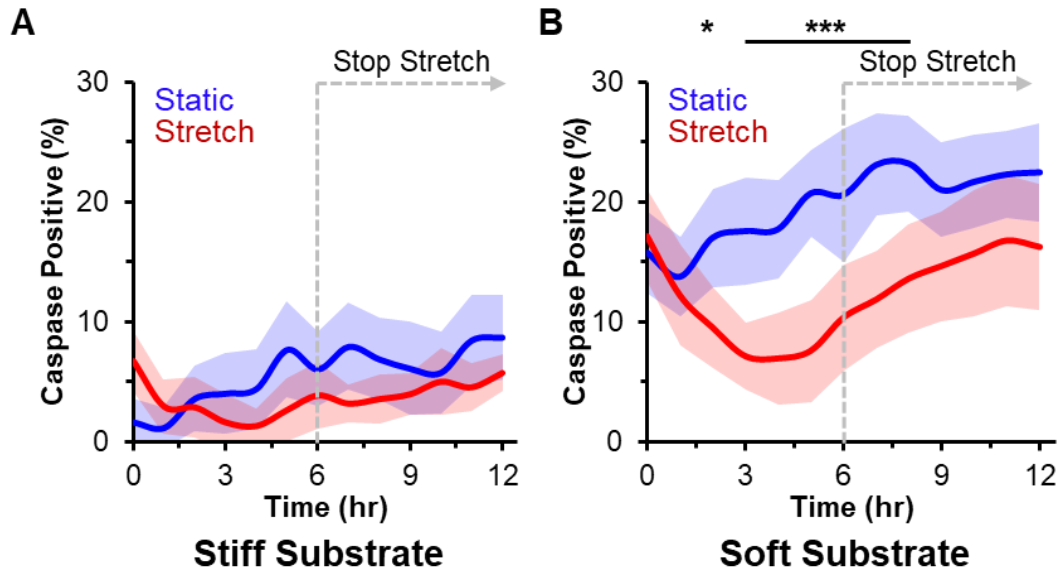


**Figure 3.7: Changes in apoptosis due to cyclic stretch depend on substrate stiffness.** Mechanical stretch causes little changes in caspase activity in cells on (A) stiff gels compared to the large decrease in apoptosis in cells on (B) soft gels. When stretch is removed after 6 hr, caspase activity increases again but to levels less than static controls. N = 15 cells (Stretch: 2 replicates, Static: 3 replicates). \* $p < 0.05$  (2 hr) and \*\*\* $p < 0.001$  (3-8 hr) for two-way ANOVA with Tukey post-hoc test between static and stretch conditions.

### 3.4 Discussion

In this study, we show that external cyclic stretch provides sufficient mechanical input to cells cultured on very soft substrates to allow them to spread and reorient, increase cell-generated tension, and decrease their instances of apoptosis. Contrary to other studies that have found stretching cells on soft gels led to parallel alignment, we find that cyclically stretching cells on soft substrates enables cells to elongate parallel to stretch before reorienting away from stretch. Previous studies differ from ours as cells are stretched for shorter time durations, at different strain rates, or on different substrate types, all of which can lead to the differences found in cellular reorientation angle. The behavior of cells cultured on soft substrates is distinctly different than cells cultured on stiff substrates which are able to generate sufficient tension to avoid apoptosis without stretch. In agreement with previous experimental studies and models, with cyclic stretch, these cells reorient perpendicular to the direction of stretch to maintain desired levels of tension and survive. Here, we measure individual cells over time under continuous cyclical stretch to determine its effects on cytoskeletal remodeling, cellular reorientation, and subsequent cell survival.

### 3.4.1 Mechanism behind cell reorientation in response to cyclic stretch

Cell health can be represented as a U-shaped curve, where the minimum represents the most stable state of cellular tension and cytoskeletal stability as well as maximum cell survival (Figure 3.8). Both high and low levels of tension can adversely affect cells and induce apoptosis (Mayr *et al.*, 2000; Wang *et al.*, 2000; Sotoudeh *et al.*, 2002; Hsieh and Nguyen, 2005). Cells cultured on stiff substrates exist at the minimum of this curve, where they are capable of establishing and sustaining homeostatic tension via mature focal adhesions and reinforced stress fibers. An input of external stress, such as from cyclic stretch, can cause cells to move to the right of the curve (high internal tension) and cause rupturing of focal adhesions and stress fiber disassembly (Figure 3.8, Figure 3.9). Cells undergo a fiber disassembly before reinforcing stress fibers in the direction of minimal stress (Krishnan *et al.*, 2009, 2012). This facilitates cell reorientation away from the direction of stretch, thereby reestablishing desired levels of tension. Apoptosis can increase if cells remain in this high-tension state (Rannou *et al.*, 2004; Zhang *et al.*, 2011a; Abbott *et al.*, 2012). Cells cultured on soft substrates naturally have low levels of internal tension and fall on the left side of the tension curve. Cells in these conditions have unstable stress fibers, immature focal adhesions, and a higher propensity for apoptosis (Tilghman *et al.*, 2010; Zhang *et al.*, 2011b; Leight *et al.*, 2012). Cyclic stretch causes cells to proceed to the right on the tension curve towards homeostatic levels, which promotes stress fiber formation, focal adhesion maturation, and cell survival (Figure 3.8, Figure 3.9). If internal tension continues to build, then cells will reorient towards a direction of optimal stress to reestablish desired levels of tension.

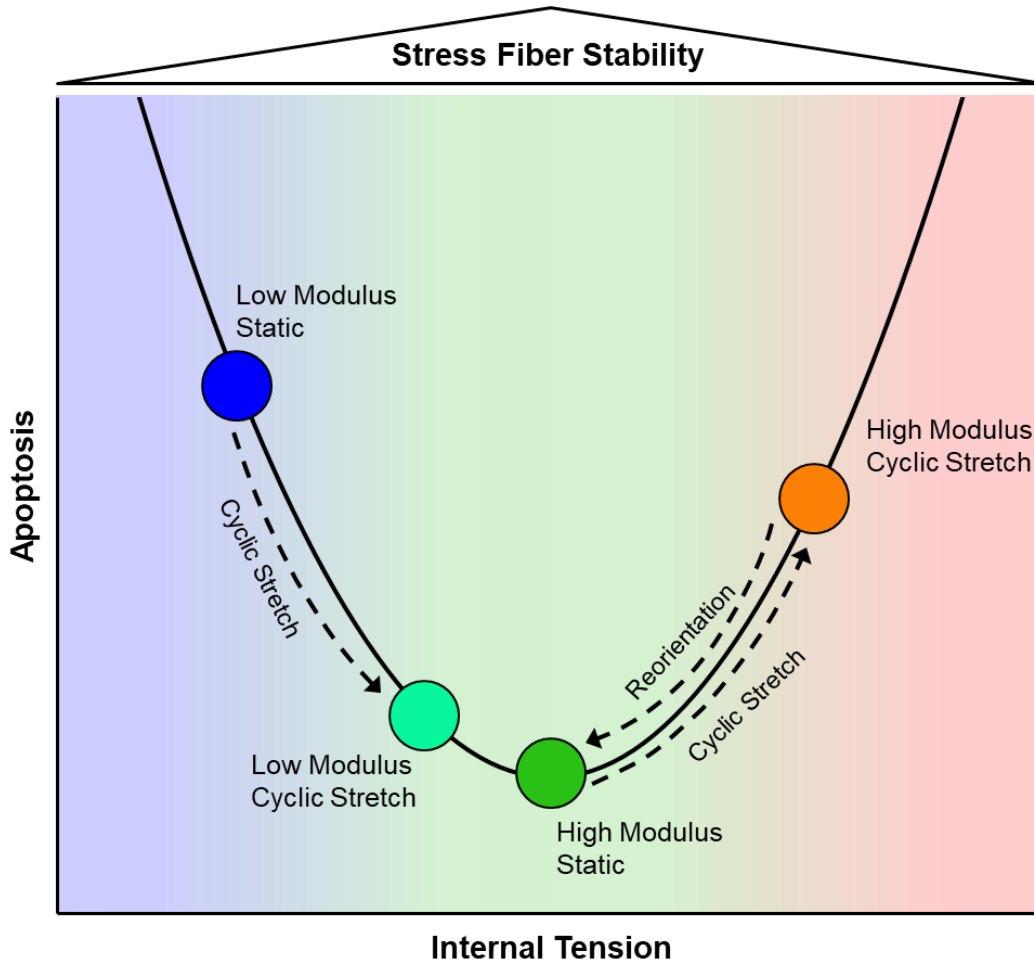


**Figure 3.8:** Relationship between cellular survival and internal cell tension. Healthy cells in physiological conditions (green region) have maximum cytoskeletal stability and are at homeostatic tension levels. Cells on stiff substrates are in this region and when cyclically stretched, increase internal tension to excessive levels (red region). Cells reorient to reduce stress and return to lower tension levels to maintain cellular survival. Cells on soft substrates exist in low-tension states (blue region) and when stretched, can increase internal tension towards homeostatic levels thereby reducing apoptotic levels.

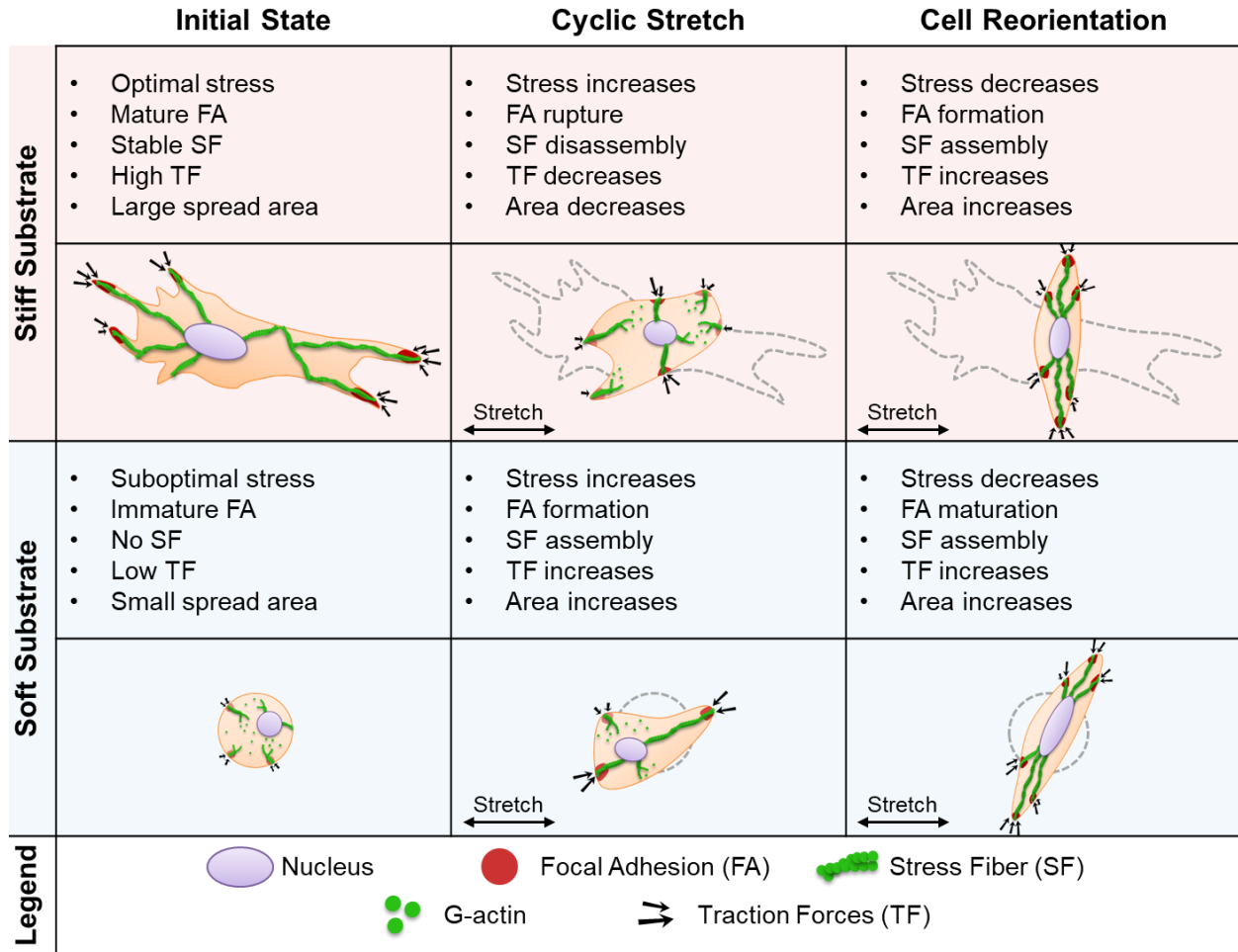


**Figure 3.9:** Schematic of possible mechanism behind strain avoidance behavior in response to cyclic stretch in cells on stiff and soft substrates. Cells have varying behavior in response to cyclic stretch dependent on substrate stiffness. Cells on stiff substrates begin at optimal tension levels, increase in tension when stretched, and reorient perpendicular to stretch to return to homeostatic tension levels. Cells on soft substrates start at suboptimal tension levels, are able to build stress fibers and elongate when stretched and orient in the direction of optimal tension, which may be less than perpendicular to stretch. Dotted outline indicates state of initial cell.

Previous studies have found that cells follow basic principles of mechanics, where steady state angles of reorientation can be predicted by the direction of minimal strain (Wang *et al.*, 1995; Zhong *et al.*, 2011). These models capture well the behavioral response of cells cultured on stiff substrates, but unanswered questions remain for cells on soft substrates. What cellular mechanisms are at play when maintaining internal tension? How do these mechanisms differ based on initial level of cellular tension? What role do these mechanisms play in cell survival?

We first have to consider what factors play a role in cell reorientation and how they differ in cells on soft versus stiff substrates. Cell reorientation requires coordination between numerous elements such as the actin cytoskeleton, focal adhesions, and ECM resistance, all of which are dependent on substrate stiffness (Quinlan and Billiar, 2012; Gupta *et al.*, 2015). Cells on stiff substrates form mature focal adhesions and stress fibers while cells on soft substrates cannot. The disassembly and reassembly of stress fibers enable cellular reorientation on stiff substrates, but cells on soft substrates must first generate stress fibers and mature focal adhesions before they can be reorganized during reorientation. Some models of cell tension on soft substrates predict that cyclic stretch should not provide sufficient mechanical input for proper stress fiber assembly (Deshpande *et al.*, 2006; Ronan *et al.*, 2014). However, we and others show that cells can spread out on very soft substrates when under moderate (10%) cyclic stretch. The model of Zhong *et al.* predicts that cells prefer to reorient on soft substrates while cells will not reorient at all on stiff substrates (Zhong *et al.*, 2011). Xu *et al.* predict cells prefer to align along the tensile direction when on very compliant substrates (Xu *et al.*, 2018). These results are consistent with the findings of Tondon and Kaunas, although they stretch cells on top of fibrous substrates for only 1 hr (Tondon and Kaunas, 2014). We show here that cells on soft PA substrates elongate parallel to stretch after 1 hr before reorienting away from stretch, possibly settling on an angle relative to stretch that provides optimal stress. These differences may be due to several factors, such as differences in substrate (PA gel versus fibrous collagen), stretch duration, or the combination of strain and modulus that leads to where cells fall on the tension curve (Figure 3.8).

### 3.4.2 Cells on stiff substrates reorient away from stretch

Cells cultured on stiff substrates are able to generate homeostatic tension levels, which is evident by the high traction forces generated as well as low instances of apoptosis. We study cells on stiff substrates to directly compare with the response of cells on soft substrates. After uniaxial external mechanical stretch is introduced, we find that cells decrease in spread area, aspect ratio, and traction forces while becoming more rounded, which has been shown previously in the literature (Krishnan *et al.*, 2009, 2012; Cirka *et al.*, 2016). This behavior may be due to stress fibers depolymerization causing a reduction in spread area, retraction of filopodia, and decreases in traction forces. Cells generate fewer protrusions which causes the aspect ratio to increase;

however, the balance between increased elongation of the cell body and lower protrusions can cause circularity to remain similar between groups. Over time, cells reorient, on average, close to perpendicular to the direction of stretch, which is consistent with previous studies (Hayakawa *et al.*, 2000; Wang *et al.*, 2001; Hsu *et al.*, 2010; Tondon and Kaunas, 2014; Zielinski *et al.*, 2018). By reorienting, cells can reestablish homeostatic levels of tension, thereby maintaining low occurrences of apoptosis.

### 3.4.3 Mechanical stretch enables cells on soft substrates to elongate

Cells cultured on soft substrates have low spread areas, low traction forces, and high instances of apoptosis. Once cyclic stretch is introduced, stress fiber assembly is reinforced in the direction of stretch and cells spread out and elongate along the direction of stretch. Over time, continuous cyclic stretch causes too high of stress on newly formed stress fibers, causing cells to reorient away from the direction of stretch. Cells settle on an intermediate angle since they receive an input of stress from mechanical stretch, but unlike cells on stiff substrates, do not receive enough resistance from the soft substrate to cause complete perpendicular reorientation. We hypothesized that lower modulus or lower strain would decrease the mechanical input on cells and that cells would remain aligned parallel to stretch. We experimented with lower strain since lower modulus PA gels can be problematic with viscosity or being partially non-polymerized. We did not find any apparent differences in cell behavior or orientation between 10% and 5% strain, although it is possible we did not try a low enough strain. Lower strains were not used as 5% strain represents the lower bound shown to elicit cell orientation with stretch (Kaunas *et al.*, 2005). Future work should include a parametric study testing varying combinations of moduli and strain values.

### 3.4.4 Cells revert to initial state after cessation of cyclic stretch

We find that after 6 hr of continuous stretching, ceasing cyclic stretch causes cells to revert to their initial pre-stretch state rather than maintain their post-stretch state of elongation. This behavior is similar to previous studies that show cells on stiff substrates reestablish baseline traction forces upon cessation of stretch (Krishnan *et al.*, 2009, 2012). We find on soft substrates that cells round up again, decrease spread area, and have increases in instances of apoptosis. This

behavior may be indicative of stress fiber and focal adhesion disassembly due to a lack of mechanical feedback from the substrate and stretch.

### 3.4.5 Relevant mechanosensitive signaling pathways

When studying what mechanisms regulate cell survival, the Hippo pathway and its transcriptional cofactor, YAP, have been shown to be both mechanosensitive and anti-apoptotic (Cui *et al.*, 2015; Seo *et al.*, 2020). YAP is a potential mechanism to link cyclic stretch and cell survival; however, most studies only correlate YAP and cyclic stretch. More work needs to be done to determine how YAP mechanistically connects cyclic stretch and subsequent cell survival. As promising as YAP is as a potential mechanism for cell survival, there are other mechanosensitive pathways that should be explored, such as the MRTF pathway.

## 3.5 Conclusions

In this study, we examine how substrate modulus affects cell reorientation and survival in response to cyclic stretch. External mechanical stretch causes cells on stiff substrates to undergo strain avoidance, where they reorient perpendicular to the direction of stretch, to reestablish what is hypothesized as homeostatic tension levels. Here, we show that in low-stiffness environments, cells on very soft substrates have initial low-tension levels and can exploit external mechanical strain to elongate, greatly increase their cell spread area, and reduce instances of apoptosis. Initially, cells on soft substrates orient towards the direction of stretch before reorienting partially away to a new intermediate angle, one of optimally applied stress. Additionally, we show that an input of continual external mechanical stimuli is required for cells on soft substrates to maintain their stress levels and cell health, and once the stimulus is removed, cells revert to their initial state and susceptibility to apoptosis. More work needs to be performed to obtain traction force measurements and YAP localization over time, both which are indicative of cell tension and are implicated in apoptosis. Further, experiments that identify the mechanism how YAP bridges mechanical stretch and apoptosis are needed. This study highlights the importance of understanding tension homeostasis and what role it plays in apoptosis.

## 3.6 Acknowledgements

This work was funded by a grant from the National Science Foundation (CMMI 1761432).

## 3.7 References

- Abbott, R. D., Howe, A. K., Langevin, H. M., and Iatridis, J. C. (2012). Live free or die: Stretch-induced apoptosis occurs when adaptive reorientation of annulus fibrosus cells is restricted. *Biochem. Biophys. Res. Commun.* *421*, 361–366.
- Brown, R. A., Prajapati, R., McGrouther, D. A., Yannas, I. V., and Eastwood, M. (1998). Tensional homeostasis in dermal fibroblasts: Mechanical responses to mechanical loading in three-dimensional substrates. *J. Cell. Physiol.* *175*, 323–332.
- Chen, C. S., Mrksich, M., Huang, S., Whitesides, G. M., and Ingber, D. E. (1997). Geometric control of cell life and death. *Science* *276*, 1425–1428.
- Cirka, H. A., Uribe, J., Liang, V., Schoen, F. J., and Billiar, K. L. (2017). Reproducible in vitro model for dystrophic calcification of cardiac valvular interstitial cells: insights into the mechanisms of calcific aortic valvular disease. *Lab Chip* *17*, 814–829.
- Cirka, H., Monterosso, M., Diamantides, N., Favreau, J., Wen, Q., and Billiar, K. (2016). Active traction force response to long-term cyclic stretch is dependent on cell pre-stress. *Biophys. J.* *110*, 1845–1857.
- Cui, Y., Hameed, F. M., Yang, B., Lee, K., Pan, C. Q., Park, S., and Sheetz, M. (2015). Cyclic stretching of soft substrates induces spreading and growth. *Nat. Commun.* *6*, 6333–6340.
- De, R., Zemel, A., and Safran, S. A. (2007). Dynamics of cell orientation. *Nat. Phys.* *3*, 655–659.
- Deshpande, V. S., McMeeking, R. M., and Evans, A. G. (2006). A bio-chemo-mechanical model for cell contractility. *PNAS* *103*, 14015–14020.
- Ghibaudo, M., Saez, A., Trichet, L., Xayaphoummine, A., Browaeys, J., Silberzan, P., Buguin, A., and Ladoux, B. (2008). Traction forces and rigidity sensing regulate cell functions. *Soft Matter* *4*, 1836–1843.
- Gould, R. A., and Butcher, J. T. (2011). Isolation of Valvular Endothelial Cells. *J. Vis. Exp.*, 6–10.
- Gupta, M., Sarangi, B. R., Deschamps, J., Nematbakhsh, Y., Callan-Jones, A., Margadant, F., Mège, R. M., Lim, C. T., Voituriez, R., and Ladoux, B. (2015). Adaptive rheology and ordering of cell cytoskeleton govern matrix rigidity sensing. *Nat. Commun.* *6*.
- Hayakawa, K., Hosokawa, A., Yabusaki, K., and Obinata, T. (2000). Orientation of Smooth Muscle-Derived A10 Cells in Culture by Cyclic Stretching: Relationship between Stress Fiber Rearrangement and Cell Reorientation. *Zoolog. Sci.* *17*, 617–624.

- Hsieh, M. H., and Nguyen, H. T. (2005). Molecular mechanism of apoptosis induced by mechanical forces. *Int. Rev. Cytol.* *245*, 45–90.
- Hsu, H.-J., Lee, C.-F., Locke, A., Vanderzyl, S. Q., and Kaunas, R. (2010). Stretch-induced stress fiber remodeling and the activations of JNK and ERK depend on mechanical strain rate, but not FAK. *PLoS One* *5*, e12470.
- Humphrey, J. D., Dufresne, E. R., and Schwartz, M. A. (2014). Mechanotransduction and extracellular matrix homeostasis. *Nat. Rev. Mol. Cell Biol.* *15*, 802–812.
- Ingber, D. E. (2003). Mechanobiology and diseases of mechanotransduction. *Ann. Med.* *35*, 564–577.
- Jaalouk, D. E., and Lammerding, J. (2009). Mechanotransduction gone awry. *Nat. Rev. Mol. Cell Biol.* *10*, 63–73.
- Kaunas, R., Nguyen, P., Usami, S., and Chien, S. (2005). Cooperative effects of Rho and mechanical stretch on stress fiber organization. *Proc Natl Acad Sci* *102*.
- Krishnan, R. *et al.* (2009). Reinforcement versus Fluidization in Cytoskeletal Mechanoresponsiveness. *PLoS One* *4*, e5486.
- Krishnan, R., Canović, E. P., Jordan, A. L., Rajendran, K., Manomohan, G., Pirentis, A. P., Smith, M. L., Butler, J. P., Fredberg, J. J., and Stamenović, D. (2012). Fluidization, resolidification, and reorientation of the endothelial cell in response to slow tidal stretches. *Am. J. Physiol. - Cell Physiol.* *303*, 368–375.
- Leight, J. L., Wozniak, M. A., Chen, S., Lynch, M. L., and Chen, C. S. (2012). Matrix rigidity regulates a switch between TGF- $\beta$ 1-induced apoptosis and epithelial-mesenchymal transition. *Mol. Biol. Cell* *23*, 781–791.
- Mayr, M., Li, C., Zou, Y., Huemer, U., Hu, Y., and Xu, Q. (2000). Biomechanical stress-induced apoptosis in vein grafts involves p38 mitogen-activated protein kinases. *FASEB J* *14*, 261–270.
- Mih, J. D., Marinkovic, A., Liu, F., Sharif, A. S., and Tschumperlin, D. J. (2012). Matrix stiffness reverses the effect of actomyosin tension on cell proliferation. *J. Cell Sci.* *125*, 5974–5983.
- Oakes, P. W., Banerjee, S., Marchetti, M. C., and Gardel, M. L. (2014). Geometry regulates traction stresses in adherent cells. *Biophys. J.* *107*, 825–833.
- Orr, A. W., Helmke, B. P., Blackman, B. R., and Schwartz, M. A. (2006). Mechanisms of mechanotransduction. *Dev. Cell* *10*, 11–20.
- Quinlan, A. M. T., and Billiar, K. L. (2012). Investigating the role of substrate stiffness in the persistence of valvular interstitial cell activation. *J. Biomed. Mater. Res. Part A* *135*, 1–19.
- Rannou, F., Lee, T. S., Zhou, R. H., Chin, J., Lotz, J. C., Mayoux-Benhamou, M. A., Barbet, J. P., Chevrot, A., and Shyy, J. Y. J. (2004). Intervertebral Disc Degeneration: The Role of the

Mitochondrial Pathway in Annulus Fibrosus Cell Apoptosis Induced by Overload. *Am. J. Pathol.* *164*, 915–924.

Rape, A. D., Guo, W. H., and Wang, Y. L. (2011). The regulation of traction force in relation to cell shape and focal adhesions. *Biomaterials* *32*, 2043–2051.

Ronan, W., Deshpande, V. S., McMeeking, R. M., and McGarry, J. P. (2014). Cellular contractility and substrate elasticity: a numerical investigation of the actin cytoskeleton and cell adhesion. *Biomech. Model. Mechanobiol.* *13*, 417–435.

Seo, B. R. *et al.* (2020). Collagen microarchitecture mechanically controls myofibroblast differentiation. *Proc. Natl. Acad. Sci.*, 201919394.

Sotoudeh, M., Li, Y.-S., Yajima, N., Chang, C.-C., Tsou, T.-C., Wang, Y., Usami, S., Ratcliffe, A., Chien, S., and Shyy, J. Y.-J. (2002). Induction of apoptosis in vascular smooth muscle cells by mechanical stretch. *Am. J. Physiol. Circ. Physiol.* *282*, H1709–H1716.

Throm Quinlan, A. M., Sierad, L. N., Capulli, A. K., Firstenberg, L. E., and Billiar, K. L. (2011). Combining dynamic stretch and tunable stiffness to probe cell mechanobiology in vitro. *PLoS One* *6*, e23272.

Tilghman, R. W., Cowan, C. R., Mih, J. D., Koryakina, Y., Gioeli, D., Slack-Davis, J. K., Blackman, B. R., Tschumperlin, D. J., and Parsons, J. T. (2010). Matrix rigidity regulates cancer cell growth and cellular phenotype. *PLoS One* *5*, 1–13.

Tondon, A., and Kaunas, R. (2014). The direction of stretch-induced cell and stress fiber orientation depends on collagen matrix stress. *PLoS One* *9*.

Wang, H.-B. B., Dembo, M., and Wang, Y. L. (2000). Substrate flexibility regulates growth and apoptosis of normal but not transformed cells. *Am J Physiol Hear. Cell Physiol* *279*, C1345–C1350.

Wang, H., Ip, W., Boissy, R., and Grood, E. S. (1995). Cell orientation response to cyclically deformed substrates: Experimental validation of a cell model. *J. Biomech.* *28*, 1543–1552.

Wang, J. H. C., Goldschmidt-Clermont, P., Wille, J., and Yin, F. C. P. (2001). Specificity of endothelial cell reorientation in response to cyclic mechanical stretching. *J. Biomech.* *34*, 1563–1572.

Xu, G. K., Feng, X. Q., and Gao, H. (2018). Orientations of Cells on Compliant Substrates under Biaxial Stretches: A Theoretical Study. *Biophys. J.* *114*, 701–710.

Zhang, Y. H., Zhao, C. Q., Jiang, L. S., and Dai, L. Y. (2011a). Cyclic stretch-induced apoptosis in rat annulus fibrosus cells is mediated in part by endoplasmic reticulum stress through nitric oxide production. *Eur. Spine J.* *20*, 1233–1243.

Zhang, Y. H., Zhao, C. Q., Jiang, L. S., and Dai, L. Y. (2011b). Substrate stiffness regulates apoptosis and the mRNA expression of extracellular matrix regulatory genes in the rat annular cells. *Matrix Biol.* *30*, 135–144.

Zhong, Y., Kong, D., Dai, L., and Ji, B. (2011). Frequency-dependent focal adhesion instability and cell reorientation under cyclic substrate stretching. *Cell. Mol. Bioeng.* 4, 442–456.

Zielinski, A., Linnartz, C., Pleschka, C., Dreissen, G., Springer, R., Merkel, R., and Hoffmann, B. (2018). Reorientation dynamics and structural interdependencies of actin, microtubules and intermediate filaments upon cyclic stretch application. *Cytoskeleton* 75, 385–394.

## Chapter 4: Heterogeneity profoundly alters emergent stress fields in constrained multicellular systems

Zachary E. Goldblatt<sup>1</sup>, Habibeh Ashouri Choshali<sup>2</sup>, Heather A. Cirka<sup>1</sup>, Vivian Liang<sup>1</sup>, Qi Wen<sup>3</sup>, Dannel McCollum<sup>4</sup>, Nima Rahbar<sup>2</sup>, Kristen L. Billiar<sup>1</sup>

1. Department of Biomedical Engineering, Worcester Polytechnic Institute, Worcester, MA
2. Department of Civil Engineering, Worcester Polytechnic Institute, Worcester, MA
3. Department of Physics, Worcester Polytechnic Institute, Worcester, MA
4. Department of Biochemistry & Molecular Pharmacology, University of Massachusetts Medical School, Worcester, MA

The following chapter appears in Goldblatt et al. “Heterogeneity profoundly alters emergent stress fields in constrained multicellular systems.” *Biophysical Journal*. (2019) 1:118 (2020) and is reproduced here with permission from Biophysical Society. Sections involving constitutively active YAP are new additions. Supporting information from the manuscript was brought into the body of the chapter.

## 4.0 Abstract

Stress fields emerging from the transfer of forces between cells within multicellular systems are increasingly being recognized as major determinants of cell fate. Current analytical and numerical models used for the calculation of stresses within cell monolayers assume homogeneous contractile and mechanical cellular properties; however, cell behavior varies by region within constrained tissues. Here, we show the impact of heterogeneous cell properties on resulting stress fields that guide cell phenotype and apoptosis. Using circular micropatterns, we measured biophysical metrics associated with cell mechanical stresses. We then computed cell-layer stress distributions using finite element contraction models and monolayer stress microscopy. In agreement with previous studies, cell spread area, alignment, and traction forces increase, while apoptotic activity decreases, from the center of cell layers to the edge. The distribution of these metrics clearly indicates low cell stress in central regions and high cell stress at the periphery of the patterns. However, the opposite trend is predicted by computational models when homogeneous contractile and mechanical properties are assumed. In our model, utilizing heterogeneous cell-layer contractility and elastic moduli values based on experimentally measured biophysical parameters, we calculate low cell stress in central areas and high anisotropic stresses in peripheral regions, consistent with the biometrics. These results clearly demonstrate that common assumptions of uniformity in cell contractility and stiffness break down in post-confluence confined multicellular systems. Finally, when YAP was constitutively active in cells occurrences of apoptosis in central regions decreased in aggregates. This work highlights the importance of incorporating regional variations in cell mechanical properties when estimating emergent stress fields from collective cell behavior.

## 4.1 Significance

Mechanical stress fields within tissues generated by force transmission between cells play a critical role in cell behaviors ranging from proliferation to differentiation to death. The intracellular stresses are currently calculated using computational models assuming homogeneous mechanical properties. When applied to dense cell monolayers with geometrically constrained growth, these models predict distributions of stresses that are inconsistent with experimentally measured stress-related biological markers. Here, using a series of finite element models with experimentally measured heterogeneous cell material properties, we compute stresses that strongly correlate with a wide range of biophysical markers. Our results demonstrate that an understanding of the underlying mechanics that regulate collective cell behavior in dynamic biological tissues requires analyses of the heterogeneity of the cell material properties.

## 4.2 Introduction

Emergent mechanical stress fields arising from force transmission between cells in monolayers and multicellular aggregates are increasingly being recognized as major contributors to the regulation of collective cell behavior. Diffusion of growth factors and cytokines are not sufficient to explain the diversity seen in behaviors of cells just microns apart. Emergent stress fields have been studied in the context of proliferation (Nelson *et al.*, 2005), differentiation (Li *et al.*, 2009; Wan *et al.*, 2010), nuclear transcription factor localization (Aragona *et al.*, 2013), tumorigenicity (Lee *et al.*, 2016), cellular alignment (He *et al.*, 2015; Liu *et al.*, 2016), and collective migration speed (Brugués *et al.*, 2014). There is growing evidence that mechanical stress fields are pivotal in controlling these events.

There is considerable interest in quantifying the cellular stresses within monolayers to better understand the mechanical factors that drive migration, proliferation, and differentiation. For forward predictions of emergent stress fields, researchers use continuum models with pre-strain or finite element models with thermal cooling to simulate active cell contraction (Nelson *et al.*, 2005; Li *et al.*, 2009; Banerjee and Cristina Marchetti, 2013; He *et al.*, 2015). To calculate cell-layer stress fields from measured substrate traction forces, monolayer stress microscopy (MSM) (Treat *et al.*, 2009) and other force balancing methods (Maruthamuthu *et al.*, 2011; Moussus *et al.*, 2014; Liu *et al.*, 2016; Nier *et al.*, 2016) have been developed.

Calculation of stresses within a cluster of cells requires assumptions about the isotropy, thickness, elastic constants, and uniformity of the cell layer (Ng *et al.*, 2014). In both predictions and calculations of cell-layer stress, the mechanical properties of cells are assumed to be uniform in past studies. Assumptions of material homogeneity may be acceptable for cell monolayers where unconstrained migration and spreading results in regional uniformity in cell density and orientation (Tambe *et al.*, 2013); however, in constrained systems (e.g., micropatterned protein islands *in vitro* and tissues with confined growth *in vivo*), regional differences in cell behavior markers indicative of variations in cell properties are commonly reported. Higher rates of proliferation (Li *et al.*, 2009), increased circumferential alignment (Liu *et al.*, 2016), enhanced

tumorigenicity (Lee *et al.*, 2016), and heightened contractility markers (Li *et al.*, 2009; Cirka *et al.*, 2017) are reported near multicellular system edges compared to central regions (Nelson *et al.*, 2005; Li *et al.*, 2009; Wan *et al.*, 2010).

Here, we test the hypothesis that incorporation of heterogeneous mechanical parameters in calculations and simulations are necessary to accurately determine cell-layer stresses in geometrically constrained multicellular systems. We culture cells on micropatterned collagen islands to post-confluence and measure a broad range of biophysical markers indicative of cell stress state. We then predict and compute in-plane cell stress distributions using thermal contraction finite element models and monolayer stress microscopy. The models are run with homogeneous and heterogeneous assumptions of cell-layer contractility and elastic modulus based on cell spread area, indentation stiffness, and traction force measurements.

## 4.3 Materials and Methods

### 4.3.1 Cell Culture

Valvular interstitial cells (VIC) were isolated from porcine hearts obtained from a local abattoir (Gould and Butcher, 2011). Cells were expanded and cultured in Dulbecco's Modified Eagle Medium (DMEM; 4.5 g/L glucose, Life Technologies, Grand Island, NY), supplemented with 10% fetal bovine serum (FBS; GE Healthcare HyClone, Chicago, IL) and 1% antibiotic/antimycotic (Life Technologies). Cells were maintained in a temperature- (37 °C), CO<sub>2</sub>- (5%), and humidity-regulated incubator. Passages 2-6 were used for all experiments. VICs were seeded at 2,000 cells/cm<sup>2</sup> and 10,000 cells/cm<sup>2</sup> for low cell density experiments of individual cells and high cell density experiments of aggregates, respectively, and allowed to adhere overnight. Media was changed after 24 hr to remove any non-adhered cells. Aggregates were cultured for 48 hr prior to traction force microscopy measurements.

### 4.3.2 Microcontact Substrate Preparation

Polyacrylamide (PA) gels (~40 kPa modulus) were attached to glass coverslips and used as the substrate for all experiments. Formulations of polyacrylamide/bisacrylamide to known mechanical modulus had been previously validated in a prior study (Throm Quinlan *et al.*, 2011). Individual cell studies used PA gels coated with monomeric collagen by functionalization of the surface using Sulfo-SANPAH (Thermo Fischer, Waltham, MA). Multicellular aggregate studies used PA gels that were microcontact printed with monomeric collagen using PDMS stamps of 200–400  $\mu\text{m}$  diameter circular posts, as previously described (Cirka *et al.*, 2017).

### 4.3.3 Live Cell Imaging

CellEvent Caspase-3/7 reagent (Thermo Fisher) was added to cultures and allowed to incubate for 1 hr prior to imaging. Phase images of aggregates and fluorescent images of caspase signal were obtained using a Zeiss Axiovert 200M microscope equipped with a CCD camera, AxioVision software, and a 40x Zeiss objective. A custom MATLAB (MathWorks, Natick, MA) program was developed for image processing to determine regional caspase location.

### 4.3.4 Traction Force Microscopy

PA gels were prepared and uniformly coated with 0.2  $\mu\text{m}$  fluorescent beads (Life Technologies) as previously described (Cirka *et al.*, 2016). Images of aggregates were taken in phase-contrast. Hoechst (Thermo Fisher) was added to media, incubated for 15 min, and imaged to count the number of cells within each aggregate. Fluorescent images of the substrate were taken before and after the addition of trypsin. Aggregate substrate traction data were obtained by calculating stresses in ANSYS (Ansys Inc., Canonsburg, PA) from displacement fields that were computed using mass particle image velocimetry from a custom MATLAB code (Cirka *et al.*, 2016).

### 4.3.5 Atomic Force Microscopy

Atomic force indentation stiffness was measured for individual VICs cultured on compliant substrates of varying moduli. For each cell, a 20  $\mu\text{m}$  x 20  $\mu\text{m}$  force map was completed over the cell body. The indentation rate was 1  $\mu\text{m/s}$  (0.06 N/m cantilever, conical tip; Asylum Research, Santa Barbara, CA). Sixteen measurements comprised each map. A custom MATLAB script was then used to extract the Young's modulus from each curve by fitting the first 200 nm of indentation data to the Hertz model for a conical indenter. The extracted values were averaged to determine the mean modulus for each cell. Similar experimental technique was used for aggregates where 20  $\mu\text{m}$  x 20  $\mu\text{m}$  force maps were produced over the center and edge of aggregates. One map in each category was performed per aggregate. Data analysis was identical to that of individual cells.

### 4.3.6 Immunocytochemistry

To determine the distribution of the various biometric markers, cells were fixed with 4% paraformaldehyde and permeabilized with 0.25% Triton-X. Visualization of G-actin was accomplished by staining VICs with deoxyribonuclease I, Alexa Fluor 594 conjugate (Life Technologies) for 30 min. Cells were counter-stained for F-actin with Alexa Fluor 488 phalloidin (Thermo Fisher) and Hoechst diluted in PBS, also for 30 min. The intensities were compared between the G-actin channel and F-actin channel to generate a ratio for all cells and aggregates. An F-actin alignment index was determined by processing phalloidin-stained actin images with a 2D fast Fourier transform (FFT) on sequential 8  $\mu\text{m}$  sub-images. The F-actin alignment index was then calculated as one minus the ratio of minor/major axis of the fitted ellipse from the thresholded FFT image. An index of zero indicates no stress fiber alignment and a value of 1 indicates perfect fiber alignment.  $\alpha$ -SMA stained cells were first blocked with 1.5% goat serum (Invitrogen, Carlsbad, CA) and then stained for  $\alpha$ -SMA (Sigma-Aldrich, St. Louis, MO). Confocal imaging was completed on a Leica SP5 microscope using the same laser intensities for all samples.

### 4.3.7 Modeling

A schematic outlining the different stress components as well as the different models can be found in Figure 4.1.

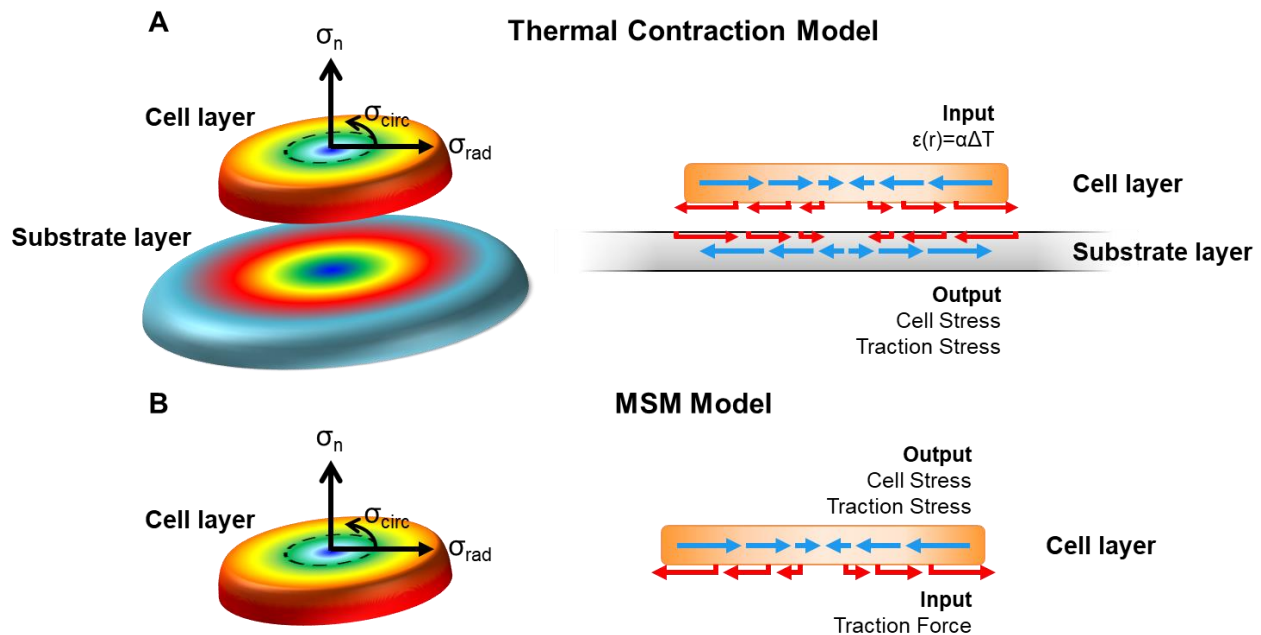


**Figure 4.1: Schematics of stress components for each computational model. A)** Representative thermal contraction model with the cell layer and its stress components (*radial*, *circumferential*, and *normal direction*) and the substrate layer (polyacrylamide gel), both with simulated stress distributions. The thermal contraction model imposes a simulated temperature drop (*input*) in the cell layer. The cell layer is fixed to the substrate layer and therefore, cannot contract, which causes stresses to be generated (*output*) in both the cell layer (*cell stress*) and substrate layer (*traction stress*). These stresses are dependent on the distribution of mechanical parameters such as the modulus and coefficient of thermal expansion value ( $\alpha$ ). **B)** Representative monolayer stress microscopy (MSM) model which consists of a cell layer alone; stress components are shown. Experimentally measured traction forces are input into the MSM model, and then cell stress and traction stress are calculated from FE models which are dependent on the distribution of modulus ( $E$ ) for the cell layer.

#### Thermal Contraction Model

A three-dimensional finite element model of the cell layer and substrate was constructed using the commercial software ABAQUS (Dassault Systemes, Velizy-Villacoublay, France). The cell layer is modeled as a continuous three-dimensional layer where the contractility is simulated with a temperature drop equivalent to applying a uniform pre-strain. The constitutive equation for the isotropic cell layer is the same as the thermoelasticity equation:

$$\sigma_{ij} = \frac{E_c}{1+\nu_c} \left( \varepsilon_{ij} + \frac{\nu_c}{1-2\nu_c} \varepsilon_{kk} \delta_{ij} \right) - \frac{E_c}{1-2\nu_c} \alpha \Delta T \delta_{ij} \quad (1)$$

where,  $E_c$  is elastic modulus,  $\nu_c$  is Poisson's ratio,  $\alpha$  is the coefficient of thermal expansion,  $\Delta T$  is the temperature change,  $\delta_{ij}$  is the Dirac delta function, and  $\sigma_{ij}$  and  $\varepsilon_{ij}$  are the stress and strain fields respectively which are obtained numerically using finite element methods.

Cell layer contraction was modeled by introducing a thermal strain using a temperature drop of 1 K. The thickness of cells and substrate layers were 3.2  $\mu\text{m}$  and 1  $\mu\text{m}$  respectively; the bottom surface of the substrate was fixed. The cell layer and substrate layer were modeled as elastic, isotropic materials with Young's moduli of 40 kPa and 0.4 kPa respectively, both with a Poisson's ratio of 0.49 (nearly incompressible). The substrate layer undergoes a softening effect due to the inclusion of the adhesive bonding layer between the cell layer and the substrate. A two-spring model was used to acquire the effective stiffness of the substrate and molecular bond based on values from Ji and colleagues (He *et al.*, 2015). We performed a parametric study showing the sensitivity of substrate stiffness on cell stress distribution and found that the qualitative results do not change over three orders of magnitude of the chosen modulus (i.e., 0.04 kPa – 4 kPa). The quantitative values do change but are normalized to radius and stress since the overall level of contraction set by the thermal coefficient and temperature drop is arbitrary (Figure 4.2). In the first model iteration, the modulus was assumed uniform to highlight the effect of varying contractility. A second parametric study was performed showing that both contractility and substrate modulus affect stress distribution independently from one another (Figure 4.3).

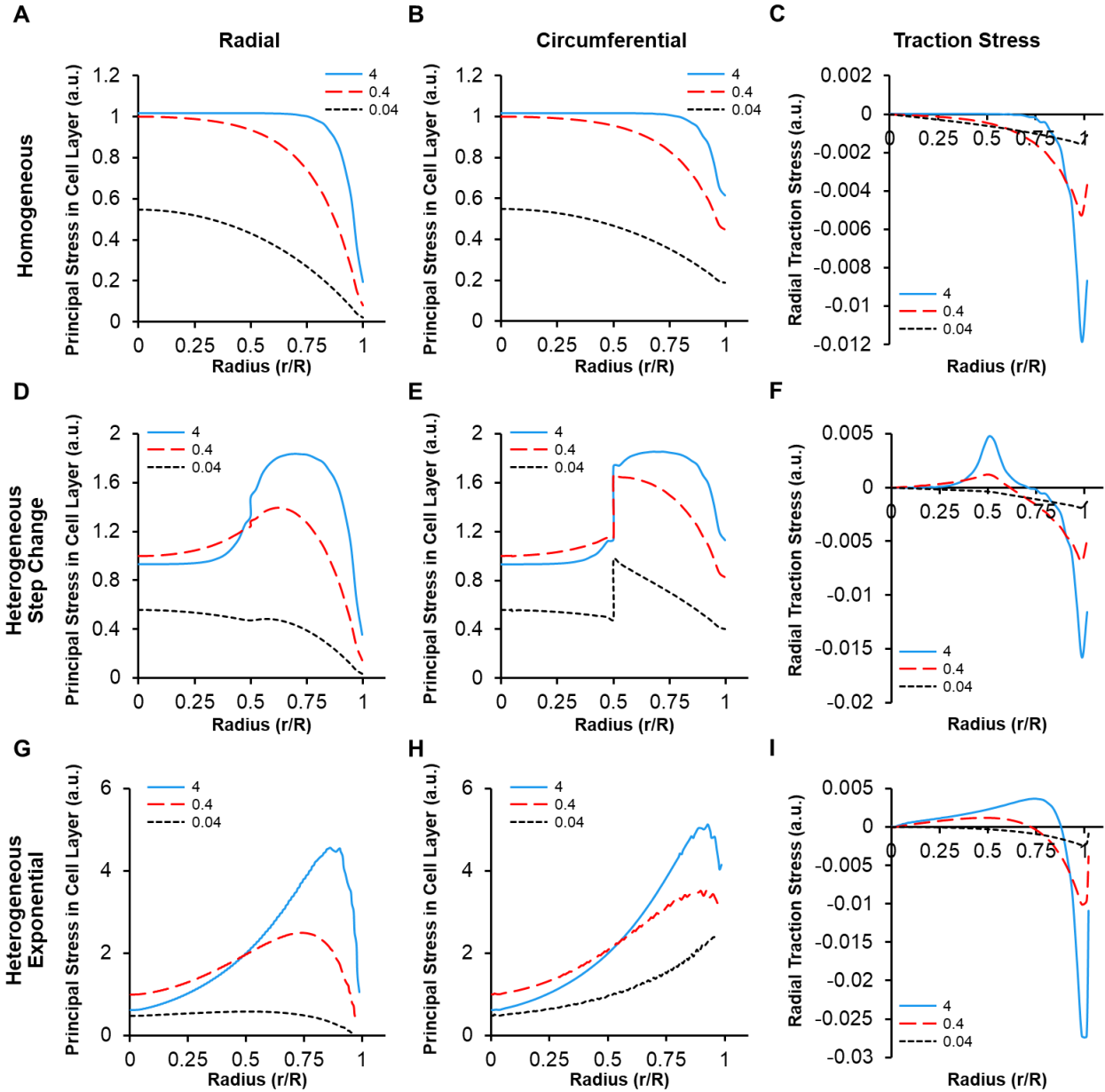


**Figure 4.2: Parametric study shows sensitivity of the stress distributions to the substrate modulus within  $\pm$  one order of magnitude from chosen baseline of thermal contraction model ( $E = 0.4$  kPa).** For radial (*left column*), circumferential (*middle column*), and traction (*right column*) stresses, qualitative distributions of stresses remain consistent; however, the magnitude of stresses correlate positively with magnitude of modulus. These distribution trends are observed in all modeling cases: homogeneous (A-C), heterogeneous step change (D-F), and heterogeneous exponential (G-I).

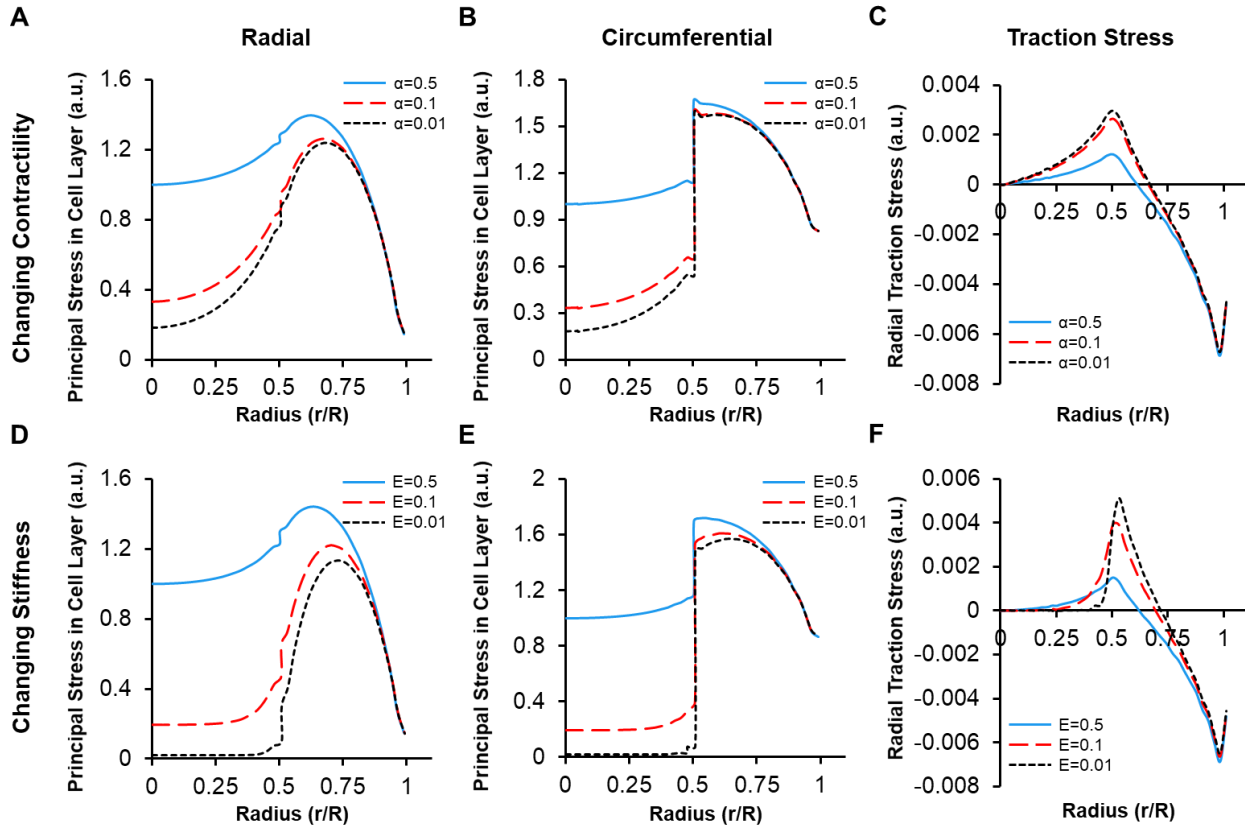


**Figure 4.3: Parametric study changing  $\alpha$  (A-C) or the substrate modulus (D-F) individually demonstrates that each has a significant effect on the stress magnitude but not the qualitative stress distributions.** Radial (A), circumferential (B), and traction (C) stresses are shown for cases where substrate modulus is uniform and coefficient of thermal contraction ( $\alpha$ ) changes at  $r = 0.5R$  by 0.5 (solid blue line), 0.1 (dashed red line), and 0.01 (dotted black line). As  $\alpha$  decreases, the stress distribution remains qualitatively consistent, but the magnitude drastically decreases. Radial (D), circumferential (E), and traction (F) stresses are shown for the cases where the coefficient of thermal contraction is uniform (homogeneous contraction) and substrate modulus changes at  $r = 0.5R$  by 0.5 (solid blue line), 0.1 (dashed red line), and 0.01 (dotted black line). As modulus decreases, the stress distribution also remains qualitatively consistent, but the magnitude drastically decreases.

The coefficient of thermal expansion,  $\alpha$ , was set to the exponential function  $\alpha'(r) = 0.9e^{2.34r}$  for the exponential heterogeneous case based on the relationship of cell area vs. aggregate radius,  $r$ . This equation was normalized to its maximum value at  $r = R$ , the maximum radius, and multiplied by 0.1 in order to achieve an  $\alpha = 0.1 \text{ K}^{-1}$  at the aggregate edge based off of values from Ji and colleagues (He *et al.*, 2015), yielding equation 2:

$$\alpha(r) = \frac{0.9e^{2.34r}}{0.9e^{2.34R}} \times 0.1 = 0.0096e^{2.34r} \quad (2)$$

The values for  $\alpha$  in each condition were normalized to each other so that the area under each  $\alpha$  vs. radius curve remains equivalent. This causes the  $\alpha$  values for the homogeneous cell layer to be  $0.0357 \text{ K}^{-1}$ . For the step heterogeneity case, the  $\alpha$  value in the peripheral region ( $r > 0.5R$ ) was set to be  $0.0476 \text{ K}^{-1}$ , and the  $\alpha$  value in the central region was set to be  $0.0238 \text{ K}^{-1}$ , i.e., the center was half as contractile as the edges.

For the simulation, the radius of the substrate was  $400 \mu\text{m}$ , and the radius of the cell layer was  $200 \mu\text{m}$ . Standard 3-D-stress hexahedral elements with an approximate global mesh size of  $2 \mu\text{m}$  were used. Stress and strain tensors were calculated throughout the model, and the radial and circumferential cell-layer stresses at the cell-substrate interaction were reported. Consistent with previous simulations (Nelson *et al.*, 2005), we assumed uniform focal adhesions between the cell layer and substrate layer to focus on only one variable (contractility). Localization of focal adhesions varies by region within aggregates and is likely higher at aggregate edges (Kilian *et al.*, 2010; Rape *et al.*, 2011; Oakes *et al.*, 2014); however, they are still present within the central region (just not as dense or large). We performed a simulation where only a thin ring ( $5 \mu\text{m}$  thick) around the edge of the cell layer is attached to the substrate layer, simulating focal adhesions only at the aggregate edge. In this case, the circumferential stresses are slightly accentuated as they progress towards the aggregate edge, yet the qualitative stress distributions remain consistent with the uniform attachment case (Figure 4.4).

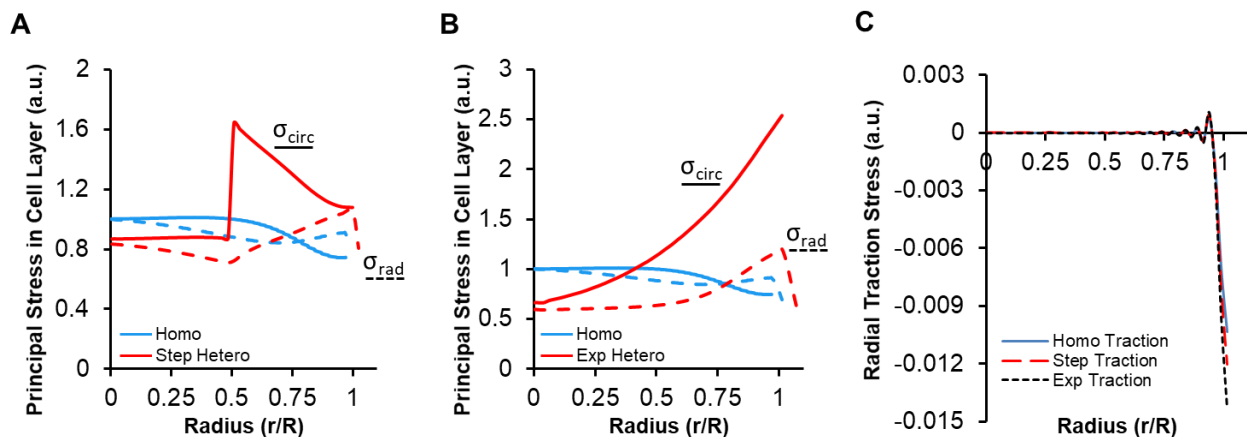


**Figure 4.4: Cell-layer and substrate stresses simulated by thermal contraction when cell layer edge is attached to the substrate and rest of cell layer is free.** This simulates focal adhesion localization only at the edge of an aggregate with no focal adhesions in the inner region. **A)** Cell-layer radial (*dotted*) and

circumferential (*solid*) stresses are shown for homogeneous (*blue*) and step change heterogeneous (*red*) conditions for contractility. **B**) Cell-layer radial (*dotted*) and circumferential (*solid*) stresses are shown for homogeneous (*blue*) and exponential heterogeneous (*red*) conditions for contractility. The stress distribution is consistent in radial and circumferential stresses; however, circumferential stresses are accentuated as they progress towards the aggregate edge over the case where the cell layer is uniformly attached to the substrate (see Fig. 4 *a* and Fig. S6 *a*). **C**) Traction forces remain localized at the aggregate edge and do not vary between the different modeling conditions.

## Monolayer Stress Microscopy (MSM)

The in-plane stresses in the cell layer were calculated using experimentally measured tractions. The displacement field from traction force microscopy was applied to a semi-infinite substrate with Young's modulus of 40 kPa and the tractions were obtained. A two-dimensional finite element model of the cell layer was constructed using ABAQUS, where tractions were applied to the bottom surface of the cell layer. The cell layer is modeled as a continuous flat, thin layer under plane-stress conditions such that all out of plane stress/traction components are negligible ( $\sigma_{zz} = \sigma_{rz} = \sigma_{\theta z} = T_z = 0$ ). Under static conditions, the two-dimensional equilibrium equations in polar coordinates are:

$$\frac{\partial \sigma_{rr}}{\partial r} + \frac{1}{r} \frac{\partial \sigma_{r\theta}}{\partial \theta} + \frac{1}{r} (\sigma_{rr} - \sigma_{\theta\theta}) = \frac{T_r}{t_c} \quad (3)$$

$$\frac{\partial \sigma_{r\theta}}{\partial r} + \frac{1}{r} \frac{\partial \sigma_{\theta\theta}}{\partial \theta} + \frac{2}{r} \sigma_{r\theta} = \frac{T_\theta}{t_c} \quad (4)$$

where,  $T_r$  and  $T_\theta$  are the measured radial and circumferential traction components, respectively, applied to the lower surface of the model,  $r$  is radius,  $\sigma_{ij}$  are the stress components, and  $t_c$  is the monolayer thickness.

The general form for Hook's law in standard tensor notation is expressed as:

$$\sigma_{ij} = C_{ijkl} \varepsilon_{kl} \quad (5)$$

When under homogeneous, isotropic plane-stress, the above equation in polar coordinates can be simplified to:

$$\varepsilon_{rr} = \frac{1}{E} (\sigma_{rr} - \nu \sigma_{\theta\theta}) \quad (6)$$

$$\varepsilon_{\theta\theta} = \frac{1}{E} (\sigma_{\theta\theta} - \nu \sigma_{rr}) \quad (7)$$

$$\varepsilon_{r\theta} = \frac{1+\nu}{E} (\sigma_{r\theta}) \quad (8)$$

Then, the compatibility equation for plane-stress in polar coordinates is given by:

$$\nabla^2 (\sigma_{rr} + \sigma_{\theta\theta}) = \frac{(1+\nu)}{t_c} \left( \frac{\partial T_r}{\partial r} + \frac{T_r}{r} + \frac{1}{r} \frac{\partial T_\theta}{\partial \theta} \right) \quad (9)$$

$$\nabla^2 = \frac{\partial^2}{\partial r^2} + \frac{1}{r} \frac{\partial}{\partial r} + \frac{1}{r^2} \frac{\partial^2}{\partial \theta^2} \quad (10)$$

The stresses are numerically calculated. The standard plane stress four node element was used to mesh the cell layer with an approximate mesh size of 1.5  $\mu\text{m}$ . Homogeneous, step heterogeneous, and exponential heterogeneous cell properties were considered. For the exponential case, an elastic modulus was exponentially increased from the center to the edge using the function  $E(r) = 0.9e^{2.34r}$ , such that the modulus at the edge was  $E = 40$  kPa. Similar to the calculations for  $\alpha$ , the values for the moduli in each condition were normalized so the area under each modulus vs. radius curve remains equal. With the elastic modulus of the exponential case set to 40 kPa at the aggregate edge, the modulus of the homogeneous case is reduced to 18.6 kPa, while for step heterogeneity, the moduli were 12.5 kPa and 24.9 kPa for the central region ( $r < 0.5R$ ) and peripheral region, respectively. This modulus range is within values for average cell-layer stiffness found in our AFM experiments. The tractions at the cell-layer nodes corresponding to the model mesh were found by interpolation of the tractions at the substrate nodes. The radial and circumferential stresses in the cell layer were reported.

### 4.3.8 Developing Stable YAP-VIC Cell Line

YAP-6A, an activated version of YAP that cannot be inhibited by LATS, was obtained from Addgene (#42562), packaged into lentivirus particles, and transduced into VIC cells. Lentiviral particles were generated by transfecting 293T cells with pLX304-YAP-S6A-V5, pSPAX.2, and PMD2.G. After 48 hr, the supernatant was collected and filtered through a 45  $\mu\text{m}$  sterile filter. Viral supernatant was then mixed 1:1 with culture media, added with 1  $\mu\text{g}/\text{mL}$  of polybrene (Millipore), and incubated with VIC cells overnight. The next day, cells were fed with culture media and after 24 hr, cells were selected with 1  $\mu\text{g}/\text{ml}$  of Puromycin until all control cells died

(approximately 48 hr). Expression of the YAP S6A-V5 construct was visualized in pooled puromycin resistant cells through immunofluorescence using anti-V5 (Invitrogen).

### 4.3.9 Magnetic Induction of Stress

To apply external forces to the cells within a subset of aggregates, ferrous beads were attached to the cells and a magnetic force was applied. Ferric oxide microbeads (5  $\mu\text{m}$  diameter; Sigma-Aldrich) were mixed vigorously and allowed to incubate in collagen solution prepared by mixing 1 mg/mL collagen (Advanced Biomatrix, Carlsbad, CA) with 10% 0.1 M NaOH to achieve a pH of 7.4 for 1 hr to ensure proper collagen coating on the beads. The solution was then spun down, supernatant aspirated, and beads were resuspended in DPBS. Prior to application onto aggregates, the microbeads were sonicated for an additional 10 min to reduce clumping. The microbead mixture was added to new cell media (1:100 V/V) for aggregates that had been cultured overnight. Aggregates were incubated with bead mixture on a rocker for 40 min to allow for dispersion of beads over aggregates. After incubation, aggregates were rinsed with DPBS to ensure that any excess beads were removed. Ceramic magnets (Duramagnetics, Sylvania, OH) were placed atop the Petri dishes. The magnetic field (618 G) produced by the magnets pulled on the microbeads and exerted an upward force (173 pN) on the cellular aggregates. Control cells without magnetic microbeads were cultured within the magnetic field, as well as additional control samples cultured with magnetic microbeads but not under a magnetic field. Samples were allowed to incubate underneath the magnets for 1 week.

## 4.4 Results and Discussion

### 4.4.1 Homogeneous models predict high stresses and low traction forces in the center of multicellular aggregates

Microcontact printing, a technique used to pattern protein shapes onto cell culture surfaces, is frequently used to create confined shapes for single cells and multicellular assemblies to examine the effects of geometric constraint on cell phenotype and fate (Nelson *et al.*, 2005; Li *et al.*, 2009; Wan *et al.*, 2010; Liu *et al.*, 2016). In this study, we cultured groupings of fibroblastic

cells (porcine valvular interstitial cells, VIC) onto 200–400  $\mu\text{m}$  diameter circular collagen micropatterns on controlled-stiffness polyacrylamide gels. Each multicellular aggregate contained 100–200 cells in a monolayer that were able to interact with the substrate and other neighboring cells. Traction stresses in the substrate were studied via displacement of fluorescent beads to understand cell interactions by region.

To determine the cell-layer stresses within aggregates, we performed two different types of modeling: a forward predicting thermal contraction model pioneered by Chen and colleagues (Nelson *et al.*, 2005) and a direct calculation of stresses using MSM developed by Fredberg and colleagues (Tambe *et al.*, 2011). For the thermal contraction model, we induced homogeneous contraction by setting a uniform coefficient of thermal expansion throughout the cell layer and applying a simulated temperature drop per the methods of Li and colleagues (Li *et al.*, 2009). We found that predicted traction stresses in the substrate below the cell layer are highest along the aggregate edge and lowest in the center (Figure 4.5A), which agrees with previous findings (Nelson *et al.*, 2005; Li *et al.*, 2009; Banerjee and Cristina Marchetti, 2013). The predicted average normal stress  $((\sigma_1 + \sigma_2)/2)$ , where  $\sigma$  is principal stress) in the cell layer has the opposite trend, with normal cell stress low at the edge and high in the center (Figure 4.5B).

For our homogeneous MSM model, experimentally measured traction forces were applied to the lower surface of a finite element model with uniform modulus throughout the cell layer based on the methods of Ji and colleagues (Figure 4.5C) (Liu *et al.*, 2016). These directly measured traction forces were averaged from six different aggregates to create a representative aggregate with a radially symmetric prototypical traction force distribution. On average, traction forces were highest at the edge and lowest in the center, as seen in previous studies (Liu *et al.*, 2016; Cirka *et al.*, 2017). For the homogeneous model, the calculated average normal stresses are highest in the center and lowest along the edge (Figure 4.5D) in agreement with previous predictions and calculations for constrained cell layers (Tambe *et al.*, 2011; He *et al.*, 2015).

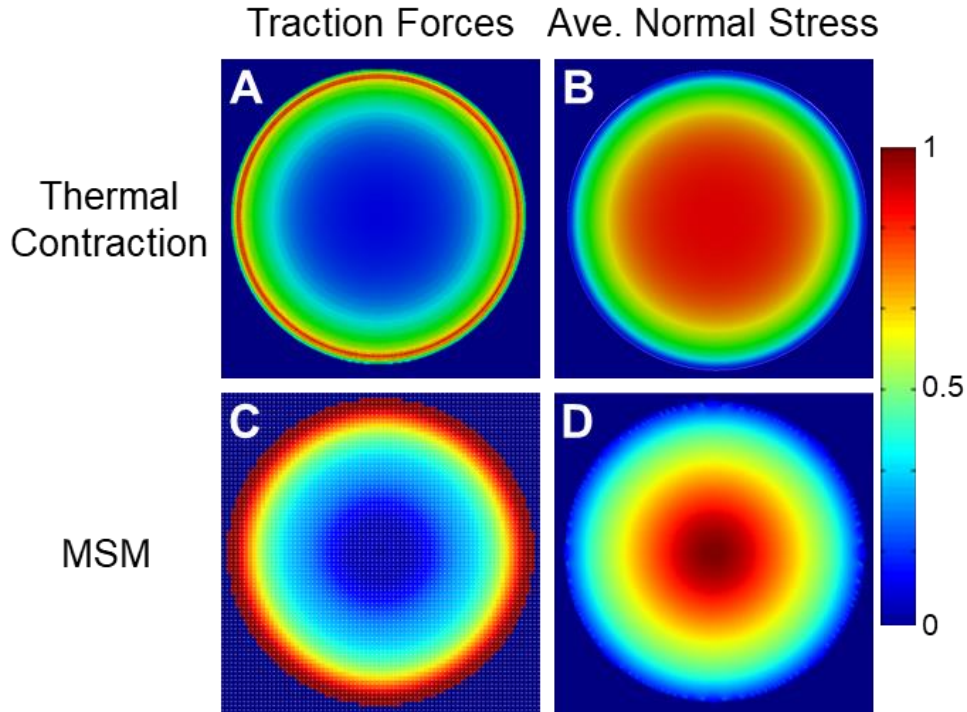


**Figure 4.5: Homogeneous thermal contraction and MSM modeling reveal high cell stress in aggregate center and high tractions at edge.** Heat maps of traction forces for homogeneous thermal contraction (A) and MSM model (C) show high tractions along aggregate periphery. Heat maps of cell-layer stress for homogeneous thermal contraction (B) and MSM model (D) display high stresses in aggregate center.

In contrast to these homogeneous model predictions and calculations, high cell stress associated biomarkers including cell spreading (Cirka *et al.*, 2016), elongation (He *et al.*, 2015), alpha-smooth muscle actin ( $\alpha$ -SMA)-rich stress fibers (Chen *et al.*, 2007), proliferation (Nelson *et al.*, 2005), and traction force generation (Li *et al.*, 2009; Cirka *et al.*, 2017) have all been reported at the edges of constrained multicellular aggregates. The homogenous models may be applicable to just-confluent layers and freely expanding monolayers where cell density remains relatively uniform. However, it appears that when cell populations grow within geometrically constrained areas, cell density increases nonuniformly and cell behavior changes regionally (Zimmermann *et al.*, 2016). We posit that when this non-uniform behavior occurs, the assumption of homogeneity is no longer valid.

#### 4.4.2 Distributions of high-stress biomarkers localize to aggregate periphery

To obtain more refined distributions of mechanical stress-related biomarkers, we quantified two cytoskeletal markers associated with cell contractility:  $\alpha$ -SMA, the hallmark of the contractile myofibroblast phenotype (Hinz, 2010), and the ratio of globular actin (G-actin) to filamentous actin (F-actin). Additionally, the distributions of three mechanosensitive indicators of cell fate were analyzed: apoptosis (Gourlay and Ayscough, 2005; Desouza *et al.*, 2012), yes-associated protein (YAP) nuclear localization (Aragona *et al.*, 2013; Das *et al.*, 2016; Elosegui-Artola *et al.*, 2017), and myocardin-related transcription factor A (MRTF-A).

Incorporation of  $\alpha$ -SMA into stress fibers correlates with the increase in contractile force in populations of fibroblasts cultured in 3-D protein gels (Hinz *et al.*, 2001) and on compliant gels (Chen *et al.*, 2007). We observed a doubling of  $\alpha$ -SMA intensity and incorporation into stress fibers from the center to the periphery in our patterned aggregates (Figure 4.6A), which agrees with previous studies of patterned fibroblasts assemblies (Li *et al.*, 2009). Under tension, F-actin stress fibers polymerize G-actin monomer units, thereby increasing the persistence length of fibers, while unloaded F-actin filaments depolymerize into G-actin (Dos Remedios *et al.*, 2003). If the total actin within a cell is conserved, G/F-actin ratios should be high for cells under low cell stress. We observed high G/F-actin ratio values in the center and low values at the edge further indicating lower cell-layer stress in central regions compared to the periphery (Figure 4.6B).

Previous evidence indicates that cells require a basal level of homeostatic tension to survive and that apoptosis is linked to states of low cell stress (Egerbacher *et al.*, 2008; Humphrey *et al.*, 2014). Increased rates of apoptosis have been found in single cells restricted in spreading by culturing on small protein islands (<20  $\mu\text{m}$  diameter) (Chen *et al.*, 1997), in adherence-dependent cells that are detached from a substrate (termed anoikis) (Frisch and Ruoslahti, 1997), and in cells cultured on soft substrates (Wang *et al.*, 2000). In our multicellular aggregates, the predominant apoptotic activity occurs in the aggregate center and decreases towards the

aggregate edge (Figure 4.6C). Additionally, compared to central cells, peripheral cells create larger, more persistent F-actin fibers, have higher fiber alignment, and align more circumferentially, indicating anisotropic stress (Figure 4.6, D and E).

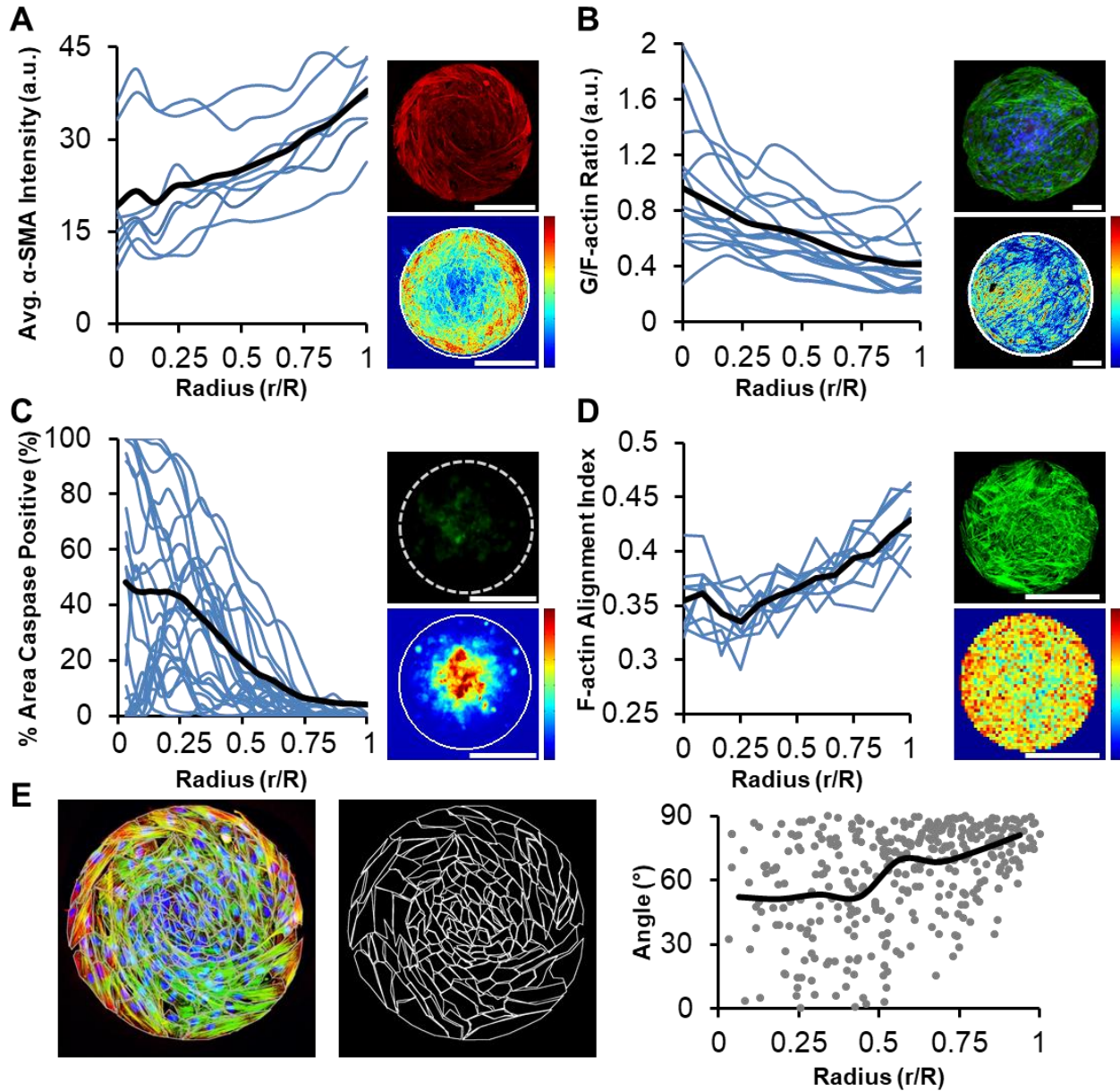


**Figure 4.6: Protein measurements for cell-layer stress indicate low stress state within the center of VIC aggregates.** **A)**  $\alpha$ -SMA intensity doubles from center to edge of aggregate. Inset shows aggregate stained for  $\alpha$ -SMA (top; red) and a heat map of average  $\alpha$ -SMA intensity (bottom).  $n = 8$  images (2 replicates). **B)** G/F-actin ratio with respect to aggregate radius decreases from center to periphery. Inset shows aggregate (top) stained for F-actin (green), G-actin (red), and nuclei (blue), and a heat map of average G/F-actin intensity (bottom).  $n = 14$  images (3 replicates). **C)** Cleaved caspase-3/7 presence decreases from center to edge of aggregate. Inset shows aggregate stained for caspase-3/7 (top; green,

dotted line indicates aggregate edge). A heat map was generated for average caspase-3/7 intensity (bottom). **D**) F-actin alignment index increases from center to edge of aggregate. An index of zero indicates no stress fiber alignment while an index of one indicates perfect fiber alignment. Inset shows aggregate stained for F-actin (top; green) and a heat map for average alignment index (bottom). **E**) Left: Aggregate with individual cells outlined and measured for cell angle. Center: Individual cell outlines. Right: Angle of cell in relation to radial angle ( $90^\circ$  indicates perpendicular to radial angle) shows that peripheral cells circumferentially align more than central cells.  $n = 2$  images (2 replicates). Scale bars =  $100 \mu\text{m}$ .

Restricting cell contractility by culturing cells at high density, culturing cells on low modulus substrates, or inhibiting contractility with ROCK inhibitors results in cytoplasmic YAP and MRTF-A localization (Dupont, 2016). In our aggregates, we observe YAP and MRTF-A nuclear exclusion within central cells and nuclear localization in peripheral cells (Figure 4.7). Combined, these distributions of stress-related biomarkers strongly suggest that low cell-layer stress occurs within the center of constrained multicellular aggregates, while edge cells generate relatively high anisotropic internal stress.

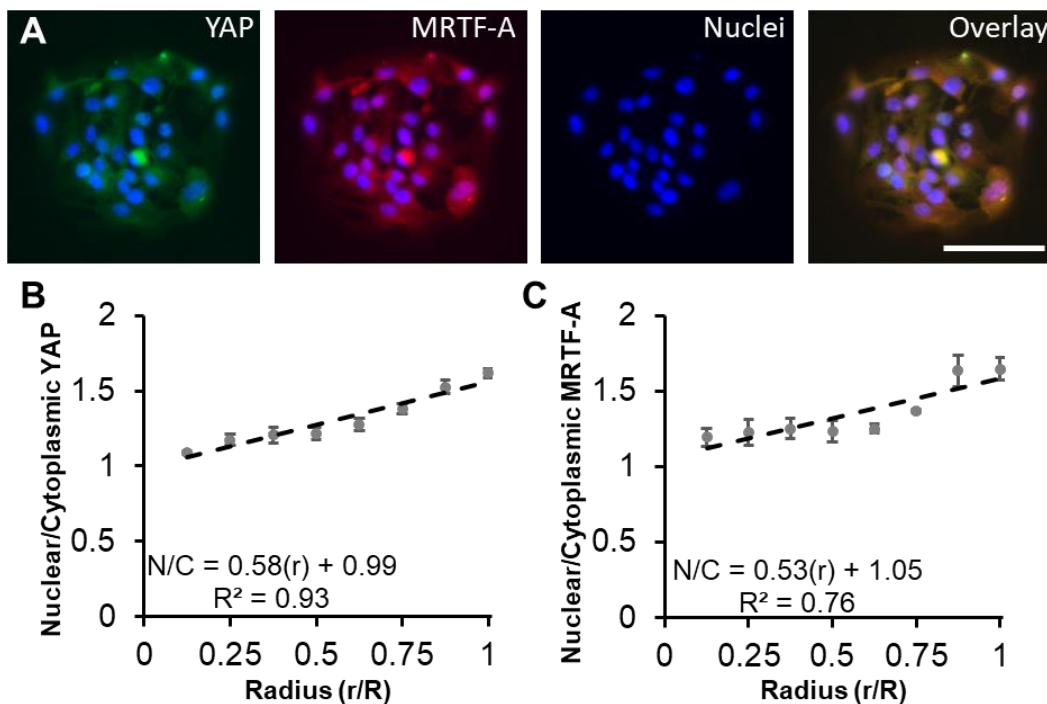


**Figure 4.7: YAP and MRTF-A localize in the nucleus of peripheral cells in multicellular aggregates.** **A**) Fluorescent image of YAP (green), MRTF-A (red), Hoechst (blue), and YAP/MRTF-A overlay in one aggregate. Hoechst localizes in all nuclei while YAP/MRTF-A are seen only in edge cells. Scale bar =  $100 \mu\text{m}$ . **B**) Scatterplot reveals that YAP nuclear/cytoplasmic ratio increases with respect to radial

location within an aggregate.  $n = 464$  cells (3 replicates). **C)** Scatterplot reveals that MRTF-A nuclear/cytoplasmic ratio increases with respect to radial location within an aggregate. Scatterplots are represented as mean  $\pm$  standard error.  $n = 320$  cells (3 replicates). \*\*\* indicates  $p < 0.001$  for the regression slope using a linear regression statistical test.

Similar to our micropatterned cell layers, in geometrically constrained multicellular systems *in vivo* (e.g. the *Drosophila* wing), increased proliferation along the edge region increases crowding of central cells and reduces cell spread area (LeGoff *et al.*, 2013). Constrained cell growth induces compression on central cells leading to apoptosis (Mao *et al.*, 2013; Diaz de la Loza and Thompson, 2017). This major difference in cell behavior with respect to wing location suggests that the local environment sensed by cells is non-uniform. This dynamic phenomenon requires heterogeneous parameters to accurately predict cell-layer stresses.

#### 4.4.3 Central cells vary in morphology, behavior, and properties compared to peripheral cells

It is well established that cell-generated forces increase with increasing spread area (Wang *et al.*, 2000; LeGoff *et al.*, 2013; Oakes *et al.*, 2014; Dupont, 2016). To obtain a rough estimate of the radial variation of contractility of the cells within our aggregates, we first determined a relationship between cell spread area and radius within aggregates ( $Area = A(r)$ ) by outlining individual cells within one aggregate. We found that cells elongated along the periphery had spread areas approximately eight times larger than centrally located cells (Figure 4.8, A and B). We then segmented aggregates into two regions (center:  $0 \leq r < 0.5R$  and periphery:  $0.5R \leq r \leq R$ , where  $r$  = radius and  $R$  = max radius) and calculated the average spread area for each region over time. After one day post-confluence, the average cell spread area in the central region was approximately 50% of peripheral cells (Figure 4.8C). In contrast, Ji and colleagues report uniform cell area of MC3T3 cells regardless of their position on circular and ring-shaped micropatterns (He *et al.*, 2015). This discrepancy may be due to their experimental timing being immediately at confluence rather than after cell crowding. In confluent cell-layers on constrained patterns, cells proliferate at the edge (Nelson *et al.*, 2005; Li *et al.*, 2009; Aragona *et al.*, 2013) and then migrate inwards, causing crowding in the center. After one week post-confluence in our aggregates, the average cell spread area decreases by over 50% in both central and peripheral

regions (Figure 4.8C). The increase in cell number over time results in smaller average spread areas in aggregate centers, decreasing to constrained single cell sizes previously shown to induce apoptosis (Chen *et al.*, 1997).

Next, we established a quantitative relationship between cell-generated traction forces and cell spread area ( $Force = F(A)$ ) by measuring traction forces of individual VICs on 7.5 kPa PA gels (Figure 4.8D). Similar to previous findings (Califano and Reinhart-King, 2010; Rape *et al.*, 2011; Oakes *et al.*, 2014), we observed a positive linear relationship between traction forces and spread area and also between maximum substrate stress and spread area. On softer substrates the cells generate even lower forces, yet a linear relationship between traction force and cell area remains. In multicellular aggregates, traction stresses exert local forces to neighboring cells, and transfer forces between them. Traction stresses and strain energy increase with individual cell or multicellular aggregate size, localize along the cell or aggregate periphery, and are independent of the number of cells present (Mertz *et al.*, 2012; Oakes *et al.*, 2014). Further, during the seeding process, natural variation occurs in the number of cells that attach to any given protein pattern. Similar to Dufresne and colleagues, we found that total traction force generated by a multicellular colony scales with the total area of the colony yet is surprisingly insensitive to the number of cells present (Mertz *et al.*, 2012). Thus, the average traction force per cell in an aggregate (total aggregate traction force divided by number of cells) decreases with increased cell density in multicellular aggregates (Figure 4.8E). Combined, these results strongly suggest that, within saturation limits, cells generate traction forces roughly proportional to their spread area over a large range of areas, regardless of whether the cells are isolated or in multicellular aggregates. This behavior forms the basis for how we model contractility with respect to radius in our heterogeneous model.

The cell stiffness also appears to follow the trend of cell area. Using AFM stiffness mapping, we observed stiffness values approximately half as large in central regions compared to peripheral regions in aggregates (Figure 4.8F). Indentation stiffness measured by AFM is related to both the intrinsic modulus of cells and the level of tension in their cytoskeletons (Canović *et al.*, 2014).

Together, these results demonstrate that central cells have smaller spread areas, generate lower tension, and have lower cell moduli compared to peripheral cells.

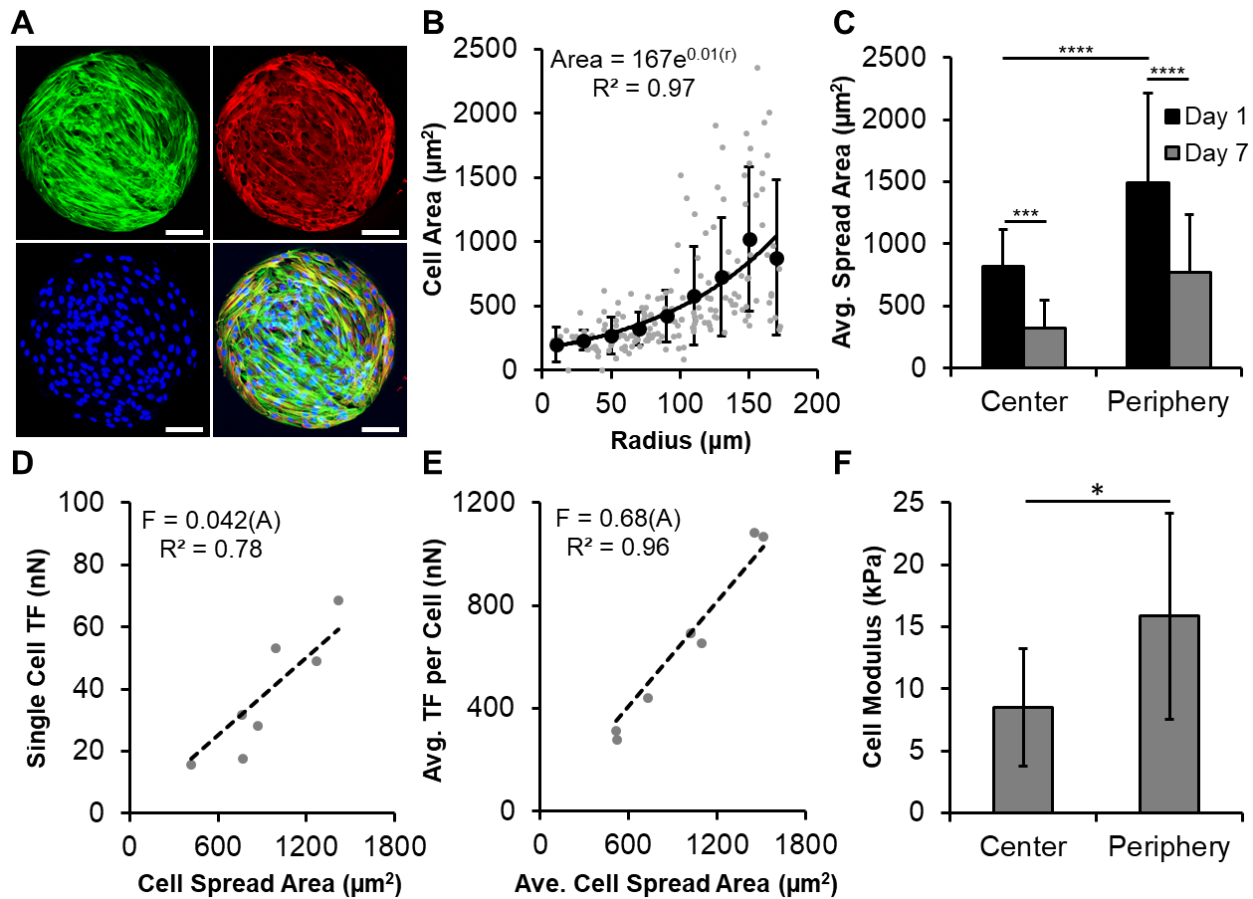


**Figure 4.8: Cells within the central region of aggregates have on average, lower spread area, lower traction force (TF), and lower indentation stiffness compared to those in the peripheral area. A)** Aggregate stained for F-actin (green),  $\alpha$ -SMA (red), nuclei (blue), and merge. Scale bar = 50  $\mu\text{m}$ . **B)** The measured relationship for cell area as a function of radius for one aggregate. Gray dots are raw data, black dots are mean  $\pm$  st. dev. for 20  $\mu\text{m}$  bins, and exponential trendline is fit to binned means. **C)** Central cell spread area is approximately half that of peripheral cells. Cell spread area decreases over one week in culture in both central and peripheral regions.  $n = 22$  cells for both center and periphery at Day 1,  $n = 16$  cells for both center and periphery at Day 7 (2 replicates). Data represented as mean  $\pm$  st. dev. \*\*\* $p < 0.001$  and \*\*\*\* $p < 0.0001$  for two-way ANOVA with Sidak's post-hoc test. **D)** The relationship for traction force as a function of cell area for individual VICs. **E)** Relationship of average traction force as a function of average area per cell in multicellular aggregates. **F)** Central cells in aggregates have a lower modulus from AFM indentation analysis than peripheral cells.  $n = 8$  aggregates (3 replicates). Data represented as mean  $\pm$  SEM, \* $p < 0.05$  for Student t-test.

#### 4.4.4 Heterogeneous models predict stress distributions inverse to homogeneous models

To predict the cell-layer stress within aggregates, we induced contraction in our finite element model with a simulated temperature drop (Li *et al.*, 2009). In the homogeneous case (uniform coefficient of thermal expansion), cell-layer stress increases from the edge to the center as previously reported for similar simulations (Nelson *et al.*, 2005; Li *et al.*, 2009; Liu *et al.*, 2016). For our heterogeneous model, we approximated contractility as a continuous exponential heterogeneous distribution based on experimentally measured data. Alternatively, we utilized a heterogeneous step function which gives results comparable to the exponential distribution but is less realistic (Figure 4.9). However, it allows a clearer visualization of how the stresses change with an abrupt change in properties. Our step function heterogeneous model results in stress distributions consistent with Edwards and Schwarz, who show a sudden change in stress at the transition point between the two values of contractility (Edwards and Schwarz, 2011). Using the linear regression of traction forces for individual cells and the exponential relationship between cell area and radius (see Figure 4.8, B and D), we generated a quantitative relationship between traction force and radial location. In our model, we assumed that  $\alpha(r)$  follows the same trend as  $F(r)$ , which provided us with the coefficient of thermal expansion as a function of radius ( $\alpha(r) = 0.9e^{2.34r}$ ) and normalized to its initial value. The circumferential stress profile for this exponential heterogeneous case decreases 3.5-fold from the edge to the center (Figure 4.10A), which is the inverse of the homogeneous case, where the stress increases 2-fold. Additionally, the radial stress in the heterogeneous case is highest towards the edge and decreases by half towards the center. The stress predictions from the heterogeneous models match biological markers of cell-layer stress state far better than the homogeneous model.

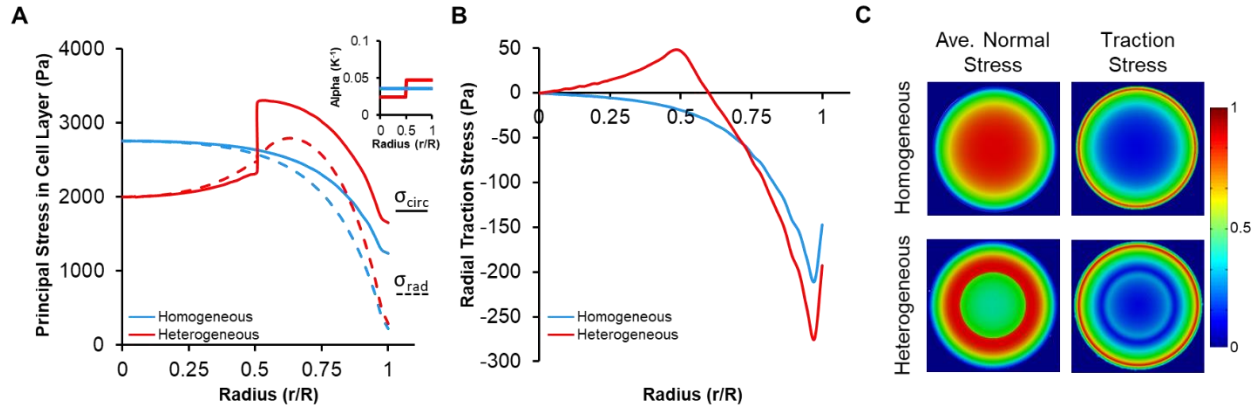


**Figure 4.9: Cell-layer and substrate stresses simulated by thermal contraction for both homogeneous and step change heterogeneous parameters for cell contractility.** **A)** Cell-layer radial (*dotted*) and circumferential (*solid*) stresses with homogeneous (*blue*) and step change heterogeneous (*red*) conditions for contractility (coefficient of thermal expansion,  $\alpha$ , is shown graphically at the top of panel A). **B)** Predicted radial traction stresses for homogeneous (*blue*) and step change heterogeneous (*red*) models of cell contractility as a function of radius. **C)** Heat maps of predicted average normal stress and traction stresses for the homogeneous and step change conditions.

Considering the roughly inverse patterns of cell-layer stress, predicted substrate traction stress patterns are surprisingly similar for the homogeneous and heterogeneous models (Figure 4.10, B and C). In the heterogeneous cases, small positive (outward) tractions are generated in the center due to relatively high contraction of the peripheral region pulling on the central region. We found this result to be evident in some experimental traction force maps (Figure 4.11). This phenomenon has also been reported in another study where modeling contraction as a step change caused positive displacements (outward) to form even though the layer as whole was retracting (Edwards and Schwarz, 2011). These results demonstrate that variations in collective cell contractility greatly affect cell-layer stress distributions but have little effect on substrate traction stresses, which suggests that using accurate cell-layer mechanical properties is critical for accurately estimating cell-layer stresses from measured traction stresses.

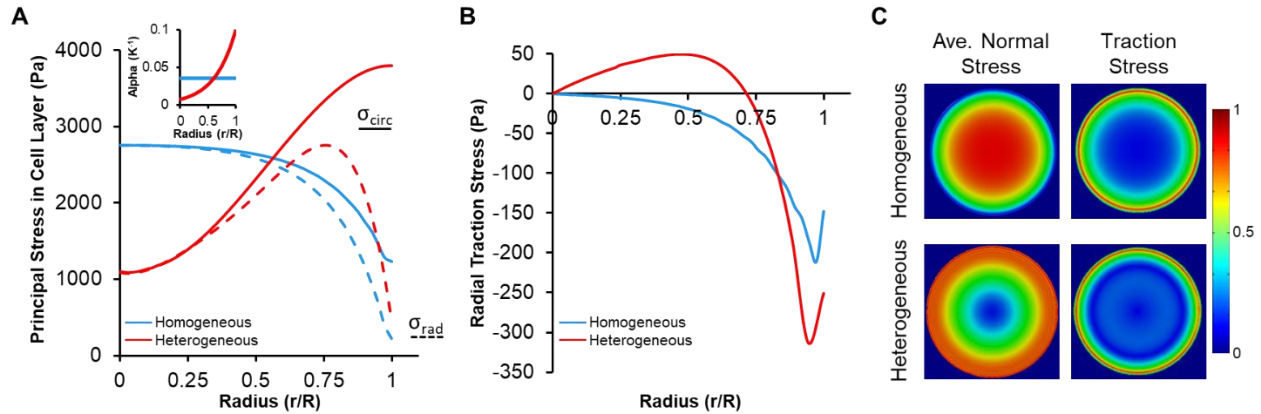


**Figure 4.10: Continuous distribution for contractile stresses as a function of radius is used to simulate cell-layer and substrate stresses. A)** Cell-layer radial (dotted) and circumferential (solid) stresses with homogeneous (blue) and exponential heterogeneous (red) conditions for contractility (coefficient of thermal expansion,  $\alpha$ , is shown graphically at the top of panel B). **B)** Predicted radial traction stresses for homogeneous (blue) and exponential heterogeneous (red) models of cell contractility as a function of radius. **C)** Heat maps of predicted average normal stress and traction stresses for the homogeneous and exponential conditions.

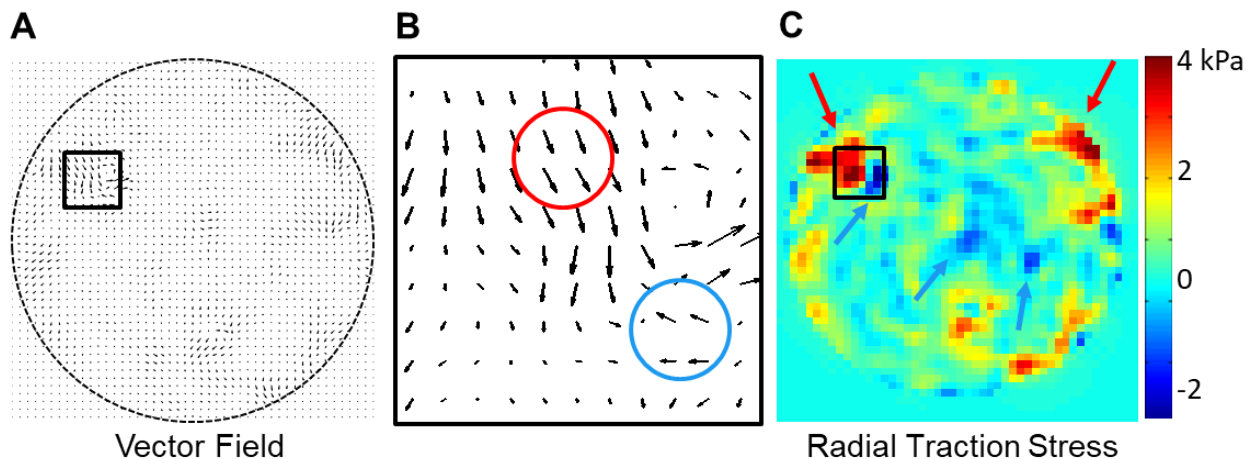


**Figure 4.11: Cell aggregates generate both positive (inward) and negative (outward) stresses. A)** Vector field of cell aggregate (outlined in dotted line) shows stress localization in different regions. **B)** Zoomed in vector field in subregion (black square) from panel A and panel C. The red circle highlights positive forces directed inwards towards the aggregate center, while the blue circle shows negative forces directed outwards towards the aggregate periphery. **C)** Heat map of radial traction stresses for representative aggregate. Positive (red arrows) forces indicate inward displacements while negative (blue arrows) forces indicate outward facing displacements. High contraction can cause strong positive (inward) forces which can then create smaller negative (outward) forces to occur.

#### 4.4.5 MSM trends agree with thermal contraction models

We then directly calculated the in-plane stress distribution using MSM (Liu *et al.*, 2016). We modeled the cell layer as a passive uniform-thickness linear elastic disc and applied measured

substrate traction forces to the lower surface of the model (Figure 4.12). In an approach analogous to the simulations, we calculated the stresses for three cases: homogeneous elastic modulus, step function modulus (Figure 4.13A), and an exponentially increasing modulus ( $E(r) = 0.9e^{2.34r}$ ) from the center to the edge. Similar to the coefficients of thermal expansion, these moduli values were normalized to have the same average value. Average stress values substantially decrease in central regions of aggregates and increase in the peripheral region when introducing heterogeneous conditions (Figure 4.12).

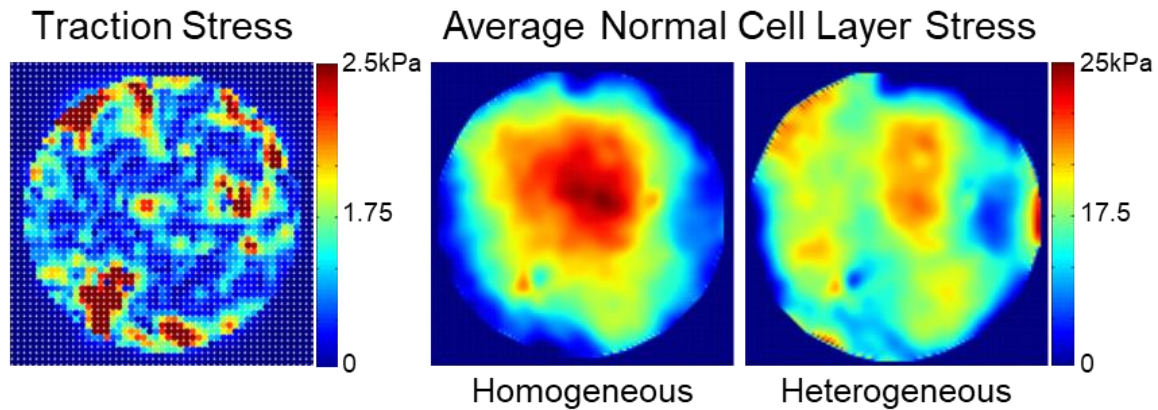


**Figure 4.12:** Heat maps from left to right show measured traction stresses and output average normal stresses for homogeneous and exponential models for a representative aggregate. Distributions of cell-layer elastic moduli are homogeneous and exponentially varying modulus per equation  $E(r) = 0.9e^{2.34r}$ .

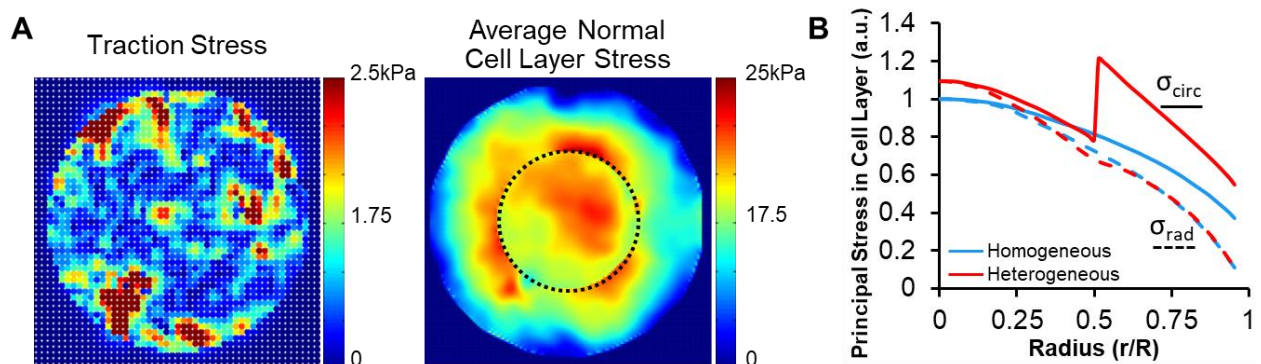


**Figure 4.13: Cell-layer stresses calculated by MSM for step change heterogeneous condition from traction forces averaged over many aggregates. A)** Heat maps from left to right show measured traction stresses and output average normal stresses for step change model in a representative aggregate. Distribution of cell-layer elastic moduli is 50% lower modulus at  $r = 0.5R$  (black dotted circle). **B)** Predictive models from input average traction stresses for cell-layer radial (*solid*) and circumferential (*dotted*) stresses with homogeneous (*blue*) and step change heterogeneous (*red*) conditions for modulus.

The individual cell-layer stress patterns from each aggregate are nonuniform, but different in magnitude and form. In all cases, the heterogeneous conditions had lower stresses in the center compared to the homogeneous case. Experimentally measured substrate stresses from six different aggregates were binned together with respect to their radial location from the center of the aggregate. An average traction force per radial bin was calculated and a best fit curve was fitted to represent any traction force for a given radius (Figure 4.14A). The equation for the best fit curve is:

$$T(r) = (-7.01E - 8)r^6 + (1.96E - 5)r^5 - (2.03E - 3)r^4 + (9.52E - 2)r^3 - (1.93E)r^2 + (1.62E + 1)r \quad (11)$$

where  $r$  is the radius,  $E$  is Young's modulus, and  $T(r)$  is the average traction stress in Pa. On average, the traction stress near the aggregate edge is high and then decreases towards the center. These average traction stresses were input into the three different case models to obtain radial and circumferential cell-layer stresses for an average aggregate using MSM (Figure 4.14B, Figure 4.13B).

In the homogeneous disc (uniform elastic modulus), both radial and circumferential stresses are highest in the center and decrease towards the edge. For the exponential function heterogeneous disc, radial stress increases rapidly from the edge and then levels out towards the center, whereas the circumferential stress is high at the edge and decreases towards the center (Figure 4.14B). The stress distributions calculated with the average tractions are similar to those simulated with the thermal contraction model (cf. Figure 4.14B and Figure 4.10A). These results further emphasize that cell-layer stress cannot be solely inferred from substrate tractions without additional specification of cell-layer material properties.

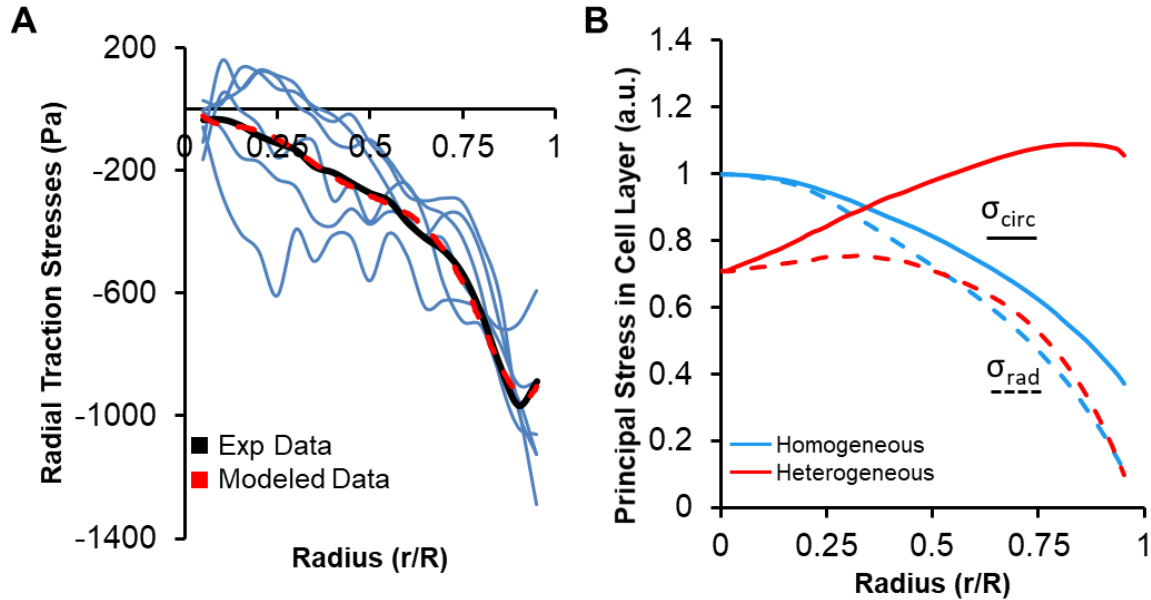


**Figure 4.14: Cell-layer stresses calculated by MSM for homogeneous and heterogeneous conditions from traction forces averaged over many aggregates. A)** The average radial traction stresses measured from six aggregates (blue lines) were averaged (black line) and a best fit curve (red dashed) was determined. **B)** Inputting average traction stresses vs. radius generates predictive models for cell-layer radial (dotted) and circumferential (solid) stresses with homogeneous (blue) and exponential heterogeneous (red) conditions for modulus.

#### 4.4.6 Activation of YAP decreases apoptosis in multicellular aggregates

It has been shown in previous studies that cells require a homeostatic tension to survive, for example states of low cell stress can initiate apoptosis (Egerbacher *et al.*, 2008; Humphrey *et al.*, 2014). As previously mentioned, indicators of high cell-tension are localized to the edges of our aggregates, while indicators of low cell-tension are found in central regions. Apoptosis activity occurs in regions of low cell-tension (as calculated by our heterogeneous models), observed being highest at aggregate centers and decreasing towards the aggregate edge (Figure 4.15A).

Activated YAP has been correlated to cells with large spread areas, defined stress fibers, and low instances of apoptosis. If apoptosis is caused by cells having low tension states and deactivated YAP, is it possible that if YAP is active, cells can survive, even in a low stress environment such as the center of an aggregate? In order to test this, we transfected VICs to constitutively express YAP and cultured them in multicellular aggregates. Active YAP promotes transcription of pro-survival genes (Zhang *et al.*, 2011; Lin *et al.*, 2015; Codelia *et al.*, 2017), which can stimulate

cell survival in the central region of aggregates. We find a dramatic decrease in apoptotic activity in VICs with constitutively active YAP compared to normal VICs (Figure 4.15B). These results demonstrate that active YAP, even in cells with low tension, can reduce occurrences of apoptosis and increase cell survival. The mechanism behind how active YAP reduces apoptotic levels still needs to be studied to determine if active YAP increases actin polymerization and therefore cytoskeletal tension, or if it instead has a direct effect on the nucleus where transcription of survival genes increases.

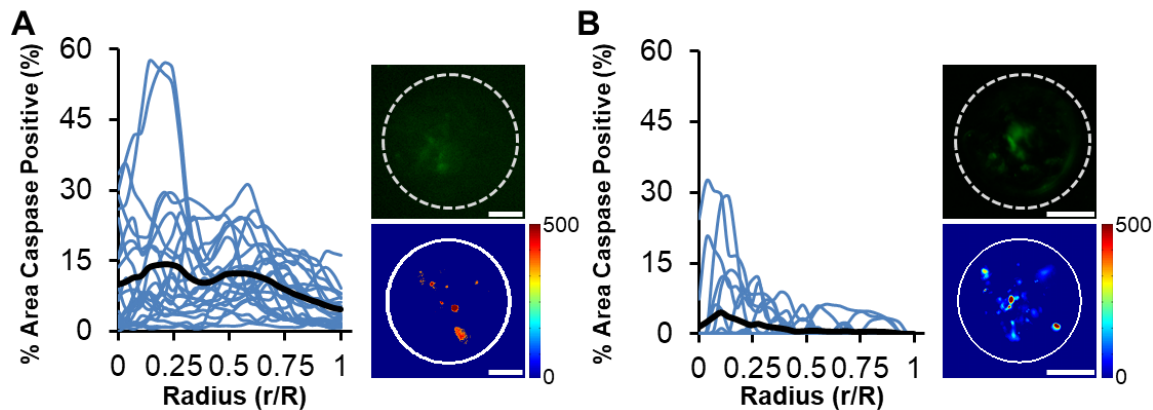


**Figure 4.15: Constitutively active YAP decreases occurrences of apoptosis in central region in aggregates.** **A)** Cleaved caspase-3/7 presence in normal VICs decreases from center to edge of aggregate. Inset shows aggregate stained for caspase-3/7 (top; green, dotted line indicates aggregate edge) and heat map for average caspase-3/7 intensity (bottom).  $n = 24$  aggregates (3 replicates). **B)** VICs with constitutively active YAP have much less caspase-3/7 presence compared to normal VICs. The general trend for caspase-3/7 decreases from center to edge of aggregate. Inset shows aggregate stained for caspase-3/7 (top; green, dotted line indicates aggregate edge), and heat map for average caspase-3/7 intensity (bottom).  $n = 23$  aggregates (3 replicates). Scale bars =  $50 \mu\text{m}$ .

#### 4.4.7 Interpretation of stress measurements relative to biological markers

In past studies, certain biomarkers have been related to regions of “high stress” that are predicted by computational models. In these cases, the authors refer to predicted substrate traction stresses, not cell-layer stress. While it is possible that traction stresses drive some cell behaviors, it is more likely that many markers related to intracellular stresses are driven by the cell-layer stress state rather than substrate traction stresses. For example, when increasing stress in cell clusters via mechanical stretching,  $\alpha$ -SMA increases throughout aggregates (Li *et al.*, 2009).

Additionally, actin stress fiber formation, amounts of F-actin and G-actin, and proliferation markers are also likely related to be driven by the internal stress state within a cell. On the other

hand, one biomarker that is likely dependent on traction stresses rather than cell-layer stress would be focal adhesion size. Focal adhesion size has previously been correlated to traction stress magnitude (Goffin *et al.*, 2006). These markers are found to be highest at cell cluster edges, yet homogeneous models predict highest stresses in the center.

When averaged over many post-confluent aggregates, stress-related biomarkers, such as  $\alpha$ -SMA, F-actin, and traction forces, clearly localize to aggregate edges. However, when considering cases where cells are able to move more independently, a large variability between aggregates has been observed. Large traction forces have been shown to accumulate in inner regions in aggregates below or at confluence and in aggregates with highly motile cells (Dumbali *et al.*, 2017; Schaumann *et al.*, 2018). Thus, the emergent cell behavior and stress distributions predicted by our models are likely only valid for post-confluent aggregates wherein heterogeneity in cell density is established due to the geometric constraints.

Previous studies have also utilized results from homogenous models to explain circumferential cell alignment near the edges of patterned multicellular systems. Ji and colleagues attribute the alignment to stress anisotropy, defined by the difference in principal in-plane stresses (equivalent to twice the maximum in-plane shear stress) (He *et al.*, 2015; Liu *et al.*, 2016). Cell alignment along the maximum principal stress direction is also found in other systems (Yuan *et al.*, 2017). Our heterogeneous models accentuate the anisotropy of stresses present at the edges while also predicting low magnitude average normal stresses in the center, which correspond to the high levels of apoptosis at the center. The biological factors that we measured are clear indicators of cellular stress, and it is therefore unlikely that anisotropy is the cause of the distribution of biomarkers but rather the cell-layer stress itself that is the main contributor.

To the best of our knowledge, all current models that calculate cell-layer stress use homogeneous models with the exception of Tambe *et al.* (Tambe *et al.*, 2013). In that study, the local elastic modulus was increased in proportion to the local stress that was pre-calculated assuming a

homogeneous elastic modulus and little change in the distribution of stresses was found. However, they focused on ruggedness of the stress landscape in migrating monolayers and did not consider geometrically constrained aggregates of proliferating cells. In contrast, our simulations decrease the contractility or modulus distribution from the edge to the center based on independent biophysical parameters, and we focus our attention on the distribution of stress magnitude and how this corresponds to certain biological responses.

To experimentally test whether the change in stress predicted by homogeneous or heterogeneous models is more likely the driver of the observed radial distribution in biomarkers, we increased the cell-layer stress in the central region by applying an external load using magnetic micro-beads (Pinto *et al.*, 2014). Magnetic micro-beads coated with collagen were uniformly deposited and attached to cultured cells and exposed to external loads via a magnetic force (Figure 4.16A). Over the course of 7 days, the magnetic beads accumulated in the central region of the aggregate, indicating migration of periphery cells to the center of the aggregates. Applying the magnetic force for one week decreased the apoptotic activity within aggregates and resulted in more uniform and diffuse  $\alpha$ -SMA staining (Figure 4.16, B and C). Application of the magnetic field also increased the nuclear aspect ratio for center cells such that they were equivalent to that of edge cells (Figure 4.16D). Together, these results suggest that the additional out-of-plane mechanical load in the center results in higher intracellular stress and therefore more uniform biological behavior across the aggregate, which supports the heterogeneous model. If the central region had initially higher stress than the edges, as predicted by the homogeneous model, the additional loading would enhance the differences in biomarkers from the center to edge.

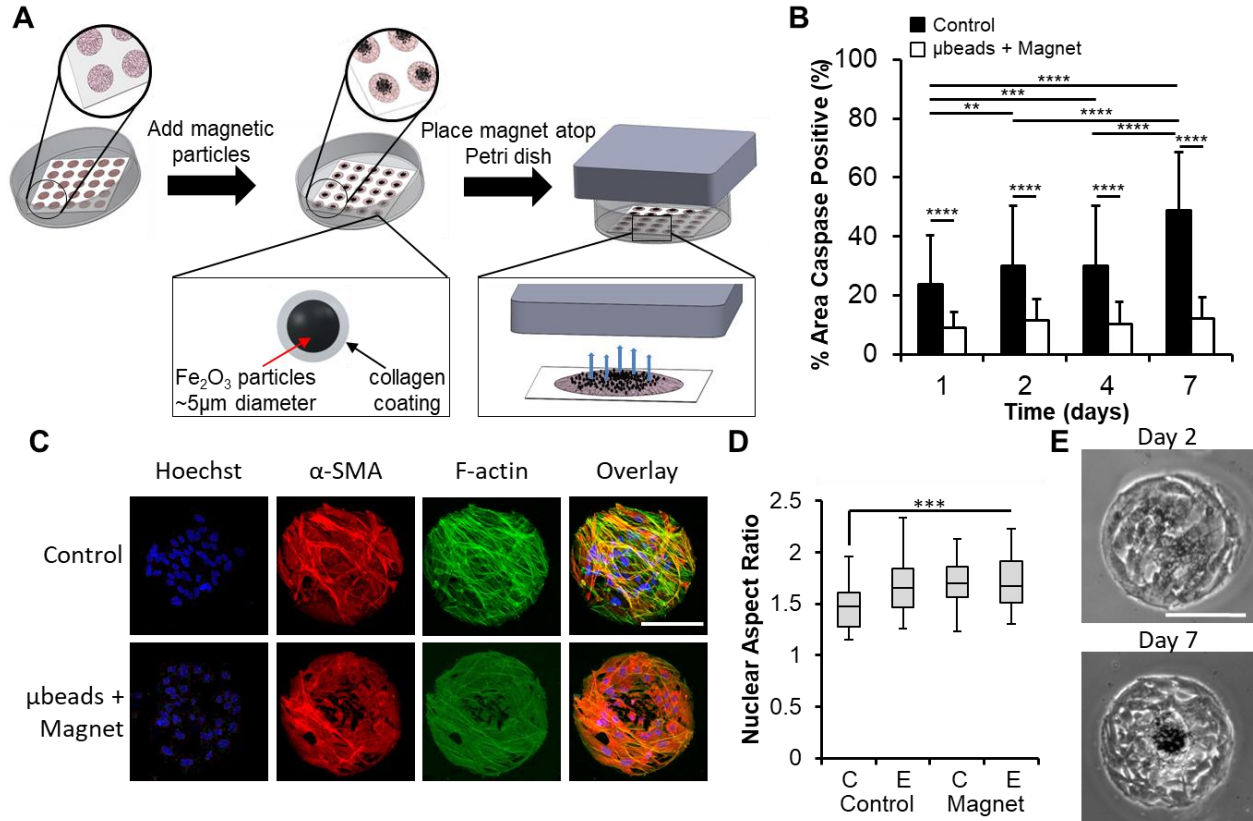


**Figure 4.16: Additional mechanical load in aggregate center increases intracellular stress and results in a more uniform biological behavior across aggregate.** **A)** Schematic of applying collagen coated magnetic beads onto cell aggregates and magnet to create an upward tensile force in the out-of-plane direction on cells. **B)** Caspase-3/7 activity reduces over time in the presence of magnetic beads.  $n > 97$  aggregates (3 replicates). Data represented as mean  $\pm$  standard deviation. \*\* indicates  $p < 0.01$ , \*\*\* indicates  $p < 0.001$ , and \*\*\*\* indicates  $p < 0.0001$  for two-way analysis of variance with Sidak's post-hoc test. **C)** Representative fluorescent images of an aggregate stained for F-actin (green),  $\alpha$ -SMA (red), and Hoechst (blue). Presence of magnetic field reduces  $\alpha$ -SMA incorporation into stress fibers. Scale bar = 100  $\mu$ m. **D)** Nuclear aspect ratio increases for central cells (C) relative to edge cells (E) when under magnetic stress.  $n > 50$  cells (3 replicates). Box and Whisker plots show medians, 25<sup>th</sup>/75<sup>th</sup>, and 5<sup>th</sup>/95<sup>th</sup> percentiles. \*\*\* indicates  $p < 0.001$  for one-way analysis of variance with Tukey's HSD post-hoc test. **E)** Phase images of aggregates at day 2 and day 7 of culture. Magnetic beads appear to localize in the central region, possibly due to cell migration towards the center. Scale bar = 100  $\mu$ m.

## 4.5 Conclusions

In this study, we present experimental and computational evidence that incorporation of heterogeneity in regional cell properties is critical for accurate estimation of distributed cell-layer stresses. By incorporating heterogeneous cell contractility and mechanical parameters, our enhanced finite element model yields cell-layer stress contours that agree with multiple

biological measures of local cell stress, all of which indicate low stress in the center of multicellular aggregates and high circumferentially aligned stress at the periphery. Constitutively activating YAP in aggregates reduces levels of apoptosis in central regions but the mechanism behind this result remains untested. Homogeneous models may be sufficient for estimating stress distributions in unconstrained systems and/or for short culture times where cell density remains constant. However, our results strongly suggest that in constrained systems over longer timeframes, proliferation and growth lead to regional changes in cell shape, size, and physical properties that must be considered in mechanical analysis of multicellular systems.

## 4.6 Author Contributions

Z.G., H.C., K.B. designed experiments. Z.G. and H.C. conducted biological experiments and H.A.C. performed modelling experiments. Z.G., H.A.C., H.C. analyzed data and V.L. contributed data. Q.W. and D.M. helped with experimental methods and N.R. helped with modeling methods. Z.G., H.A.C., Q.W., D.M., N.R., and K.B. interpreted the data. Z.G., H.C., and K.B. wrote the manuscript.

## 4.7 Acknowledgements

Will Linthicum is acknowledged for his help and expertise with AFM experiments. We thank Sebastian Mana-Capelli for his help producing the constitutively active YAP cell line. This work was funded in part by grants from the National Science Foundation (CMMI 761432), the National Institutes of Health (2R15HL087257-02A1), and a WPI-UMass Medical School Seed Grant.

## 4.8 References

Aragona, M., Panciera, T., Manfrin, A., Giulitti, S., Michielin, F., Elvassore, N., Dupont, S., and Piccolo, S. (2013). A mechanical checkpoint controls multicellular growth through YAP/TAZ regulation by actin-processing factors. *Cell* 154, 1047–1059.

- Banerjee, S., and Cristina Marchetti, M. (2013). Controlling cell-matrix traction forces by extracellular geometry. *New J. Phys.* 15.
- Brugués, A., Anon, E., Conte, V., Veldhuis, J. H., Gupta, M., Colombelli, J., Muñoz, J. J., Brodland, G. W., Ladoux, B., and Trepap, X. (2014). Forces driving epithelial wound healing. *Nat. Phys.* 10, 683–690.
- Califano, J. P., and Reinhart-King, C. A. (2010). Substrate stiffness and cell area predict cellular traction stresses in single cells and cells in contact. *Cell. Mol. Bioeng.* 3, 68–75.
- Canović, E. P., Seidl, D. T., Barbone, P. E., Smith, M. L., and Stamenović, D. (2014). Stiffness versus prestress relationship at subcellular length scale. *J. Biomech.* 47, 3222–3225.
- Chen, C. S., Mrksich, M., Huang, S., Whitesides, G. M., and Ingber, D. E. (1997). Geometric control of cell life and death. *Science* 276, 1425–1428.
- Chen, J., Li, H., SundarRaj, N., and Wang, J. H. C. (2007). Alpha-smooth muscle actin expression enhances cell traction force. *Cell Motil. Cytoskeleton* 64, 248–257.
- Cirka, H. A., Uribe, J., Liang, V., Schoen, F. J., and Billiar, K. L. (2017). Reproducible in vitro model for dystrophic calcification of cardiac valvular interstitial cells: insights into the mechanisms of calcific aortic valvular disease. *Lab Chip* 17, 814–829.
- Cirka, H., Monterosso, M., Diamantides, N., Favreau, J., Wen, Q., and Billiar, K. (2016). Active traction force response to long-term cyclic stretch is dependent on cell pre-stress. *Biophys. J.* 110, 1845–1857.
- Codelia, V. A., Sun, G., and Irvine, K. D. (2017). Regulation of YAP by mechanical strain through Jnk and Hippo signaling. *Curr. Biol.* 24, 2012–2017.
- Das, A., Fischer, R. S., Pan, D., and Waterman, C. M. (2016). YAP nuclear localization in the absence of cell-cell contact is mediated by a filamentous actin-dependent, Myosin II and Phospho-YAP-independent pathway during extracellular matrix mechanosensing. *J. Biol. Chem.* 291, 6096–6110.
- Desouza, M., Gunning, P. W., and Stehn, J. R. (2012). The actin cytoskeleton as a sensor and mediator of apoptosis. *Bioarchitecture* 2, 75–87.
- Diaz de la Loza, M. C., and Thompson, B. J. (2017). Forces shaping the *Drosophila* wing. *Mech. Dev.* 144, 23–32.
- Dumbali, S. P., Mei, L., Qian, S., and Maruthamuthu, V. (2017). Endogenous Sheet-Averaged Tension Within a Large Epithelial Cell Colony. *J. Biomech. Eng.* 139, 101008.
- Dupont, S. (2016). Role of YAP/TAZ in cell-matrix adhesion-mediated signalling and mechanotransduction. *Exp. Cell Res.* 343, 42–53.
- Edwards, C. M., and Schwarz, U. S. (2011). Force localization in contracting cell layers. *Phys.*

Rev. Lett. 107, 1–5.

Egerbacher, M., Arnoczky, S. P., Caballero, O., Lavagnino, M., and Gardner, K. L. (2008). Loss of homeostatic tension induces apoptosis in tendon cells: an in vitro study. *Clin. Orthop. Relat. Res.* 466, 1562–1568.

Elosegui-Artola, A. et al. (2017). Force triggers YAP nuclear entry by regulating transport across nuclear pores. *Cell* 171, 1397-1410.e14.

Frisch, S. M., and Ruoslahti, E. (1997). Integrins and anoikis. *Curr. Opin. Cell Biol.* 9, 701–706.

Goffin, J. M., Pittet, P., Csucs, G., Lussi, J. W., Meister, J. J., and Hinz, B. (2006). Focal adhesion size controls tension-dependent recruitment of  $\alpha$ -smooth muscle actin to stress fibers. *J. Cell Biol.* 172, 259–268.

Gould, R. A., and Butcher, J. T. (2011). Isolation of Valvular Endothelial Cells. *J. Vis. Exp.*, 6–10.

Gourlay, C. W., and Ayscough, K. R. (2005). The actin cytoskeleton: a key regulator of apoptosis and ageing? *Nat. Rev. Mol. Cell Biol.* 6, 583–589.

He, S., Liu, C., Li, X., Ma, S., Huo, B., and Ji, B. (2015). Dissecting Collective Cell Behavior in Polarization and Alignment on Micropatterned Substrates. *Biophys. J.* 109, 489–500.

Hinz, B. (2010). The myofibroblast: Paradigm for a mechanically active cell. *J. Biomech.* 43, 146–155.

Hinz, B., Celetta, G., Tomasek, J. J., Gabbiani, G., and Chaponnier, C. (2001). Alpha-Smooth Muscle Actin Expression Upregulates Fibroblast Contractile Activity. *Mol. Biol. Cell* 12, 2730–2741.

Humphrey, J. D., Dufresne, E. R., and Schwartz, M. A. (2014). Mechanotransduction and extracellular matrix homeostasis. *Nat. Rev. Mol. Cell Biol.* 15, 802–812.

Kilian, K. A., Bugarija, B., Lahn, B. T., and Mrksich, M. (2010). Geometric cues for directing the differentiation of mesenchymal stem cells. *Proc. Natl. Acad. Sci.* 107, 4872–4877.

Lee, J., Abdeen, A. A., Wycislo, K. L., Fan, T. M., and Kilian, K. A. (2016). Interfacial geometry dictates cancer cell tumorigenicity. *Nat. Mater.* 15, 856–862.

LeGoff, L., Rouault, H., and Lecuit, T. (2013). A global pattern of mechanical stress polarizes cell divisions and cell shape in the growing *Drosophila* wing disc. *Development* 140, 4051–4059.

Li, B., Li, F., Puskar, K. M., and Wang, J. H. C. (2009). Spatial patterning of cell proliferation and differentiation depends on mechanical stress magnitude. *J. Biomech.* 42, 1622–1627.

Lin, Z., Zhou, P., Von Gise, A., Gu, F., Ma, Q., Chen, J., Guo, H., Van Gorp, P. R. R., Wang, D. Z., and Pu, W. T. (2015). Pi3kcb links Hippo-YAP and PI3K-AKT signaling pathways to

promote cardiomyocyte proliferation and survival. *Circ. Res.* 116, 35–45.

Liu, C., He, S., Li, X., Huo, B., and Ji, B. (2016). Mechanics of cell mechanosensing on patterned substrate. *J. Appl. Mech.* 83, 1–8.

Mao, Y., Tournier, A. L., Hoppe, A., Kester, L., Thompson, B. J., and Tapon, N. (2013). Differential proliferation rates generate patterns of mechanical tension that orient tissue growth. *EMBO J.* 32, 2790–2803.

Maruthamuthu, V., Sabass, B., Schwarz, U. S., and Gardel, M. L. (2011). Cell-ECM traction force modulates endogenous tension at cell-cell contacts. *Proc. Natl. Acad. Sci.* 108, 4708–4713.

Mertz, A. F., Banerjee, S., Che, Y., German, G. K., Xu, Y., Hyland, C., Marchetti, M. C., Horsley, V., and Dufresne, E. R. (2012). Scaling of traction forces with the size of cohesive cell colonies. *Phys. Rev. Lett.* 108, 1–5.

Moussus, M., Loughian, C. Der, Fuard, D., Courçon, M., Gulino-Debrac, D., Delanoë-Ayari, H., and Nicolas, A. (2014). Intracellular stresses in patterned cell assemblies. *Soft Matter* 10, 2414–2423.

Nelson, C. M., Jean, R. P., Tan, J. L., Liu, W. F., Sniadecki, N. J., Spector, A. A., and Chen, C. S. (2005). Emergent patterns of growth controlled by multicellular form and mechanics. *Proc. Natl. Acad. Sci.* 102, 11594–11599.

Ng, M. R., Besser, A., Brugge, J. S., and Danuser, G. (2014). Mapping the dynamics of force transduction at cell-cell junctions of epithelial clusters. *Elife* 3, e03282.

Nier, V., Jain, S., Lim, C. T., Ishihara, S., Ladoux, B., and Marcq, P. (2016). Inference of Internal Stress in a Cell Monolayer. *Biophys. J.* 110, 1625–1635.

Oakes, P. W., Banerjee, S., Marchetti, M. C., and Gardel, M. L. (2014). Geometry regulates traction stresses in adherent cells. *Biophys. J.* 107, 825–833.

Pinto, V. I., Senini, V. W., Wang, Y., Kazembe, M. P., and McCulloch, C. A. (2014). Filamin A protects cells against force-induced apoptosis by stabilizing talin- and vinculin-containing cell adhesions. *FASEB J.* 28, 453–463.

Rape, A. D., Guo, W. H., and Wang, Y. L. (2011). The regulation of traction force in relation to cell shape and focal adhesions. *Biomaterials* 32, 2043–2051.

Dos Remedios, C. G., Chhabra, D., Kekic, M., Dedova, I. V, Tsubakihara, M., Berry, D. A., and Nosworthy, N. J. (2003). Actin binding proteins: Regulation of cytoskeletal microfilaments. *Physiol Rev* 83, 433–473.

Schaumann, E. N., Staddon, M. F., Gardel, M. L., and Banerjee, S. (2018). Force localization modes in dynamic epithelial colonies. *Mol. Biol. Cell* 29, 2835–2847.

Tambe, D. T., Croutelle, U., Trepate, X., Park, C. Y., Kim, J. H., Millet, E., Butler, J. P., and

Fredberg, J. J. (2013). Monolayer Stress Microscopy: Limitations, Artifacts, and Accuracy of Recovered Intercellular Stresses. *PLoS One* 8.

Tambe, D. T., Hardin, C. C., Angelini, T. E., Rajendran, K., Weitz, D. a, Fredberg, J. J., and Trepap, X. (2011). Collective cell guidance by cooperative intercellular forces. *Nat. Mater.* 10, 469–475.

Throm Quinlan, A. M., Sierad, L. N., Capulli, A. K., Firstenberg, L. E., and Billiar, K. L. (2011). Combining dynamic stretch and tunable stiffness to probe cell mechanobiology in vitro. *PLoS One* 6, e23272.

Trepap, X., Wasserman, M. R., Angelini, T. E., Millet, E., Weitz, D. A., Butler, J. P., and Fredberg, J. J. (2009). Physical forces during collective cell migration. *Nat. Phys.* 5, 426–430.

Wan, L. Q., Kang, S. M., Eng, G., Grayson, W. L., Lu, X. L., Huo, B., Gimble, J., Guo, X. E., Mow, V. C., and Vunjak-Novakovic, G. (2010). Geometric control of human stem cell morphology and differentiation. *Integr. Biol.* 2, 346–353.

Wang, H. B., Dembo, M., and Wang, Y. L. (2000). Substrate flexibility regulates growth and apoptosis of normal but not transformed cells. *Am. J. Physiol. Physiol.* 279, C1345–C1350.

Yuan, H., Marzban, B., and Parker, K. K. (2017). Myofibrils in Cardiomyocytes Tend to Assemble Along the Maximal Principle Stress Directions. *J. Biomech. Eng.* 139, 1210101–1210108.

Zhang, H., Pasolli, H. A., and Fuchs, E. (2011). Yes-associated protein (YAP) transcriptional coactivator functions in balancing growth and differentiation in skin. *Proc Natl Acad Sci* 108, 2270–2275.

Zimmermann, J., Camley, B. A., Rappel, W., and Levine, H. (2016). Contact inhibition of locomotion determines cell – cell and cell – substrate forces in tissues. *PNAS* 113.

## Chapter 5: Conclusions, Limitations, and Future Work

### 5.1 Conclusions

This dissertation examines the mechanisms by which the extracellular mechanical environment affects intracellular stresses and subsequent cell behavior including cell orientation and apoptosis. Two aims were completed to explore these research areas. The first aim focused on how dynamic mechanical stress and substrate modulus affect alignment of the cytoskeletal network and apoptosis in single cells. And the second aim experimentally measured and modeled the distribution of stresses within the cell-layer in multicellular aggregates. Studying how cells that are isolated and within monolayers regulate their intracellular tensional levels in response to their extracellular mechanical environment has provided valuable insight into how mechanical stress regulates cell fate through mechanosensitive pathways.

#### 5.1.1 Conclusions: Aim 1

In Aim 1, we investigated the effects of cyclical stretch on cellular reorientation and survival in cells cultured in low-stress conditions. Cells were first cultured on high-modulus (stiff) substrates, where cells are able to generate optimal homeostatic cell-stress levels and cells have high spread area and elongate. We then cyclically stretched these cells to study typical strain-avoidance behavior. Similar to previous studies, we found that stretched cells quickly reoriented perpendicular to stretch, presumably to reestablish their homeostatic stress level (Hayakawa *et al.*, 2000; Wang *et al.*, 2001; Hsu *et al.*, 2010; Tondon and Kaunas, 2014; Zielinski *et al.*, 2018). We then cultured VICs on low-modulus (soft) substrates to create conditions with insufficient mechanical resistance for cells to generate optimal stress levels. Here, cells have small spread area and are rounded. Dynamic mechanical stretch was introduced to modulate cell-stress levels and cytoskeletal arrangement. Over time, stretched cells were able to increase spread area and elongate, first parallel to the direction of stretch before reorienting to an angle significantly less than perpendicular to stretch, presumably to a condition in which their stress is optimized. These results directly contradict current models that predict cell orientation to align along the direction of stretch for cells cultured on soft (low elastic modulus) substrates (Tondon and Kaunas, 2014; Xu *et al.*, 2018). Differences between these studies and ours include stretch duration, cell type,

substrate composition, and combinations of mechanical parameters, all of which affect internal tension levels and could affect the reorientation of cells.

In agreement with previous studies, we have found that cells on stiff substrates have very low instances of apoptosis. When cyclically stretched, cells reorient away from the direction of stretch and maintain low levels of apoptosis. On the other hand, cells on soft substrates have substantially higher occurrences of apoptosis. We hypothesize that this apoptosis is due to the low-tension state of cells. Cyclic stretch acts as a stress input and can enable cells to increase in tension which should theoretically decrease apoptosis. We find that cyclically stretching cells significantly reduces the amount of apoptosis present, while stopping stretch ultimately increases apoptosis back to its initial values.

Our results show that the effect of mechanical stretch on morphology and cell behavior is reversible in cells on soft substrates. Cells on soft substrates require a continuous input of mechanical strain to retain their spread area and survival. After removing cyclic stretch, cells reverted to their initial state within two hours, having low spread area and aspect ratio and high circularity. Additionally, a slight increase in apoptosis occurs in cells once stretch is stopped and cells are no longer able to achieve an optimal state of stress. In this aim, we uncovered how mechanical stimuli initiate cytoskeletal reorganization thereby regulating cell survival.

### 5.1.2 Conclusions: Aim 2

In Aim 2, we presented experimental and computational evidence indicating that accurately estimating the distributions of cell-layer stresses requires incorporation of regional heterogeneity in cell properties (modulus and/or contractility). We cultured cells in multicellular aggregates of defined size, which enabled us to systematically examine the relationship between cell geometry, mechanical stress, and apoptosis. We were able to measure the radial distribution of various stress-associated biomarkers within aggregates. Biomarkers and cell properties indicative of high cell-stress, such as  $\alpha$ -SMA incorporation, F-actin stress fibers, traction forces, cell area, cell stiffness, and nuclear localization of YAP and MRTF-A were all observed at aggregate edges. Low cell-stress-associated biomarkers such as G-actin localization, cytoplasmic localization of

YAP and MRTF-A, and instances of apoptosis were detected in central regions of aggregates. These data indicate that multicellular aggregates have higher stress along aggregate peripheries compared to their central regions. The regional distributions of these biomarkers and cell properties were similar to the findings of others (Nelson *et al.*, 2005; Théry *et al.*, 2006; Li *et al.*, 2009; Rape *et al.*, 2011; Oakes *et al.*, 2014; He *et al.*, 2015).

Previous studies have used homogeneous mechanical properties for cells when using computational models to estimate cell- and substrate-stress levels (Nelson *et al.*, 2005; Tambe *et al.*, 2011; Kim *et al.*, 2013; He *et al.*, 2015; Liu *et al.*, 2016). Homogeneous finite element models may be sufficient for estimating stress distributions in unconstrained systems and/or for short culture times where cell density remains constant. However, our results show that proliferation and growth lead to regional differences in cellular properties in constrained systems over long timeframes. These differences in physical properties among neighboring cells need to be considered in the stress analysis of the entire system. By incorporating heterogeneous cell contractility and stiffness parameters into our finite element model, we found cell-layer stress contours that agreed with the distribution of multiple stress-associated biomarkers. That is, high cell-layer stress localized to aggregate peripheries while low cell-layer stress was concentrated in aggregate centers. These estimated stress distributions result in the opposite trend for what models using homogeneous mechanical properties predict. This discrepancy in estimated stress distribution highlights the importance of incorporating regional differences in mechanical properties of cells when predicting emergent stress fields in multicellular systems.

The mechanosensitive Hippo pathway was studied to determine its role in mechanically initiated apoptosis. Present in high stress conditions, activated YAP is essential for cell survival. We hypothesize that activating YAP in low-tension cells can decrease apoptosis. To test this hypothesis, we transfected VICs to express constitutively active YAP even in low-stress conditions. We then determined differences in cell behavior in multicellular aggregates. We found that by activating YAP, central cells in aggregates had reduced instances of cell death compared to normal VICs. This indicates that active YAP is able to promote continued cell survival and could be exploited to help rescue cells in low-stress environments. In this aim, we

determined a spatial relationship between intracellular cell-stress, mechanosensitive pathways, and apoptosis within multicellular aggregates.

## 5.2 Experimental Limitations and Next Steps

There were several limitations in Aims 1 and 2 that can be contributed to inherent deficiencies of the experiments and modeling performed. These limitations did not take away from the overall findings that we discovered concerning how apoptosis is affected in single cells and multicellular systems depending on the conditions of their mechanical environment. Next steps should address some of these limitations by improving experimental procedures and modeling parameters.

### 5.2.1 Study Limitations: Aim 1

#### 5.2.1.1 3-D versus 2-D environmental conditions

While the studies described in this dissertation have produced important insights into how cell mechanics is connected to apoptosis, they were all performed in 2-D, nonfibrous, elastic polyacrylamide (PA) gels that are well controlled but not biofidelic of *in vivo* environments. In heart valves, the ECM is a 3-D, fibrous network comprising various proteins components that exhibit viscoelastic and strain-stiffening behavior with anisotropic stiffness. Cells *in vivo* can adjust their mechanical properties as well as the properties of the ECM in response to mechanical stimuli and stresses. It is known that cell behavior differs in 3-D vs 2-D (Soares *et al.*, 2012). For instance, when cyclically stretched, cells align away from the direction of stretch in 2-D but parallel to stretch in 3-D gels (Lee *et al.*, 2012; Tondon and Kaunas, 2014; Zielinski *et al.*, 2018). This may be due to contact guidance and stiffening of collagen fibers when stretched, which encourage alignment along the direction of stretch. Future work should expand the scope of our experiments and investigate cell behavior differences in 3-D environments when under similar conditions to our 2-D experiments.

#### 5.2.1.2 Increasing the reproducibility of PA gels

There is variability between each PA gel that is polymerized to a CellScale well used in the reorientation studies in Aim 1. It is important to increase the fidelity between different gels, having each one as even and uniform as possible to one another. Gels of lower modulus are more

viscous and stick to the glass coverslip when it is being removed. This sometimes forms grooves in the gel rather than a uniform smooth layer. Cells respond to these topographic features through contact guidance, which can cause unexpected behavior for the given conditions. For instance, in time-lapse experiments, it is common to see some cells that are initially spread out on soft substrates, cells in the same region aligned in the same direction, or cells not reorient away from the direction of stretch (these cells are seen adhered near ridges in the gel). Future work should focus on the reproducibility of PA gel polymerization and coverslip removal to ensure the uniformity of the gel layer independent of the substrate modulus.

### 5.2.1.3 Increasing resolution of real-time traction force generation

Traction force generation is directly dependent on cytoskeletal tension. Higher tensional forces stored in stress fibers allows for higher pulling forces on focal adhesions, which leads to larger traction forces. It is important to measure traction forces over time when cyclically stretching cells, as the variation and magnitude of traction forces are indicative of tensional homeostasis. Cells on very soft substrates generate low traction forces, and the fluorescent bead displacement in gels due to these tractions is also very low. It is necessary to image cells at higher magnifications to accurately measure this low bead displacement; however, sometimes traction forces/bead displacements are so low that they are below the resolution of the microscope even under high magnification (40X). Additionally, over the course of an entire time-lapse experiment, the imaging position drifts as the mechanical stage of the microscope moves between positions. Although this drift is low over 12 hr (50-100  $\mu\text{m}$ ), it still can affect the calculation of traction forces and lead to inaccurate values. This drift is especially evident when under higher magnifications (40X), which as previously said, is necessary to capture very low bead displacement and traction forces. One possible solution is using fluorescently labeled adhesive protein dots in a patterned grid (Polio *et al.*, 2012). These adhesive dots act as small focal adhesion islands where cells can attach. Using this method, any drift that occurs would be inconsequential since the grid of fluorescent dots can always be used as a reference point. Future experiments should focus on minimizing these issues to accurately measure traction forces over time in individual cells to better characterize tensional homeostasis.

## 5.2.2 Study Limitations: Aim 2

### 5.2.2.1 Modeling cell-stresses

The established models for cell and substrate stresses have been largely formulated with homogeneous assumptions for various mechanical cell properties (Nelson *et al.*, 2005; Tambe *et al.*, 2011; Kim *et al.*, 2013; He *et al.*, 2015; Liu *et al.*, 2016). These properties include but are not limited to the isotropy of the system, thickness of layers, elastic constants, and uniformity of the cell layer. As a next iteration, we expanded this model twice by including two different heterogeneous mechanical cell properties. First, we assumed contractility (thermal contraction model) or modulus (monolayer stress microscopy) followed a stepwise function where it halved in the central region of the circular aggregate, beginning at half the radius. Next, we iterated again, assuming contractility or modulus followed a continuous function that we matched to the trend of experimental traction forces. These iterations resulted in our model showing stress distributions that were opposite of those using homogeneous assumptions (high cell-stress along the periphery of the aggregate, low cell-stress in central region). However, these iterations were only a first step in accurately estimating the stresses present within a multicellular aggregate. Our model was still simplified by assuming multiple parameters to be uniform or a non-factor. Future iterations should focus on measuring different parameters and varying them regionally in order to expand our model further and generate more realistic stress distributions that are better representatives of what cells experience within the aggregate.

Cellular properties are not isotropic within each cell, let alone in a whole aggregate. For instance, cells generally contract along their long axis, as this is the direction that most fibers are aligned in and cells can generate force (Abhilash *et al.*, 2014). This behavior implies that cell contraction is anisotropic, which then means that a multicellular aggregate would also contract anisotropically. Aggregates should then contract in different directions depending on the elongation angle of each cell. A higher order model would include this anisotropic contraction, such as having non-uniform cooling in the thermal contraction model. This parameter would require modeled aggregates to contract in different directions based on the distribution of cellular alignment.

The heterogeneity within an aggregate is due to the many differences inherent within each cell. When modeling cell-stresses, we currently use a continuum model where we merge together all elements of a modeled aggregate layer and assume similar properties throughout the single layer. Material properties like modulus and contraction are assigned as a function of radius based off a mathematical function that is derived from experimental data of a representative aggregate. In reality, an agent-based model where each cell has its own individual properties and rules would be more appropriate for modeling the entirety of the aggregate. Here, we would look at individual components of each cell and incorporate the varying structural heterogeneity into the whole aggregate. Individual components to apply to the model would be the local distribution and differing strength of experimentally measured focal adhesions, cytoskeletal stress fibers, traction forces generated, cell moduli, and even propensity for apoptosis (dependent on cell stress and cytoskeletal properties). All these markers and values should be measured in actual aggregates and then applied to their respective regions within the modeled aggregate. Focal adhesion distribution would affect where cells can pull on the substrate and generate traction stresses in the model. Stress fiber alignment and density affects to what extent and in what direction cells will contract within the aggregate. Measured traction forces would indicate where cells are contracting the most in aggregates. And finally, atomic force microscopy experiments can show which cells are stiffest. Individual cell properties would help create a more accurate representation of the whole aggregate when predicting cell and traction stresses.

In addition to measuring and applying biomarker distributions to a discrete cell-by-cell model, we should also aim to model cell and traction stresses in specific aggregates rather than in a radially symmetric representative one. Parameters indicative of prototypical aggregates are valuable for predicting overall stress distributions in the collective aggregate population. It would be more beneficial to understand how stresses are localized in a single, specific aggregate. Stress localization can then be correlated to specifically observed biomarkers that are present in a particular aggregate.

Another characteristic of our stress model is that it serves as a snapshot of the stress distributions in a representative aggregate. These stresses are estimated at a time point that essentially serves as a steady state, where certain parameters that are inputs will produce a final equilibrium of

stress distributions. Aggregates are very active, where cells continually migrate, proliferate, and change in shape and size. This cellular activity suggests that internal and external forces would continually change which would therefore change the intracellular stresses that are present. A higher-order model would predict stresses in aggregates over many iterations, where estimated stresses would be inputs in the next iteration. Additionally, the constitutive equations that define the model could include time as a variable. These parameters would allow us to model changing cell-stresses with respect to time.

There is an inherent randomness in cell behavior in aggregates, where random events can occur outside of normal cell behavior. This randomness is not a parameter in our stress model. Therefore, given a specific set of inputs, our model always gives the exact same output of stress distribution. The next iteration of our higher order model should include stochasticity, which would apply a factor of randomization to the model. Sometimes cell behavior does not follow the pattern that is normally observed, and so, there is always a chance that some localization of stress would not occur as expected.

#### 5.2.2.2 Time course of aggregate behavior

Aggregates are highly active clusters that have continually changing properties over time. In large enough aggregates or monolayers, local whorling occurs and regional differences in cell behavior can be seen (Vedula *et al.*, 2012; Kim *et al.*, 2013). This swirling effect is due to migrating cells, even in dense monolayers, which causes the whole aggregate to rotate. We have shown this behavior in preliminary experiments. The active migration of cells within aggregates will affect the generation of cell stresses. Additionally, the balance between proliferation and apoptosis should be characterized over time. Presumably, as cells proliferate along the edges, cells also apoptose in the central regions. If cells migrate between central and peripheral regions, when does apoptosis initiate in cells? Time-lapse microscopy would shed light on how proliferating cells replace cells undergoing apoptosis. Additionally, time-lapse experiments should measure changes in traction forces, focal adhesions, and stress fibers over time. Seeing how these three measurements colocalize and correlate to one another could increase our understanding into the mechanisms behind observed cell behavior. Disease progression, such as

in our *in vitro* calcific aortic valve disease model, could also be studied with time-lapse microscopy of multicellular aggregates.

### 5.2.2.3 Increasing the reproducibility of aggregate generation

Each PDMS stamp used for microcontact printing has hundreds of identical “islands” in its pattern and can therefore produce hundreds of identical multicellular aggregates. However, this is not normally the case. In a usual experiment, one can get up to 30-40 good aggregates (completely confluent) to form and have even more partial aggregates. This may be due to numerous reasons, which include but are not limited to poor collagen transfer from the PDMS stamp to the PA gel, imperfect patterns on the PDMS stamp, and poor stamping technique. Additionally, after multiple days of culturing, the number of good aggregates continues to decrease. What parameters result in better aggregate formation and longevity? What are ways to have uniform aggregates form? Future work should strive to generate better fidelity for microcontact printing which will enable the collection of more data.

## 5.3 Long-term Future Work for the Field

The data presented in this thesis have supported that cells optimize their intracellular tensional levels in response to the dynamic nature of their mechanical environment. When insufficient mechanical feedback occurs, cells undergo apoptosis. This process is evident in single isolated cells that apoptose when cultured on very soft substrates and in multicellular systems where cells undergo compressive apoptosis in the central region of aggregates. In addition to the conditions that were presented in this thesis, there are additional properties, markers, and experiments that have yet to be tested. Future work will greatly strengthen our understanding of the relationship between mechanical cues and stress-associated apoptosis.

### 5.3.1 Future Work: Aim 1

#### 5.3.1.1 Varying levels of stiffness and stretch

In the realignment study from Aim 1, we characterized differences in cellular realignment due to 5% and 10% cyclical mechanical strain when cultured on low-modulus (1.2 kPa) and high-modulus (38.6 kPa) PA gels. We observed differences in cell behavior between just these two

moduli values at both 5% and 10% strain. Future studies should look at changes in cell behavior with cells cultured on an entire array of stiffness levels. The substrate modulus acts as an initial stress input for cells which sets up the intracellular stress levels that cells can generate. As substrate stiffness increases, cell-stress can increase to levels that are comparable to *in vivo*. By experimenting with an array of substrate moduli, we can better define cell behavior at these intermediate levels of stress, such as partially elongated cells or cells generating medium level traction forces.

In addition to substrate modulus, cyclic strain magnitude is another important feature in cell-stress. Most of the experiments in our study used 10% strain. We did lower the strain to 5% to determine if cell behavior would change with lower strain (such as realigning to parallel the direction of stretch). We did not see any significant differences between cells stretched at 10% vs 5% strain. However, future studies should consider lower strains as well as other strain levels and substrate modulus levels to determine any critical differences that may arise. It has been shown in studies that stretch less than 3% strain does not elicit a cellular response at lower frequencies such as 1 Hz (Kaunas *et al.*, 2005; Cui *et al.*, 2015). There should be a theoretical strain that results in cells realigning to any specific angle, whether this be 30° from the direction of stretch or parallel to it. What combination of strain magnitude and substrate stiffness will lead to parallel alignment? Models of cell reorientation should guide future experiments, as every pairing of modulus, waveform, strain rate, and strain cannot be performed. These parameters would lead to conditions that are favorable for cells to generate moderate intracellular stress but may not be their desired equilibrium state.

It has been shown that multiple aspects of stretch have different effects on cell behavior. These different aspects can include substrate modulus, strain magnitude, frequency, rate, and waveform type. In our study, we used 10% strain that increased and decreased at an even triangular rate of 1 Hz. The effects of stretching cells at different frequencies and strain rates (e.g., fast strain and slow relaxation or slow strain and fast relaxation) should also be studied.

### 5.3.1.2 Stress-associated biomarkers

Biomarkers indicative of intracellular stress levels, such as traction force and apoptosis, were measured in our studies. Characterizing other proteins, such as  $\alpha$ -SMA, F-actin, G-actin, and YAP/MRTF-A localization would help increase our understanding of the cellular mechanisms used to reduce stress inputs from cyclic stretch and maintain tensional homeostasis.  $\alpha$ -SMA is a contractility protein that is incorporated into F-actin as cells generate high internal tension. As cells on soft substrates spread out when stretched, a time-lapse showing increases in  $\alpha$ -SMA would be important to analyze. Additionally, increases in F-actin and decreases in G-actin would be important to characterize. F-actin realignment has been shown to precede cell body realignment (Greiner *et al.*, 2013; Zielinski *et al.*, 2018). A time-lapse experiment with live stains of F-actin (e.g., LifeAct) would show fiber reorganization as well as cellular reorientation. These data could then be used to help inform model parameters for cellular realignment model fidelity. Additionally, experiments that stimulate or inhibit YAP/MRTF-A can clarify the role the two proteins have in signaling apoptosis.

### 5.3.1.3 Coupling microcontact printing and cyclic stretch

From previous studies as well as our own, we know that cells undergo strain avoidance behavior in response to cyclic stretch. Cells on stiff substrates will reorient perpendicular to the direction of stretch, while cells on soft substrates reorient away from the direction of stretch but settle at an angle significantly lower than the 90° mark. In the experiments from Aim 1, cells are completely unrestricted, whether on stiff or soft substrates, and are able to spread out in any direction. For instance, cells on soft substrates are able to initially spread parallel to the direction of stretch before reorienting away from it.

Future experiments should use microcontact printing to restrict cell size, shape, and direction and determine how these restrictions alter cell behavior. If a cell is restricted as an ellipse parallel to the direction of stretch, what happens when the cell cannot reorient to avoid the applied stress/stretch? Will apoptosis increase? Do cytoskeletal stress fibers realign perpendicular while the cell body remains perpendicular? In our preliminary studies, we have seen that cells adhered to micropatterned ellipses in the direction of stretch attempt to reorient away from stretch but cannot due to the restricted adhesion area, causing cells to form a diamond shape. Changes in

traction forces, stress fiber alignment, apoptosis, and morphology should be measured and characterized in these experiments. Additionally, these experiments can determine the effects of substrate modulus (high vs intermediate vs low) as well as the difference in microcontact printed patterns, which can change in size and shape. These patterns can range from circles to ellipses at varying angles from the direction of stretch as well as ranging from small single cell islands (20  $\mu\text{m}$  diameter; 314  $\mu\text{m}^2$  area) to large multicellular aggregates (400  $\mu\text{m}$  diameter; 125,000  $\mu\text{m}^2$  area).

#### 5.3.1.4 Modeling cytoskeletal reorganization and cellular reorientation

The established models for cellular reorientation and cytoskeletal reorganization are limited to focusing on changes in single cellular characteristics (e.g., only stress fibers) and final reorientation at steady state. The basic parameters used in modeling cell reorientation are concentrated into three steps: changes in focal adhesions, dynamics of cytoskeletal fibers, and finally, subsequent cellular realignment. These are mostly dependent on strain magnitude, but substrate stiffness and strain frequency are also shown to affect reorientation (Kaunas *et al.*, 2005; Throm Quinlan *et al.*, 2011; Cui *et al.*, 2015). Current models accurately predict reorientation of cells cultured on stiff substrates, but still fail to capture cellular behavior on very compliant substrates. Cell reorientation requires coordination between the actin cytoskeleton, focal adhesions, and ECM resistance, all of which are dependent on one another as well as substrate stiffness (Quinlan and Billiar, 2012; Gupta *et al.*, 2015). Most models are unidirectional where changes in focal adhesion cause changes in stress fibers and then cell orientation. However, these parameters affect one another where changes in focal adhesions can cause changes in stress fibers that then reinforce or disassemble focal adhesions. Capturing this cyclical dependence is difficult to model as it greatly increases the complexity of the model.

It has been shown that cells on stiff substrates in static conditions form mature focal adhesions and stress fibers. Cells can then reorient through cytoskeletal disassembly and reassembly. On the other hand, cells on soft substrates cannot generate stress fibers and have immature focal adhesions. Cells in these conditions need to first assemble stress fibers and focal adhesions before they can remodel them. Future models of cells on soft substrates need to capture this cellular behavior to accurately characterize cytoskeletal reorganization and cellular reorientation.

A few current models of cell tension predict that mechanical stretch is not enough for stress fiber assembly in cells on soft substrates (Deshpande *et al.*, 2006; Ronan *et al.*, 2014). However, we and others show that cells can spread out when cyclically stretched on very compliant substrates. Other models predict that cells will preferentially align parallel to the direction of stretch when on soft substrates, which is consistent with the findings from Tondon and Kaunas (Tondon and Kaunas, 2014; Xu *et al.*, 2018). We find that cells on very soft substrates elongate along the direction of stretch before reorienting away. There are many possibly reasons behind the differences in cell reorientation in the different studies. One probable cause is the grouping of mechanical parameters (e.g., specific substrate modulus, strain rate, strain magnitude) which will affect how much internal tension is increased in low-tension cells. As cells on soft substrates increase in internal tension, they are able to spread out. However, if that tension increases past desired levels, then cells may reorient to reduce stress. Future models need to be iterative, where cells on soft substrates start small and rounded and over time, there are intermediate stages of higher stress states in elongated cells. These models need to improve the characterization and measurement of internal cell tension in order to better determine how different mechanical parameters influence this tension (separately or collectively), which leads to subsequent reorientation or even cell survival.

### 5.3.1.5 Constitutively active Hippo and MRTF signaling pathways

Hippo and MRTF are mechanosensitive signaling pathways that promote cell survival. Cells under optimal stress conditions (e.g., adhered to a stiff substrate) have nuclear localization of both transcriptional cofactors, YAP and MRTF-A, which acts as pro-survival and anti-apoptotic signals (Yu *et al.*, 2016). Future studies should experiment with VICs that have constitutively active YAP or MRTF-A and characterize how these cells are different than normal VICs when being cyclically stretched on soft substrates.

Differences in cell morphology, reorientation behavior (speed, final angle), apoptosis, traction forces, and dynamics of the cytoskeletal network should all be quantified and evaluated. For instance, soft substrates cause normal VICs to be small and rounded, but active YAP/MRTF-A will increase the stability of the cytoskeletal network. Will this allow constitutively active

YAP/MRTF-A cells to spread out on these soft substrates? Or will the promotion of F-actin polymerization be offset by the lack of tension that fibers are able to produce? In the same instance, will apoptosis decrease or remain the same? If active YAP/MRTF-A are able to maintain tension within the cytoskeletal network, will cells on soft substrates reorient to a different angle of that to which normal VICs reorient? It is important to determine the differences in the aforementioned cellular characteristics between constitutively active YAP/MRTF-A VICs and normal VICs in order to ascertain how active YAP/MRTF-A affect cell survival. Only then can we manipulate the Hippo and MRTF pathways to produce desired outcomes such as inhibiting apoptotic events.

### 5.3.2 Future Work: Aim 2

#### 5.3.2.1 Focal adhesion staining in aggregates

We have previously shown that aggregates generate higher traction forces along the edges of aggregates compared to the central regions. There is a dependency on focal adhesions for traction force generation and therefore stands to reason that there would be larger and stronger focal adhesions at aggregate peripheries compared to central regions (Kilian *et al.*, 2010; Rape *et al.*, 2011; Oakes *et al.*, 2014). In our studies, we did not experimentally measure focal adhesions nor apply them to our stress model. Focal adhesion uniformity was assumed between the cell layer and substrate layer to focus on one variable (contractility) at a time. Focal adhesions likely are present throughout the entire aggregate but localization would vary by region. Focal adhesion location and density would affect where and how strong a cell could pull on the substrate. Future work should characterize this focal adhesion distribution to better understand the cell-substrate traction stresses that form regionally within aggregates as well as apply to the stress model as a mechanical parameter.

#### 5.3.2.2 Decoupling cell-stress and traction-stress

The convolution of the effects of cell-stress and traction-stress on cell behavior remain a fundamental problem in mechanobiology. For instance, in the central region of aggregates, apoptosis is high while traction-stresses and estimated cell-stresses (by our heterogenous model) are low. However, does low cell-stress or low traction-stress cause the observed cellular

responses? Future works should include experiments that decouple cell-stresses and traction-stresses to determine the effects of each type of stress individually. Separating out cell-stress from traction-stress or manipulated one at a time can be a hard endeavor. For example, can we increase cell-stress in central cells while keeping traction-stresses low? Is high cell-stress or high traction-stress important for cell survival? One possible method for decoupling these two stresses is culturing aggregates on poly-L-lysine. Substrates coated in poly-L-lysine allow cells to ionically bond directly to the substrate in an integrin-independent manner. No focal adhesions form and therefore, no traction-stresses are generated. Cell-stresses are present, but the cytoskeleton does not generate defined stress fibers. Another possible solution is to generate full aggregates with regions that have no adhesion proteins. For instance, if two aggregates are close enough together, could a bridge of cells form between them via cell-cell contacts only? Or if a microcontact printed pattern is ring, is there a way to have cells accumulate in the non-adhesive middle region? In these scenarios, only cell-cell contacts would be present and no focal adhesions, which should allow the generation of stress fibers and cell-stresses while preventing traction-stress generation. Separating out cell-stress and traction-stress would help shed insight on answering fundamental questions about what stresses initiate what cellular behavior within multicellular aggregates.

### 5.3.2.3 Remove cell-cell contact

Cells in multicellular monolayers form cell-ECM adhesions to the substrate as well as cell-cell contacts with one another via cadherins. Cell-cell contact has been shown to change behavior of cells, such as normalizing their morphology independent of substrate stiffness (Discher *et al.*, 2005; Yeung *et al.*, 2005). Additionally, cell-cell contact is more important for cells in the central regions of aggregates compared to the edges. In fact, it has been shown that cells in the central region of aggregates have increased cell-cell forces compared to cell-integrin forces found at edge cells (Maruthamuthu *et al.*, 2011). We hypothesize that apoptosis results from low cell tension in central cells, arising from high cell densities causing cell compression. This compression causes low cell-integrin forces to form and cell-cell forces to bypass the central region and concentrate around aggregate edges. However, it is difficult to experimentally measure cell tension; rather it needs to be inferred from models. For instance, future experiments should use techniques like laser-ablation, which will cause aggregates to retract from the middle.

If central cells have lower tension, then aggregates will demonstrate lower retraction. Additional experiments removing cell-cell contact should also be performed. For example, EDTA initiates cadherin internalization and inhibits cell-cell contacts. As central cells already cannot generate high cell-ECM forces through integrins, EDTA would cause cells to have even lower intracellular tension as cell-cell contacts are removed. This could possibly greatly increase instances of apoptosis.

#### 5.3.2.4 FRET tension sensor

Researchers have developed various ways for visualizing and measuring the mechanical nature of cells, such as determining cell force generation via traction force microscopy. Molecular-scale deformations within the cell, such as the amount of stretch on a load-bearing protein, can be measured using molecular tension microscopy (MTM) sensors. MTM sensors are molecular springs with a donor and acceptor fluorophore attached to either end. Using the principle of Forster resonance energy transfer (FRET), the amount of fluorescence detected is dependent on the distance and angle between the two fluorophores. For instance, the less force on the protein, the closer the two fluorophores are and the higher the amount of FRET (fluorescence) detected; the more force on a protein, the further away the two fluorophores are and the lower amount of FRET detected. The force generation on these proteins can then be calculated from simple spring equations. Future experiments should employ this technique at cell-cell junctions and cell-ECM focal adhesions. FRET tension sensors integrated with cadherins will allow for the measurement of cell-cell forces, while FRET tension sensors combined with focal adhesions will allow calculation of force generation in specific focal adhesions. The regional distribution of forces can then be correlated to aggregate radius and inform on the actual internal forces that cells are generating within the cell layer.

#### 5.3.2.5 Cyclic stretching of aggregates

In our multicellular aggregates, we observe higher instances of apoptosis in central regions compared to peripheral regions. We postulate that this apoptotic trend is due to the central region being a low stress environment which leads to cells having low intracellular stress. This theory is supported by our thermal contraction and MSM models that use heterogeneous mechanical properties and show low cell-stresses in the central regions. The physical attributes observed in

these central cells are similar to single cells that are seeded on soft substrates; cells in both conditions are small, rounded, and have higher rates of apoptosis compared to cells on stiff substrates (Zhang *et al.*, 2011; Cirka *et al.*, 2017; Goldblatt *et al.*, 2020). It has been shown that cyclic stretch, which acts as an external stress input, has been able to reduce levels of apoptosis in single cells experiments (Liu *et al.*, 2003). It is feasible that cyclically stretching micropatterned aggregates could act as an external stress input in central cells, allowing them to increase their intracellular stress equal to those of periphery cells. This increase in internal stress could then lead to central cells having reduced numbers of apoptosis.

It is important to cyclically stretch our aggregates as these conditions better represent what happens *in vivo* during diseased states, where cells aggregate together in heart valves and undergo continual cyclic strain from each heartbeat. Future experiments should include characterizing changes in apoptosis, F-actin alignment, F-actin/G-actin ratio,  $\alpha$ -SMA localization, and YAP/MRTF-A nuclear localization. We expect similar results to those of our magnetic bead experiment, where a magnet increases the stresses on cells throughout the entire aggregate. These conditions made observed biomarkers ( $\alpha$ -SMA intensity) of cells be more uniform throughout the aggregate (central region comparable to peripheral region) and had decreased levels of apoptosis. This leads us to hypothesize that the central region would have increased F-actin/G-actin ratios as well as increased levels of YAP and MRTF-A nuclear localization. Additionally, uniaxial cyclic stretch inputs a directional force on the aggregate producing anisotropic strains. It would be interesting to see how this anisotropy of force affects different cell behaviors (e.g., cell body alignment vs. cytoskeletal fiber alignment).

#### 5.3.2.6 Regulating Hippo and MRTF mechanotransduction pathways

Hippo and MRTF act as pro-survival pathways that are mechanosensitive. Cells in good health with optimal intracellular stress levels have nuclear localization of both transcriptional cofactors, YAP and MRTF-A, which promotes proliferation and inhibits apoptosis (Yu *et al.*, 2016). In our preliminary studies, we have shown that aggregates with constitutively active YAP have lower instances of apoptosis in central regions compared to normal VICs. Additional studies should be performed to determine other critical differences between constitutively active YAP VICs and normal VICs, such as localization and magnitude of traction force generation, presence of  $\alpha$ -

SMA, and F-actin fiber density and thickness. MRTF-A localization in these active YAP cells should also be studied. Theoretically, active YAP should help cell survival, possibly by retaining high intracellular stress or by directly activating survival genes, which should in turn promote nuclear localization of active MRTF-A, even in central cells in aggregates.

Similar to constitutively active YAP, a second cell line of VICs with constitutively active MRTF-A should also be studied for similar outcomes. Apoptosis, traction forces,  $\alpha$ -SMA presence, and F-actin fiber density should be similarly measured and associated to regional locations within aggregates. We expect comparable results to constitutively active YAP, with lower instances of apoptosis. Additionally, YAP localization in active MRTF-A cells should be studied. Active MRTF-A should also help maintain intracellular stress which should promote nuclear localization of YAP, even in central cells in aggregates. Along with our collaborators, we have attempted to transfect VICs with constitutively active MRTF-A. However, there appears to be incompatibility issues transfecting MRTF-A into primary cells and further testing needs to be performed.

We hypothesize that constitutively active YAP and MRTF-A help reduce apoptosis in VICs by retaining cell tension in stress fibers. What is the mechanism behind this reduction of apoptosis? Would deactivating YAP and MRTF-A increase apoptosis? Knockout studies need to be performed to test whether YAP and MRTF-A promote cell survival through cytoskeletal stability or by simply increasing transcription of survival genes. Having knockdowns of both proteins raises many interesting questions in multicellular aggregates, such as do edge cells now act comparable to central cells or does apoptosis increase in peripheral cells. Future experiments should study changes in traction forces, F-actin density,  $\alpha$ -SMA presence, and cytoskeletal genes between YAP and MRTF-A knockouts vs normal VICs. Single and double siRNA knockouts should be performed since the efficiency and efficacy of siRNA is better than inhibitors that simply downregulate the two proteins. Additionally, in single knockouts, the nuclear localization of the non-knockout protein should be studied. For instance, if YAP is knocked out, will MRTF-A also be inactive and localize to the cytoplasm, even in peripheral cells? And in the instance for MRTF-A knockout, will YAP localize to the cytoplasm, even at the edge of aggregates? Sheetz's group showed that depletion of MRTF-A also downregulated YAP while siRNA depletion of

YAP did not affect the expression of MRTF-A (Cui *et al.*, 2015). Manipulating YAP and MRTF-A signaling opens interesting avenues to study the regulation of different cell behaviors, especially apoptosis.

### 5.3.2.7 Long term aggregate culture

In the *in vitro* aggregate model that we employ in our experiments, aggregates are cultured for a maximum of seven days. Within seven days, aggregates become hyperconfluent, form non-uniform densities, undergo apoptosis, and form calcification nodules. Future work should explore longer time durations to determine how long cells can survive as an aggregate.

Theoretically, cells should be able to maintain an aggregate indefinitely. As central cells apoptose and detach from the surface thereby creating vacant spots, cells on the edges continue to proliferate and migrate towards the middle, filling these vacancies. However, we experience issues with aggregates compacting so much that they pop off the substrate. This can happen anytime between two to seven days of aggregate culture. Future experiments will need to create better conditions for aggregate culture that increase the total lifespan of aggregates.

## 5.4 References

- Abhilash, A. S., Baker, B. M., Trappmann, B., Chen, C. S., and Shenoy, V. B. (2014). Remodeling of fibrous extracellular matrices by contractile cells: Predictions from discrete fiber network simulations. *Biophys. J.* *107*, 1829–1840.
- Cirka, H. A., Uribe, J., Liang, V., Schoen, F. J., and Billiar, K. L. (2017). Reproducible *in vitro* model for dystrophic calcification of cardiac valvular interstitial cells: insights into the mechanisms of calcific aortic valvular disease. *Lab Chip* *17*, 814–829.
- Cui, Y., Hameed, F. M., Yang, B., Lee, K., Pan, C. Q., Park, S., and Sheetz, M. (2015). Cyclic stretching of soft substrates induces spreading and growth. *Nat. Commun.* *6*, 6333–6340.
- Deshpande, V. S., McMeeking, R. M., and Evans, A. G. (2006). A bio-chemo-mechanical model for cell contractility. *PNAS* *103*, 14015–14020.
- Discher, D. E., Janmey, P., and Wang, Y.-L. (2005). Tissue cells feel and respond to the stiffness of their substrate. *Science* *310*, 1139–1143.
- Goldblatt, Z. E., Ashouri Choshali, H., Cirka, H. A., Liang, V., Wen, Q., McCollum, D., Rahbar, N., and Billiar, K. L. (2020). Heterogeneity profoundly alters emergent stress fields in constrained multicellular systems. *Biophys. J.* *118*, 15–25.
- Greiner, A. M., Chen, H., Spatz, J. P., and Kemkemer, R. (2013). Cyclic Tensile Strain Controls

Cell Shape and Directs Actin Stress Fiber Formation and Focal Adhesion Alignment in Spreading Cells. *PLoS One* 8.

Gupta, M., Sarangi, B. R., Deschamps, J., Nematbakhsh, Y., Callan-Jones, A., Margadant, F., Mège, R. M., Lim, C. T., Voituriez, R., and Ladoux, B. (2015). Adaptive rheology and ordering of cell cytoskeleton govern matrix rigidity sensing. *Nat. Commun.* 6.

Hayakawa, K., Hosokawa, A., Yabusaki, K., and Obinata, T. (2000). Orientation of Smooth Muscle-Derived A10 Cells in Culture by Cyclic Stretching: Relationship between Stress Fiber Rearrangement and Cell Reorientation. *Zoolog. Sci.* 17, 617–624.

He, S., Liu, C., Li, X., Ma, S., Huo, B., and Ji, B. (2015). Dissecting Collective Cell Behavior in Polarization and Alignment on Micropatterned Substrates. *Biophys. J.* 109, 489–500.

Hsu, H.-J., Lee, C.-F., Locke, A., Vanderzyl, S. Q., and Kaunas, R. (2010). Stretch-induced stress fiber remodeling and the activations of JNK and ERK depend on mechanical strain rate, but not FAK. *PLoS One* 5, e12470.

Kaunas, R., Nguyen, P., Usami, S., and Chien, S. (2005). Cooperative effects of Rho and mechanical stretch on stress fiber organization. *Proc Natl Acad Sci* 102.

Kilian, K. A., Bugarija, B., Lahn, B. T., and Mrksich, M. (2010). Geometric cues for directing the differentiation of mesenchymal stem cells. *Proc. Natl. Acad. Sci.* 107, 4872–4877.

Kim, J. H. *et al.* (2013). Propulsion and navigation within the advancing monolayer sheet. *Nat. Mater.* 12, 856–863.

Lee, S. L. *et al.* (2012). Physically-Induced Cytoskeleton Remodeling of Cells in Three-Dimensional Culture. *PLoS One* 7.

Li, B., Li, F., Puskar, K. M., and Wang, J. H. C. (2009). Spatial patterning of cell proliferation and differentiation depends on mechanical stress magnitude. *J. Biomech.* 42, 1622–1627.

Liu, C., He, S., Li, X., Huo, B., and Ji, B. (2016). Mechanics of cell mechanosensing on patterned substrate. *J. Appl. Mech.* 83, 1–8.

Liu, X. M., Ensenat, D., Wang, H., Schafer, A. I., and Durante, W. (2003). Physiologic cyclic stretch inhibits apoptosis in vascular endothelium. *FEBS Lett.* 541, 52–56.

Maruthamuthu, V., Sabass, B., Schwarz, U. S., and Gardel, M. L. (2011). Cell-ECM traction force modulates endogenous tension at cell-cell contacts. *Proc. Natl. Acad. Sci.* 108, 4708–4713.

Nelson, C. M., Jean, R. P., Tan, J. L., Liu, W. F., Sniadecki, N. J., Spector, A. A., and Chen, C. S. (2005). Emergent patterns of growth controlled by multicellular form and mechanics. *Proc. Natl. Acad. Sci.* 102, 11594–11599.

Oakes, P. W., Banerjee, S., Marchetti, M. C., and Gardel, M. L. (2014). Geometry regulates traction stresses in adherent cells. *Biophys. J.* 107, 825–833.

Polio, S. R., Rothenberg, K. E., Stamenović, D., and Smith, M. L. (2012). A micropatterning and image processing approach to simplify measurement of cellular traction forces. *Acta Biomater.* 8, 82–88.

- Quinlan, A. M. T., and Billiar, K. L. (2012). Investigating the role of substrate stiffness in the persistence of valvular interstitial cell activation. *J. Biomed. Mater. Res. Part A* *135*, 1–19.
- Rape, A. D., Guo, W. H., and Wang, Y. L. (2011). The regulation of traction force in relation to cell shape and focal adhesions. *Biomaterials* *32*, 2043–2051.
- Ronan, W., Deshpande, V. S., McMeeking, R. M., and McGarry, J. P. (2014). Cellular contractility and substrate elasticity: a numerical investigation of the actin cytoskeleton and cell adhesion. *Biomech. Model. Mechanobiol.* *13*, 417–435.
- Soares, C. P., Midlej, V., de Oliveira, M. E. W., Benchimol, M., Costa, M. L., and Mermelstein, C. (2012). 2D and 3D-organized cardiac cells shows differences in cellular morphology, adhesion junctions, presence of myofibrils and protein expression. *PLoS One* *7*.
- Tambe, D. T. *et al.* (2011). Collective cell guidance by cooperative intercellular forces. *Nat. Mater.* *10*, 469–475.
- Théry, M., Pépin, A., Dressaire, E., Chen, Y., and Bornens, M. (2006). Cell distribution of stress fibres in response to the geometry of the adhesive environment. *Cell Motil. Cytoskeleton* *63*, 341–355.
- Throm Quinlan, A. M., Sierad, L. N., Capulli, A. K., Firstenberg, L. E., and Billiar, K. L. (2011). Combining dynamic stretch and tunable stiffness to probe cell mechanobiology in vitro. *PLoS One* *6*, e23272.
- Tondon, A., and Kaunas, R. (2014). The direction of stretch-induced cell and stress fiber orientation depends on collagen matrix stress. *PLoS One* *9*.
- Vedula, S. R. K., Leong, M. C., Lai, T. L., Hersen, P., Kabla, A. J., Lim, C. T., and Ladoux, B. (2012). Emerging modes of collective cell migration induced by geometrical constraints. *Proc. Natl. Acad. Sci.* *109*, 12974–12979.
- Wang, J. H. C., Goldschmidt-Clermont, P., Wille, J., and Yin, F. C. P. (2001). Specificity of endothelial cell reorientation in response to cyclic mechanical stretching. *J. Biomech.* *34*, 1563–1572.
- Xu, G. K., Feng, X. Q., and Gao, H. (2018). Orientations of Cells on Compliant Substrates under Biaxial Stretches: A Theoretical Study. *Biophys. J.* *114*, 701–710.
- Yeung, T., Georges, P. C., Flanagan, L. A., Marg, B., Ortiz, M., Funaki, M., Zahir, N., Ming, W., Weaver, V., and Janmey, P. A. (2005). Effects of substrate stiffness on cell morphology, cytoskeletal structure, and adhesion. *Cell Motil. Cytoskeleton* *60*, 24–34.
- Yu, O. M., Miyamoto, S., and Brown, J. H. (2016). Myocardin-Related Transcription Factor A and Yes-Associated Protein Exert Dual Control in G Protein-Coupled Receptor- and RhoA-Mediated Transcriptional Regulation and Cell Proliferation. *Mol. Cell. Biol.* *36*, 39–49.
- Zhang, Y. H., Zhao, C. Q., Jiang, L. S., and Dai, L. Y. (2011). Substrate stiffness regulates apoptosis and the mRNA expression of extracellular matrix regulatory genes in the rat annular cells. *Matrix Biol.* *30*, 135–144.
- Zielinski, A., Linnartz, C., Pleschka, C., Dreissen, G., Springer, R., Merkel, R., and Hoffmann,

B. (2018). Reorientation dynamics and structural interdependencies of actin, microtubules and intermediate filaments upon cyclic stretch application. *Cytoskeleton* 75, 385–394.

## Appendix: Protocols

### A.1 Valvular interstitial cell isolation

Protocol modified from *Gould R.A., Butcher J.T. (2010). Isolation of Valvular Endothelial Cells. JoVE. 46. <http://www.jove.com/details.php?id=2158>, doi: 10.3791/2158*

#### Preparation (do day before tissue harvest)

1. Autoclave
  - a. Serrated tissue forceps
  - b. Tissue scissors
  - c. Cotton swaps
2. Make sterile collagenase media (at least 2hr prior)
  - a. Use normal media 10% FBS + 1% Anti-Anti in DMEM
  - b. Measure 600 U/ml collagenase II
    - i. Use about 30mL of media for 3 leaflets
    - ii. 270 U/mg → 66.67mg in 30mL
  - c. Add collagenase type II to media
  - d. Filter sterile
    - i. 0.2 µm filter on syringe or vacuum
  - e. Keep on rocker to ensure homogenized solution (RT overnight)

#### Steps to isolate valve leaflets

1. Excise the aortic root
2. Thoroughly rinse the aortic root with cold, sterile DPBS
3. Isolate valve leaflets (3 per valve) from the root and place directly in sterile 15 ml conical tube filled with 12 mL cold DPBS
4. Shake several times to remove debris
5. Keep on ice
6. Place tissues in sterile hood

#### Steps to isolate valvular interstitial cells

1. Fill a sterile 15 mL centrifuge tube with 10 mL collagenase solution per valve
2. Immediately place them in the appropriate 15 mL conical tube with collagenase solution
3. Make sure to check the samples after 6 hours
  - a. If sufficient digestion has occurred at 6 hours, immediately proceed to step 4
4. Mix the degraded tissue gently with a stereological pipette until the cell suspension becomes homogenized
5. Centrifuge the digest for 5 min at 1000 rpm and aspirate the supernatant
6. Add 5mL of media to the tube and centrifuge a second time, and aspirate the supernatant
7. Re-suspend the centrifuged endothelial cells in 5 mL of porcine media and plate in a T-75 flask

- Let the cells grow 1-2 days before changing the media. Tissue debris is normal.

## A.2 Preparation of Leibovitz's L-15 culture media

The following media was used for culture of VICs in all time-lapse experiments.

L-15 media is a CO<sub>2</sub> free media for cells (still require 37 °C and humidity).

Final concentrations: 10% FBS, 1% antibiotic/antimycotic, 0.45% Glucose

Complete media was made in 50 mL aliquots.

### Materials:

- 500 mL bottle of 1x Leibovitz's L-15 medium
- Fetal bovine serum (FBS), stored in -20 °C
- Antibiotic-antimycotic, stored in -20 °C
- 45% glucose, stored at room temperature on chemical shelf
- 50 mL conical tube

### Methods:

1. Thaw FBS and anti-anti aliquots at room temperature or in warm water bath
2. Add 42.5 mL of L-15 media to 50 mL conical tube
3. Once thawed, add 5 mL FBS and 0.5 mL anti-anti to conical tube
4. Add 0.5 mL of glucose to conical tube
5. Label conical tube with initials, date, final concentrations of 10% FBS, 1% anti-anti, and 0.45% glucose, and indicate complete L-15 media
6. Store in 4 °C refrigerator

## A.3 Activation of polyacrylamide gel

Activation of polyacrylamide (PA) gel makes gel susceptible for collagen transfer during micro-contact printing.

Protocol modified from Vesna Damljanovic

### Materials:

- 55% hydrazine hydrate
- 0.05 N glacial acetic acid
- DI water
- Tweezers
- Ceramic rack
- **Note 1:** it is best that all glassware used for hydrazine hydrate activation be used only for this activation protocol and kept separate from other laboratory equipment

- **Note 2:** Hydrazine hydrate is extremely carcinogenic and should only be used in a fume hood
- **Note 3:** Hydrazine hydrate comes at 78-82% solution, 55% hydrazine hydrate diluted in DI water was used for the activation of all gels

**Methods:**

1. Fill ceramic rack with coverslips with PA gels attached
2. In fume hood, use tweezers to carefully lower ceramic rack into beaker with 55% hydrazine hydrate
  - a. Incubate in hydrazine hydrate for 2 hours
3. Carefully remove ceramic rack from hydrazine hydrate and lower into second beaker with 0.05 N acetic acid
  - a. Dispose of hydrazine hydrate into appropriate waste container
    - i. Can reuse hydrazine hydrate a few extra times (have done as much as 10x)
  - b. Incubate in acetic acid for 30 min
4. Transfer gels to DI water
  - a. Dispose of acetic acid into appropriate waste container
  - b. Incubate in DI water for 30 min
5. Store gels in HEPES in 4 °C fridge until ready for micro-contact printing
  - a. Gels will remain activated for several months

## A.4 Micro-contact printing protocol

**Materials:**

- Activated polyacrylamide (PA) gels on glass coverslips
- 0.1 N glacial acetic acid
- Type I collagen solution
- 50 mM sodium acetate buffer
- Sodium n-periodate crystals
- PDMS stamps
- Plasma cleaner
- N<sub>2</sub> air gun
- Vacuum/Desiccator
- PBS, DI water (diH<sub>2</sub>O), Ethanol (EtOH)

**Methods:**

1. Prepare collagen solution in 1.6mL Eppendorf tube:
  - a. 1 mL solution is good for 4 stamps
  - b. 100 µL of 1 mg/mL collagen
    - i. Dilution of 4.33 mg/mL collagen in 0.1 N acetic acid
  - c. 900 µL of 50 mM sodium acetate buffer
  - d. 0.36 mg of sodium periodate

2. Incubate solution at room temperature for 1hr
3. Clean PDMS stamps with diH<sub>2</sub>O, EtOH, and diH<sub>2</sub>O again, and dry completely with air gun
4. Plasma treat PDMS stamps for 2 min in plasma cleaner
5. Place PDMS stamps with patterned side facing up
6. Pipette ~250  $\mu$ L of collagen solution on top of pattern for 1hr at room temperature
7. Dry activated PA gels in vacuum ~10min (time varies) until gel surface appears dry
8. Partially dry stamps with N<sub>2</sub> gun until they are damp, but no visible droplets
9. Place stamps on PA gel for >5 min
10. Remove stamp and soak gel in PBS/antibiotics in 4 °C overnight

## A.5 Attachment of polyacrylamide gels onto CellScale wells

### Materials:

- CellScale well – composed of Elastosil
- Plasma cleaner
- Ethanol
- 1% aminopropyl trimethoxysilane solution (made from Albrecht Lab)
- 0.5% glutaraldehyde
- N<sub>2</sub> air gun
- Polyacrylamide (PA) gel
- DI water

### Methods:

1. Sonicate CellScale well in ethanol if not new well package
2. Plasma treat CellScale well for 2 min
3. Pipette 100  $\mu$ L of 1% aminopropyl trimethoxysilane onto each well – make sure it covers the entire bottom (easy spreading indicates good plasma treatment)
  - a. Incubate for 5 min
4. Remove all silane solution from wells and add 100  $\mu$ L of 0.5% glutaraldehyde
  - a. Incubate for 5 min
  - b. Dispose of silane solution into appropriate waste container
5. Remove all 0.5% glutaraldehyde and dry with N<sub>2</sub> gun if necessary
  - a. Dispose of glutaraldehyde into appropriate waste container
6. Add 4  $\mu$ L PA gel to center of each well and place 5 mm diameter coverslip over each
  - a. Make sure coverslip/gel does not touch sides of well – will cause gel to not form
7. Quickly put CellScale wells with PA gels into vacuum chamber and flush with N<sub>2</sub> for 1 min
8. Polymerize PA gels under N<sub>2</sub> for required time based off gel stiffness
  - a. Soft gels polymerize for ~1.5 hours
  - b. Stiff gels polymerize for ~45 min
9. Soak gels in DI water for required time based off gel stiffness

- a. Soft gels soak for ~1 hour
- b. Stiff gels soak for ~30 min
10. Carefully remove coverslips
11. Soak gels in DI water at 4 °C for long term storage

## A.6 Collagen attachment to control polyacrylamide gels

### Materials:

- Type I collagen
- Sulpho-SANPAH
- HEPES
- 0.02 N glacial acetic acid
- UV light
- Polyacrylamide (PA) gels

### Methods:

1. Thaw sulpho-SANPAH aliquots from -80 °C freezer
2. Dilute solution into HEPES
3. Achieve concentration of 0.5 mg/mL (1:100 dilution – 10 µL in 1 mL of HEPES)
4. Place ~250 µL of solution onto each PA gel (square 22mm gels) – less for smaller gels
5. Irradiate gel and solution under UV light for 10 minutes
6. Rinse with HEPES 3x for 5 min, 3 min, and 2 min for a total of 10 min
7. Apply collagen solution to PA gel, ensure gel is uniformly covered
  - a. Dilute collagen with 0.02 N acetic acid to create 200 µg/mL concentration
8. Incubate at overnight at 4 °C

## A.7 Preparing fluorescent micro-bead coat on glass coverslips

The purpose of this protocol is to evaporate micro-beads onto glass coverslips. The coverslips can then be placed on unpolymerized polyacrylamide gel droplets so that a uniform layer of beads attaches to the polymerized gel.

### Materials:

- 100% ethanol
- 0.2 µm diameter fluorescent beads
- Plasma cleaner
- Coverslip
- 1.6 mL Eppendorf tube
- Vacuum Oven
- Ceramic coverslip rack

- Sonicator
- Coverslip tweezers
- Brass test tube rack – ensures coverslips have level surface to rest on in the oven

### Methods:

1. Preheat oven to 140-150 °C – temperature is critical
  - a. Too hot: bead solution evaporates causing bead clumping
  - b. Too cold: beads clump together forming a cobble stone appearance
2. Create a 0.5% bead solution in Eppendorf tube
  - a. 1 mL of 100% ethanol
  - b. 5 uL of bead stock solution
3. Place coverslips in coverslip rack
4. Add to 500 mL with ethanol.
5. Place coverslips in ethanol and sonicate for 5 min along with bead solution
6. Remove coverslips and place in oven to dry
7. When dry, use tweezers to remove from coverslip rack and place in a petri dish to plasma treat
8. Plasma treat coverslips for 30 s – 2 min at full power
  - a. **Note:** use coverslips soon after cleaning (<10 min)
  - b. Wait until oven is sufficiently hot prior to starting this step
9. Place 6 coverslips (no more than six at one time, if doing more see note below) on flat surface (brass test-tube rack) that is compatible with high temperature
10. Add bead solution to coverslip – adjust volume for different size coverslips
  - a. 35 µL of bead solution to 22 mm square coverslip
  - b. 1.5 µL of bead solution to 5 mm diameter circle coverslip
11. Wait 10 seconds as the ethanol solution spreads out along the coverslip prior to placing in the oven
12. After placing in the oven, pull a vacuum until the gauge reads -20 torr
13. Release vacuum, coverslips are ready to use.

**Note:** If doing more than six coverslips, the brass test tube rack must be cooled prior to reuse.

## A.8 Caspase-3/7 live cell detection

This reagent was purchased and used according to the manufacturer's instructions:

<https://www.thermofisher.com/order/catalog/product/C10423>

It was used at working concentration of 5 µM. 2.5 µL of reagent was added for every 1 mL of culture media. Reagent was incubated at 37 °C with cells for 1 hour prior to imaging.

## A.9 Image acquisition for Traction Force Microscopy

### Materials:

- Traction force sample
- 0.25% EDTA Trypsin
- Fine tipped transfer pipettes
- Waste container
- PBS
- Zeiss microscope

### Methods:

1. Change media in sample to PBS
2. Securely fix sample on microscope and remove lid
  - a. It is critical that the petri dish not be bumped or moved once it has been placed on the microscope and cell positions have been acquired
3. Find desired cells and mark positions with AxioVision software
  - a. Suggested to have between 10-15 cells per sample
4. Acquire a phase (cell) and fluorescent (bead) image for each cell
5. Carefully, use fine tipped transfer pipette to remove PBS
6. Add trypsin
7. Check to ensure all cells have detached from the substrate before taking final fluorescent image of the beads

## A.10 Immunofluorescence staining protocol

This protocol is for staining phalloidin (F-actin), deoxyribonuclease I (DNase-1; G-actin), and Hoechst (Nuclei).

### Materials:

- Phalloidin
  - Alexa Fluor 488
  - Life Technologies – A12379
- Deoxyribonuclease I (DNase-1)
  - Alexa Fluor 594
  - Life Technologies – D12372
- Hoechst 33342
  - Life Technologies – H3570
- PBS
- Aluminum foil
- Fixed sample

**Methods:**

1. Aspirate and rinse fixed samples with PBS
2. Stain with phalloidin
  - a. 1:100 in PBS (10  $\mu$ L/1 mL)
  - b. Cover samples w/ foil and allow 40-60 min at room temp
3. Stain with DNase-1 (can co-stain with phalloidin)
  - a. 1:500 in PBS (2  $\mu$ L/1 mL)
  - b. Cover samples w/ foil and allow 40-60 min at room temp
4. Aspirate and rinse 2x with PBS.
5. Apply Hoechst stain for 5-20 minutes
  - a. 1:200 in PBS (5  $\mu$ L/1 mL)
  - b. ~50  $\mu$ L on top of sample
  - c. Keep covered from light
6. Aspirate and rinse 2x with PBS
7. Image within 3 days
8. Store covered samples in PBS in 4 °C fridge

**Notes:**

- Keep in foil out of light
- Store phalloidin and DNase-1 in -20 °C freezer
- Hoechst is stored in fridge NOT, freezer
- Stain with lights off

**A.11 Immunocytochemistry staining protocol for  $\alpha$ -SMA**

This protocol is for staining alpha-smooth muscle actin ( $\alpha$ -SMA).

**Materials:**

- Primary antibody: anti- $\alpha$ SMA (alpha-smooth muscle actin)
  - Mouse
  - 0.2mL
  - Sigma-Aldrich – A2547
- Secondary antibody: anti-Mouse IgG (H+L) Highly Cross-Adsorbed Secondary Antibody
  - Goat
  - Alexa Fluor Plus 555
  - 1mg
  - ThermoFisher – A32727
- 0.25% Triton-X
- Goat serum
- PBS
- Aluminum foil
- Fixed sample

**Methods:**

1. Permeabilize cells with 0.25% Triton-X 100 in diH<sub>2</sub>O for 15-20 min at RT
2. Aspirate and rinse with PBS once
3. Block with 1.5% normal goat serum (NGS) in PBS for 30 min at RT
4. Add primary antibody, diluted in 1.5 % NGS (dilution 1:100), for 1 hour at RT
  - a.  $\alpha$ -SMA at necessary dilution
5. Wash three times with PBS (5 min each with gentle agitation)
6. Add secondary antibody, diluted in 1.5% NGS (dilution 1:500); incubate for 45 min at RT
  - a. Add secondary at necessary dilution
  - b. Protect samples from light from this point
7. Rinse with PBS three times (5 min each)
8. Counterstain with phalloidin if desired
9. Counterstain with Hoechst if desired (3- 4 min)
10. Rinse twice with PBS.

**Notes:**

- Keep in foil out of light
- Stain with lights off
- Primary antibody incubation can be carried out overnight at 4 °C
- Store in 4 °C fridge until ready to image

**A.12 Immunocytochemistry staining protocol for YAP and MRTF-A**

This protocol is for staining Yes-associated protein (YAP), phosphorylated YAP (YAP-P), myocardin-related transcription factor A (MRTF-A), TRP-6, Vinculin, and N-cadherin.

Protocol from McCollum Lab

**Materials:**

- Primary antibody: YAP, YAP-P, MRTF-A, TRP-6, Vinculin, and N-cadherin
  - Goat/Mouse
- Secondary antibody
  - Goat/Mouse
- 0.05% Triton-X 100
- 4% paraformaldehyde (PFA)
- Universal Buffer (UB: 150 mM NaCl, 50 mM Tris pH 7.6, 0.01% NaN<sub>3</sub>)
- Bovine serum albumin (BSA)
- Aluminum foil
- Fixed sample

**Methods:**

1. Wash samples with PFA for 10 min
2. Permeabilize samples with UB + 0.05% Triton-X 100 for 5 min
3. Block samples in UB + 10% BSA for 30 min
4. Incubate samples with primary antibody in UB + 10% BSA for 1-2 hr at RT
  - a. YAP mouse 1:200
  - b. YAP-P rabbit 1:500
  - c. MRTF-A rabbit 1:500
  - d. TRP-6 mouse 1:500
  - e. Vinculin mouse 1:500
  - f. N-cadherin rabbit 1:500
5. Wash 3x in UB for 5 min each
6. Incubate samples with secondary antibody in UB + 10% BSA for 1 hr at RT
  - a. Alexa Fluor 488 anti-mouse 1:1000
  - b. Alexa Fluor 568 anti-rabbit 1:1000
7. Wash 3x in UB for 5 min each
8. Mount and image

**A.13 MATLAB code for radial distribution of caspase in aggregates**

% Script determines center of every aggregate and translates it to the middle of the image. It then determines max, average, and counts for corresponding caspase images and graphs them with respect to radial distribution.

```

dishNo = 1;           % dish number
baseNo = 1;          % starting circle number
nImages = 27;        % total number of circles including starting circle
tau = 500;           % threshold for minimum intensity counting –
                    % tau = 0 if subtracting Null Background image
delta = 30;          % # of rings for radial distribution

mkdir(['dish' num2str(dishNo)]); % make directory – make sure it is part of path

% base image - calculates the center of the IMAGE (not aggregate)
% name phase images dish#_phase_circle## - where # is what dish (normally “1”) and ##
changes for each aggregate
% name caspase images dish#_caspase_circle## - where # is what dish (normally “1”) and ##
changes for each aggregate

imPhase=imread(['dish' num2str(dishNo) '_phase_circle' num2str(baseNo) '.TIF']);
[SizeY, SizeX] = size(imPhase);
CenterX = SizeX/2;
CenterY = SizeY/2;

```

```

for i = baseNo:nImages % cycles from first aggregate to last aggregate
    % Read in images
    im_phase = imread(['dish' num2str(dishNo) '_phase_circle' num2str(i) '.TIF']);
    im_caspase = imread(['dish' num2str(dishNo) '_caspase_circle' num2str(i) '.TIF']);

    % subtract out background noise from caspase images from NULL image
    im_Background = imread('NullBackground8.TIF');
    im_caspase = im_caspase - im_Background;

    % trace the edge of aggregates to calculate centroid
    figure, imshow(im_phase)
    title(['Trace the aggregate outline, #', num2str(i), ' out of ', num2str(nImages)]);
    [bwc,xc,yc]=roipoly;
    reg=bwlabel(bwc);
    [s,l]=bwboundaries(bwc);
    g=regionprops(l,'PixelList','centroid');
    Cell_Centroid=g.Centroid;
    close all;
    xcenter = Cell_Centroid(1,1);
    ycenter = Cell_Centroid(1,2);

    % translate image to overlay aggregates on top of each other
    xtrans = CenterX - xcenter;
    ytrans = CenterY - ycenter;
    trans_phase = imtranslate(im_phase,[ytrans,xtrans]);
    trans_caspase = imtranslate(im_caspase,[ytrans,xtrans]);
    caspaseAll(:, :, i) = trans_caspase;
    figname_phase = ['dish' num2str(dishNo) '\dish' num2str(dishNo) 'trans_phase_circle'
num2str(i) '.tif'];
    figname_caspase = ['dish' num2str(dishNo) '\dish' num2str(dishNo) 'trans_caspase_circle'
num2str(i) '.tif'];
    imwrite(trans_phase,figname_phase);
    imwrite(trans_caspase,figname_caspase);
    close all;
end

% show 1st translated image to find the edge of the aggregates
imPhase=imread(['dish1trans_phase_circle' num2str(baseNo) '.TIF']);
imshow(imPhase)
title('Select the edge of the cell');

% x,y coordinates of radius from phase image
h=impoint;
j=wait(h);
xrad = j(1,1);

```

```

yrad = j(1,2);
close all
x = CenterX-xrad; y = CenterY-yrad;
radius = sqrt(x^2+y^2);

%%%%%%%%%%%%%%%%%%%%%%%%%%%%%%%%%%%%%%%%%%%%%%%%%%%%%%%%%%%%%%%%%%%%%%%%

% The following generate different graphs for the translated data

% Max projection of caspase images at each pixel
caspaseMax = max(caspaseAll,[],3);
temp = double(caspaseMax(:));
maxlim = mean(temp)+3*std(temp);
figure, imagesc(caspaseMax); caxis([0 maxlim]);
viscircles([CenterX CenterY],radius,'EdgeColor','w'); % draw white circle from radius
title('Max Projection of Caspase'); colorbar; colormap jet;

filename_caspaseMax = ['dish' num2str(dishNo) '\dish' num2str(dishNo)
'trans_caspase_circle_max.tif'];
filename_caspaseMax_color = ['dish' num2str(dishNo) '\dish' num2str(dishNo)
'trans_caspase_circle_max_color.tif'];
imwrite(caspaseMax,filename_caspaseMax);
saveas(gcf,filename_caspaseMax_color);

%%%%%%%%%%%%%%%%%%%%%%%%%%%%%%%%%%%%%%%%%%%%%%%%%%%%%%%%%%%%%%%%%%%%%%%%

% Average caspase image at each pixel
caspaseAve = mean(caspaseAll,3);
temp = double(caspaseAve(:));
maxlim = mean(temp)+3*std(temp);
figure, imagesc(caspaseAve); caxis([0 maxlim]);
viscircles([CenterX CenterY],radius,'EdgeColor','w'); %draw white circle from radius
title('Average Caspase Intensity at each Location'); colorbar; colormap jet;

filename_caspaseAve = ['dish' num2str(dishNo) '\dish' num2str(dishNo)
'trans_caspase_circle_ave.tif'];
filename_caspaseAve_color = ['dish' num2str(dishNo) '\dish' num2str(dishNo)
'trans_caspase_circle_ave_color.tif'];
imwrite(caspaseAve,filename_caspaseAve);
saveas(gcf,filename_caspaseAve_color);

%%%%%%%%%%%%%%%%%%%%%%%%%%%%%%%%%%%%%%%%%%%%%%%%%%%%%%%%%%%%%%%%%%%%%%%%

% Visit each pixel and see if the value is above the threshold. If value is above threshold, makes
intensity 1, to normalize all counts. Will calculate the average caspase value at each radius as
well as number of counts of caspase at each radius.

```

```

caspaseCount = zeros(SizeY,SizeX,nImages,'uint16');
for i=1:SizeY
    for j = 1:SizeX
        for k = 1:nImages
            if caspaseAll(i,j,k) < tau
                caspaseCount(i,j,k) = 0;
            else
                caspaseCount(i,j,k) = 1;
            end
        end
    end
end
caspaseCountSum = sum(caspaseCount,3);

x = 1:1:SizeX;
y = 1:1:SizeY;

% Creates matrix of equal dimensions of aggregate images and signifies the radial distance for
each pixel
for kx = 1:length(x)
    for ky = 1:length(y)
        r(ky,kx) = sqrt((kx-CenterX)^2 + (ky-CenterY)^2);
    end
end

% Average caspase value and count value at each radius
rad=0:radius/(delta):radius; % breakdown of radii into number of rings selected previously
idx=zeros(1,length(rad)); % creating index to store values for each radius

for kx = 1:length(x)
    for ky = 1:length(y)
        for kz = 2:length(rad)
            if r(ky,kx)<=rad(kz) && r(ky,kx)>rad(kz-1)
                idx(kz-1)=idx(kz-1)+1;
                vector(kz-1,idx(kz-1))=caspaseAve(ky,kx);
                Count(kz-1,idx(kz-1))=caspaseCountSum(ky,kx);
            end
        end
    end
end

for i=2:length(rad)
    Average(i-1)=sum(vector(i-1,1:idx(i-1)))/idx(i-1);
    Countave(i-1)=((sum(Count(i-1,1:idx(i-1)))/idx(i-1))/nImages*100);
end

```

```

end

% Implementing the average per radius
% Implementing the counts per radius
% Anything outside of the aggregate limits is zero
for kx = 1:length(x)
    for ky = 1:length(y)
        for kz = 2:length(rad)
            if r(ky,kx)<=rad(kz) && r(ky,kx)>rad(kz-1)
                caspaseAveRing(ky,kx)=Average(kz-1);
                caspaseCountRing(ky,kx)=Countave(kz-1);
            elseif r(ky,kx)>max(rad)
                caspaseAveRing(ky,kx)=0;
                caspaseCountRing(ky,kx)=0;
            end
        end
    end
end
end

% % % % % % % % % % % % % % % % % % % % % % % % % % % % % % % % % % %

% Graphing average caspase intensity as a function of radius
temp = double(caspaseAveRing(:));
maxlim = mean(temp)+3*std(temp);
figure, imagesc(caspaseAveRing); caxis([0 maxlim]);
viscircles([CenterX CenterY],radius,'EdgeColor','w'); %draw white circle from radius
title('Average Caspase Intensity at Specific Radii'); colorbar; colormap jet;

filename_caspaseAveRing = ['dish' num2str(dishNo) '\dish' num2str(dishNo)
'trans_caspase_circle_avering.tif'];
filename_caspaseAveRing_color = ['dish' num2str(dishNo) '\dish' num2str(dishNo)
'trans_caspase_circle_avering_color.tif'];
imwrite(caspaseAveRing,filename_caspaseAveRing);
saveas(gcf,filename_caspaseAveRing_color);

% Graphing average count of caspase as a function of radius
figure, imagesc(caspaseCountRing); caxis([0 100]);
viscircles([CenterX CenterY],radius,'EdgeColor','w'); %draw white circle from radius
title('Frequency of Caspase Presence at Specific Radii'); colorbar; colormap jet;

filename_caspaseCountRing = ['dish' num2str(dishNo) '\dish' num2str(dishNo)
'trans_caspase_circle_countring.tif'];
filename_caspaseCountRing_color = ['dish' num2str(dishNo) '\dish' num2str(dishNo)
'trans_caspase_circle_countring_color.tif'];
imwrite(caspaseCountRing,filename_caspaseCountRing);
saveas(gcf,filename_caspaseCountRing_color);

```

```
%%%%%%%%%%%%%%%%%%%%%%%%%%%%%%%%%%%%%%%%%%%%%%%%%%%%%%%%%%%%%%%%%%%%%%%%%
```

```
% Make scatterplot/line graph of average/counts as a function of radius
z = radius/delta:radius/delta:radius;
z = z/radius*90; % aggregate is roughly 180um diameter --> 90um radius
figure, scatter(z,Countave)
hold on
plot(z,Countave)
axis([0 z(end) 0 100]);
%set(gca,'XTick',z);
%set(gca,'XTickLabel',ceil(z));
xlabel('Distance from center (\mum)');
ylabel('Percent of area positive for caspase (%)')
title('Frequency of Caspase Presence at Specific Radii');
hold off
```

```
%%%%%%%%%%%%%%%%%%%%%%%%%%%%%%%%%%%%%%%%%%%%%%%%%%%%%%%%%%%%%%%%%%%%%%%%%
%%%%%%%%%%%%%%%%%%%%%%%%%%%%%%%%%%%%%%%%%%%%%%%%%%%%%%%%%%%%%%%%%%%%%%%%%
```

```
% % % CODE TO GRAPH INDIVIDUAL AGGREGATES PLOTS % % %
% Going through each image and making rings for average intensity and count
```

```
for k = 1:nImages
    idx=zeros(1,length(rad));
    for kx = 1:length(x)
        for ky = 1:length(y)
            for kz = 2:length(rad)
                if r(ky,kx)<=rad(kz) && r(ky,kx)>rad(kz-1)
                    idx(kz-1)=idx(kz-1)+1;
                    vectorInd(kz-1,idx(kz-1))=caspaseAll(ky,kx,k);
                    CountInd(kz-1,idx(kz-1))=caspaseCount(ky,kx,k);
                end
            end
        end
    end
    vectorIndAll(:,k)=vectorInd;
    CountIndAll(:,k)=CountInd;
end

for i=2:length(rad)
    AverageInd(i-1,:)=sum(vectorIndAll(i-1,:,:))/idx(i-1);
    CountaveInd(i-1,:)=(sum(CountIndAll(i-1,:,:))/idx(i-1))*100;
end
```

```
%%%%%%%%%%%%%%%%%%%%%%%%%%%%%%%%%%%%%%%%%%%%%%%%%%%%%%%%%%%%%%%%%%%%%%%%%
```

```
% Plotting individual graphs for each image
```

```
z = radius/delta:radius/delta:radius;
z = z/radius*90; % aggregate is roughly 180um diameter --> 90um radius
hold on
plot(z,CountaveInd)
axis([0 z(end) 0 100]);
%set(gca,'XTick',z);
%set(gca,'XTickLabel',z);
xlabel('Distance from center (\mum)');
ylabel('Percent of area positive for caspase (%)')
title('Frequency of Caspase Presence at Specific Radii in Individual Aggregates');

m=mean(CountaveInd,2); err=std(CountaveInd,[],2)/sqrt(nImages);
errorbar(z,m,err,'o')
%scatter(z,m)
hold off
```